Volume 55
Number 6
23 March 2026
Pages 2997–3728

Chem Soc Rev

Chemical Society Reviews

rsc.li/chem-soc-rev

ISSN 0306-0012

ROYAL SOCIETY OF CHEMISTRY

REVIEW ARTICLE

Vitaly L. Sushkevich *et al.*

Formation of active sites in copper-exchanged zeolites for the direct methane-to-methanol conversion

Chem Soc Rev

REVIEW ARTICLE

View Article Online
View Journal | View Issue

Cite this: *Chem. Soc. Rev.*, 2026, **55**, 3078

Formation of active sites in copper-exchanged zeolites for the direct methane-to-methanol conversion

Jörg W. A. Fischer, †‡[a] Andreas Brenig, ‡[b] Johannes Wieser, ‡[b] Jeroen A. van Bokhoven [bc] and Vitaly L. Sushkevich *[c]

Cu-exchanged zeolites are extensively studied for their promising properties in the direct and selective conversion of CH_4 to CH_3OH at low temperatures. Their performance has been attributed to the presence of multiple oxygenated Cu(II) active sites, which can co-exist in a given zeolite framework. Most emphasis has been placed on identifying these Cu-oxo centers, understanding their structural development during reaction with CH_4, and establishing a correlation between the Cu speciation and the zeolite's Cu loading, Si/Al ratio, and topology. On the contrary, the processes underlying the oxidative formation of Cu(II) active sites have received comparatively little attention. This critical review presents an overview of the current understanding of the generation of Cu(II) active centers and highlights the impact of the oxidant type and the reaction conditions on the nature of the formed Cu(II) species. Key knowledge gaps are identified by addressing prevailing misconceptions and conflicting reports in the literature. To remedy these issues, strategies are proposed to resolve discrepancies and to gain new insight into the processes preceding the CH_4-to-CH_3OH conversion in Cu-exchanged zeolites, aiming to better understand and control the generation of these Cu(II) active sites in zeolites.

Received 30th June 2025

DOI: 10.1039/d5cs00747j

rsc.li/chem-soc-rev

[a] *Department of Chemistry and Applied Biosciences, ETH Zurich, Vladimir-Prelog-Weg 1-5/10, 8093 Zurich, Switzerland*
[b] *Institute for Chemical and Bioengineering, ETH Zurich, Vladimir-Prelog-Weg 1-5/10, 8093 Zurich, Switzerland*
[c] *Center for Energy and Environmental Sciences, Paul Scherrer Institute, Forschungsstrasse 111, 5232 Villigen, Switzerland. E-mail: vitaly.sushkevich@psi.ch*
† Current address: Institute for Catalysis, Hokkaido University, N-21, W-10, Sapporo 001-0021, Japan.
‡ These authors have contributed equally to this work.

Jörg W. A. Fischer

Jörg Fischer studied chemistry at the University of Konstanz, with academic stays at the University of Washington and at the University of Tübingen. He joined ETH in 2020 for his PhD with Prof. Jeschke. During that time, he focused on the development of operando EPR spectroscopy and its application to transition metal exchanged zeolites. In 2025, he obtained a postdoctoral fellowship from the Japan Society for the Promotion of Science (JSPS) and moved to Japan working at the Hokkaido University on CO2 hydrogenation over metal oxides. Recently he joined Utrecht University for a postdoctoral research stay, where he focuses on coke speciation in zeolites.

Andreas Brenig

Dr Andreas Brenig earned his Bachelor's and Master's degrees in Chemistry from the Technical University of Munich, where he specialized in Chemical Engineering and Catalysis. He then completed his doctoral studies at the Center for Energy and Environmental Sciences at Paul Scherrer Institute and is currently working as a postdoctoral researcher at the Institute for Chemical and Bioengineering at ETH Zurich. His research focuses on the physicochemical characterization of materials for energy applications and the implementation of chemometric methods.

1. Introduction

Natural gas sources in remote or stranded locations are notoriously difficult to utilize, as the low volumetric energy density of CH_4, the main constituent of natural gas, makes long-distance transportation economically unfeasible, frequently leading to gas flaring at extraction sites.[1] Liquefaction of natural gas can be used for natural gas transportation from remote production facilities, but the relatively high cost of this process and the expensive infrastructure have limited its commercial application to large natural gas reserves. Alternatively, converting CH_4 to condensable or value-added chemicals on-site is a promising route for CH_4 valorization. The transformation of CH_4 to CH_3OH continues to attract attention as CH_3OH is an important energy carrier (*e.g.*, fuel, direct methanol fuel cells (DMFCs))[2] and a chemical building block for producing olefins.[3] The industrial production of CH_3OH based on CH_4 consists of two consecutive steps: (1) CH_4 steam reforming into syngas (mixture of CO and H_2) and (2) conversion of syngas to CH_3OH at high pressures using a $Cu/ZnO/Al_2O_3$ (CZA) catalyst. This approach, especially the steam reforming of CH_4 to syngas, is energy-intensive and only feasible for large-scale operations.[4]

Scale-flexible and direct approaches for the CH_4-to-CH_3OH conversion are an attractive solution, but face one major challenge: the higher reactivity of CH_3OH compared to CH_4, leading to overoxidation of the former.[5,6] Transition metal ion (TMI)-exchanged zeolites have emerged as promising materials for the selective oxidation of CH_4 to CH_3OH, attracting considerable attention over the past two decades.[6,7] These materials can stabilize monomeric, dimeric, and multimeric metal-oxo sites that resemble the active centers of C–H bond activating enzymes, such as Cu containing particulate methane monooxygenase (pMMO) and Fe containing soluble methane monooxygenase (sMMO).[8,9] The active species in TMI containing zeolites are usually generated by an oxidant such as O_2, N_2O, NO, or H_2O_2. Among the TMI-zeolites employed for the CH_4-to-CH_3OH conversion, Cu- and Fe-exchanged zeolites are the most studied ones. Cu-exchanged zeolites are considered to have the greatest economic potential, as the Cu-oxo sites can be generated using O_2, whereas the activation of Fe-exchanged zeolites typically requires expensive oxidants such as N_2O or H_2O_2, which are more costly than the produced CH_3OH.[10–12]

The generation of these Cu(II) active centers is of fundamental importance, as they govern the reactivity of the material. While the existing literature predominantly focuses on the structural characterization of the Cu-oxo species and on optimizing the CH_3OH productivity by varying the process parameters during CH_4 conversion, it often overlooks how the activation conditions influence the formation and nature of the Cu(II) active sites. A comprehensive understanding of the

Johannes Wieser

Johannes Wieser received his BSc and MSc degrees in Chemistry from the Technical University Munich (TUM). He subsequently joined the Department of Chemical and Applied Biosciences (D-CHAB) at ETH Zürich, where he is currently pursuing his PhD under the supervision of Professor Jeroen A. van Bokhoven. His research at ETH focuses on the development of processes for the selective oxidation of methane to value-added products, primarily via copper-exchanged zeolitic systems.

Jeroen A. van Bokhoven

Jeroen A. van Bokhoven completed a degree in chemistry at Utrecht University (Netherlands) in 1995 and went on to obtain a PhD in inorganic chemistry and catalysis from the same university in 2000 (with honours). From 1999 until 2002, he was head of the XAS (X-ray absorption spectroscopy) user-support group at Utrecht University. In 2002, he moved to the ETH, where he worked as a researcher in the group of Prof. Prins. In 2006, he obtained an SNF assistant professorship in the Department of Chemistry and Applied Biology. He was the 2008 recipient of the Swiss Chemical Society Werner Prize. Since 2010, Jeroen A. van Bokhoven has a Chair in Heterogeneous Catalysis at the Institute for Chemical and Bioengineering at ETH Zurich and is Head of Laboratory for Catalysis and Sustainable Chemistry at the Paul Scherrer Institute.

Vitaly L. Sushkevich

Vitaly Sushkevich earned his PhD from Lomonosov Moscow State University in 2014, where he led the development of novel catalysts and catalytic processes for producing monomers for synthetic rubbers from renewable feedstocks. In 2019, he joined the Paul Scherrer Institute as a Scientist, focusing on challenges in selective alkane oxidation and dehydrogenation. More recently, he has taken on a leading role in advancing research on the understanding of the mechanisms of synthesis of solid catalysts and porous materials.

mechanism of Cu–zeolite activation is essential for selectively generating specific Cu(II) active centers and maximizing their population within the zeolite framework. In general, the formation of Cu(II) active species in the (non-)isothermal chemical looping as well as in the continuous CH_4-to-CH_3OH processes (see Section 2.3) remains poorly understood. In particular, contradictory findings regarding the effect of the activation temperature and duration on the CH_3OH productivity have been reported,[13–22] and disagreements concerning the influence of the partial pressure of the oxidizing agent persist.[16,17,21,23] Therefore, an in-depth understanding of the formation of Cu(II) active sites is essential to obtain a holistic picture of the overall redox cycle.

In this review, the formation of various Cu-oxo centers, which are active in the CH_4-to-CH_3OH conversion, is discussed in detail, and misconceptions and knowledge gaps are presented. The article is structured as follows: First, a brief introduction to zeolites and the Cu(II) sites stabilized within these materials is provided alongside their key spectroscopic fingerprints. This is followed by showcasing different approaches in which Cu–zeolites have been employed in the CH_4-to-CH_3OH transformation. Subsequently, the generation of distinct Cu(II) centers by various oxidizing agents, namely O_2, N_2O, NO, H_2O, CO_2, and H_2O_2, is reviewed, and their role in the stoichiometric stepwise chemical looping and catalytic processes is critically examined. To avoid ambiguities, the Lewis structures of each Cu(II) active site and selected intermediates are compiled in Scheme S1 in the Supporting Information, along with their corresponding names, potential resonance structures, and Cu oxidation states. Next, common misconceptions and conflicting literature reports are identified and discussed, and knowledge gaps are pointed out. Finally, recommendations are given to gain the needed in-depth understanding of the processes leading to the formation of Cu(II) active species. Whenever specific Cu–zeolites are addressed, their Cu/Al and Si/Al ratios are provided as reported in the original publications, using the notation Cu_XZEO_Y, where *X*, ZEO, and *Y* correspond to the Cu/Al ratio, the framework type code, and the Si/Al ratio. If either the Cu/Al or Si/Al ratio is not specified in the literature, it is omitted from the material description. In cases where the Cu/Al ratio is not provided, *X* is replaced by a hyphen, *i.e.*, Cu-ZEO_Y, for improved readability.

2. Zeolites

Zeolites are microporous crystalline aluminosilicates built from primary building units (PBUs), consisting of a central Si or Al atom tetrahedrally coordinated by four O atoms (T-sites). These PBUs connect *via* corner-sharing O atoms to form unique secondary building units (SBUs), whose arrangement defines the framework-specific porous system. Depending on the particular arrangement of the SBUs, the porous network features regular cavities interconnected by channels ranging from 3 to 15 Å in diameter.[24] These channels are either straight or puckered and can intersect each other. Generally, the diffusion through zeolites is governed by the molecule's size since a molecule can only pass through when the free diameter of the pore is equal to or greater than the molecule's dimensions (molecular-scale porosity).[9] This size restriction imposes steric constraints on molecular diffusion through the microporous network to reach adsorption sites. Therefore, zeolites belong to a class of materials called "molecular sieves". Depending on the pore interconnectivity/dimensionality, zeolites can be classified into 1, 2, or 3D materials. Scheme 1 shows three zeolite frameworks, which are employed most frequently in the CH_4-to-CH_3OH conversion, and which feature different dimensionalities. While the mordenite (MOR) framework is a 1D structure (due to its pore openings being larger than 3.4 Å), the chabazite (CHA) and MFI frameworks exhibit a 3D structure.[25] Scheme 1 also highlights the crystallographically distinct T-sites in each framework.

The distribution of Al over crystallographic T-sites obeys the Loewenstein rule, which states that whenever two T-sites are

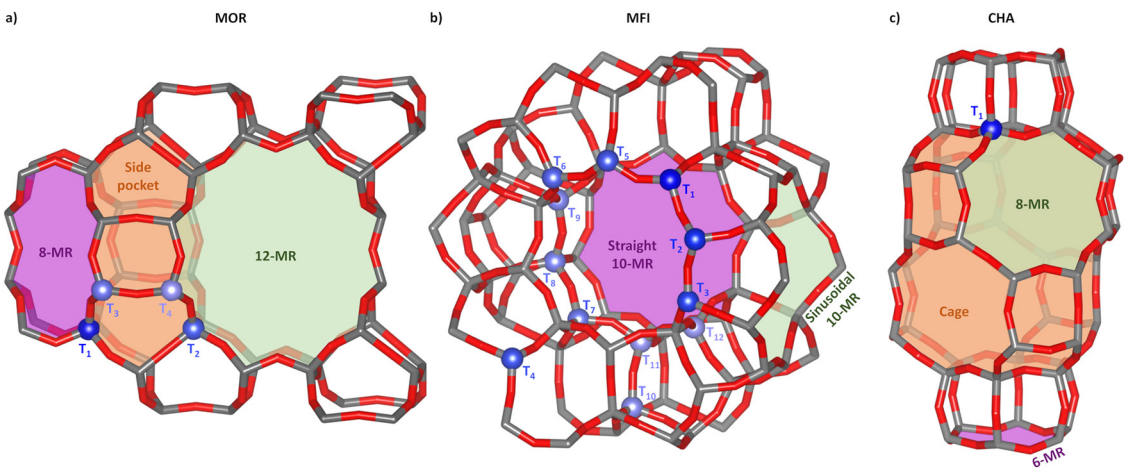

Scheme 1 Different zeolite frameworks employed most frequently in the CH_4-to-CH_3OH conversion: MOR (a), MFI (b), and CHA (c). The two largest ring openings, as well as characteristic lattice structures, are highlighted in transparent colors. Crystallographically distinct T-sites are indicated in different shades of blue. Si and framework O atoms are marked in grey and red, respectively.

linked by one O atom of the framework (O_{fw}), only one of them can be an Al atom.[26] Therefore, the resulting upper limit of isomorphous substitution of Si by Al is defined by a minimum Si/Al ratio of 1. Additionally, the Al substitution strives for an even distribution over the lattice in naturally occurring zeolites.[27] However, experimental evidence has suggested that the Al distribution in synthetic zeolites exhibits non-random patterns and deviates from simple statistical distributions.[28–30] While Loewenstein's rule does remain valid, Al substitutions are found to be in closer proximity than expected for a random distribution.[9] The difference in bond length between Al–O_{fw} (~1.7 Å) and Si–O_{fw} (~1.6 Å) distorts the lattice locally and influences the shape and free diameter of the rings. Therefore, the fraction of Al can affect the stability of the zeolite, with MOR and MFI being stable only above a Si/A ratio of 5 and 10, respectively.[31,32] For CHA, Si/Al ratios as low as 2 have been reported in gas absorption studies.[33]

The replacement of Si by Al introduces a net negative charge on the zeolite lattice, which requires an extra-framework cation for charge balance. Different extra-framework cations affect the properties of the zeolite and enable optimization of the material for a given application. When H^+ serves as the counter-ion, a Brønsted acid site (BAS) is created, which imparts the characteristic acidity of the zeolite. Introduction of TMIs is a widely employed strategy to modify the zeolite's adsorption and redox properties.[34] The most common approach for the incorporation of other cations, such as Cu(II), involves an ion exchange of the parent material in an aqueous medium, where the original cations, *e.g.*, H^+, NH_4^+, or Na^+, are exchanged with a Cu(II)-aqua complex. Notably, exchange conditions critically influence the final speciation and material properties, and precise control is essential to prevent undesired side reactions. For example, at high pH, both the participation of deprotonated surface Si–OH groups in the exchange reaction and the precipitation of Cu(II)-aqua complexes, which form CuO clusters upon calcination, contribute to the formation of non-stoichiometric and over-exchanged zeolites. Stoichiometric exchange occurs when the positive charge of the incorporated TMIs exactly balances the framework's negative charge, corresponding to a TMI/Al ratio of 0.5 for a divalent TMI species such as a monomeric bare Cu^{2+} site or a dimeric Cu(II) center (see Sections 2.1.1 and 2.1.3). It is important to point out that the stoichiometric exchange with other Cu(II) species, such as monomeric $[CuOH]^+$ or tri- and multimeric Cu(II) sites (see Sections 2.1.2 and 2.1.4), leads to a different TMI/Al ratio. Instead of aqueous ion exchange, Cu(II) can also be introduced into the zeolite pores *via* incipient wetness impregnation (IWI).[35,36] Another possibility is the so-called "solid-state" ion exchange. Here, the parent zeolite is mechanically mixed with a TMI containing precursor, such as CuCl, and the mixture is subsequently heated up, leading to an ion exchange.[37] While solid-state ion exchange is a relatively straightforward procedure, the method is limited by potential degradation of the zeolite framework at high temperatures and incomplete reaction of the precursor.[38–40] Alternatively, TMIs can also be directly incorporated during the synthesis of the zeolite by employing TMI containing structure directing agents (SDAs). This approach has been demonstrated for the preparation of Cu-exchanged small-pore zeolites, such as Cu–CHA, where the narrow pore size might hinder diffusion of the Cu(II)-aqua complex during a conventional ion exchange, preventing a full ion exchange.[41] All the above-mentioned methods for the introduction of Cu into zeolites typically give rise to a complex mixture of various co-existing Cu(II) active sites upon oxidative treatment. These species are discussed in more detail in the following section.

2.1 Definition of potential Cu(II) species in specific zeolite frameworks

2.1.1 Monomeric Cu^{2+} species. Two distinct monomeric Cu^{2+} sites have been identified in the 6-membered ring (MR) of various zeolites such as Cu–MOR, Cu–CHA, and Cu-MFI. These bare Cu^{2+} species have been reported to be the dominant Cu(II) sites at low Cu loadings across different framework topologies and Si/Al ratios.[42–46] The structure of these centers has been clarified with the help of electron paramagnetic resonance (EPR), NO-adsorption Fourier-transform infrared (NO-FTIR), and photoluminescence (PL) measurements.[42–44,47] These species balance the charge of two Al T-sites and are coordinated by up to four O_{fw} atoms. They do not feature any extra-framework O (O_{ef}) ligands and are thus sometimes referred to as "bare" Cu^{2+} centers. A schematic representation of these species is shown in Scheme 2 and Schemes S1a, b. One of these sites is located in a 6-MR where the Al T-sites are arranged in a *para* configuration (Cu^{2+}_{para}), whereas the Al T-sites of the second center are positioned in a *meta* arrangement (Cu^{2+}_{meta}). Although the presence of these two different species is generally accepted, the clear differentiation of their spectroscopic fingerprints continues to pose a challenge. Based on density functional theory (DFT) and electrostatic considerations, Godiksen *et al.* correlated an EPR signal around g_{II} = 2.325 in Cu–CHA to Cu^{2+}_{para}, whereas a feature at approximately g_{II} = 2.358 was attributed to Cu^{2+}_{meta}.[47] In contrast, theoretical calculations by Bruzzese *et al.* led to the opposite assignment.[45] As in Cu–CHA, the correlations in Cu-MFI and Cu–MOR suffer from the same ambiguity. However, in Cu–MOR and Cu-MFI, a second bare Cu^{2+} is only observable at very low Cu loadings and has not been investigated in detail. Similarly, in other Cu–zeolites, including Linde type A (LTA) and faujasite (FAU), distinct EPR

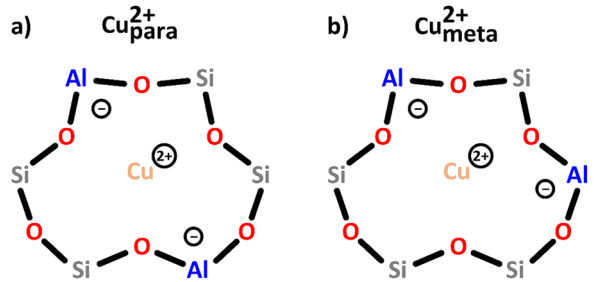

Scheme 2 Bare monomeric Cu^{2+} charge-balanced by two Al T-sites positioned in either the *para* (a) or *meta* (b) arrangement. Color code: Al = blue, Si = grey, framework O = red, Cu = orange.

signals of isolated Cu^{2+} have been associated with different Al T-site arrangements.[9,48] In addition to their characteristic EPR features, bare Cu^{2+} centers have been identified in several Cu–zeolites using NO-FTIR experiments, giving rise to distinct absorption bands in the region from 1940 to 1900 cm^{-1}.[44] By analyzing the NO-FTIR and Cu(I) PL spectra of oxidized and reduced Cu-exchanged zeolites, Dědeček *et al.* have been able to differentiate *meta* and para Al T-site configurations in several zeolites.[44] However, in Cu–CHA, a differentiation between these two species on the basis of NO-FTIR spectroscopy is often not possible.[49,50] Further, a band around 14 000–12 000 cm^{-1} in the ultraviolet-visible (UV-Vis) spectra of various Cu–zeolites with different frameworks has been attributed to these bare Cu^{2+} sites.[50–54]

In an *operando* EPR study, Godiksen *et al.* demonstrated that these two centers differ in their reactivity toward oxidation in gas mixtures relevant for the NH_3-mediated selective catalytic reduction of NO_x (NH_3-SCR), indicating that the Al T-site arrangement has a major impact on their redox behavior.[55] Furthermore, recent studies have suggested that even though these sites lack O_{ef} ligands, they can still participate in the CH_4-to-CH_3OH conversion when present as a Cu^{2+}/$[CuOH]^+$ pair.[46,50,56]

2.1.2 Monomeric $[CuOH]^+$ species. Upon saturation of 6-MRs featuring two Al T-sites by Cu(II), monomeric Cu^{2+} is exchanged into ion exchange positions featuring a single Al T-site.[46,57,58] The existence of a Cu(II) exchange site characterized by just one Al T-site has been shown decades ago, but the presence of an OH^- ligand for charge compensation has frequently been rejected in the past due to disagreements between experimentally observed g values and those obtained from DFT calculations.[59–61] However, recent studies have confirmed the existence of the OH^- ligand based on EPR and Raman measurements as well as DFT calculations.[44,50,58,62,63] A schematic representation of $[CuOH]^+$ is shown in Scheme 3 and Scheme S1c.

In Cu–MOR, $[CuOH]^+$ exhibits a g_{II} value of 2.27, similar to that in Cu-MFI, and both species are believed to exhibit a bidentate coordination to the O_{fw} atoms of a single Al T-site. In contrast, DFT calculations have indicated that $[CuOH]^+$ is coordinated by three O_{fw} atoms in Cu–CHA.[58] Nevertheless, since the experimentally observed *g* value of $[CuOH]^+$ in Cu–CHA (g_{II} = 2.40) deviates significantly from that in Cu–MOR and Cu-MFI, a different coordination mode of $[CuOH]^+$ in Cu–CHA compared to Cu–MOR and Cu-MFI seems plausible. Apart from the ligation, the zeolite framework also governs the location of $[CuOH]^+$. In Cu–MOR, $[CuOH]^+$ has originally been assumed to reside within a 6-MR, but a recent study by Heyer *et al.* has suggested that it is actually located in the 8-MR of the MOR side pocket (Scheme 1), facing the 8-MR channel.[61,62] Other ion exchange positions were, however, not excluded by the authors. In Cu–CHA, $[CuOH]^+$ is also positioned within the 8-MR, whereas it is situated in the 10-MR in Cu-MFI.[46,50,58,59,64] In addition to EPR spectroscopy, $[CuOH]^+$ has also been characterized by NO-FTIR and UV-Vis measurements, yielding absorption bands around 1900 cm^{-1} and between 16 000 and 12 000 cm^{-1}, respectively.[44,50,51,60] The participation of $[CuOH]^+$ in CH_4 partial oxidation has been demonstrated in the past years.[46,50,56,62,63,65]

2.1.3 Dimeric Cu-Oxo species. In their seminal work, Groothaert *et al.* defined a dimeric Cu-oxo center as the active site for the CH_4-to-CH_3OH conversion in Cu-MFI.[7] Initially, the Cu(II) species was attributed to $[Cu_2(\mu\text{-}O)_2]^{2+}$ based on the observation of a characteristic UV-Vis signal around 22 700 cm^{-1}, but subsequent Raman and DFT studies by the same research group revised this assignment to $[Cu_2(\mu\text{-}O)]^{2+}$.[66] Furthermore, Ipek *et al.* proposed the presence of $[Cu_2(trans\text{-}\mu\text{-}1,2\text{-}O_2)]^{2+}$ in Cu–CHA based on the identification of broad UV-Vis features in the 35 000–22 200 cm^{-1} range and distinct Raman signals (see Section 3).[20] The different dimeric oxygenated Cu(II) centers are summarized in Scheme 4 and Scheme S1d–f. Depending on the zeolite's Si/Al ratio, these sites become dominant in materials characterized by a higher Cu loading than that needed for the generation of monomeric Cu(II) species.[46,50,57] Notably, the spin–spin exchange interaction of the Cu(II) ions usually renders dimeric Cu-oxo motifs EPR invisible under standard measurement conditions, *e.g.*, at X-band frequencies (9.5 GHz).[46,47,67]

In Cu–MOR, three distinct $[Cu_2(\mu\text{-}O)]^{2+}$ cores have been proposed based on Raman measurements by Vanelderen *et al.* and Plessers *et al.*[51,68] One of these Cu(II) centers has been suggested to reside within the 8-MR of the MOR side pocket (Scheme 1), oriented toward the 12-MR channel, whereas the other two Cu-oxo sites have been shown to span across the 8-MR channel.[68,69] Remarkably, $[Cu_2(\mu\text{-}O)]^{2+}$ positioned in the more restricted 8-MR channel is more active in CH_4 hydroxylation than its geometrically less confined counterpart.[51,69] According to DFT calculations, the higher activity of the former Cu(II) species originates from the stronger van der Waals interaction between CH_4 and the narrow zeolite lattice surrounding this Cu(II) active center. Notably, the nature of the dimeric Cu-oxo site has been shown to be influenced by the co-cation, which in turn affects the material's reactivity. In Cu–MOR and Cu-MFI, Brezicki *et al.* demonstrated that $[Cu_2(\mu\text{-}O)]^{2+}$, characterized by a UV-Vis signal at ~27 500 cm^{-1}, is the dominant dimeric Cu(II) species in the absence of Na^+ co-cations, whereas $[Cu_2(trans\text{-}\mu\text{-}1,2\text{-}O_2)]^{2+}$, featuring a UV-Vis band at around 22 000 cm^{-1}, becomes the prevalent Cu(II) center in the presence of Na^+.[70] Compared to $[Cu_2(\mu\text{-}O)]^{2+}$, $[Cu_2(trans\text{-}\mu\text{-}1,2\text{-}O_2)]^{2+}$ was found to promote CH_4 overoxidation

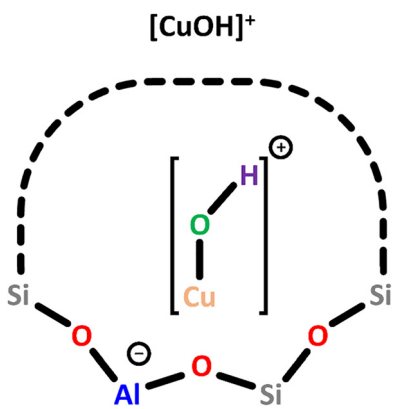

Scheme 3 Monomeric $[CuOH]^+$ charge-balanced by a single Al T-site. Color code: Al = blue, Si = grey, framework O = red, Cu = orange, extra-framework O = green, H = violet.

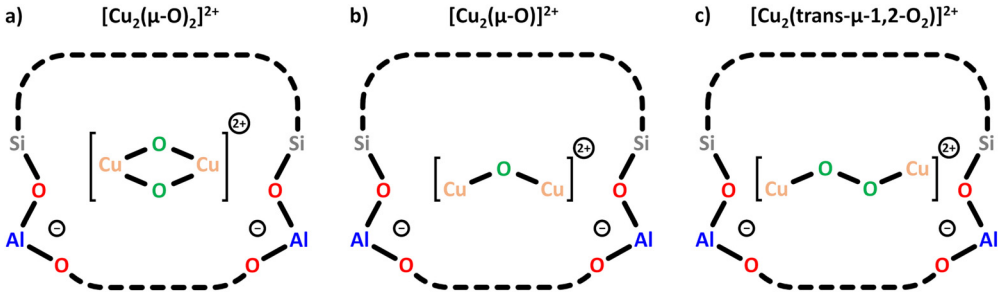

Scheme 4 Dimeric $[Cu_2(\mu\text{-}O)_2]^{2+}$ (a), $[Cu_2(\mu\text{-}O)]^{2+}$ (b) and $[Cu_2(trans\text{-}\mu\text{-}1,2\text{-}O_2)]^{2+}$ (c) charge-balanced by two Al T-sites. Color code: Al = blue, Si = grey, framework O = red, Cu = orange, extra-framework O = green.

due to the greater number of reactive O_{ef} atoms in this Cu(II) site. In contrast to Brezicki *et al.*, Artsiusheuski *et al.* assigned the two features at approximately 27 200 and 21 900 cm^{-1} in the UV-Vis spectrum of Cu-MFI to two distinct $[Cu_2(\mu\text{-}O)]^{2+}$ motifs within the 10-MR (Scheme 1), which differ in their reactivity toward CH_4. Using Fourier-transform extended X-ray absorption fine structure (FT-EXAFS) spectroscopy, the Cu–Cu distance of the two $[Cu_2(\mu\text{-}O)]^{2+}$ species was determined to amount to 2.9 and 3.2 Å.[71]

Two different Cu(II) dimers have been proposed to co-exist in Cu–CHA. Originally, one of them has been attributed to a $[Cu_2(trans\text{-}\mu\text{-}1,2\text{-}O_2)]^{2+}$ center, whereas the other one has been identified as a $[Cu_2(\mu\text{-}O)]^{2+}$ species.[20] However, a recent study has provided evidence that instead of $[Cu_2(trans\text{-}\mu\text{-}1,2\text{-}O_2)]^{2+}$ and $[Cu_2(\mu\text{-}O)]^{2+}$, Cu–CHA might host two different $[Cu_2(\mu\text{-}O)]^{2+}$ motifs, which differ in their activity, Cu–Cu distance, and location within the framework.[69] Their exact structure and the origin of the variation in their activity remain elusive.[20,50] Furthermore, Göltl *et al.* proposed the presence of two different $[Cu_2(\mu\text{-}O)_2]^{2+}$ centers in Cu–CHA to explain the difference in material reactivity after activation in either O_2 or N_2O.[72] They concluded that activation with N_2O leads to $[Cu_2(\mu\text{-}O)_2]^{2+}$, whereas activation with O_2 results in the corresponding hydroxylated Cu(II) dimer ($[Cu_2(\mu\text{-}OH)_2]^{2+}$, Scheme S1g), which, however, requires the presence of H_2O.

It is worth mentioning that a recent study by Heyer *et al.*, focusing on dimeric Cu(II) species in Cu–CHA and Cu-MFI, contradicts the aforementioned observations by proposing the existence of only a single type of $[Cu_2(\mu\text{-}O)]^{2+}$ located within the 8-MR of Cu–CHA and the 10-MR of Cu-MFI. This study attributes the differences in reactivity between frameworks to variations in the coordination of $[Cu_2(\mu\text{-}O)]^{2+}$ to the zeolite lattice, which result in different ground spin states of S = 0 and S = 1 for $[Cu_2(\mu\text{-}O)]^{2+}$ in Cu-MFI and Cu–CHA, respectively.[67]

2.1.4 Trimeric $[Cu_3(\mu\text{-}O)_3]^{2+}$ species and Cu-Oxo nanoclusters. The selective transformation of CH_4 to CH_3OH *via* a trimeric Cu-oxo-cluster (Scheme 5 and Scheme S1h) has first been suggested in a contribution by Grundner *et al.* in 2015.[73]

To enable the formation of these trimeric Cu(II) sites, the authors selected a MOR framework with a high concentration of Al T-sites in the 8-MR of the side pockets (Scheme 1) and employed an optimized synthesis procedure.[73] In a subsequent theoretical study on Cu-MFI, the same research group proposed that trinuclear Cu-oxo clusters are the most stable Cu(II) species at elevated O_2 partial pressures.[74] A UV-Vis band around

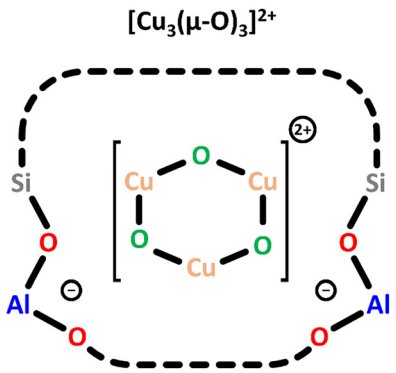

Scheme 5 Trimeric $[Cu_3(\mu\text{-}O)_3]^{2+}$ charge-balanced by two Al T-sites. Color code: Al = blue, Si = grey, framework O = red, Cu = orange, extra-framework O = green.

31 000 cm^{-1} has been assigned to the $[Cu_3(\mu\text{-}O)_3]^{2+}$ species, but no experimental EPR signature or NO-FTIR features have been reported yet. Notably, only Ikuno *et al.* and Kim *et al.* have observed similar UV-Vis absorption features in the range from 39 000 to 30 000 cm^{-1} and attributed them to $[Cu_3(\mu\text{-}O)_3]^{2+}$.[19,21]

Furthermore, theory-based studies have identified an increased stability of Cu-oxo clusters with even higher nuclearity.[75] Using FT-EXAFS spectroscopy, Sushkevich *et al.* and Artsiusheuski *et al.* suggested the presence of Cu_XO_Y clusters in the large pores of Cu-FAU and Cu-exchanged beta (BEA), which also participate in the conversion of CH_4 to CH_3OH.[76,77] In addition, Tomkins *et al.* suggested multimeric dispersed Cu-oxo clusters in Cu–MOR as active species based on transmission electron microscopy (TEM) and FT-EXAFS measurements, and the reduction of a large fraction of Cu(II) in the studied material after exposure to CH_4 was reported.[17]

2.3 CH_4-to-CH_3OH conversion in Cu–zeolites

Scheme 6 illustrates a possible reaction mechanism for the selective CH_4-to-CH_3OH conversion *via* $[Cu_2(\mu\text{-}O)]^{2+}$.[78] The first steps include a dehydration of the material and the formation of the Cu(II) species with an oxidizing agent (1) and (2). Exposure to CH_4 results in its adsorption on the Cu(II) active site (3), where it is subsequently converted to CH_3OH, which induces a reduction of the Cu(II) center. The CH_3OH formation can proceed either *via* homolytic (4.1) or heterolytic (4.2) C–H bond activation. Theoretical calculations by Phung *et al.*,

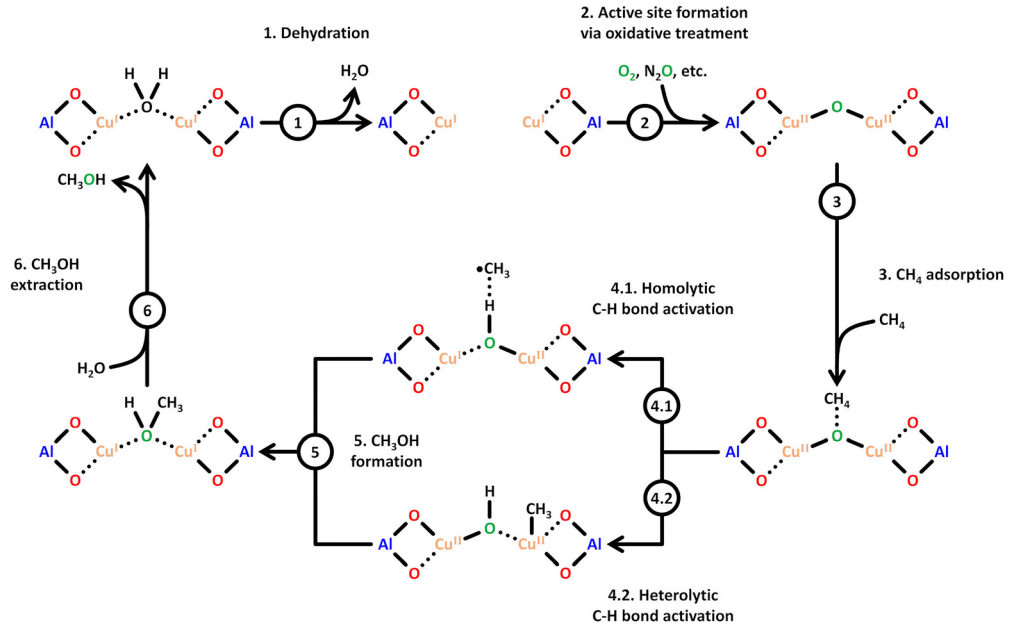

Scheme 6 Proposed mechanism of CH_4 hydroxylation by $[Cu_2(\mu\text{-}O)]^{2+}$. Starting from a reduced state after H_2O-assisted CH_3OH extraction, the redox cycle consists of: dehydration (1), active site formation *via* exposure to an oxidizing agent such as O_2 or N_2O (2), CH_4 adsorption at the Cu(II) active site (3), C–H bond activation *via* either homolytic or heterolytic (4.1 or 4.2) C–H bond activation, CH_3OH formation (5), and CH_3OH extraction with H_2O (6). Dotted bonds correspond to dative interactions. Color code: Al = blue, framework O = red, Cu = orange, extra-framework O = green. Adapted from ref. 78 with permission from the American Chemical Society (Copyright 2018).

employing complete active space perturbation theory (CASPT2), favored the heterolytic pathway, thereby questioning the general validity of the radical rebound step in the homolytic reaction mechanism.[79] After CH_3OH formation (5), the material is exposed to H_2O to facilitate the extraction of CH_3OH from the framework (6). These steps complete the cycle, and the Cu(II) active site can be regenerated upon dehydration and oxidation.

Various strategies have been explored for the effective transformation of CH_4 into CH_3OH. In a stepwise process (chemical looping, *vide infra*), the outlined steps (activation (1) and (2), reaction (3)–(5), and product extraction (6)) are separated, while in the continuous (catalytic) operation mode, the oxidizing agent, *e.g.*, O_2, as well as CH_4 and H_2O, are introduced simultaneously. The primary issue of continuous CH_4 hydroxylation lies in the significantly lower CH_3OH yield and selectivity compared to the stepwise approach.[13,80] Achieving high CH_4 conversion at equally high CH_3OH yield and selectivity is challenging due to both kinetic and thermodynamic constraints. High CH_3OH yield is only attainable if the CH_4 partial oxidation is faster than the subsequent oxidation of CH_3OH to deeper oxidation products such as CO_2. However, the C–H bond activation in CH_4 is slower than in CH_3OH, resulting in a substantial decrease in CH_3OH selectivity at elevated CH_4 conversion.[8] This phenomenon is known as the "selectivity-conversion limit".[81–84]

To overcome this limitation, product protection strategies can be employed. Of these, the chemical looping approach has been most frequently used for Cu–zeolites. This scheme involves a stoichiometric and stepwise process and is often combined with a temperature swing, but an isothermal operation mode is also possible.[17,85,86] In detail, the stepwise process involves three consecutive steps: (1) generation of the active Cu(II) sites within the zeolite by an oxidant at temperatures between 423–753 K, (2) the reaction with CH_4 at 423–623 K, and (3) the extraction of CH_3OH using liquid H_2O at ambient temperature or H_2O vapor. After reaction with CH_4, molecularly adsorbed CH_3OH or an intermediate in the form of a CH_3O methoxy species stabilized at a BAS or a reacted Cu(I) center may be present. The CH_3O species are converted to CH_3OH upon contact with H_2O. The main drawback of this process is the non-continuous operation. Moreover, the desorption of CH_3OH requires a solvent-based extraction technique, which leads to a dilute CH_3OH solution and necessitates an energy-intensive concentration of CH_3OH. Importantly, this issue is not limited to CH_4 hydroxylation *via* chemical looping, but also arises in the continuous process. The main advantage of the stepwise process is the protection of the adsorbed CH_3O against overoxidation, which generally leads to a higher CH_3OH yield and selectivity compared to the catalytic process. For the sake of completeness, it should be mentioned that Panov *et al.* were the first to employ chemical looping for CH_4 partial oxidation *via* Fe-exchanged zeolites.[6]

3. Formation of Cu(II) active sites during dehydration of as-prepared/hydrated Cu–zeolites under inert gas or vacuum

3.1 Generation of monomeric sites and spectroscopic characterization of Cu–zeolite dehydration

Considering that the oxidant represents an integral component in the CH_4-to-CH_3OH conversion for closing the Cu(II)/Cu(I)

redox cycle and generating active Cu-oxo sites, it may seem counterintuitive to begin with a discussion of CH_4 hydroxylation by Cu–zeolites that have been subjected to thermal treatment under inert gas or vacuum instead. Nevertheless, multiple studies have reported a non-negligible CH_3OH productivity of various Cu–zeolites (Cu-ferrierite (FER), Cu–MOR, Cu–CHA) in CH_4 partial oxidation following their activation in inert gas at elevated temperatures, occasionally reaching levels comparable to those achieved after conventional calcination.[16,17,20,22,62,87–92] For example, Passini *et al.* observed that the CH_3OH productivity of $Cu_{0.23}FER_{10.0}$ decreased only marginally from 7.3 to 6.5 $\mu mol_{CH_3OH}\ g_{ZEO}^{-1}$ when treating the material in He instead of air at 823 K prior to interaction with CH_4 at 483 K.[87] Similarly, Tomkins *et al.* demonstrated that the performance of $Cu–MOR_{6.0}$ during reaction with 6 bar CH_4 at 473 K was comparable after an initial activation in either He or O_2 at 473 K (20.0 and 21.2 $\mu mol_{CH_3OH}\ g_{ZEO}^{-1}$, respectively).[17] At first glance, these observations could suggest that the generation of oxygenated Cu(II) active species during thermal treatment of Cu–zeolites in inert gas is similarly efficient as in the presence of an oxidant. However, it is important to highlight that the Cu–zeolites in the aforementioned studies were synthesized *via* conventional aqueous ion exchange using $Cu(NO_3)_2$ or $Cu(CH_3COO)_2$ and remained in the as-prepared/hydrated state prior to treatment with inert gas at elevated temperatures.[16,17,20,22,87–92] Under these conditions, Cu is already present in the oxidation state +2 and forms mobile $[Cu(H_2O)_6]^{2+}$ and $[Cu(OH)(H_2O)_5]^{+}$ adducts at low temperatures, which are detached from the zeolite lattice.[57,93] The transformation of ligated H_2O into OH^- is facilitated by the electrostatic field imposed by the framework and yields H^+ as a byproduct.[94] As a result, the two hydrated complexes exist in a pH-dependent equilibrium as indicated by eqn (3.1) and Scheme 7.[95–97]

$$[Cu(H_2O)_6]^{2+} \leftrightarrow [Cu(OH)(H_2O)_5]^{+} + H^{+} \qquad (3.1)$$

Upon raising the temperature from ambient temperature to 473–673 K in inert gas or vacuum, $[Cu(H_2O)_6]^{2+}$ and $[Cu(OH)(H_2O)_5]^{+}$ undergo dehydration and migrate to the cation exchange positions, where Cu(II) starts to interact with the O_{fw} atoms of the zeolite lattice.[19,90,92,98–104] Exchange positions featuring proximal Al T-sites in a second- (–Al–O–Si–O–Al–) or third-nearest-neighbor (NN, –Al–O–(Si–O–)$_2$Al–) arrangement, host Cu(II) as bare Cu^{2+} ions, whereas isolated Al T-sites are charge-balanced by $[CuOH]^+$ (see Sections 2.1.1 and 2.1.2).[54,57,105,106] In principle, the simple dehydration already serves as a pathway for the formation of Cu(II) active sites since paired Cu^{2+}/$[CuOH]^+$ [46,50,106,107] and $[CuOH]^+$/$[CuOH]^+$ [62,65,108–111] have been demonstrated to participate in CH_4 partial oxidation. The facile formation of Cu^{2+}/$[CuOH]^+$ as well as $[CuOH]^+$/$[CuOH]^+$ *via* dehydration of Cu(II)-aqua complexes is illustrated in Scheme 7.

The transformation of $[Cu(H_2O)_6]^{2+}$ and $[Cu(OH)(H_2O)_5]^{+}$ into framework-bound Cu(II) has been extensively investigated in different Cu–zeolites using UV-Vis spectroscopy.[15,53,98,112] In the as-prepared/hydrated state, the spectrum is dominated by a very intense signal at higher energies as well as a broad and asymmetric band at $\sim$12 500 cm^{-1}, which correspond to an

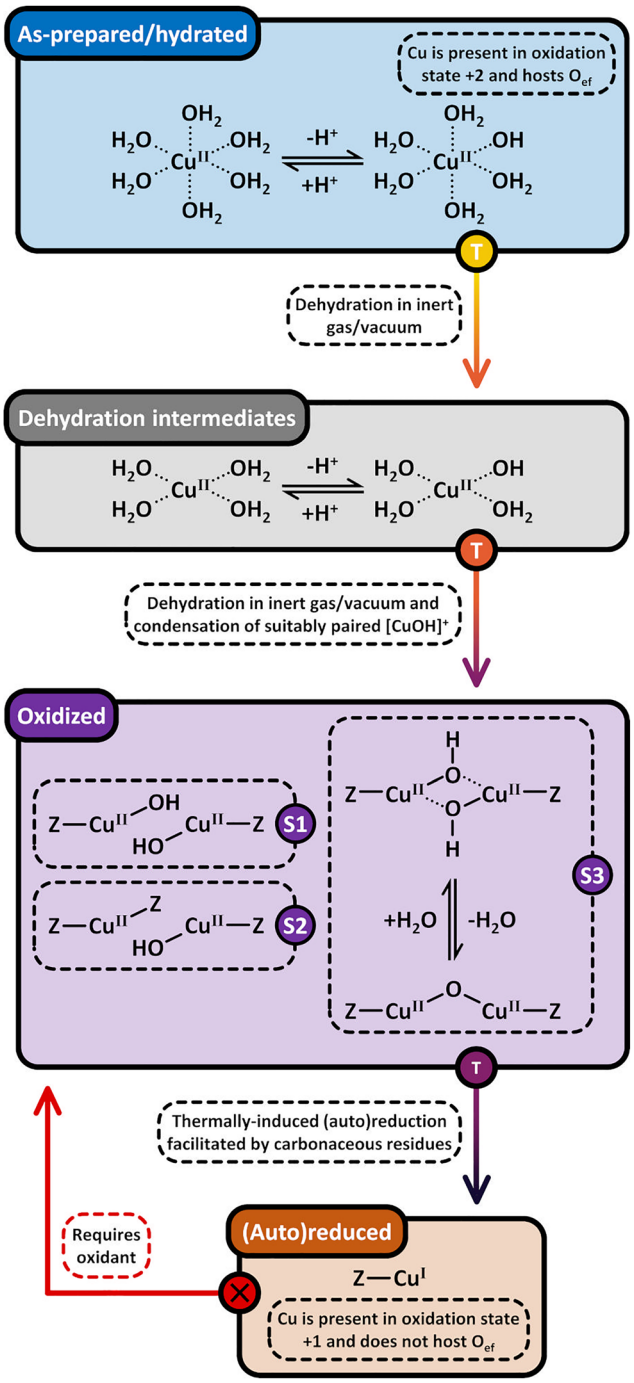

Scheme 7 Formation pathways of $[CuOH]^+$/$[CuOH]^+$ (S1), Cu^{2+}/$[CuOH]^+$ (S2), and $[Cu_2(\mu\text{-}O)]^{2+}$ (S3, violet background) *via* dehydration of $[Cu(H_2O)_6]^{2+}$ and $[Cu(OH)(H_2O)_5]^{+}$ (blue background) under inert gas or vacuum. $[Cu_2(\mu\text{-}O)]^{2+}$ potentially evolves from the intramolecular condensation of $[Cu_2(\mu\text{-}OH)_2]^{2+}$. The dehydration proceeds through $[Cu(H_2O)_4]^{2+}$ and $[Cu(OH)(H_2O)_3]^{+}$ intermediates (grey background). Upon surpassing a material specific temperature threshold, the Cu-oxo sites are subjected to (auto)reduction in inert gas and vacuum, yielding Cu(I) (brown background). The latter can only be converted into oxygenated Cu(II) species in the presence of an oxidant (starting point marked by an "X"). Dotted bonds correspond to dative interactions. The term "Z" describes the negatively charged zeolite lattice. The color gradient from yellow to violet of the different starting points and arrows indicates the progressively increasing temperature.

O_{ef} → Cu(II) ligand-to-metal charge transfer (LMCT) and unresolved d–d transitions of octahedral Cu(II)-aqua complexes, subjected to tetragonal elongation by Jahn–Teller distortion (Fig. 1a).[15,53,98,112] Depending on the specific coordination environment of Cu(II) within the exchange positions, the substitution of H_2O by O_{fw} throughout dehydration under inert gas or vacuum induces a topology-specific shift of the feature at ~12 500 cm^{-1}.[15,53,98,112] This is accompanied by an increase in the intensity of the d–d transitions due to symmetry reduction, *i.e.*, rearrangement from a quasi-octahedral to a distorted four- or three-fold coordination mode. The ligand exchange is also evident from the bathochromic shift of the LMCT transition, arising from the lower optical electronegativity of O_{fw} relative to H_2O.[53,112–115]

The insights provided by UV-Vis experiments have been further validated by X-ray absorption spectroscopy (XAS). The X-ray absorption near edge structure (XANES) spectrum of as-prepared/hydrated Cu–zeolites, collected at ambient temperature, is characterized by a smooth rising edge and an intense white line at ~8997 eV, which are characteristic of Cu(II)-aqua complexes in a distorted octahedral environment (Fig. 1b).[89,92,98–100,102,104] This is in accordance with the corresponding FT-EXAFS spectrum that displays a signal at ~1.93 Å (phase uncorrected), corresponding to a first shell Cu–O scattering path with a Cu–O coordination number (CN) of 3.5–4.9.[57,98–100,116,117] The absence of well-defined higher coordination shell peaks is indicative of the high degree of disorder and mobility of the solvated Cu(II).[57,104,116,117] The decrease of the first shell CN due to the removal of H_2O during dehydration in inert gas or vacuum is apparent from the gradual decline of the white line in the XANES spectrum and the simultaneous intensity loss of the first shell Cu–O signal in the FT-EXAFS spectrum.[19,89,98–102,104,118] This occurs alongside a bathochromic shift of the rising edge, which emerges from the change in the Cu(II) coordination environment from a six- to a four-/three-fold binding mode.[99,100,102] In addition, the rising edge becomes more structured and develops a distinct feature at ~8986 eV, originating from the dipole-allowed 1s → 4p transition of Cu(II) combined with a shakedown charge transfer from a ligand p valence orbital into the metal $3d^9$ orbital.[89,98,99,102,116,119,120] Moreover, a pre-edge signal at ~8977 eV emerges, which stems from the dipole-forbidden but quadrupole-allowed 1s → 3d transition of non-centrosymmetric Cu(II).[89,98–102,120,121] Based on multivariate curve resolution (MCR), Martini *et al.* proposed that the dehydration of $[Cu(H_2O)_6]^{2+}$ and $[Cu(OH)(H_2O)_5]^+$ into Cu^{2+} and $[CuOH]^+$ proceeds *via* $[Cu(H_2O)_4]^{2+}$ and $[Cu(OH)(H_2O)_3]^+$ intermediates.[53,102] The formation of these partially hydrated square planar complexes is in line with ^1H hyperfine sublevel correlation (HYSCORE) experiments by Bruzzese *et al.*, which indicated that the axially coordinated H_2O ligands are lost first during vacuum treatment of $Cu_{0.005}CHA_{15.4}$ from ambient temperature to 323 K.[45] The generation of these intermediates throughout the dehydration process is depicted in Scheme 7. Crucially, XANES spectroscopy demonstrates that, depending on the specific Cu–zeolite, dehydration under inert gas or vacuum at temperatures up to 473–673 K does not result in a pronounced Cu(II) (auto)reduction (*vide infra*), as evident from the absence of an intense rising edge feature at ~8983 eV, corresponding to the 1s → $4p_{x/y}$ transition of quasi-linear Cu(I).[16,19,51,89,90,92,98–104,106,122–125]

EPR spectroscopy has provided complementary insight into the dehydration process. The continuous wave (CW) X-band EPR

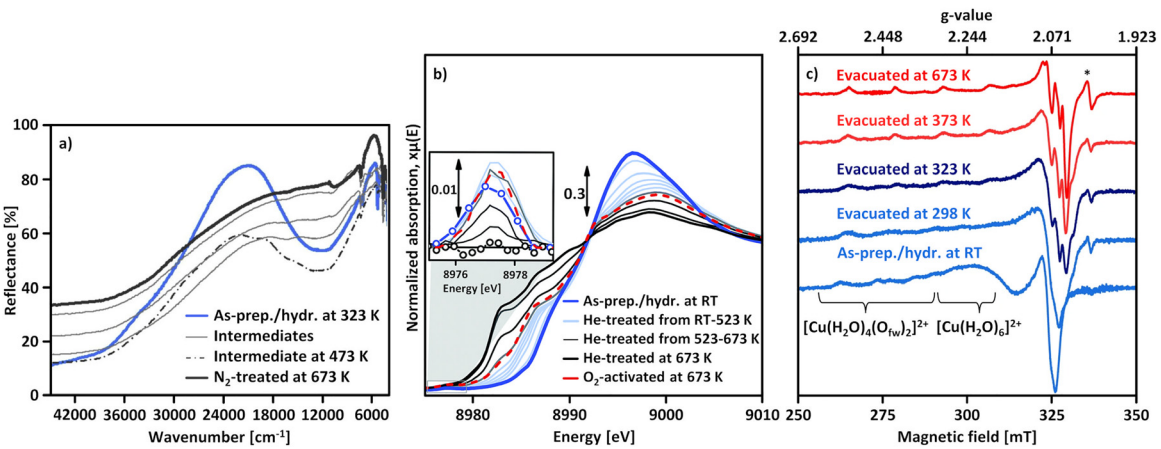

Fig. 1 UV-Vis spectra of $Cu_{0.5}CHA_{15.0}$ during interaction with N_2 at temperatures in the range from 323 to 673 K (a). The thick blue spectrum corresponds to the as-prepared/hydrated material at 323 K, whereas thin grey spectra were recorded throughout the temperature increase. The dashed black spectrum indicates the state at 473 K at which the intensity of the d–d transitions is maximized. The thick black spectrum corresponds to the N_2-treated material at 673 K. XANES spectra of $Cu_{0.4}CHA_{13.1}$ during dehydration in He from ambient temperature to 673 K (b). The thick blue spectrum corresponds to the as-prepared/hydrated material at ambient temperature, whereas thin blue and black spectra were recorded throughout the temperature increase between ambient temperature and 523 K, as well as 523 and 673 K, respectively. The thick black spectrum corresponds to the He-treated material at 673 K. The spectrum of the material after calcination at 673 K (thick dashed red) is provided for comparison. The inset in (b) depicts a magnified, background-subtracted region, where the Cu(II) pre-edge signal can be observed. CW X-band EPR spectra of $Cu_{0.005}CHA_{15.4}$ during evacuation at progressively increasing temperatures in the range from ambient temperature to 673 K (c). The spectral features of mobile $[Cu(H_2O)_6]^{2+}$ and rigid $[Cu(H_2O)_4(O_{fw})_2]^{2+}$ are indicated. The asterisk (*) corresponds to a carbon radical signal. Adapted from ref. 45, 53 and 104 with permission from Elsevier (Copyright 2019), the Royal Society of Chemistry (Copyright 2014), and the Nature Publishing Group (Copyright 2021).

spectrum of as-prepared/hydrated Cu–zeolites, collected at ambient temperature, is characterized by a broad, motion-averaged isotropic signal in the range of g = 2.14–2.17 without a resolved parallel hyperfine structure, which originates from mobile, solvated Cu(II) (Fig. 1c).[43,45,47,98,99] Interestingly, an additional anisotropic feature with a g_{II} of 2.37 and a weak hyperfine structure has been identified in the CW X-band EPR spectrum of as-prepared/hydrated $Cu_{0.005}CHA_{15.4}$, arising from a $[Cu(H_2O)_4(O_{fw})_2]^{2+}$ complex within the 8-MR (Scheme 1), which suggests that a certain fraction of Cu(II) already interacts with the zeolite lattice under these conditions.[43,45,47] The transition from mobile $[Cu(H_2O)_6]^{2+}$ and $[Cu(OH)(H_2O)_5]^{+}$ into rigid fully framework-bound Cu(II) by dehydration under inert gas or vacuum is evident from the disappearance of the motion-averaged component and the simultaneous emergence of new signals featuring resolved hyperfine interactions, whose g and A parameters depend on the Cu(II) coordination geometry, the nature of the complexing ligands (O_{fw}, OH^-), and the specific topology.[43,45,47,98,99,126] This occurs alongside a decrease in overall spectral intensity. By combining EPR and XANES spectroscopy, Palomino *et al.* and Xamena *et al.* demonstrated that this effect does not arise from a conversion of paramagnetic Cu(II) ($3d^9$, S = 1/2) into diamagnetic Cu(I) ($3d^{10}$, S = 0) *via* (auto)reduction (*vide infra*), but from the formation of EPR-silent moieties instead.[98,99] The latter have been associated with isolated $[CuOH]^+$, adopting a distorted trigonal planar coordination.[43,47,55,58,98,99] Owing to their near-degenerate ground state, these Cu(II) sites were proposed to be subjected to a pseudo Jahn–Teller effect, yielding a low-lying excited state. The EPR transition can couple to this vibration, which provides a pathway for fast energy dissipation that shortens the spin–lattice relaxation time. This results in a broadening of the spectral line shape, effectively rendering $[CuOH]^+$ EPR-invisible. However, complementary CW X-band EPR and ^{1}H HYSCORE experiments with $Cu_{0.005}CHA_{15.4}$ by Bruzzese *et al.* showed that $[CuOH]^+$ is rather present in a distorted square-planar environment and does in fact exhibit a distinct EPR signature, which is in line with results from Sushkevich *et al.* and Fischer *et al.*[46,50,58,109,127] The intensity drop can also be explained by the formation of $[Cu_2(\mu\text{-}O)]^{2+}$, which is typically not observable by EPR spectroscopy regardless of its specific electronic configuration.[43,58,98,99,128] In the S = 0 ground state, the unpaired electrons of the two Cu(II) ions are coupled antiferromagnetically, whereas in the S = 1 ground state, the large zero-field splitting of the ferromagnetically interacting electrons typically makes $[Cu_2(\mu\text{-}O)]^{2+}$ undetectable by conventional CW X-band EPR spectroscopy.[67] A noticeable exception to this are dimeric Cu(II) species in Y-type zeolites as reported by Chao *et al.*[129] The exchange positions in Y-type zeolites allow for a unique geometric arrangement, resulting in ferromagnetically coupled Cu(II) pairs with a zero field splitting of D = 0.0476 cm^{-1}, small enough to be detected at x-band frequencies.

3.2 Generation of dimeric sites *via* condensation or (auto)reduction

According to eqn (3.2), the generation of $[Cu_2(\mu\text{-}O)]^{2+}$ throughout dehydration of as-prepared/hydrated Cu–zeolites under inert gas or vacuum can proceed *via* the condensation of adjacent $[CuOH]^+$ sites, possibly *via* a $[Cu_2(\mu\text{-}OH)_2]^{2+}$ intermediate.[16,20,54,92–94,98–101,106,130–134] The equilibrium between the latter two species is controlled by the H_2O partial pressure, with $[Cu_2(\mu\text{-}O)]^{2+}$ being favored at low H_2O pressures.[54,105,135]

$$2[Cu(OH)(H_2O)_5]^+ \rightarrow 2[CuOH]^+ + 10H_2O \rightarrow [Cu_2(\mu\text{-}OH)_2]^{2+} \leftrightarrow [Cu_2(\mu\text{-}O)]^{2+} + H_2O \quad (3.2)$$

The extent of $[Cu_2(\mu\text{-}O)]^{2+}$ formation is governed by the number of $[CuOH]^+$ pairs characterized by a suitable inter-site distance to undergo condensation.[16,20,53,54,105,106,136] Upon exceeding this spatial limit, which depends on the zeolite framework, the Si/Al ratio, the distribution of Al T-sites, and the Cu loading, $[CuOH]^+$ remains as an isolated Cu(II) species. Eqn (3.2) thus provides another plausible pathway for the evolution of Cu-oxo active sites during treatment of as-prepared/hydrated Cu–zeolites under inert gas or vacuum, which could be responsible for the finite reactivity of the corresponding materials in CH_4 partial oxidation. The formation of $[Cu_2(\mu\text{-}O)]^{2+}$ *via* intramolecular condensation of $[Cu_2(\mu\text{-}OH)_2]^{2+}$ during thermal treatment of as-prepared/hydrated Cu–zeolites in inert gas or vacuum is also highlighted in Scheme 7. Evidence for the generation of $[Cu_2(\mu\text{-}O)]^{2+}$ in the absence of an oxidant has been provided by Ipek *et al.*, who compared the Raman spectrum of $Cu_{0.45}CHA_{12.0}$ following treatment in either He or O_2 at 723 K (Fig. 2a).[20] The authors observed that the spectrum recorded after dehydration in He displayed the same characteristic band at ~617 cm^{-1}, attributed to the ν(Cu–O) vibration of $[Cu_2(\mu\text{-}O)]^{2+}$, as the one collected after calcination.

Further proof was presented by Ikuno *et al.*, who monitored the evolution of the FT-EXAFS spectrum of $Cu_{0.31}MOR_{11.0}$ throughout dehydration in He in the temperature range from 323 to 723 K (Fig. 2b).[19] From 373 K onward, the authors noted an increase in the intensity of a peak at ~2.3 Å (phase uncorrected) that subsequently diminished as the temperature exceeded 573 K. This signal was correlated to the second shell Cu–Cu scattering path in $[Cu_2(\mu\text{-}O)]^{2+}$, which develops below 573 K *via* eqn (3.2) and undergoes (auto)reduction (*vide infra*) when surpassing this temperature threshold. The decline in the intensity of the Cu–Cu scattering peak during $[Cu_2(\mu\text{-}O)]^{2+}$ (auto)reduction was linked to the dispersion of Cu(I) across the framework. Notably, an elongation of the Cu–Cu distance in $[Cu_2(\mu\text{-}O)]^{2+}$ in Cu–MOR upon (auto)reduction has indeed been identified using wavelet-transform (WT) EXAFS spectroscopy.[137–139]

Above 473–673 K in inert gas or vacuum, Cu(II) is subjected to (auto)reduction as evident from the loss in absorbance of the LMCT and d–d transitions in the UV-Vis spectra (Fig. 1a),[53,98,106] the appearance of the Cu(I) rising edge signal in the XANES spectra (Fig. 1b), which develops at the expanse of the features of Cu(II),[16,19,89,98–102,104,106] and the intensity decrease of the first shell Cu–O scattering signal due to the loss of O_{ef} ligands.[16,19,90,92,98–104] As already indicated, this process is believed to involve the direct liberation of O_2 from $[Cu_2(\mu\text{-}O)]^{2+}$ (eqn (3.3)).[93,130,134] At this point, it should already be mentioned that (auto)reduction is facilitated by potentially present carbonaceous impurities (see Section 4.2.1).[101,128,140,141]

$$2[Cu_2(\mu\text{-}O)]^{2+} \rightarrow 4Cu^+ + O_2 \quad (3.3)$$

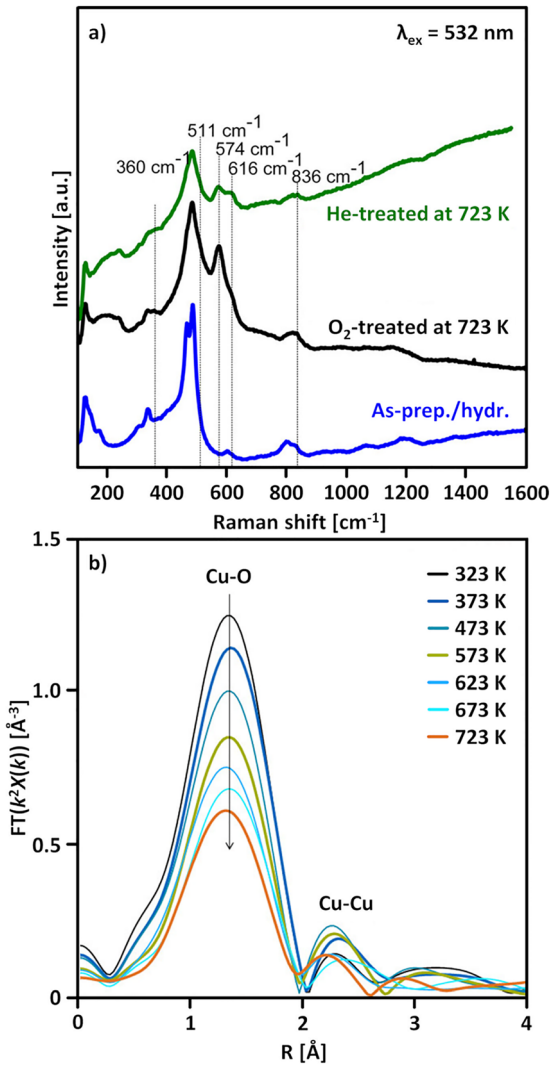

Fig. 2 Raman spectrum (λ_{ex} = 532 nm) of as-prepared/hydrated $Cu_{0.45}CHA_{12.0}$ (blue) as well as the corresponding spectra after interaction with O_2 (black) and He (green) at 723 K (a). FT-EXAFS spectra (k^2-weighted) of $Cu_{0.31}MOR_{11.0}$ during thermal treatment in He at temperatures between 323 and 723 K (b). Adapted from ref. 19 and 20 with permission from the American Chemical Society (Copyright 2017 and 2019).

The transformation of Cu-oxo species into Cu(I) *via* (auto)reduction at elevated temperatures is also illustrated in Scheme 7. The (auto)reduction of $[Cu_2(\mu\text{-}O)]^{2+}$ diminishes the concentration of oxygenated Cu(II) active sites, which may account for the generally lower CH_3OH productivity of Cu–zeolites activated in inert gas or vacuum at elevated temperatures when compared to materials activated in O_2.[16,20,22,89,92] However, considering that the mechanism depicted in eqn (3.3) requires the presence of proximal Cu(II) dimers, it is reasonable to assume that a certain fraction of isolated $[Cu_2(\mu\text{-}O)]^{2+}$ may persist.[142] Alternatively, Cu(II) (auto)reduction has also been suggested to proceed *via* $^{\bullet}OH$ loss from $[CuOH]^+$ (eqn (3.4)).[16,20,53,98–100,104,112,143,144] Interaction of the radical with a second $[CuOH]^+$ site may yield H_2O and $[CuO^{\bullet}]^+$ (eqn (3.5), Scheme S1i), which could be followed by further decomposition of paired $[CuO^{\bullet}]^+$ centers into Cu(I) and O_2 (eqn (3.6)).[9,16,20,52,53,98–100,112,145]

$$[CuOH]^+ \rightarrow Cu^+ + {}^{\bullet}OH \quad (3.4)$$

$$[CuOH]^+ + {}^{\bullet}OH \rightarrow [CuO^{\bullet}]^+ + H_2O \quad (3.5)$$

$$2[CuO^{\bullet}]^+ \rightarrow 2Cu^+ + O_2 \quad (3.6)$$

Notably, the formation of $[CuO^{\bullet}]^+$ opens up an additional pathway for the generation of dimeric Cu-oxo centers *via* recombination into *trans*/*cis* $[Cu_2(\mu\text{-}1,2\text{-}O_2)]^{2+}$ (eqn (3.7), Scheme S1j), $[Cu_2(\mu\text{-}O)_2]^{2+}$ (eqn (3.8)), or $[Cu_2(\mu\text{-}\eta^2\text{:}\eta^2\text{-}O_2)]^{2+}$ (eqn (3.8) and Scheme S1k).[16,20,106,146] The latter may subsequently convert into $[Cu_2(\mu\text{-}O)]^{2+}$ *via* O–O bond rupture (see Section 4.2.2).[16,20,22,147]

$$2[CuO^{\bullet}]^+ \rightarrow \textit{trans/cis}\ [Cu_2(\mu\text{-}1,2\text{-}O_2)]^{2+} \quad (3.7)$$

$$2[CuO^{\bullet}]^+ \rightarrow [Cu_2(\mu\text{-}O)_2]^{2+} \quad (3.8)$$

$$2[CuO^{\bullet}]^+ \rightarrow [Cu_2(\mu\text{-}\eta^2\text{:}\eta^2\text{-}O_2)]^{2+} \rightarrow [Cu_2(\mu\text{-}O)]^{2+} + 1/2O_2 \quad (3.9)$$

DFT calculations have indicated that the self-organization of $[CuO^{\bullet}]^+$ in Cu-MFI into $[Cu_2(\mu\text{-}O)_2]^{2+}$ or $[Cu_2(\mu\text{-}\eta^2\text{:}\eta^2\text{-}O_2)]^{2+}$ is a strongly exothermic reaction, which is driven by the high Lewis basicity of the O_{ef} ligands and the tendency of Cu(II) to maximize its CN.[9,52,60,146,148,149] The possibility of $[Cu_2(\textit{trans}\text{-}\mu\text{-}1,2\text{-}O_2)]^{2+}$ formation *via* $[CuO^{\bullet}]^+$ recombination is again supported by the comparative Raman study of Ipek *et al.*, which focused on the examination of $Cu_{0.45}CHA_{12.0}$ activation in either O_2 or He at 723 K.[20] Apart from the feature at ~617 cm^{-1} (*vide supra*), the spectrum of both the O_2- and He-treated material exhibited signals at ~510 and ~580 cm^{-1}, associated with the ν(Cu–O) stretching vibrations of $[Cu_2(\textit{trans}\text{-}\mu\text{-}1,2\text{-}O_2)]^{2+}$ (Fig. 2a). Hence, eqn (3.4)–(3.7) illustrate another potential reaction network for the development of oxygenated Cu(II) active sites during thermal treatment of Cu–zeolites in inert gas or vacuum. Nevertheless, the generation of O_2-bridged Cu(II) dimers *via* $[CuOH]^+$ (auto)reduction is thermodynamically not particularly favorable. For example, Wilcox *et al.* used DFT to calculate the Gibbs free energy of (auto)reduction for various oxygenated Cu(II) species in Cu–CHA at 723 K, 0.021 mbar O_2, and 0.1 mbar H_2O.[106] In most ion exchange positions, the (auto)reduction of *trans*/*cis* $[Cu_2(\mu\text{-}1,2\text{-}O_2)]^{2+}$, $[Cu_2(\mu\text{-}O)_2]^{2+}$, and $[Cu_2(\mu\text{-}\eta^2\text{:}\eta^2\text{-}O_2)]^{2+}$ was found to be considerably more exergonic compared to that of $[CuOH]^+$. Only $[Cu_2(\textit{trans}\text{-}\mu\text{-}1,2\text{-}O_2)]^{2+}$, $[Cu_2(\mu\text{-}O)_2]^{2+}$, and $[Cu_2(\mu\text{-}\eta^2\text{:}\eta^2\text{-}O_2)]^{2+}$ stabilized in an 8-MR featuring two Al T-sites positioned in a 4NN arrangement were characterized by a more endergonic (auto)reduction (by ~4–21 kJ mol^{-1}) than $[CuOH]^+$. Consequently, *trans*/*cis* $[Cu_2(\mu\text{-}1,2\text{-}O_2)]^{2+}$, $[Cu_2(\mu\text{-}O)_2]^{2+}$, and $[Cu_2(\mu\text{-}\eta^2\text{:}\eta^2\text{-}O_2)]^{2+}$ demonstrate a higher tendency to undergo (auto)reduction than $[CuOH]^+$, calling the formation of the former by (auto)reduction of the latter into question. Moreover, the existence of $[CuO^{\bullet}]^+$ has yet to be experimentally verified.[16,20,101,106,131,150] This is complemented by the fact that the formation of this Cu(II) site, although under oxidative conditions, has been deemed unfavorable in both the 8- and 6-MR of Cu–CHA at any temperature in the range from 323 to 723 K at 0.2–0.95 bar O_2 and 0.02–0.05 bar H_2O.[57,107]

In this context, it is also important to note that the assignment of the bands at ~510 and ~580 cm^{-1} by Ipek *et al.* has recently been revised by Rhoda *et al.*, who correlated them to the vibration of a T-site ligand and the ν_{sym}(Cu–O) stretch of a different $[Cu_2(\mu\text{-}O)]^{2+}$ center, casting further doubt on the relevance of eqn (3.7).

Based on the preceding discussion, it can be concluded that the thermal treatment of as-prepared/hydrated Cu–zeolites under inert gas or vacuum is sufficient to induce the generation of Cu-oxo active sites as Cu is already present in the oxidation state +2 and bares reactive O_{ef} in the form of OH^- ligands.[93,130] As illustrated in Scheme 7, the oxygenated Cu(II) active sites can manifest as paired Cu^{2+}/$[CuOH]^+$ and $[CuOH]^+$/$[CuOH]^+$, formed *via* simple dehydration of the corresponding Cu(II)-aqua complexes, or as $[Cu_2(\mu\text{-}O)]^{2+}$, arising from the condensation of neighboring $[CuOH]^+$. At elevated temperatures, $[Cu_2(\mu\text{-}O)]^{2+}$ and $[CuOH]^+$ are subjected to (auto)reduction, which decreases the CH_3OH productivity of materials thermally treated in inert gas or vacuum compared to those activated in the presence of an oxidant. Crucially, the development of Cu(II) active sites in inert gas or vacuum is only feasible in as-prepared/hydrated samples, indicating that an oxidative activation is required if the Cu–zeolite is in an (auto)reduced state. As a final note of caution, the CH_3OH productivity of materials, thermally treated under inert gas or vacuum, may be artificially inflated by the presence of O_2 impurities.[90] Nevertheless, since the extent of O_2 contamination is usually undefined, it is challenging to assess the impact of residual O_2 traces on the CH_3OH output of these samples.

4. Utilization of O_2 for the formation of active Cu(II) sites in chemical looping and continuous CH_4 partial oxidation

4.1 Changing the multiplicity of O_2 by reductive activation with Cu(I)

Conceptually, the transformation of CH_4 and O_2 into CH_3OH is a spin-forbidden process.[9,81,151–154] This arises from the fact that CH_4 and CH_3OH are both characterized by a closed-shell singlet (S = 0) electronic structure, whereas O_2 is a diradical featuring a triplet (S = 1) ground state. As a result, the spin states of the reactants ($|S_{CH_4} \pm S_{O_2}|$) and product ($|S_{CH_3OH}|$) do not have a common term, rendering this reaction spin-forbidden according to Wigner's selection rule. Therefore, direct CH_4 hydroxylation formally requires a change in the multiplicity of O_2 *via* its transformation into reactive $^{\bullet}O_2^-$, O_2^{2-}, or O^{2-} species upon interaction with a metal center. In the case of Cu-exchanged zeolites, the reductive activation of O_2 involves the oxidation of Cu(I) into Cu(II), which represents a transition from a diamagnetic $3d^{10}$ into a paramagnetic $3d^9$ configuration.[93] The possible ground states of the formed Cu-oxo sites are governed by their chemical formula and spin orientations. End-on/side-on $[Cu(\eta\text{-}O_2^{\bullet})]^+$ (Schemes S1l and m),[155] $[Cu_2(\mu\text{-}O)]^{2+}$,[66,74,90,156–159] *trans*/*cis* $[Cu_2(\mu\text{-}1,2\text{-}O_2)]^{2+}$[70] as well as $[Cu_2(\mu\text{-}\eta^2\text{:}\eta^2\text{-}O_2)]^{2+}$[70,156,160] can adopt either a triplet or open-shell singlet state, whereas $[Cu_3(\mu\text{-}O)_3]^{2+}$ may exist in either a doublet, quartet, or sextet state.[73,74,158,159,161] Isolated Cu^{2+} and $[CuOH]^+$ are exclusively present in the doublet state.[56,62,107] However, since these species can participate in CH_4 conversion only in the presence of a second proximal Cu(II) center (*e.g.*, in $[CuOH]^+$/$[CuOH]^+$[62,65,109–111,162] and Cu^{2+}/$[CuOH]^+$ pairs[46,50,56,106,107]), the total spin state of these active sites effectively corresponds to either a triplet or an open-shell singlet.[56,62] In contrast to their high-spin counterparts, CH_4 partial oxidation *via* dimeric Cu-oxo species in the singlet state and trimeric oxygenated Cu(II) centers in the doublet state is not accompanied by a spin inversion and hence does not violate Wigner's selection rule.[74,150,157–159,163] For example, multiple theoretical studies have demonstrated that CH_4 hydroxylation on triplet $[Cu_2(\mu\text{-}O)]^{2+}$ proceeds *via* a spin flip at the radical rebound step in the homolytic C–H bond activation mechanism (Scheme 6), whereas no such transition is required in the case of singlet $[Cu_2(\mu\text{-}O)]^{2+}$.[157,158,164] Consequently, the reductive activation of O_2 by Cu(I) and the transformation of the latter into a reactive Cu-oxo site with a suitable ground state are essential to facilitate the oxo-functionalization of CH_4.[9,81,151,153,163,165] Notably, Mahyuddin *et al.* determined that the different spin states of $[Cu_2(\mu\text{-}O)]^{2+}$ and $[Cu_3(\mu\text{-}O)_3]^{2+}$ are essentially isoenergetic.[154,157–159] Depending on the zeolite framework, the singlet–triplet splitting of $[Cu_2(\mu\text{-}O)]^{2+}$ in Cu-exchanged AEI, AFX, CHA, MFI, MOR, and mazzite (MAZ) was found to amount to just 0.8–5.0 kJ mol^{-1}.[157,158] Likewise, the energetic difference between the quartet and doublet state of $[Cu_3(\mu\text{-}O)_3]^{2+}$ in Cu–MOR and Cu-MAZ is only 3.3–7.9 kJ mol^{-1}.[158] Theoretical studies by various other authors resulted in similarly small splittings between the high- and low-spin state of various Cu-oxo motifs in different Cu–zeolites.[66,70,73,74,155] As a result, the formation of high-spin Cu-oxo species, whose participation in CH_4 partial oxidation necessitates a spin crossover, is thermodynamically as feasible as the generation of their low-spin counterparts. In fact, the former have been reported to be even more active due to a higher spin density at the O_{ef} ligand, which increases their reactivity in the H atom abstraction (HAA).[67,73,74,95,107,157–159,161,166,167] Nevertheless, the magnitude of the energetic difference between distinct spin states is strongly affected by the chosen computational method and functional, as well as the location and geometry of the Cu(II) model structure.[70,106,155,159,161,164,168] For the sake of completeness, Heyer *et al.* combined variable-temperature, variable-field magnetic circular dichroism (VTVHMCD) spectroscopy and DFT calculations to show that the ground state of $[Cu_2(\mu\text{-}O)]^{2+}$ is governed by the relative orientation of the planes of the bidentate coordinating Al T-sites, which, in turn, depends on the specific zeolite framework (see Section 2.1.3).[67] Thus, $[Cu_2(\mu\text{-}O)]^{2+}$ hosted in Cu-MFI adopts a singlet state due to the parallel arrangement of the bidentate coordinating Al T-sites, which maximizes the superexchange interaction between the two half-filled Cu(II) 3d orbitals. On the contrary, this interaction is minimized in the case of $[Cu_2(\mu\text{-}O)]^{2+}$ in Cu–CHA owing to the perpendicular orientation of the planes of the chelating framework ligands, which results in a triplet ground state.

4.2 Formation of Cu(II) sites using O_2 during non-isothermal looping

As outlined in Section 2.3 and Scheme 6, the activation of Cu–zeolites for CH_4 partial oxidation *via* non-isothermal looping is initiated by a heating ramp to a specific temperature, followed by a dwell period for a certain duration and a subsequent cool down (ideally in the presence of the oxidant) to a set temperature for CH_4 hydroxylation.[7,72,133,144] After CH_3OH extraction, this procedure must be repeated to reactivate the material for the next reaction sequence. In the following sections, the available literature concerning each of the above mentioned periods will be reviewed, aiming to reconstruct the formation mechanism of different Cu(II) sites and to elucidate the impact of activation conditions on Cu speciation and material performance in CH_4 hydroxylation. The behavior of Cu–zeolites in successive redox cycles is also addressed to assess the regenerability of the Cu(II) active centers.

4.2.1 Cu(II) structural evolution and (auto)reduction during the heating ramp – the impact of carbonaceous impurities. Similar to the processes described in Section 3, the treatment of as-prepared/hydrated Cu–zeolites in flowing O_2 during the initial heating ramp is coupled to the transformation of mobile $[Cu(H_2O)_6]^{2+}$ and $[Cu(OH)(H_2O)_5]^{+}$ complexes into framework-coordinated Cu^{2+} and $[CuOH]^{+}$ as indicated by the analogous changes in the UV-Vis,[15,20,21,53] XANES,[19,89,92,100,101,104,116,118,139,169–174] FT-EXAFS,[19,100,104,175] and EPR spectra.[43,45,112] This is also accompanied by the condensation of proximal $[CuOH]^{+}$ into $[Cu_2(\mu\text{-}O)]^{2+}$ *via* $[Cu_2(\mu\text{-}OH)_2]^{2+}$ (eqn (3.2)).[20,22,54,93,105,106] The development of these oxygenated Cu(II) centers throughout the progressive dehydration in O_2 is outlined in Scheme 8.

Surprisingly, multiple studies have indicated that Cu(II) may still undergo (auto)reduction during thermal treatment in O_2 despite the presence of an oxidant.[21,51,103,127,132,174,176] Andersen *et al.*, for example, analyzed the evolution of the XANES spectra of $Cu_{0.48}CHA_{15.1}$ during dehydration in O_2 by linear combination fitting (LCF) and observed a decrease in the Cu(II) fraction by 37% upon raising the temperature from 683 to 773 K.[103] Notably, the Cu(II) fraction did not recover when the material was kept in O_2 at 773 K for ~27 min, suggesting that the Cu(II) reduction did not originate from the oxidative decomposition of carbonaceous impurities (*vide infra*) but rather from a thermally driven change in the Cu(II)/Cu(I) equilibrium. Andersen *et al.* attributed this effect to the (auto)reduction of $[CuOH]^{+}$ *via* $^{\bullet}OH$ loss as depicted in eqn (3.4). Nevertheless, this process does not necessarily need to be limited to $[CuOH]^{+}$. Several theoretical studies have highlighted that the conversion of Cu(I) and O_2 into various mono- and multimeric oxygenated Cu(II) centers is strongly exothermic.[155,156,164,177–180] For instance, DFT calculations by Mahyuddin *et al.* revealed that the oxidation of two Cu(I) pairs, each situated in one of the opposing 8-MRs of the side pocket in Cu–MOR (Scheme 1), into two $[Cu_2(\mu\text{-}O)]^{2+}$ moieties is characterized by a reaction enthalpy of about −463 kJ mol^{-1}.[179] Consequently, the reverse process, *i.e.*, the transformation of Cu(II) into Cu(I) *via* O_{ef} loss, is thermodynamically favorable at elevated temperatures, shifting the reaction equilibrium toward (auto)reduction.[19,21] This correlation is supported by work from Brenig *et al.* focused on the generation of Cu(II) active sites in reduced Cu–$MOR_{10.0}$, Cu-$MFI_{11.5}$, and Cu–$CHA_{11.0}$.[127] After activating the materials in O_2 at 753 K, these authors noted a progressive increase in the intensity of UV-Vis features between 27 300–26 400 and 2200–21 800 cm^{-1}, corresponding to the LMCT transition of two different classes of $[Cu_2(\mu\text{-}O)]^{2+}$, during a cool down to 313 K in the presence of the oxidant. This clearly highlights that the formation of these dimeric Cu-oxo species is preferred at lower temperatures, whereas they are subjected to a reversible (auto)reduction at elevated temperatures. Additional evidence for this was provided by an LCF analysis of the XANES spectra recorded during temperature-programmed oxidation (TPO) of the three reduced samples with O_2, which unveiled that the Cu(II) fraction first reaches a framework-dependent maximum at a certain temperature and then declines upon further raising the temperature. An analogy to this behavior is the redox equilibrium between Cu_2O and CuO (eqn (4.1)), which shifts toward the former upon increasing the temperature.[181–184]

$$2Cu_2O + O_2 \leftrightarrow 4CuO \qquad (4.1)$$

This can be rationalized when considering the standard enthalpy and entropy of the oxidation (forward) reaction, which amount to approximately −283 kJ mol^{-1} and −219 J mol^{-1} K^{-1}.[185–187] Despite its exothermic nature, the reaction becomes progressively

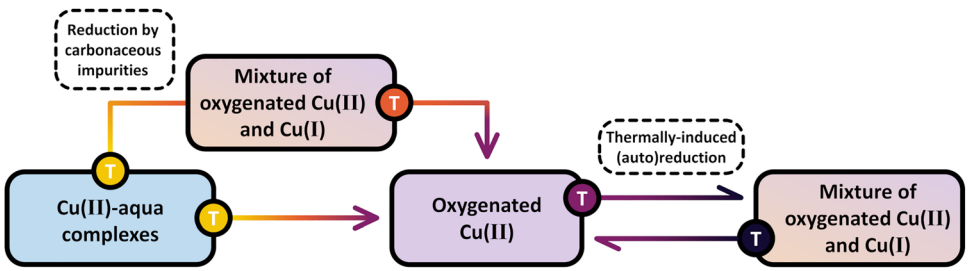

Scheme 8 Evolution of Cu(II) species during treatment of as-prepared/hydrated Cu–zeolites (blue background) in O_2 at progressively increasing temperatures. In the presence of carbonaceous impurities, calcination leads to the momentary reduction of a fraction of Cu(II) centers to Cu(I) (brown/violet background). Upon further increasing the temperature, Cu(I) is re-oxidized, and the material predominantly contains oxygenated Cu(II) species (violet background). This state is directly reached in the absence of carbonaceous impurities. At even higher temperatures, the Cu-oxo centers are subjected to a reversible temperature-controlled (auto)reduction in O_2. The color gradient from yellow to violet of the different starting points and arrows indicates the progressively increasing temperature.

endergonic at elevated temperatures due to the negative entropic term. Consequently, the sign of the Gibbs free energy turns positive above ~1292 K, and the equilibrium and rate constant of the oxidation reaction steadily diminish. Notably, this is also reflected by the change in the sign of the activation energy, which has been demonstrated to become negative after surpassing a certain temperature threshold.[181,184,188] While this example serves as a useful illustration, it is important to keep in mind that the redox behavior of crystalline bulk oxides is not representative of that of Cu centers stabilized within zeolites, as neither the involved chemical species nor the applied conditions are comparable.[189] Moreover, the Cu_2O/CuO system does not capture any characteristic enthalpic or entropic (de)stabilization effects arising in Cu-exchanged zeolites. As a result, the thermodynamic considerations presented above cannot directly be transferred to the (auto)reduction of oxygenated Cu(II) sites in O_2 at high temperatures. Therefore, an in-depth investigation of this effect by combining experimental and theoretical studies is essential to determine its thermodynamic driving forces. The relationship between the Cu(II)/Cu(I) equilibrium and the calcination temperature is outlined in Scheme 8.

A similar yet distinct phenomenon has been reported by Kvande *et al.* and Borfecchia *et al.*, who tracked the evolution of the XANES spectra of Cu–MOR and Cu–CHA during dehydration from ambient temperature to 773 K in O_2.[139,175] Apart from the gradual loss of the white line intensity and the emergence of the rising and pre-edge feature of Cu(II), the authors observed a progressive development of the rising edge signal of Cu(I) upon increasing the temperature from ambient temperature to 623–653 K. Notably, the absorbance of the Cu(I) feature decreased again when further raising the temperature and completely vanished at 773 K. The same behavior, although in a different temperature regime, has been detected in the XANES spectra of $Cu_{0.2}FER_{11.0}$ collected during activation in O_2 (Fig. 3a).[169]

This transient Cu(II) reduction was interpreted based on the FTIR spectra of $Cu_{0.53}CHA_{14.8}$ recorded during dehydration from 303 to 673 K in flowing O_2, which exhibited a continuous intensity loss of a feature at ~3650 cm^{-1}, assigned to the ν(O-H) stretching vibration of $[CuOH]^+$ (Fig. 3b).[15,16,53,57,104,112,130,174,190] Based on the apparent decomposition of $[CuOH]^+$ at elevated temperatures in O_2, the temporary appearance of the Cu(I) signal in the XANES spectra was associated with the (auto)reduction of $[CuOH]^+$ into Cu(I) *via* eqn (3.4).[16,118,175,191] The subsequent diminution of this feature above 623–653 K was attributed to the re-oxidation of Cu(I) by O_2, yielding $[Cu(\eta^1\text{-}O_2^{\bullet})]^+$ (eqn (4.1)) or $[Cu_2(trans\text{-}\mu\text{-}1,2\text{-}O_2)]^{2+}$ (eqn (4.2)). Consequently, $[CuOH]^+$ was envisioned as a precursor for the formation of mono- and dimeric Cu-oxo sites *via* its (auto)reduction into Cu(I). The tricoordinate $[Cu(\eta^1\text{-}O_2^{\bullet})]^+$ and $[Cu_2(trans\text{-}\mu\text{-}1,2\text{-}O_2)]^{2+}$ were suggested to undergo a thermally-induced rearrangement into four-fold coordinated $[Cu(\eta^2\text{-}O_2^{\bullet})]^+$ and $[Cu_2(\mu\text{-}\eta^2\text{:}\eta^2\text{-}O_2)]^{2+}$ during a cool down in O_2 (see Section 4.2.5).[16,172,175,192]

$$Cu^+ + O_2 \rightarrow [Cu(\eta^1\text{-}O_2^{\bullet})]^+ \quad (4.2)$$

$$2Cu^+ + O_2 \rightarrow [Cu_2(trans\text{-}\mu\text{-}1,2\text{-}O_2)]^{2+} \quad (4.3)$$

Evidence for the formation of $[Cu(\eta^1\text{-}O_2^{\bullet})]^+$ and $[Cu_2(trans\text{-}\mu\text{-}1,2\text{-}O_2)]^{2+}$ was provided by the Raman spectrum of calcined $Cu_{0.53}CHA_{14.8}$, which exhibited bands centered in the 1155–1100 cm^{-1} range, along with distinct features at ~580 and ~510 cm^{-1}.[16,53,193] The higher-energy signals were associated with the ν(O–O) vibration of end-on/side-on $[Cu(\eta\text{-}O_2^{\bullet})]^+$, whereas the latter two bands were attributed to the ν(Cu–O) stretching vibrations of $[Cu_2(trans\text{-}\mu\text{-}1,2\text{-}O_2)]^{2+}$.[16,20,53,193] However, as already mentioned in Section 3.2, a different interpretation concerning the origin of the signals at ~580 and ~510 cm^{-1} has been presented by Rhoda *et al.*[194] These authors also suggested that the features at 1155 and 1100 cm^{-1} originate from the first ν_{sym}(Cu–O) overtone

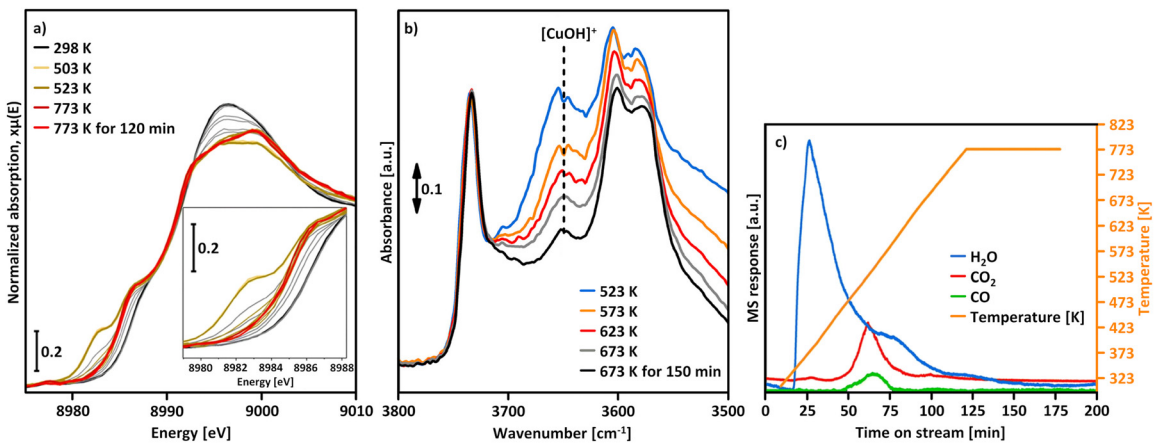

Fig. 3 Cu K-edge XANES spectra of $Cu_{0.2}FER_{11.0}$ during activation in O_2 at temperatures between 298 and 773 K, as well as after 120 min at 773 K (a). The inset in (a) shows a magnification of the spectral region where the transient appearance of the Cu(I) signal can be observed. MS response (left axis) during interaction with O_2 as well as the temperature profile (right axis); the masses corresponding to H_2O (m/z = 18), CO_2 (m/z = 44), and CO (m/z = 28) were followed during the experiment (b). FTIR spectra of the ν(O–H) region of $Cu_{0.53}CHA_{14.8}$ during treatment in O_2 in the 523–673 K range, as well as after 150 min at 673 K (c). The dotted line highlights the progressive decrease in intensity of the band at ~3650 cm^{-1} corresponding to $[CuOH]^+$. Adapted from ref. 16 and 169 with permission from Springer Nature Link (Copyright 2019) and the American Chemical Society (Copyright 2017).

vibration of $[Cu_2(\mu\text{-}O)]^{2+}$ and the combination mode of the ν_{sym}(Cu–O) stretch of this Cu(II) dimer and a vibration of a T-site ligand. Additionally, it is worth mentioning that the materials explored by Kvande *et al.* and Borfecchia *et al.* were not pre-calcined prior to their investigation by XAS.[139,175] This is important as multiple authors have demonstrated that Cu–zeolites can contain carbonaceous impurities capable of reducing Cu(II) at elevated temperatures.[101,128,140,141] For instance, Sushkevich *et al.* employed XANES spectroscopy to compare the temperature onset of excessive Cu(I) generation in as-prepared/hydrated and pre-calcined $Cu_{0.39}MOR_{10.0}$ during treatment in He from 300 to 1100 K.[101] LCF analysis of the recorded spectra revealed a pronounced increase in the fraction of Cu(I) already at ~495 K in the as-prepared/hydrated material, whereas a temperature above ~650 K was necessary to induce a noticeable decrease in the amount of Cu(II) in the pre-calcined sample. Complementary temperature-programmed desorption (TPD) experiments highlighted that considerable amounts of CO_2 were released throughout thermal treatment of the as-prepared/hydrated Cu–zeolite, emphasizing that the facile Cu(I) formation was not related to thermally-induced (auto)reduction of Cu(II), but to its reduction by carbonaceous deposits. Therefore, it is reasonable to assume that the transient appearance of the Cu(I) rising edge feature in the XANES spectra collected by Kvande *et al.* and Borfecchia *et al.* originated from the momentary reduction of Cu(II) by carbonaceous impurities rather than the (auto)reduction of $[CuOH]^+$. This hypothesis is further supported by Pappas *et al.*, who coupled the analysis of the dehydration of $Cu_{0.2}FER_{11.0}$ in flowing O_2 by XANES spectroscopy to online mass spectrometry (MS).[169] The authors noted the development of CO_2 and CO in the same temperature regime in which the temporary Cu(II) reduction took place, highlighting that this phenomenon does not arise from the $^{\bullet}OH$ loss from $[CuOH]^+$ (Fig. 3c). Instead of $[CuOH]^+$ (auto)-reduction *via* eqn (3.4), the frequently observed decrease in the intensity of the FTIR band at ~3650 cm^{-1} throughout activation could derive from $[CuOH]^+$ condensation *via* eqn (3.2).

Scheme 8 highlights the differences between the reduction of Cu(II) by carbonaceous residues and the thermally-induced (auto)reduction of Cu(II) during calcination of Cu–zeolites at progressively increasing temperatures.

4.2.2 Influence of activation temperature on Cu(II) active site formation. Most studies have reported an almost linear relationship between CH_3OH productivity and activation temperature.[13–16,18,19] For example, Park *et al.* investigated the performance of Cu–MOR and Cu-MEI in CH_4 partial oxidation after treatment with O_2 at different temperatures and observed that, depending on the specific sample, the CH_3OH output more than doubled (on a $mmol_{CH_3OH}$ mol_{Cu}^{-1} basis) upon increasing the calcination temperature from 623 to 823 K.[14] Pappas *et al.* described a similar effect of the activation temperature on the CH_3OH productivity of $Cu_{0.49}CHA_{12.1}$.[16] A notable exception to this general trend are Cu–zeolites exhibiting a high Cu loading ($\geq$6 wt%), whose performance in CH_4 hydroxylation exhibits a volcano-type dependence on the O_2 treatment temperature.[14] This was attributed to a temperature-induced aggregation of Cu into inactive clusters in materials featuring a high Cu content. Interestingly, a similar behavior has been reported for $Cu_{0.2}FER_{11.0}$, featuring a Cu loading of just ~1.9 wt%, suggesting that thermally driven clustering of Cu could also be affected by the zeolite framework.[89] Kim *et al.* also noted a bell-shaped correlation between the CH_3OH output of $Cu_{0.4}MOR_{20.0}$, featuring a Cu content of ~2.0 wt%, and the calcination temperature.[21] They argued that elevated temperatures are necessary to convert an ill-defined O_2-bridged intermediate into $[Cu_3(\mu\text{-}O)_3]^{2+}$. As the formation of this intermediate is exothermic, it undergoes O_2 loss upon exceeding the optimal activation temperature of 723 K, resulting in a reduced CH_3OH productivity. Nevertheless, the reversibility of this process in the CH_4 partial oxidation experiments was not taken into account (see Section 4.2.5).

The origin of the beneficial impact of elevated activation temperatures on the CH_3OH productivity was explored by Smeets *et al.* and Groothaert *et al.*, who studied the development of the LMCT transition of $[Cu_2(\mu\text{-}O)]^{2+}$ at ~22 700 cm^{-1} in as-prepared/hydrated Cu-MFI as a function of the calcination temperature by UV-Vis spectroscopy.[133,136] Starting from ~623 K, the intensity of this characteristic band progressively increased upon raising the temperature and reached a maximum at about 923 K (Fig. 4a). Notably, the absorbance of this feature started to decrease again upon further increasing the temperature to 1023 K. The loss in signal intensity could not be reversed during a subsequent O_2 treatment at 723 K and was thus attributed to an irreversible decomposition of $[Cu_2(\mu\text{-}O)]^{2+}$.

Oord *et al.* observed a similar enhancement in the intensity of a band at 29 000 cm^{-1} in the UV-Vis spectrum of $Cu\text{–}CHA_{20.0}$, attributed to a not precisely defined dimeric Cu-oxo active site, when raising the O_2 treatment temperature from 723 to 823 K.[15] The necessity of high activation temperatures has also been highlighted by Wijerathne *et al.*, who combined DFT calculations and Monte Carlo (MC) simulations to reveal that the transformation of the $[Cu_2(\mu\text{-}OH)_2]^{2+}$ intermediate into $[Cu_2(\mu\text{-}O)]^{2+}$ in Cu–CHA and Cu–MOR, characterized by a random Al T-site arrangement, only takes place above ~730 K at 1×10^{-5} mbar H_2O and 200 mbar O_2 (H_2O/O_2 ratio: 5×10^{-8}).[105] This is in qualitative agreement with theoretically predicted phase diagrams from Hutton *et al.*, indicating that $[Cu_2(\mu\text{-}O)]^{2+}$ becomes thermodynamically more stable than $[Cu_2(\mu\text{-}OH)_2]^{2+}$ above ~680 K at the same H_2O/O_2 ratio in Cu–CHA, featuring a distinct Al T-site distribution.[135] In contrast, a computationally derived phase diagram from Li *et al.* suggested that the conversion of $[Cu_2(\mu\text{-}OH)_2]^{2+}$ into $[Cu_2(\mu\text{-}O)]^{2+}$ in Cu–CHA occurs already above 280 K, at the same H_2O-to-O_2 ratio.[54] Using DFT, Suleiman *et al.* determined the minimal activation temperature required for the generation of $[Cu_2(\mu\text{-}O)]^{2+}$, $[Cu_2(\mu\text{-}O)_2]^{2+}$, $[Cu_2(\mu\text{-}\eta^2\text{:}\eta^2\text{-}O_2)]^{2+}$, and $[Cu_3(\mu\text{-}O)_3]^{2+}$ in the 8-MR of as-prepared/hydrated Cu–MOR featuring H^+ as co-cations.[167] Depending on the specific Cu-oxo center, the temperature at which the Gibbs free energy of formation starts to become negative amounted to 618–733 K, demonstrating once again that elevated temperatures are necessary to remove H_2O ligands from the Cu(II)-aqua complexes and to induce their aggregation into multimeric oxygenated Cu(II) species. Complete dehydration of the material is particularly important as the strongly hydrophilic Cu-oxo

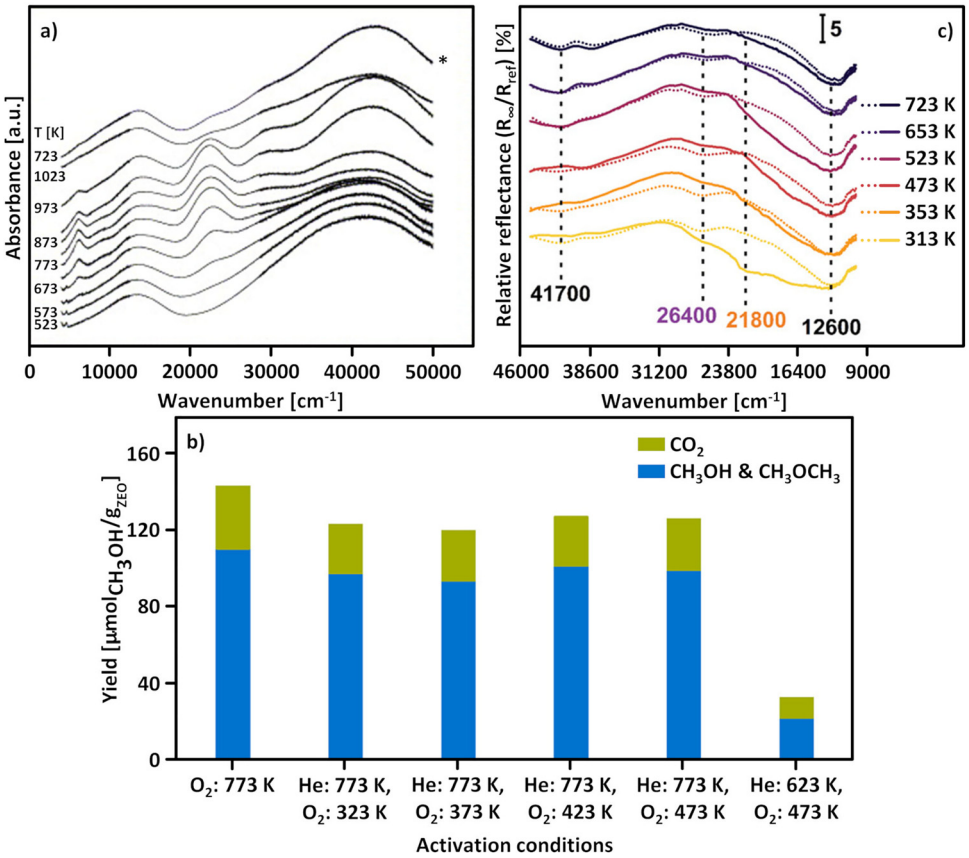

Fig. 4 UV-Vis spectra of as-prepared/hydrated $Cu_{0.54}MFI_{12.0}$ recorded at ambient temperature after calcination in O_2 at different temperatures ranging from 523 to 1023 K. The spectrum marked by an asterisk (*) corresponds to the spectrum collected after activation in O_2 at 1023 K, followed by interaction with O_2 at 723 K (a). Total productivity of $Cu_{0.31}MOR_{11.0}$ in CH_4 partial oxidation after activation in O_2 at 773 K and after treatment in He at 773 or 623 K, followed by interaction with O_2 at various temperatures ranging from 323 to 473 K (b). UV-Vis spectra of Cu–$MOR_{10.0}$ after activation (dotted lines, recorded in O_2) and reactivation (solid lines, recorded in O_2) at temperatures in the range from 313 to 723 K. The characteristic LMCT transitions of the two different $[Cu_2(\mu\text{-}O)]^{2+}$ motifs are highlighted in purple and orange (c). Adapted from ref. 19, 127 and 136 with permission from Elsevier (Copyright 2005), the American Chemical Society (Copyright 2019), and Wiley (Copyright 2025).

species readily adsorb H_2O, which saturates the coordination sphere of the Cu(II) active sites, rendering them inaccessible for CH_4 and effectively poisoning them.[100,101,171–173] The gravity of H_2O-induced passivation has been emphasized by Sushkevich *et al.*, who combined FTIR spectroscopy and NO probe molecule adsorption to determine that the interaction of a single H_2O molecule with $[Cu_2(\mu\text{-}O)]^{2+}$ and $[CuOH]^+/[CuOH]^+$ is sufficient to completely deactivate these species at low CH_4 pressures.[101] Scheme 9 highlights the necessity of high activation temperatures for the generation of various Cu-oxo sites throughout the treatment of as-prepared/hydrate Cu–zeolites with O_2.

Based on the results presented above, elevated calcination temperatures are essential for promoting the generation of di- and trimeric Cu(II) active sites in as-prepared/hydrated Cu–zeolites, which, in turn, results in an optimized performance in CH_4 partial oxidation. However, this correlation may not necessarily apply to the formation of these species in (auto)reduced materials, as the activation of as-prepared/hydrated and (auto)reduced samples involves a fundamentally different series of elementary steps. In the former case, Cu is already present in the oxidation state +2 and the generation of mono-/multimeric oxygenated Cu(II) centers proceeds *via* dehydration of Cu(II)-aqua complexes and $[CuOH]^+$ condensation (eqn (3.2)). In contrast, oxygenated Cu(II) centers in (auto)reduced Cu–zeolites develop *via* an actual oxidation of Cu(I) into Cu(II) in the presence of O_2. Ikuno *et al.* emphasized this distinction by decoupling the oxidative formation of Cu-oxo species from other thermally driven processes, such as dehydration and (auto)reduction (Fig. 4b).[19] They determined that the CH_3OH output of $Cu_{0.31}MOR_{11.0}$, initially (auto)reduced in He at 773 K and subsequently exposed to O_2 at temperatures ranging from 323 to 473 K, was comparable to that of the material directly calcined in O_2 at 773 K. Conversely, a decrease in the temperature of the initial He treatment to 623 K followed by interaction with O_2 at 473 K resulted in a substantial reduction of the CH_3OH productivity. The authors rationalized this behavior by arguing that the initial thermal treatment in He promotes the formation of $[CuOH]^+$ and $[Cu_2(\mu\text{-}O)]^{2+}$ (eqn (3.2)), which are subsequently (auto)reduced *via* eqn (3.3) and (3.4), yielding Cu(I) and $^\bullet$OH. Due to the weaker electrostatic interaction between Cu(I) and the zeolite lattice, the former is capable of dynamically reorganizing into a reduced precursor

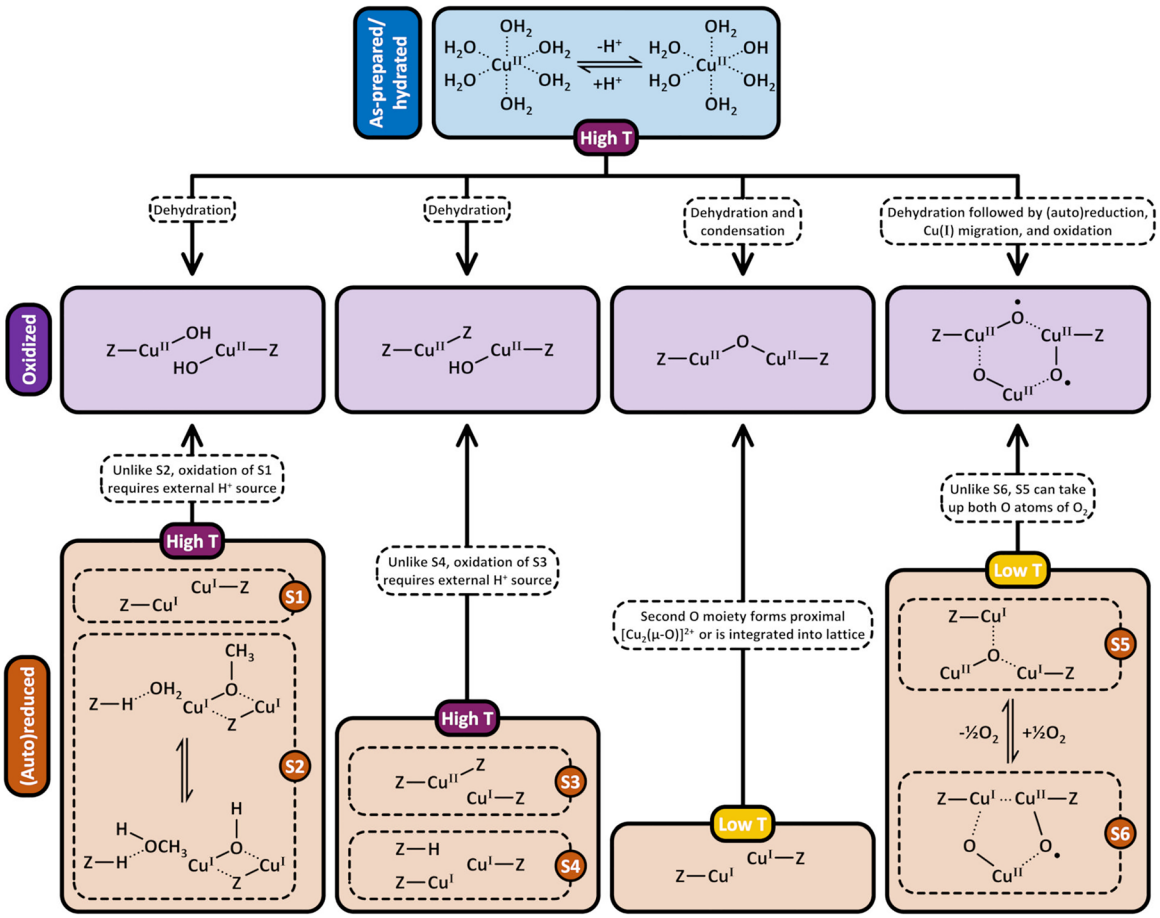

Scheme 9 Formation pathways of $[CuOH]^+/[CuOH]^+$, $Cu^{2+}/[CuOH]^+$, $[Cu_2(\mu\text{-}O)]^{2+}$, and $[Cu_3(\mu\text{-}O)_3]^{2+}$ (violet background) by treatment of as-prepared/hydrated (blue background) and (auto)reduced (brown background) Cu–zeolites with O_2. After (auto)reduction of $[CuOH]^+/[CuOH]^+$, this site may exist either as two plain Cu(I) ions (S1) or as a BAS containing site (S2). This distinction is important as, unlike in the case of S2, the generation of $[CuOH]^+/[CuOH]^+$ from S1 necessitates an external H^+ source. Similarly, the transformation of Cu^{2+}/Cu^+ (S3) into $Cu^{2+}/[CuOH]^+$ requires an additional H^+ source, which is not necessary when starting from $2Cu^+$/BAS (S4). Unlike the reaction of $[Cu_3(\mu\text{-}O)_2]^{2+}$ (S6) with O_2, the formation of $[Cu_3(\mu\text{-}O)_3]^{2+}$ *via* interaction of $[Cu_3(\mu\text{-}O)]^{2+}$ (S5) with O_2 does not require a location to accommodate the second O moiety. Dotted bonds correspond to dative interactions. The term "Z" describes the negatively charged zeolite lattice. Depending on the necessary activation temperature, the different starting points are highlighted in either violet or yellow.

of a $[Cu_3(\mu\text{-}O)_3]^{2+}$ center. This precursor can be present either in the form of three Cu(I) ions or as a mixed $[Cu_2(\mu\text{-}O)]^{2+}/Cu(I)$ moiety and is rapidly oxidized by O_2 and $^\bullet OH$ into $[Cu_3(\mu\text{-}O)_3]^{2+}$ *via* eqn (4.4) and (4.5), regardless of the activation temperature. An alternative pathway for $[Cu_3(\mu\text{-}O)_3]^{2+}$ generation in Cu-MFI has been suggested by Li *et al.*, which is based on the interaction of a $2Cu(I)/[CuOH]^+$ precursor with O_2 (eqn (4.6)).[54]

$$3Cu^+ + O_2 + {}^\bullet OH \rightarrow [Cu_3(\mu\text{-}O)_3]^{2+} + H^+ \quad (4.4)$$

$$[Cu_2(\mu\text{-}O)]^{2+} + Cu^+ + 1/2O_2 + {}^\bullet OH \rightarrow [Cu_3(\mu\text{-}O)_3]^{2+} + H^+ \quad (4.5)$$

$$2Cu^+ + [CuOH]^+ + O_2 \rightarrow [Cu_3(\mu\text{-}O)_3]^{2+} + H^+ \quad (4.6)$$

The diminished CH_3OH output after dehydration in He at 623 K prior to interaction with O_2 at 473 K was attributed to a less efficient (auto)reduction or a limited degree of Cu(I) mobility. Notably, Ikuno *et al.* suggested that $[Cu_3(\mu\text{-}O)_3]^{2+}$ evolves through the same mechanism during conventional activation of as-prepared/hydrated Cu–MOR in O_2.[19] While monitoring the XANES spectra of their material during dehydration in O_2, they noticed the appearance of the Cu(I) rising edge feature at 623 K, which vanished again after keeping the sample in O_2 at 723 K for 1 h. This behavior was attributed to the (auto)reduction of $[CuOH]^+$ or $[Cu_2(\mu\text{-}O)]^{2+}$, followed by their re-oxidation into $[Cu_3(\mu\text{-}O)_3]^{2+}$ *via* eqn (4.4) and (4.5). As discussed in Section 4.2.1, Cu-oxo species can indeed undergo (auto)reduction at elevated temperatures even under oxidative conditions. However, compared to treatment in inert gas or vacuum, the presence of O_2 should shift the reaction equilibrium toward the oxygenated Cu(II) state. Given that the generation of mobile Cu(I) was suggested to be a prerequisite for the formation of the reduced $[Cu_3(\mu\text{-}O)_3]^{2+}$ precursor, it could be expected that a conventional activation of the as-prepared/hydrated sample in O_2 should result in a drastically lower CH_3OH productivity compared to an initial treatment of the material in inert gas or vacuum followed by O_2 exposure. This is, however, not observed experimentally.

Despite this conceptual inconsistency, the work by Ikuno *et al.* provides compelling evidence that, unlike in as-prepared/hydrated Cu–zeolites, the generation of Cu-oxo active sites in (auto)reduced materials does not require elevated temperatures. This is in contrast to analogous experiments from a study by Pappas *et al.*[16] Compared to the CH_3OH productivity of $Cu_{0.49}CHA_{12.1}$ activated in O_2 at 773 K, these authors observed a decrease in the performance of the material in CH_4 partial oxidation after He treatment at 773 K, followed by interaction with O_2 at 473 K. This phenomenon was correlated to the temperature-controlled formation of less reactive four-fold coordinated Cu(II) species (see Section 4.2.5). Then again, Smeets *et al.* compared the minimal activation temperature necessary to detect the LMCT transition of $[Cu_2(\mu\text{-}O)]^{2+}$ at ~22 700 cm^{-1} in as-prepared/hydrated and (auto)reduced $Cu_{0.54}MFI_{12.0}$.[136] In the former case, the threshold temperature was 623 K, whereas it dropped to 553 K after treatment of the sample in He at 773 K, implying that the onset temperature of $[Cu_2(\mu\text{-}O)]^{2+}$ formation is controlled by the initial state of the Cu–zeolite. Similarly, Woertink *et al.* observed the emergence of this characteristic feature already at 448 K when exposing (auto)reduced $Cu_{0.54}MFI_{12.0}$ to O_2.[66] The fact that the generation of oxygenated Cu(II) species in (auto)reduced Cu–zeolites takes place even at low temperatures has additionally been highlighted by an investigation of Brenig *et al.* focused on the activation of (auto)reduced Cu–$MOR_{10.0}$, Cu-$MFI_{11.5}$, and Cu–$CHA_{11.0}$.[127] By LCF analysis of the XANES spectra recorded throughout TPO, the authors registered a continuous increase in the Cu(II) fraction starting already at 240 K. Likewise, UV-Vis spectra collected after exposing the reduced materials to O_2 at 313 K displayed a pronounced increase in the absorbance of two bands within the ranges of 27 300–26 400 and 22 000–21 800 cm^{-1}, corresponding to the LMCT transition of two distinct $[Cu_2(\mu\text{-}O)]^{2+}$ motifs (Fig. 4c). Compared to the spectra acquired after calcination at 753 K followed by a cool down to 313 K in the presence of the oxidant, the intensity in these regions was identical or even higher in the spectra of the reduced samples contacted with O_2 at 313 K. This clearly illustrates that the generation of $[Cu_2(\mu\text{-}O)]^{2+}$ in (auto)reduced Cu–zeolites is feasible at low temperatures and is equally or even more efficient than high-temperature activation. Notably, complementary CW X-band EPR experiments indicated that the oxidative formation of monomeric Cu(II) sites, including Cu^{2+}_{para}, Cu^{2+}_{meta}, and $[CuOH]^+$, requires markedly higher temperatures than that of Cu(II) dimers. In fact, O_2 treatment of the reduced materials at 723 K was necessary to attain the same signal intensity as in the spectra of as-prepared/hydrated samples calcined at 753 K. A similar phenomenon has been reported by Palomino *et al.*, who observed that temperatures of up to 670 K were necessary to maximize the signal intensity of the CW X-band EPR spectrum of (auto)reduced Cu-$MFI_{14.0}$ during interaction with O_2.[98] The origin of the nuclearity-dependent formation temperature of specific Cu(II) centers remains to be identified. The difference between the required temperature for Cu(II) di-/trimer and Cu(II) monomer formation during interaction of (auto)reduced Cu–zeolites with O_2 is depicted in Scheme 9.

The mechanism of $[Cu_2(\mu\text{-}O)]^{2+}$ generation in (auto)reduced Cu-MFI has been explored by Smeets *et al.*[147] Unlike in the case of as-prepared/hydrated materials, where $[Cu_2(\mu\text{-}O)]^{2+}$ evolves from $[CuOH]^+$ condensation (eqn (3.2)), the formation of $[Cu_2(\mu\text{-}O)]^{2+}$ in (auto)reduced samples is initiated by the reaction of O_2 with neighboring Cu(I) ions, yielding a $[Cu_2(\mu\text{-}\eta^2\text{:}\eta^2\text{-}O_2)]^{2+}$ precursor (eqn (4.7)).

$$Cu^+ + O_2 \rightarrow [Cu_2(\mu\text{-}\eta^2\text{:}\eta^2\text{-}O_2)]^{2+} \quad (4.7)$$

$$[Cu_2(\mu\text{-}\eta^2\text{:}\eta^2\text{-}O_2)]^{2+} + 2Cu^+ \rightarrow 2Cu^{2+} + O^{2-}_{fw} + [Cu_2(\mu\text{-}O)]^{2+} \quad (4.8)$$

$$[Cu_2(\mu\text{-}\eta^2\text{:}\eta^2\text{-}O_2)]^{2+} + [Si_2(\mu\text{-}O)]^{6+} \rightarrow [Cu_2(\mu\text{-}O)]^{2+} + [Si_2(\mu\text{-}1,2\text{-}O_2)]^{6+} \quad (4.9)$$

$$[Cu_2(\mu\text{-}\eta^2\text{:}\eta^2\text{-}O_2)]^{2+} + 2Cu^+ \rightarrow 2[Cu_2(\mu\text{-}O)]^{2+} \quad (4.10)$$

By monitoring the development of the $O_{ef} \rightarrow$ Cu(II) LMCT feature of $[Cu_2(\mu\text{-}\eta^2\text{:}\eta^2\text{-}O_2)]^{2+}$ at ~29 000 cm^{-1}, Smeets *et al.* determined that this precursor develops within ~2 min when contacting the (auto)reduced material with O_2 at ambient temperature (Fig. 5a).

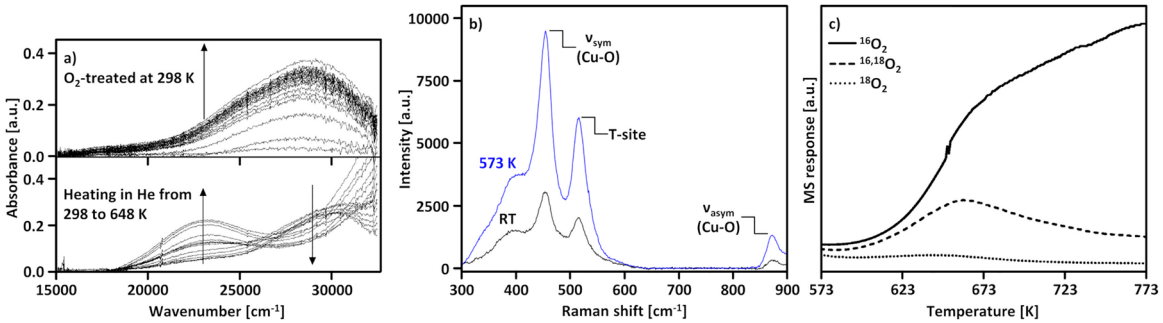

Fig. 5 UV-Vis spectra of $Cu_{0.5}MFI_{12.0}$, previously (auto)reduced in He at 723 K, during interaction with O_2 at 298 K (a, top) as well as of $Cu_{0.3}MFI_{12.0}$ throughout heating in He from 298 to 648 K following treatment in He at 723 K and exposure to O_2 at 298 K (a, bottom). Raman spectra (λ_{ex} = 457.9 nm) of (auto)reduced Cu-$MFI_{12.0}$ after interaction with O_2 at ambient temperature (black) and after raising the temperature to 573 K (blue, b). MS signal of $^{16}O_2$, $^{16,18}O_2$, and $^{18}O_2$ as a function of temperature during a TPD (2 K min^{-1}) of activated $Cu_{0.5}MFI_{12.0}$ (c). The maximum in the $^{16,18}O_2$ desorption profile occurs in the same temperature range where the LMCT band of $[Cu_2(\mu\text{-}O)]^{2+}$ at ~22 700 cm^{-1} disappears. Adapted from ref. 147 with permission from the American Chemical Society (Copyright 2010).

Upon increasing the temperature to 448 K in either O_2 or He, the intensity of the band at $\sim$29 000 cm^{-1} started to gradually decrease, which was accompanied by an absorbance gain at $\sim$22 700 cm^{-1} (Fig. 5a). This transition was attributed to the progressive conversion of $[Cu_2(\mu\text{-}\eta^2\text{:}\eta^2\text{-}O_2)]^{2+}$ into $[Cu_2(\mu\text{-}O)]^{2+}$. Importantly, complementary Raman experiments demonstrated that the characteristic signals of $[Cu_2(\mu\text{-}O)]^{2+}$ at $\sim$870, 456, and 514 cm^{-1}, corresponding to the ν_{asym}(Cu–O) and ν_{sym}(Cu–O) stretch as well as the vibration of a T-site ligand, can already be identified in the spectrum of the (auto)reduced sample after interaction with O_2 at ambient temperature (Fig. 5b).[66,147] This suggests that the transformation of the O_2-bridged precursor into $[Cu_2(\mu\text{-}O)]^{2+}$ can take place even below 448 K, which is in agreement with the results of the investigation by Brenig *et al.* of the Cu(II) dimer generation in Cu–$MOR_{10.0}$, Cu-$MFI_{11.5}$, and Cu–$CHA_{11.0}$ by UV-Vis spectroscopy (*vide supra*).[127]

A key question in the formation of $[Cu_2(\mu\text{-}O)]^{2+}$ concerns the fate of the second O moiety arising from the O–O bond rupture in $[Cu_2(\mu\text{-}\eta^2\text{:}\eta^2\text{-}O_2)]^{2+}$. Smeets *et al.* addressed this by analyzing the isotopic composition of O_2 released during TPD of $^{18}O_2$-activated $Cu_{0.5}MFI_{12.0}$ (Fig. 5c).[147] The authors detected a prominent $^{16,18}O_2$ signal in the same temperature range where the LMCT band of $[Cu_2(\mu\text{-}O)]^{2+}$ at $\sim$22 700 cm^{-1} began to disappear. Consequently, they argued that the $^{18}O_{ef}$ of $[Cu_2(\mu\text{-}O)]^{2+}$ does not recombine with $^{18}O_{ef}$ from a second Cu(II) dimer but with $^{16}O_{fw}$ instead. By invoking the concept of microscopic reversibility, Smeets *et al.* proposed that the second ^{18}O moiety, originating from the O–O bond cleavage in $[Cu_2(\mu\text{-}\eta^2\text{:}\eta^2\text{-}O_2)]^{2+}$, is incorporated into the zeolite lattice as $^{18}O_{fw}$ (eqn (4.8)). Due to the higher abundance of $^{16}O_{fw}$ compared to $^{18}O_{fw}$, the $^{18}O_{ef}$ of $[Cu_2(\mu\text{-}O)]^{2+}$ preferentially recombines with $^{16}O_{fw}$ during the TPD, leading to the pronounced $^{16,18}O_2$ signal. The two additional electrons required to convert the O_2^{2-} group of $[Cu_2(\mu\text{-}\eta^2\text{:}\eta^2\text{-}O_2)]^{2+}$ into two O^{2-} moieties were hypothesized to derive from two Cu(I) spectator ions, which are oxidized to Cu(II). At this stage, it remains unclear how the Cu(I) spectators are regenerated in the course of successive CH_4-to-CH_3OH cycles and whether the zeolite lattice can continuously serve as a reservoir for new O_{fw} groups. Moreover, the possibility of isotope scrambling between $^{18}O_{ef}$ of $[Cu_2(\mu\text{-}O)]^{2+}$ and $^{16}O_{fw}$ of the zeolite lattice, which could affect the $^{16,18}O_2$ signal, was not considered.[195,196]

Two additional scenarios regarding the positioning of the second O moiety have been suggested by Mahyuddin *et al.*, who employed DFT to investigate the generation of $[Cu_2(\mu\text{-}O)]^{2+}$ in Cu–MOR.[179] Following $[Cu_2(\mu\text{-}\eta^2\text{:}\eta^2\text{-}O_2)]^{2+}$ formation in the 8-MR of the MOR side pocket (Scheme 1) facing the 8-MR channel, the liberated O atom can be integrated into the same 8-MR of the zeolite lattice, yielding $[Si_2(trans\text{-}\mu\text{-}1,2\text{-}O_2)]^{6+}$ (Scheme S1n) and $[Cu_2(\mu\text{-}O)]^{2+}$ (eqn (4.9)). Alternatively, the O moiety can be transferred to two Cu(I) ions situated in the opposite 8-MR, leading to the formation of a second proximal $[Cu_2(\mu\text{-}O)]^{2+}$ center (eqn (4.10)). Compared to the mechanism proposed by Smeets *et al.*, the incorporation of the released O atom into the framework *via* $[Si_2(trans\text{-}\mu\text{-}1,2\text{-}O_2)]^{6+}$ generation does not necessitate an electron transfer from Cu(I) spectators, as the new O_2^{2-} group retains the same formal charge as the original O^{2-} lattice species. Although the formation of $[Cu_2(\mu\text{-}O)]^{2+}$ *via* assimilation of the O moiety into the zeolite lattice is exothermic (−61.5 kJ mol^{-1}), the true activation energy of the O–O bond cleavage is prohibitively high (250 kJ mol^{-1}), rendering this reaction unfeasible even at 723 K. On the contrary, the true activation energy of O–O bond rupture leading to the generation of two $[Cu_2(\mu\text{-}O)]^{2+}$ sites in opposing 8-MRs of the MOR side pocket (Scheme 1) is considerably smaller (43.9 kJ mol^{-1}), allowing this reaction to proceed at lower temperatures. Notably, the mechanism of proximal $[Cu_2(\mu\text{-}O)]^{2+}$ formation is characterized by two spin inversions. The first one takes place during the initial O_2 adsorption and transforms the system from a triplet to an open-singlet state, whereas the second one occurs while passing the O atom from one 8-MR to the other and induces a change from the open-shell singlet to the quintet state. Accordingly, each individual Cu(II) dimer adopts the more reactive triplet state, which, however, necessitates a spin crossover throughout the subsequent CH_4 partial oxidation (see Section 4.1).[67,73,95,107,157–159,161,164,166,167] It is important to highlight that the transfer of the O moiety across the 8-MRs of the MOR side pocket is feasible due to the short distance separating the $[Cu_2(\mu\text{-}\eta^2\text{:}\eta^2\text{-}O_2)]^{2+}$ precursor from the neighboring Cu(I) pair.[179] The migration of the second O atom might, however, not be possible anymore in Cu–zeolites featuring paired Cu(I) ions located at distant exchange positions. An intriguing hypothesis has been put forward by Alayon *et al.*, who proposed that the interaction of the liberated O moiety with gas phase O_2 may yield O_3, which could diffuse to isolated Cu(I) pairs to oxidize them.[100] Alternatively, Ikuno *et al.* mentioned that two O atoms could simply recombine to O_2 again.[19] Despite these considerations, it remains elusive at this stage how Cu-oxo generation by O_2 is affected by the spacing of Cu(I) pairs.

In their study on the activation of (auto)reduced Cu–MOR by O_2, Mahyuddin *et al.* also provided additional insight into the mechanism of $[Cu_3(\mu\text{-}O)_3]^{2+}$ generation (eqn (4.11)).[179]

$$[Cu_3(\mu\text{-}O)]^{2+} + O_2 \rightarrow [Cu_3(\mu\text{-}O)(\eta^1\text{-}O_2)]^{2+} \rightarrow [Cu_3(\mu\text{-}O)(\mu\text{-}\eta^2\text{:}\eta^2\text{-}O_2)]^{2+} \rightarrow [Cu_3(\mu\text{-}O)_3]^{2+} \quad (4.11)$$

Starting from $[Cu_3(\mu\text{-}O)]^{2+}$ (Scheme S1o) situated in the 8-MR of the MOR side pocket (Scheme 1) facing the 12-MR, O_2 adsorption yields a $[Cu_3(\mu\text{-}O)(\eta^1\text{-}O_2)]^{2+}$ (Scheme S1p) complex in the quartet state, which rearranges into an open-shell doublet $[Cu_3(\mu\text{-}O)(\mu\text{-}\eta^2\text{:}\eta^2\text{-}O_2)]^{2+}$ (Scheme S1q) intermediate. The latter converts into $[Cu_3(\mu\text{-}O)_3]^{2+}$ *via* O–O bond rupture, which is accompanied by a second spin inversion resulting in a quartet ground state. Notably, the mechanisms of $[Cu_3(\mu\text{-}O)_3]^{2+}$ formation proposed by both Ikuno *et al.* and Mahyuddin *et al.* are based on the interaction of O_2 with two-fold reacted or completely reduced $[Cu_3(\mu\text{-}O)_3]^{2+}$, which bypasses the need for a nearby Cu(I) pair to accommodate a second O atom.[19,179] However, this issue resurfaces when considering the transformation of partially reduced $[Cu_3(\mu\text{-}O)_2]^{2+}$ into $[Cu_3(\mu\text{-}O)_3]^{2+}$. This paradigm is also outlined in Scheme 9.

Finally, a conclusive reaction scheme for the oxidative generation of $[CuOH]^+$/$[CuOH]^+$ and Cu^{2+}/$[CuOH]^+$ in (auto)reduced Cu–zeolites has not been presented so far. Multiple theoretical

studies have indicated that the interaction of O_2 with isolated Cu(I) can result in end-on/side-on $[Cu(\eta\text{-}O_2^{\bullet})]^+$ (eqn (4.2) and (4.12)).[155,156,178] Santra *et al.* even resolved the rovibrational branches of the ν(O–O) stretch of $[Cu(\eta^2\text{-}O_2^{\bullet})]^+$ at about 1196, 1180, and 1170 cm^{-1} in the FTIR spectrum of Cu-FAU, prepared *via* solid-state ion exchange with CuCl, after adsorption of O_2 at 80 K.[155] Nevertheless, it is not clear if and how these monomeric Cu-oxo sites can further transform into $[CuOH]^+$ or Cu^{2+}. Envisioning a plausible pathway for the formation of $[CuOH]^+$ is further complicated by the fact that a H^+ source must be present either in the form of H_2O or as a BAS.[52,104,127] As depicted in Scheme 9, a potential H^+ source is already present or must be supplied externally, depending on the state of the (auto)reduced $[CuOH]^+$/$[CuOH]^+$ and Cu^{2+}/$[CuOH]^+$ pairs.

4.2.3 Influence of O_2 partial pressure on Cu(II) active site formation. Conflicting results regarding the impact of the O_2 partial pressure on the CH_3OH productivity have been reported. Studies by Pappas *et al.* demonstrated that the CH_3OH output (in mol_{CH_3OH} mol_{Cu}^{-1}) of $Cu_{0.49}CHA_{12.1}$ increases logarithmically upon raising the O_2 partial pressure from 67 to 187 mbar during calcination at 723 K and then levels off.[16] A similar positive correlation between the performance of $Cu_{0.4}MOR_{20.0}$ in CH_4 hydroxylation and the O_2 partial pressure throughout activation at 723 K has been described by Kim *et al.*[21] On the contrary, Álvarez *et al.* noted a decrease in the CH_3OH productivity of $Cu_{0.54}MOR_{6.5}$ from ~22.6 to ~14.4 μmol_{CH_3OH} g_{ZEO}^{-1} after treatment of the material in pure O_2 instead of synthetic air at 723 K prior to CH_4 partial oxidation.[91] Likewise, Tomkins *et al.* observed a drop in the CH_3OH productivity of Cu–$MOR_{6.0}$ from 14.4 to 7.5 μmol_{CH_3OH} g_{ZEO}^{-1} upon increasing the O_2 pressure from 1 to 6 bar during activation at 723 K, followed by reaction with 1 bar CH_4 at 473 K.[17] These authors attributed the adverse influence of the O_2 pressure to a less efficient removal of volatiles, whose nature was, however, not addressed in more detail. Notably, phase diagrams derived from *ab initio* calculations have indicated that the Cu speciation in various Cu–zeolites is strongly affected by the O_2 partial pressure.[72–74,135,168,177] Grundner *et al.*, for example, demonstrated that $[Cu_2(\mu\text{-}O)]^{2+}$ is the thermodynamically preferred Cu(II) center in Cu–MOR below ~2.2 mbar O_2 at 700 K and 1×10^{-5} mbar H_2O, whereas $[Cu_3(\mu\text{-}O)_3]^{2+}$ becomes more favorable at higher O_2 partial pressures (see Section 2.1.4).[73] Nevertheless, the O_2 partial pressure and temperature are decreased right before the actual CH_4 partial oxidation. Therefore, Cu-oxo centers, which are thermodynamically preferred under activation conditions, might not be the most favorable Cu(II) species prior to exposure of the material to CH_4.[72] A meaningful correlation between the O_2 partial pressure, the nature of the formed Cu-oxo sites, and the resulting performance in CH_4-to-CH_3OH conversion cannot be established at this point.

4.2.4 Cu(II) evolution as a function of activation duration. Ikuno *et al.* compared the performance of $Cu_{0.31}MOR_{11.0}$ in CH_4 partial oxidation after calcination at 623 K for either 1 or 3 h and detected only an insignificantly small increase in the CH_3OH productivity upon prolonging the duration of the O_2 treatment.[19] The marginal difference in the CH_3OH output decreased even further when raising the activation temperature to 773 K. Consequently, these authors argued that the generation of the oxygenated Cu(II) active site at temperatures between 623 and 773 K is purely thermodynamically controlled in Cu–MOR. Then again, other studies, focusing on both Cu–MOR and Cu–CHA, have indicated a pronounced positive correlation between CH_3OH productivity and calcination duration.[16,22,91] For instance, Pappas *et al.* demonstrated that the CH_3OH output (in mol_{CH_3OH} mol_{Cu}^{-1}) of $Cu_{0.49}CHA_{12.1}$ more than doubles upon prolonging the O_2 treatment from 60 to 720 min at 723 K.[16] Bregante *et al.* attributed the necessity for an extended activation period in Cu–CHA to the kinetically controlled transformation of an O_2-bridged Cu(II) precursor into $[Cu_2(\mu\text{-}O)]^{2+}$.[22] By tracking the changes in the Raman spectra of (auto)reduced $Cu_{0.24}CHA_{15.5}$ during contact with O_2 at 723 K, the authors observed that a timespan of up to ~3.6 h was necessary to maximize the intensity of a band at 603 cm^{-1}, which was assigned to the deformation mode of an 8-MR hosting $[Cu_2(\mu\text{-}O)]^{2+}$ (Fig. 6a) On the contrary, complementary XANES experiments indicated that the elementary conversion of Cu(I) into Cu(II) occurs at a significantly faster rate (~0.7 h). Bregante *et al.* proposed that the quick Cu(I) oxidation corresponds to the rapid formation of end-on/side-on $[Cu(\eta\text{-}O_2^{\bullet})]^+$ *via* interaction of Cu(I) with O_2 (eqn (4.12)) and the equally fast generation of a $[Cu_2(\mu\text{-}\eta^2\text{:}\eta^2\text{-}O_2)]^{2+}$ or $[Cu_2(trans\text{-}\mu\text{-}1,2\text{-}O_2)]^{2+}$ precursor upon reaction of end-on/side-on $[Cu(\eta\text{-}O_2^{\bullet})]^+$ with an adjacent Cu(I) center (eqn (4.13)). Subsequently, the O_2-bridged Cu(II) precursor evolves into $[Cu_2(\mu\text{-}O)]^{2+}$ *via* O–O bond cleavage (eqn (4.14)), which was envisioned to be the rate-determining step.

$$Cu^+ + O_2 \rightarrow \text{end-on/side-on } [Cu(\eta\text{-}O_2^{\bullet})]^+ \quad (4.12)$$

$$\text{End-on/side-on } [Cu(\eta\text{-}O_2^{\bullet})]^+ + Cu^+ \rightarrow [Cu_2(trans\text{-}\mu\text{-}1,2\text{-}O_2)]^{2+} \text{ or } [Cu_2(\mu\text{-}\eta^2\text{:}\eta^2\text{-}O_2)]^{2+} \quad (4.13)$$

$$[Cu_2(trans\text{-}\mu\text{-}1,2\text{-}O_2)]^{2+} \text{ or } [Cu_2(\mu\text{-}\eta^2\text{:}\eta^2\text{-}O_2)]^{2+} \rightarrow [Cu_2(\mu\text{-}O)]^{2+} + 1/2O_2 \quad (4.14)$$

Notably, the recorded time-resolved Raman spectra are quite peculiar as they do not display the characteristic signals of the zeolite framework vibrations right from the start of the activation procedure (Fig. 6a).

Instead, these bands progressively emerge throughout the O_2 treatment alongside the feature at 603 cm^{-1}. Since the kinetic description of the $[Cu_2(\mu\text{-}O)]^{2+}$ generation was based on MCR using a single spectral component, the extracted rate constant is convoluted by the temporal development of the signals arising from the framework vibrations. This raises the question whether the long calcination durations are actually related to the formation of $[Cu_2(\mu\text{-}O)]^{2+}$. Moreover, if the O_2-bridged precursor is present in a pseudo-steady state, one could expect to observe its corresponding features in the Raman spectra, which, however, is not the case.[147] Additionally, since the materials studied by Bregante *et al.* were in an (auto)reduced state prior to their treatment with O_2, it is crucial to keep in mind that these results cannot simply be transferred to the activation of as-prepared/hydrated Cu–zeolites. As highlighted in Section 3, the

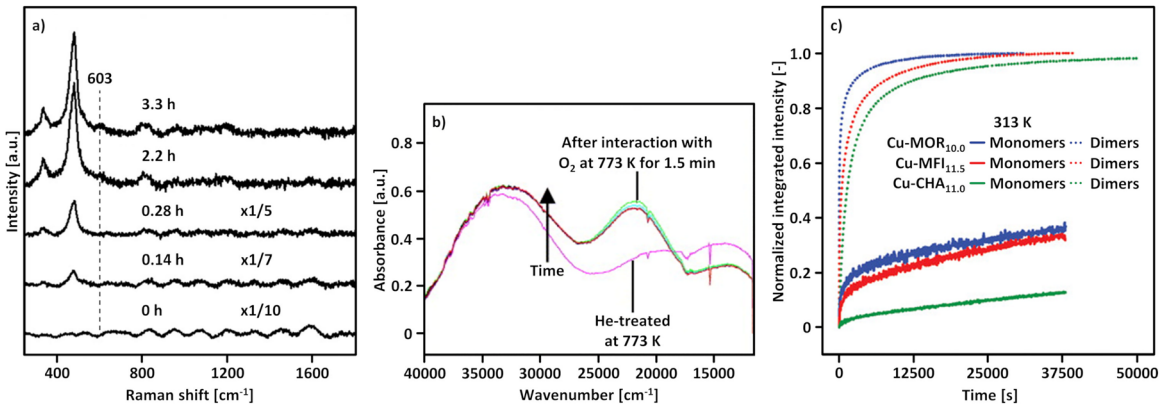

Fig. 6 Time-resolved Raman spectra (λ_{ex} = 532 nm) of $Cu_{0.24}CHA_{15.5}$, previously (auto)reduced in He at 723 K, during calcination in O_2 at 723 K (a). Spectra have been scaled by the indicated constants. UV-Vis spectra of $Cu_{0.54}MFI_{12.0}$ throughout interaction with O_2 at 773 K following treatment in He at the same temperature (b). Development of the normalized integrated signal intensity of monomeric (Cu^{2+} and $[CuOH]^+$, solid lines) as well as dimeric (two types of $[Cu_2(\mu\text{-}O)]^{2+}$, dotted lines) Cu(II) species in (auto)reduced Cu–$MOR_{10.0}$ (blue), Cu-$MFI_{11.5}$ (red), and Cu–$CHA_{11.0}$ (green) during exposure to O_2 at 313 K measured by EPR and UV-Vis spectroscopy (c). Adapted from ref. 22, 127 and 136 with permission from the American Chemical Society (Copyright 2021), Elsevier (Copyright 2005), and Wiley (Copyright 2025).

generation of $[Cu_2(\mu\text{-}O)]^{2+}$ in as-prepared/hydrated materials proceeds *via* $[CuOH]^+$ condensation (eqn (3.2)), which does not involve a potentially kinetically limiting O–O bond rupture.

Contrary to the findings of Bregante *et al.*, Smeets *et al.* reported that the formation of $[Cu_2(\mu\text{-}O)]^{2+}$ in (auto)reduced $Cu_{0.54}MFI_{12.0}$ is a rather quick process.[136] Compared to the UV-Vis spectrum of $Cu_{0.54}MFI_{12.0}$ calcined at 773 K, these authors reported that the intensity of the LMCT transition of $[Cu_2(\mu\text{-}O)]^{2+}$ at ~22 700 cm^{-1} can be fully restored within ~1.5 min upon interaction of the (auto)reduced material with O_2 at 773 K (Fig. 6b). The fact that the evolution of $[Cu_2(\mu\text{-}O)]^{2+}$ in (auto)reduced Cu–zeolites proceeds at an exceptionally fast rate is further supported by a study of Brenig *et al.* focused on the activation of reduced Cu–$MOR_{10.0}$, Cu-$MFI_{11.5}$, and Cu–$CHA_{11.0}$.[127] Depending on the framework, these authors observed that the temporal development of the bands corresponding to the LMCT transition of two different $[Cu_2(\mu\text{-}O)]^{2+}$ moieties reached a steady state after ~1.6 h during treatment of the materials with O_2 at just 313 K (Fig. 6c). Upon raising the activation temperature above 423 K, these features evolved almost instantaneously. Interestingly, the rate of $[Cu_2(\mu\text{-}O)]^{2+}$ generation was found to be dictated by the zeolite topology. Throughout the interaction of the reduced samples with O_2 at 313 K, the authors noted that the time required for the absorbance of the LMCT signals to reach 50% of their steady state intensity increased in the order of Cu–$MOR_{10.0}$ (20 s) < Cu-$MFI_{11.5}$ (410 s) < Cu–$CHA_{11.0}$ (1310 s). A comparison of the temporal behavior of the simultaneously measured O_2 consumption of the different Cu–zeolites revealed the same trend. Although the origin of this framework-dependent oxidizability remains uncertain, it can be speculated that it is related to the preferential stabilization of Cu in specific oxidation states within the distinct ion exchange positions or to variations in the proximity of Cu(I) centers. Nevertheless, a more in-depth analysis is necessary to fully reveal the influence of the zeolite's topology on the formation kinetics of specific Cu-oxo species as well as on the bulk oxidizability. Notably, complementary CW X-band EPR experiments revealed that the rate of Cu(II) monomer formation, including Cu^{2+}_{para}, Cu^{2+}_{meta}, and $[CuOH]^+$, is equally affected by the framework but remains significantly slower than the rate of Cu(II) dimer generation.

4.2.5 Cu(II) evolution during the cool down to the temperature of CH_4 partial oxidation. Multiple authors have noted an amplification of the white line intensity in the XANES spectra of Cu–MOR, Cu–CHA, and Cu-FER during cool down in O_2 to 473 K following high-temperature calcination at 773 K, which was accompanied by an increase in the intensity of the first-shell Cu–O scattering signal in the corresponding FT-EXAFS spectra.[16,138,139,169,175,197] This was attributed to a thermally-induced transition from three- to four-fold coordinated Cu(II). Pappas *et al.* and Borfecchia *et al.* suggested that this process involves the rearrangement of $[Cu(\eta^1\text{-}O_2^{\bullet})]^+$ or $[Cu_2(trans\text{-}\mu\text{-}1,2\text{-}O_2)]^{2+}$, formed *via* eqn (4.2) and (4.3), into $[Cu(\eta^2\text{-}O_2^{\bullet})]^+$ (eqn (4.15)) or $[Cu_2(\mu\text{-}\eta^2\text{:}\eta^2\text{-}O_2)]^{2+}$ (eqn (4.16)).[16,172,175,192] The latter was proposed to further convert into $[Cu_2(\mu\text{-}O)]^{2+}$ *via* O–O bond cleavage (see Section 4.2.2).[16,20,22,147] Kvande *et al.* instead argued that the increase in the first shell CN arises from the transformation of $[Cu_2(\mu\text{-}O)]^{2+}$ (eqn (4.17)) or paired $[CuOH]^+$ (eqn (4.18)) into either $[Cu_2(\mu\text{-}OH)_2]^{2+}$ or $[Cu_2(\mu\text{-}\eta^2\text{:}\eta^2\text{-}O_2)]^{2+}$.[139]

$$[Cu(\eta^1\text{-}O_2^{\bullet})]^+ \underset{T\uparrow}{\overset{T\downarrow}{\rightleftharpoons}} [Cu(\eta^2\text{-}O_2^{\bullet})]^+ \tag{4.15}$$

$$[Cu_2(trans\text{-}\mu\text{-}1,2\text{-}O_2)]^{2+} \underset{T\uparrow}{\overset{T\downarrow}{\rightleftharpoons}} [Cu_2(\mu\text{-}\eta^2\text{:}\eta^2\text{-}O_2)]^{2+} \rightarrow [Cu_2(\mu\text{-}O)]^{2+} + 1/2O_2 \tag{4.16}$$

$$[Cu_2(\mu\text{-}\eta^2\text{:}\eta^2\text{-}O_2)]^{2+} \underset{+1/2O_2}{\overset{-1/2O_2}{\underset{T\downarrow}{\overset{T\uparrow}{\rightleftharpoons}}}} [Cu_2(\mu\text{-}O_2)]^{2+} \underset{-H_2O}{\overset{+H_2O}{\underset{T\uparrow}{\overset{T\downarrow}{\rightleftharpoons}}}} [Cu_2(\mu\text{-}OH)_2]^{2+} \tag{4.17}$$

$$\left[Cu_2(\mu\text{-}\eta^2\text{:}\eta^2\text{-}O_2)\right]^{2+} + H_2O \underset{+1/2O_2}{\overset{-1/2O_2}{\underset{T\downarrow}{\overset{T\uparrow}{\rightleftharpoons}}}} 2[CuOH]^+ \underset{T\uparrow}{\overset{T\downarrow}{\rightleftharpoons}} \left[Cu_2(\mu\text{-}OH)_2\right]^{2+} \quad (4.18)$$

Notwithstanding the actual nature of the involved Cu-oxo species, Pappas *et al.* argued that three-fold coordinated Cu-oxo species are characterized by a higher reactivity than four-fold coordinated centers.[16] They based this on the observation that $Cu_{0.49}CHA_{12.1}$, initially (auto)reduced in He at 773 K, exhibited a higher CH_3OH productivity after treatment with O_2 at 773 K than at 473 K. However, it is important to emphasize that the corresponding CH_4 partial oxidation experiments were performed at 473 K, meaning that the material calcined at 773 K was cooled in O_2 to this reaction temperature. Consequently, it is surprising that the CH_3OH output differed after calcination at the two temperatures, given that the cool down from 773 to 473 K should have also resulted in the transformation of the active three-fold into the less active four-fold coordinated Cu(II) species. In this context, it is worth mentioning that Brezicki *et al.* warned that the apparent increase in the first shell CN, identified in both the XANES and FT-EXAFS spectra, during the cool down might also be attributed to the re-adsorption of H_2O impurities.[90] In general, the correlation of alleged, spectroscopically identified, temperature-induced phenomena to standardized reactivity tests, without accounting for the reversibility of these processes, appears to be a common pitfall.[13,21] As already addressed in Section 4.2.2, Kim *et al.* investigated the impact of the activation temperature on the performance of $Cu_{0.4}MOR_{20.0}$ in CH_4 partial oxidation and observed a decrease in the CH_3OH output from ~67 to ~56 $\mu mol_{CH_3OH}\ g_{ZEO}^{-1}$ upon raising the calcination temperature from 723 to 773 K.[21] UV-Vis spectra recorded throughout O_2 treatment of the as-prepared/hydrated material indicated that the intensity of a band at ~34 000 cm^{-1}, associated with $[Cu_3(\mu\text{-}O)_3]^{2+}$, peaked at 723 K before declining again at 773 K. Based on this, Kim *et al.* argued that elevated temperatures favor the desorption of O_2 from an intermediate of the $[Cu_3(\mu\text{-}O)_3]^{2+}$ site, resulting in the diminished CH_3OH productivity after activation at temperatures higher than 723 K. Yet again, the CH_4 partial oxidation experiments were conducted at 423 K after a cool down in O_2, suggesting that this desorption effect should have been reverted.

4.2.6 Cu(II) evolution during multiple redox cycles. Once formed, Cu(II) active sites appear to be fully regenerable after CH_4 partial oxidation, as the CH_3OH productivity of most Cu–zeolites remains constant throughout multiple redox cycles under the same conditions.[18,73,87,89,91,92,96,198] For example, reusability studies by Grundner *et al.* revealed a steady CH_3OH output of ~95 $\mu mol_{CH_3OH}\ g_{ZEO}^{-1}$ of Cu–MOR over eight consecutive CH_4 partial oxidation reactions, which demonstrates the high (hydro-)thermal stability of the Cu–zeolite and emphasizes that the Cu(II) centers reach the same state after each activation.[73] This is further supported by results from Negri *et al.*, who discovered that the UV-Vis spectrum of $Cu_{0.5}CHA_{15.0}$, initially present either in an as-prepared/hydrated or (auto)reduced state, does not deviate significantly from each other after an O_2 treatment at 673 K, inferring that the activation procedure restores the speciation and relative abundance of the Cu(II) sites.[53] Notably, this is in contrast to a complementary Raman analysis by the same authors, which indicated that the nature of the formed Cu-oxo centers is, in fact, influenced by the original state of the material. Contrary to the Raman spectrum of as-prepared/hydrated $Cu_{0.5}CHA_{15.0}$ recorded after O_2 treatment, no feature at 580 cm^{-1} could be identified in the spectrum of the calcined sample initially present in an (auto)reduced state. The absence of this signal was attributed to the suppression of the generation of $[Cu_2(trans\text{-}\mu\text{-}1,2\text{-}O_2)]^{2+}$ during interaction of the (auto)reduced $Cu_{0.5}CHA_{15.0}$ with O_2. It remains unclear at this point why this effect was not reflected by the analogous UV-Vis experiments.

Contrary to the work by Grundner *et al.*, Bozbag *et al.* observed that the CH_3OH productivity of $Cu_{0.38}MOR_{8.5}$ slightly increased by 5.7 $\mu mol_{CH_3OH}\ g_{ZEO}^{-1}$ between the first (12.1 $\mu mol_{CH_3OH}\ g_{ZEO}^{-1}$) and second (17.8 $\mu mol_{CH_3OH}\ g_{ZEO}^{-1}$) redox cycle and remained approximately constant thereafter.[199] They attributed this behavior to a facilitated Cu(II) active site formation in the second calcination period, which was related to the hydration of the material throughout the aqueous CH_3OH extraction of the first cycle. However, it was not verified whether the sample's H_2O content actually differed before the O_2 treatment of the first and second cycle. Additionally, the reason for the beneficial role of H_2O in the generation of the Cu(II) active sites was not elaborated in more detail. Notwithstanding these unresolved questions, an increase in the CH_3OH output in the course of multiple redox cycles has also been reported by Pappas *et al.* for Cu-FER and Cu–CHA.[16,89,169] This was related to a hydration-induced displacement of residual Cu(II) species from redox inert positions during the CH_3OH extraction and their transformation into oxygenated Cu(II) active centers in the O_2 treatment period of the subsequent reaction cycle. Nevertheless, inactive Cu(II) species usually correspond to isolated bare Cu^{2+} ions, which are charge-balanced by two Al T-sites positioned either in a 2NN or 3NN arrangement (see Section 2.1.1). Since the formation of these Cu(II) centers is characterized by a significantly lower Gibbs free energy compared to that of any other mono- or multimeric Cu-oxo species under the conditions of Cu–zeolite activation, the driving force for this redistribution phenomenon has yet to be determined.[54,57,105,106]

To further complicate matters, Wieser *et al.* and Knorpp *et al.* even noted a drop in the CH_3OH output of Cu-$MAZ_{4.3}$ by ~40% during four consecutive cycles (from ~159.8 to 96.4 $\mu mol_{CH_3OH}\ g_{ZEO}^{-1}$), which they associated with a gradual unpairing of proximal $[CuOH]^+$ centers and their migration from the 8-MR channel to the 6-MR of the gmelinite cage where they adopt the form of redox inert bare Cu^{2+} ions.[111,200] The origin of this rearrangement phenomenon was related to the extensive dehydration of the material throughout activation at 723 K, which was proposed to enable the transfer of Cu between the different ion exchange positions.[111]

The discussion above highlights that more research is necessary to resolve the impact of the initial state, the zeolite framework, and the Cu speciation on the material regenerability.

4.3. Formation of Cu(II) sites using O_2 during isothermal looping and continuous CH_4 partial oxidation

Compared to non-isothermal looping, the processes occurring throughout the oxidative activation in isothermal CH_4 partial oxidation and continuous CH_4-to-CH_3OH conversion have remained largely unexplored. As a result, a definitive correlation between the activation conditions, the nature of the generated Cu-oxo centers, and the Cu–zeolite's CH_3OH productivity has yet to be established. Given the limited number of relevant studies, the following section will provide a combined overview of the formation and regeneration of oxygenated Cu(II) species in both isothermal CH_4 hydroxylation and continuous CH_4-to-CH_3OH conversion. Where applicable, the effect of the activation conditions on the CH_3OH productivity will be assessed.

4.3.1 Development of Cu(II) sites during oxidative treatment in isothermal looping, influence of activation conditions, and material recyclability. The evolution of Cu(II) during the heating ramp of the activation period in isothermal CH_4 partial oxidation has been investigated by Knorpp *et al.*, who monitored the changes in the XANES spectra of as-prepared/hydrated Cu–$MOR_{10.0}$ and Cu-$MAZ_{4.3}$ throughout O_2 treatment from 298 to 473 K.[171,201] Consistent with the observations described in Sections 3 and 4.2.1, the recorded spectral changes are indicative of the gradual dehydration of the Cu(II)-aqua complexes and the simultaneous coordination of Cu(II) to the zeolite lattice. Nevertheless, LCF analysis of the collected spectra revealed that, depending on the material, 14–19% of the exchanged Cu remained in a hydrated state, demonstrating that calcination at 473 K is not sufficient to induce the complete removal of H_2O. This was further supported by complementary thermogravimetric analysis (TGA), which unveiled that the residual content of H_2O, persisting after activation of Cu–$MOR_{10.0}$ at 473 K, amounts to 1.6 H_2O molecules per Cu atom on average.[171] In light of the discussion in Section 4.2.2, the activation conditions employed in isothermal CH_4 partial oxidation should inhibit the efficient formation of multimeric oxygenated Cu(II) active sites in as-prepared/hydrated samples since the reduced calcination temperatures prevent the complete dehydration of the Cu(II)-aqua complexes and the aggregation of Cu(II) into di- or trimeric Cu-oxo species.[15,133,136,167] Moreover, the large amount of residual H_2O poisons any generated Cu-oxo centers (see Section 4.2.2).[100,171,173,175,202] Consequently, it is not surprising that the performance of Cu–zeolites in CH_4-to-CH_3OH conversion *via* isothermal looping is typically lower compared to that of the same material operating in a non-isothermal manner.[17,201,203] For instance, Tomkins *et al.* compared the CH_3OH output of Cu–$MOR_{6.0}$ during interaction with 1 bar CH_4 at 473 K after activation in 1 bar O_2 at either 723 K for 4 h or 473 K for 13 h.[17] Upon switching from non-isothermal to isothermal CH_4 partial oxidation, the authors noted a decrease in the CH_3OH productivity from approximately 45.3 to 2.1 $\mu mol_{CH_3OH}\ g_{ZEO}^{-1}$. Although elevated CH_4 pressures (up to 15 bar CH_4) can partially mitigate the inhibitory effect of competitive H_2O adsorption, the disparity in CH_3OH output between the two procedures generally persists.[17,201,203,204] Increasing the temperature during O_2 treatment facilitates material dehydration and the formation of oxygenated Cu(II) species. This, however, does not necessarily translate into an improved CH_3OH productivity, as elevated temperatures during the subsequent CH_4 partial oxidation can promote CH_4 overoxidation, thereby reducing CH_3OH selectivity. The ambivalent role of the process temperature has been emphasized by Wieser *et al.*, who studied the performance of $Cu_{0.25}MAZ_{4.3}$ in CH_4 partial oxidation under isothermal and isobaric conditions at temperatures ranging from 473 to 573 K.[205]

As depicted in Fig. 7a, increasing the temperature beyond 498 K during material treatment in O_2 had little effect on the final amount of dehydrated Cu(II). However, rising temperatures significantly increased the amount of reduced Cu(I) throughout CH_4 exposure (Fig. 7b). Increasing the temperature from 473 to 543 K resulted in an increase of the averaged CH_3OH output from 75 to 277 $\mu mol_{CH_3OH}\ g_{ZEO}^{-1}$ (Fig. 7c). Further raising the process temperature to 573 K led to a decline in the CH_3OH productivity to 264 $\mu mol_{CH_3OH}\ g_{ZEO}^{-1}$, highlighting the delicate balance between looping temperatures that are sufficiently high to enable dehydration and Cu-oxo active site generation, yet low enough to suppress CH_4 overoxidation. Importantly, these constraints are less stringent in the case of Cu–zeolites, which are characterized by both a high activity in CH_4 hydroxylation and CH_3OH selectivity at elevated temperatures.[204,206] An example for such a material is Cu-exchanged erionite (ERI) such as $Cu_{0.3}ERI_{5.6}$, whose CH_3OH productivity after activation at either 573 or 723 K and subsequent reaction with 30 bar CH_4 at 573 K differs by only $\sim$2 $\mu mol_{CH_3OH}\ g_{ZEO}^{-1}$.[206]

The influence of the O_2 pressure during calcination on the performance of Cu–$MOR_{6.0}$ in isothermal CH_4 partial oxidation has been studied by Tomkins *et al.*[17] Consistent with their work on the impact of the O_2 pressure on the CH_3OH productivity of materials operating under non-isothermal conditions (see Section 4.2.3), these authors determined that the CH_3OH output in isothermal CH_4 hydroxylation is inversely proportional to the O_2 pressure. This is illustrated by the fact that an increase in the O_2 pressure from 1 to 6 bar during activation at 473 K, followed by reaction with 6 bar CH_4 at the same temperature, induced a decrease in the CH_3OH productivity from 21.2 to 16.8 $\mu mol_{CH_3OH}\ g_{ZEO}^{-1}$. Nevertheless, elevated O_2 pressures do not seem to impair the general oxidizability of Cu(I), as highlighted by Wieser *et al.*, who investigated the effect of the O_2 pressure on the development of the XANES spectra of reduced $Cu_{0.25}MAZ_{4.3}$ during activation at 523 K.[205] By LCF analysis of the recorded spectra, these authors were able to show that the final Cu(I) content varies insignificantly upon increasing the O_2 pressure from 1 to 4 bar. Moreover, their results suggest that the O_2 pressure has a negligible effect on the Cu(I) oxidation rate.

Tomkins *et al.* also assessed the relation between the activation duration and the CH_3OH output of Cu–$MOR_{6.0}$.[17] They demonstrated that the CH_3OH productivity increases logarithmically from 10.4 to 25.5 $\mu mol_{CH_3OH}/g_{ZEO}$ upon extending the activation time in O_2 at 473 K from $\sim$3.3 (duration of heating ramp) to 42 h followed by reaction with 6 bar CH_4 at the same temperature.

Similar to CH_4 partial oxidation in a non-isothermal mode, the CH_3OH productivity of most Cu–zeolites operating under isothermal conditions is relatively constant throughout multiple

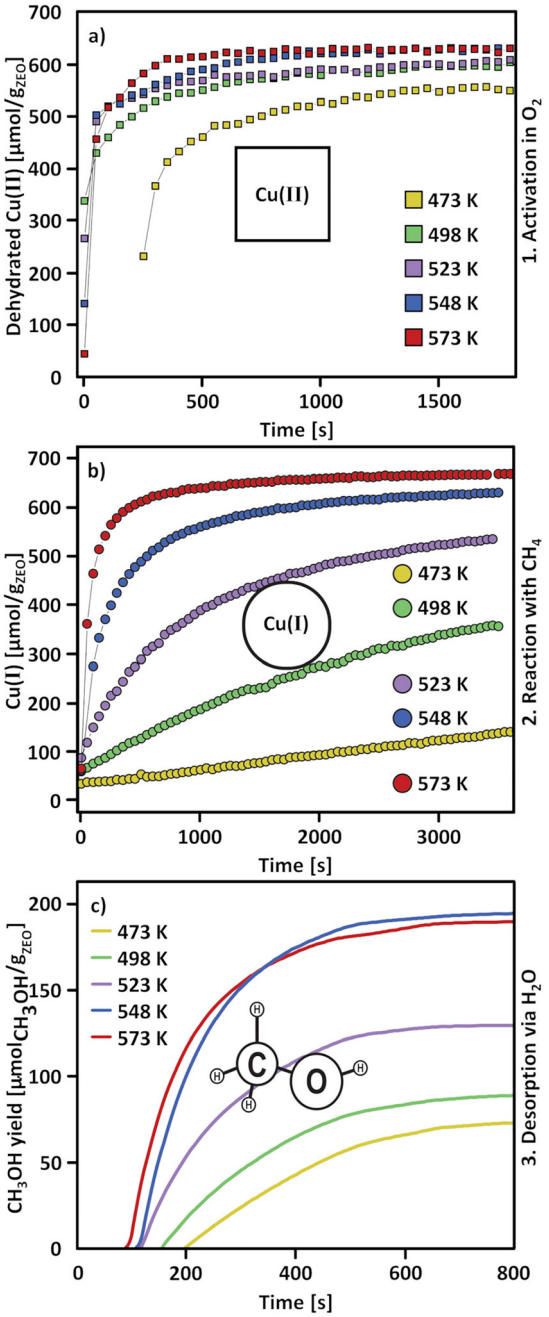

Fig. 7 Development of the amount of dehydrated Cu(II) during exposure of $Cu_{0.25}MAZ_{4.3}$ to O_2 at temperatures ranging from 473 to 573 K (a). Change in the amount of Cu(I) throughout reaction of activated $Cu_{0.25}MAZ_{4.3}$ with CH_4 at the same temperatures (b). Corresponding CH_3OH yield during aqueous product extraction (c). The CH_3OH yield is averaged over four consecutively performed cycles at each temperature. Adapted from ref. 205 with permission from Wiley (Copyright 2023).

redox cycles.[17,206] For example, Zhu *et al.* reported a stable CH_3OH productivity of ~113 $\mu mol_{CH_3OH}\ g_{ZEO}^{-1}$ during four consecutive reaction cycles of $Cu_{0.3}ERI_{5.6}$ with 30 bar CH_4 at 573 K, following activation in O_2 at the same temperature.[206] Likewise, Tomkins *et al.* observed a relatively steady CH_3OH output of ~20 $\mu mol_{CH_3OH}\ g_{ZEO}^{-1}$ throughout four successive reactions of Cu–$MOR_{6.0}$ with 6 bar CH_4 at 473 K after O_2 treatment.[17] X-ray powder diffraction (XRPD) and N_2 physisorption experiments highlighted that the Cu–zeolites are not subjected to hydrothermal degradation and retain their surface properties and crystallinity.[17,206] These results imply that a constant fraction of Cu-oxo active centers can be regenerated after each redox cycle. A noteworthy exception to this is the work by Wieser *et al.*, who studied the performance of $Cu_{0.25}MAZ_{4.3}$ in isothermal and isobaric CH_4 partial oxidation at 523–573 K.[111,205] Within this temperature regime, the authors observed a steady increase in the CH_3OH productivity throughout four consecutive redox cycles. For example, the CH_3OH output during CH_4 hydroxylation at 563 K rose from 86 to 147 $\mu mol_{CH_3OH}/g_{ZEO}^{-1}$ between the first and fourth reaction sequence.[111] Wieser *et al.* attributed this trend to the gradual pairing of $[CuOH]^+$ species *via* a hydration-induced migration through the MAZ framework.

The identification of paired $[CuOH]^+$ centers in Cu-MAZ *via* anomalous XRPD (AXRPD) by Wieser *et al.* represents the first definitive structural characterization of an oxygenated Cu(II) active site involved in isothermal CH_4 partial oxidation.[111] The formation of $[CuOH]^+/[CuOH]^+$ pairs in as-prepared/hydrated and (auto)reduced Cu–zeolites under the conditions of isothermal CH_4 hydroxylation, as well as their poisoning by residual H_2O, is depicted in Scheme 10. For the sake of completeness, it should be mentioned that AXRPD has also enabled Knorpp *et al.* to assign $[CuOH]^+/[CuOH]^+$ pairs as the active centers in Cu-$MAZ_{4.3}$ in non-isothermal CH_4-to-CH_3OH conversion.[110] Synchrotron-based XRD has also been used by Andersen *et al.* and Ipek *et al.* to study the dehydration of Cu–CHA in O_2 at temperatures up to 773 K.[20,103] At present, it is not clear whether di- and trimeric Cu-oxo centers can also develop under the activation conditions employed in isothermal CH_4 hydroxylation, and whether their structures resemble those of their counterparts generated during high-temperature calcination in non-isothermal CH_4 hydroxylation. Tomkins *et al.* excluded the formation of dimeric Cu(II) species, as the UV-Vis spectra of Cu–$MOR_{6.0}$ and Cu-$MFI_{15.0}$, recorded after O_2 treatment at 473 K for 13 h, did not exhibit the LMCT transition of $[Cu_2(\mu\text{-}O)]^{2+}$ at 22 200–22 700 cm^{-1}. Based on TEM, they proposed the participation of finely dispersed sub-nanometer Cu_XO_Y particles in the isothermal CH_4-to-CH_3OH conversion. Regarding the UV-Vis measurements, it should be noted that the adsorption of trace amounts of H_2O on $[Cu_2(\mu\text{-}O)]^{2+}$ can drastically reduce the intensity of its LMCT transition.[50,80,133,144,207] For instance, Smeets *et al.* observed a complete disappearance of the characteristic feature of $[Cu_2(\mu\text{-}O)]^{2+}$ at 22 700 cm^{-1} in the UV-Vis spectrum of $Cu_{0.56}MFI_{12.0}$ upon contacting the activated material with a H_2O-saturated stream of N_2O at 637 and 723 K.[207] This effect was fully reversible by switching to a pure N_2O flow. Brenig *et al.* observed a similar effect in the UV-Vis spectrum of calcined $Cu_{0.41}CHA_{6.5}$ during interaction with H_2O at 473 K, which resulted in a decrease in the absorbance of the LMCT bands of two different $[Cu_2(\mu\text{-}O)]^{2+}$ motifs centered at about 26 700 and 22 400 cm^{-1}.[50] Currently, it is not known whether this intensity loss arises from the actual hydrolysis of $[Cu_2(\mu\text{-}O)]^{2+}$ (inversion of eqn (3.2)) or whether it is merely a consequence of the H_2O adsorption itself. If the latter is the

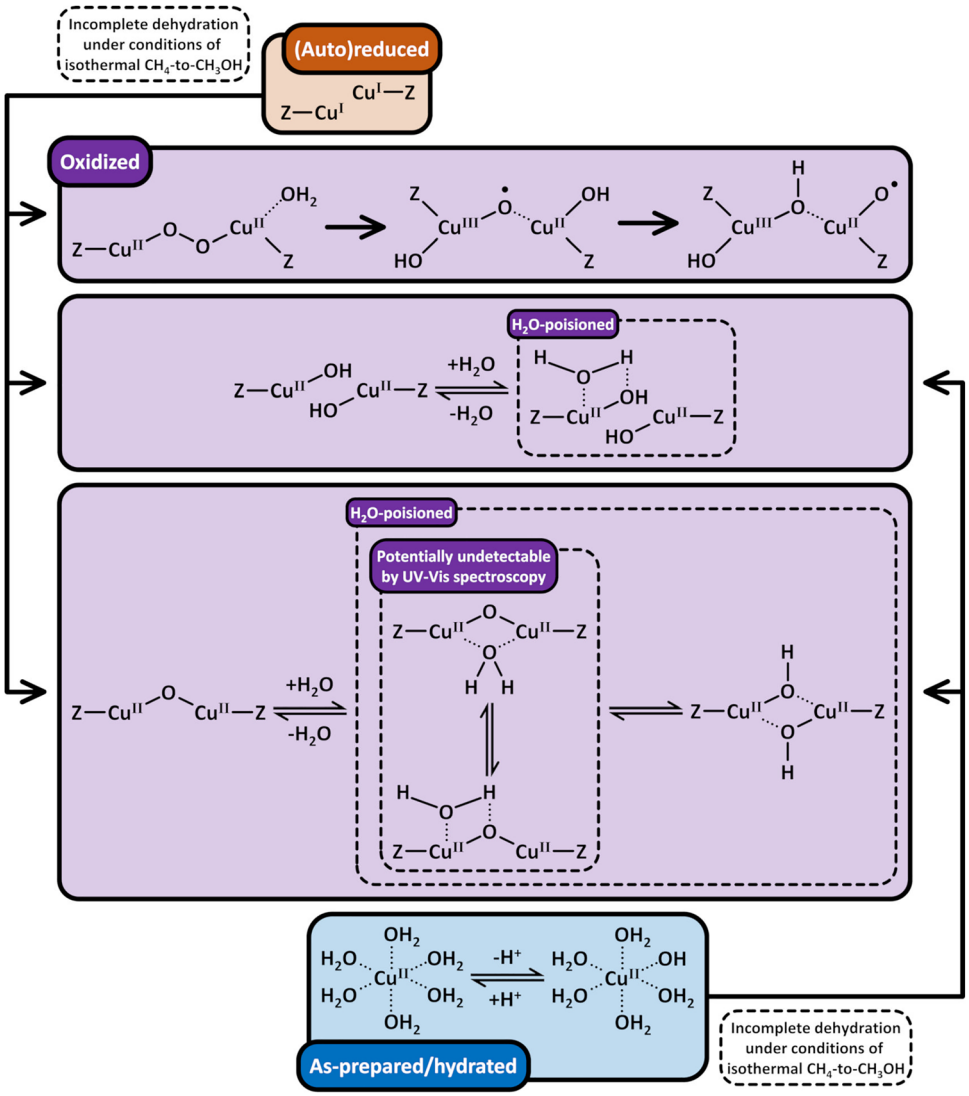

Scheme 10 Formation of $[Cu_2(\mu\text{-}O)(OH)_2]^{2+}$, $[(HO)Cu(\mu\text{-}OH)Cu(O)]^{2+}$, $[CuOH]^+/[CuOH]^+$, and $[Cu_2(\mu\text{-}O)]^{2+}$ (violet background) in O_2 under the conditions of isothermal CH_4 partial oxidation. $[Cu_2(\mu\text{-}O)(OH)_2]^{2+}$ is generated *via* multiple intramolecular H atom transfers in $[Cu_2(trans\text{-}\mu\text{-}1,2\text{-}O_2)(H_2O)]^{2+}$, which, itself arises from the interaction of Cu^+ (brown background) with O_2 and H_2O. A plausible mechanism for $[Cu_2(trans\text{-}\mu\text{-}1,2\text{-}O_2)(H_2O)]^{2+}$ formation in as-prepared/hydrated Cu–zeolites has yet to be identified. In contrast, $[CuOH]^+/[CuOH]^+$ and $[Cu_2(\mu\text{-}O)]^{2+}$ may evolve in both as-prepared/hydrated and (auto)reduced materials. Owing to the lower activation temperatures, the materials are not fully dehydrated, resulting in the adsorption of H_2O on the Cu-oxo active sites. The ligation by H_2O poisons the oxygenated Cu(II) centers and may obscure the characteristic LMCT feature of $[Cu_2(\mu\text{-}O)]^{2+}$ in the UV-Vis spectra. $[Cu_2(\mu\text{-}OH)_2]^{2+}$ does not belong to the group of oxygenated Cu(II) species that are undetectable by UV-Vis spectroscopy as it features an $(OH^-)_{ef} \rightarrow Cu(II)$ LMCT transition at 32 000–30 000 cm^{-1}.[133,144] Notably, the development of this band at the expense of the characteristic LMCT signal of $[Cu_2(\mu\text{-}O)]^{2+}$ upon hydration has not been observed so far.[50,80,207] Dotted bonds correspond to dative interactions. The term "Z" describes the negatively charged zeolite lattice.

case, virtually intact $[Cu_2(\mu\text{-}O)]^{2+}$ centers could well be present after calcination at 473 K but remain undetectable by UV-Vis spectroscopy due to the high amount of residual H_2O, emerging from the incomplete dehydration of the material. The potential generation of $[Cu_2(\mu\text{-}O)]^{2+}$ throughout activation of as-prepared/hydrated and (auto)reduced Cu–zeolites in O_2 under the conditions of isothermal CH_4 partial oxidation is illustrated in Scheme 10. The poisoning of $[Cu_2(\mu\text{-}O)]^{2+}$ by adsorption of H_2O as well as the resulting adsorption complexes, which are characterized by a masked $O_{ef} \rightarrow Cu(II)$ LMCT transition, are also shown.

An interesting proposal concerning the formation of dimeric Cu(II) active species in partially hydrated Cu–zeolites has been reported by Yumura *et al.*, who studied the interaction of O_2 and H_2O with reduced Cu-MFI using DFT.[208] According to these authors, the adsorption of O_2 and H_2O on Cu(I) ions, situated in the 10-MR and positioned in a 3NN arrangement, yields $[Cu_2(trans\text{-}\mu\text{-}1,2\text{-}O_2)(H_2O)]^{2+}$ (eqn (4.19) and Scheme S1r). The latter is transformed into $[Cu_2(trans\text{-}\mu\text{-}1,2\text{-}OOH)(OH)]^{2+}$ (Scheme S1s) *via* H atom transfer from the H_2O ligand onto the bridging O_2 moiety. Following another H atom transfer and a simultaneous O-OH bond cleavage, a $[Cu_2(\mu\text{-}O)(OH)_2]^{2+}$ (Scheme S1t) intermediate is

generated, which further converts into $[(HO)Cu(\mu\text{-}OH)Cu(O)]^{2+}$ (Scheme S1u).

$$2Cu^{+} + O_2 + H_2O \rightarrow [Cu_2(\textit{trans}\text{-}\mu\text{-}1,2\text{-}O_2)(H_2O)]^{2+} \rightarrow [Cu_2(\textit{trans}\text{-}\mu\text{-}1,2\text{-}OOH)(OH)]^{2+} \rightarrow [Cu_2(\mu\text{-}O)(OH)_2]^{2+} \rightarrow [(HO)Cu(\mu\text{-}OH)Cu(O)]^{2+} \quad (4.19)$$

The entire reaction pathway is endothermic by $\sim$15 kJ mol^{-1} relative to the initial $[Cu_2(\textit{trans}\text{-}\mu\text{-}1,2\text{-}O_2)(H_2O)]^{2+}$ complex. Notably, spin density calculations indicated that the bridging O in $[Cu_2(\mu\text{-}O)(OH)_2]^{2+}$ and the terminal O in $[(HO)Cu(\mu\text{-}OH)Cu(O)]^{2+}$ exhibit a radical character, whereas the two Cu centers in each complex adopt a mixed +3/+2 valence state. Owing to the presence of O radicals in both structures, they can participate in HAA from CH_4 with activation energies in the range of 33–44 kJ mol^{-1}. The transformation of Cu(I) and O_2 into $[Cu_2(\mu\text{-}O)(OH)_2]^{2+}$ and $[(HO)Cu(\mu\text{-}OH)Cu(O)]^{2+}$ in reduced Cu–zeolites represents a plausible route for the generation of dimeric oxygenated Cu(II) active sites, which accounts for the probable interaction of the Cu-oxo center with residual H_2O. Nevertheless, it is important to emphasize that this reaction scheme cannot simply be extended to the activation of as-prepared/hydrated materials, since there is no reasonable pathway for $[Cu_2(\textit{trans}\text{-}\mu\text{-}1,2\text{-}O_2)(H_2O)]^{2+}$ generation starting from $[Cu(H_2O)_6]^{2+}$ and $[Cu(OH)(H_2O)_5]^{+}$ (see Section 3). This paradigm is also highlighted in Scheme 10. Thus, further research is required to assess the possibility of the formation of di- and trimeric Cu-oxo centers under the activation conditions of isothermal CH_4 hydroxylation.

4.3.2 Development of Cu(II) sites during continuous CH_4-to-CH_3OH conversion, influence of process parameters, and long-term stability. Several Cu–zeolites have demonstrated a sustained performance in continuous CH_4-to-CH_3OH conversion over prolonged operation periods.[13,209–213] For example, Narsimhan *et al.* exposed $Cu_{0.37}MFI_{13.6}$ to a 2400 mL g_{ZEO}^{-1} h^{-1} stream of 981 mbar CH_4, 32 mbar H_2O, and 0.025 mbar O_2 at 483 K and observed a steady CH_3OH productivity of 0.88 $\mu mol_{CH_3OH}/g_{ZEO}^{-1}$ h^{-1} for up to 108 h.[209] A CH_3OH selectivity of 71% was reached, but the CH_4 conversion equaled to just 0.0014%. A noticeable increase in CH_4 conversion to 0.06% was reported by Hirayama *et al.* during the interaction of $Cu\text{–}CHA_{10.0}$ with a 120 010 mL g_{ZEO}^{-1} h^{-1} stream of 486 mbar CH_4, 0.08 mbar H_2O, 20 mbar O_2, and 507 mbar N_2 at 573 K.[211] This resulted in a steady CH_3OH output of 366 μmol_{CH_3OH} g_{ZEO}^{-} h^{-1} for 24 h, albeit at a significantly reduced CH_3OH selectivity of only 22%, thereby exemplifying the strict selectivity-conversion limit in catalytic CH_4 partial oxidation (see Section 2.3).[12,81–84] Notwithstanding the intrinsic restriction of the thermodynamically[214] and kinetically[215] favorable CH_4 overoxidation on the CH_3OH productivity, these results emphasize that a constant amount of oxygenated Cu(II) active sites can continuously be (re-)generated in an $O_2/CH_4/H_2O$ stream.

No consensus concerning the influence of the O_2 partial pressure on the performance of Cu–zeolites in catalytic CH_4-to-CH_3OH conversion has been reached yet. Narsimhan *et al.* varied the O_2 partial pressure between 0.025 and 2.4 mbar during continuous CH_4 hydroxylation by $Cu_{0.37}MFI_{13.6}$ at 483 K and determined that the reaction is zero order in O_2.[209] A similar result has been reported by Dinh *et al.*, who employed $Cu_{0.22}CHA_{23.0}$ in catalytic CH_4 partial oxidation at 0.08–0.87 mbar O_2 and 543 K.[212] On the contrary, Hirayama *et al.* observed a decrease in the CH_3OH production rate from 376 to 322 μmol_{CH_3OH} g_{ZEO}^{-1} h^{-1} upon increasing the O_2 partial pressure from 9 to 37 mbar during continuous CH_4-to-CH_3OH conversion by $Cu\text{–}CHA_{10}$ at 573 K.[211] Currently, it is not clear whether these variations arise from differences in the mechanism of the Cu(II) active site formation or the markedly contrasting reaction conditions. Nevertheless, the zero or even negative order dependency of O_2 on the CH_3OH production rate clearly highlights that the generation of oxygenated Cu(II) active species is not the rate-determining step in catalytic CH_4 partial oxidation.[212] As addressed in Section 4.2.4, this correlates well with the fact that the formation of $[Cu_2(\mu\text{-}O)]^{2+}$ during the activation of (auto)reduced Cu–zeolites in non-isothermal CH_4 hydroxylation proceeds at a high rate.[127,136]

The development of Cu-oxo active sites under the conditions of catalytic CH_4 hydroxylation remains poorly understood. Narsimhan *et al.* exposed (auto)reduced $Cu_{0.37}MFI_{13.6}$ to an $O_2/CH_4/H_2O$ feed and observed that the onset of steady state CH_3OH production was preceded by an initial induction period of $\sim$190 min.[209] This behavior was attributed to the H_2O-induced rearrangement of hydrated Cu(I) into the Cu-oxo active site.[209,212] According to Narsimhan *et al.*, this Cu(II) active species does not correspond to $[Cu_2(\mu\text{-}O)]^{2+}$, as complementary UV-Vis spectra collected throughout the induction period did not display a pronounced LMCT band at $\sim$22 700 cm^{-1}. Nevertheless, considering the strong impact of H_2O on the intensity of this band (see Sections 4.3.1 and 10.3), caution should be warranted when using the presence of this feature to assess the existence of $[Cu_2(\mu\text{-}O)]^{2+}$ under the conditions of continuous CH_4-to-CH_3OH conversion. In a subsequent study by the same research group, $[Cu_2(\mu\text{-}O)]^{2+}$ was identified as the Cu(II) active site for catalytic CH_4 partial oxidation in Cu–CHA by analysis of the FT-EXAFS spectrum collected at 543 K under steady state CH_3OH production.[212] Similar to their previous work, the perpetual generation of the Cu(II) dimer was proposed to occur *via* the interaction of O_2 with mobile hydrated Cu(I) ions, which are capable of dynamically migrating between the Al T-sites. The necessary charge balancing for the transfer of Cu(I) from one ion exchange position to the other was suggested to proceed *via* a simultaneous H_2O-assisted transfer of H^+ co-cations. At a sufficiently low Si/Al ratio and in the absence of co-cations that permanently block the Al T-sites (*e.g.* Na^+ or NH_4^+), this mechanism enables the transfer of Cu(I) throughout the entire framework, thereby facilitating the evolution of $[Cu_2(\mu\text{-}O)]^{2+}$ even in materials featuring a low Cu content. Whether the actual generation of $[Cu_2(\mu\text{-}O)]^{2+}$ proceeds *via* one of the pathways depicted by eqn (4.7)–(4.10) or (4.12)–(4.14) remains a matter of debate. A different hypothesis regarding the nature and formation mechanism of the Cu-oxo active site in $Cu\text{–}MOR_{10.0}$ for continuous CH_4-to-CH_3OH conversion has been presented by Ohyama *et al.*[210] These authors collected the XANES spectrum of $Cu\text{–}MOR_{10.0}$ after equilibration in an O_2/H_2O and $O_2/CH_4/H_2O$

stream at 573 K and computed the corresponding difference spectrum. This difference spectrum was compared to that obtained using simulated XANES spectra representing different Cu(II) and Cu(I) structural motifs. Based on this comparison, Ohyama *et al.* proposed that the oxygenated Cu(II) active site corresponds to a hydrated $[Cu_2(\mu\text{-}1,2\text{-}O_2)(OH)_2(H_2O)_2]$ (Scheme S1v) complex, which develops *via* interaction of O_2 with diffusion-paired mobile $[Cu(OH)(H_2O)]$ (eqn (4.20) and Scheme S1w).

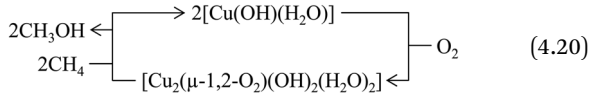

(4.20)

Notably, these Cu species are neutrally charged and fully detached from the framework, thereby functioning as a quasi-homogeneous catalyst within a zeolitic host, which is reminiscent of the NH_3-mobilized Cu centers in NH_3-SCR.[216,217] Nevertheless, a pathway for the generation of $[Cu(OH)(H_2O)]$ was not provided, and it is not clear how the Al T-sites are charge-balanced. It could be envisioned that $[Cu(OH)(H_2O)]$ is formed *via* the reaction of Cu(I) with H_2O, yielding H^+ as a byproduct to balance the charge of the Al T-site, though this remains purely speculative.

Finally, many mechanistic pathways dealing with the formation of oxygenated Cu(II) active sites during catalytic CH_4 partial hydroxylation postulate the involvement of hydrated mobile Cu(I) ions.[210,212] However, Cu(I)-aqua complexes are not stable and may disproportionate into metallic Cu and hydrated Cu(II) due to the larger hydration energy and higher CN of $[Cu(H_2O)_6]^{2+}$ relative to $[Cu(H_2O)_2]^+$.[218–221] Instead, the mobile Cu(I) species may correspond to bare Cu(I) ions, which are capable of migrating through the zeolite lattice in the absence of any ligands.[103,222] This has been demonstrated by Andersen *et al.*, who monitored the dehydration of $Cu_{0.48}CHA_{15.1}$ during He treatment *via* simultaneous XRPD and XANES spectroscopy.[103] Upon (auto)reduction of the material at temperatures above 636 K, Rietveld analysis of the corresponding XRPD patterns revealed a redistribution of Cu from the 8-MR to the 6-MR, indicating that Cu(I) could be dynamically migrating between ion exchange positions. Whether this process is relevant for the evolution of oxygenated Cu(II) species under conditions of continuous CH_4-toCH_3OH conversion, particularly concerning the migration timescale, remains an open question.

5. Usage of N_2O in chemical looping and continuous CH_4 hydroxylation for the formation of active Cu(II) species

5.1 Formation of Cu(II) sites using N_2O during the stepwise CH_4-to-CH_3OH conversion *via* looping

Prior to the usage of N_2O as an oxidizing agent for the formation of Cu-oxo active sites for CH_4 partial oxidation, the interaction of N_2O with Cu–zeolites was investigated in the context of the catalytic N_2O decomposition reaction.[133,145,207,223] Consequently, the oxidation of Cu(I) to Cu(II) by N_2O has been studied far earlier than its direct application in the CH_4-to-CH_3OH conversion.

5.1.1 Dimeric sites. The first definite characterization of a Cu(II) active site capable of abstracting an O atom from N_2O was achieved by Groothaert *et al.* with $Cu_{0.58}MFI_{31.0}$.[133,145] *In situ* UV-Vis spectra collected during N_2O exposure at 773 K revealed the emergence of an intense LMCT band at $\sim$22 700 cm^{-1} and a weaker LMCT band at $\sim$30 000 cm^{-1}, initially assigned to a $[Cu_2(\mu\text{-}O)_2]^{2+}$ center. The dimeric nature of this oxygenated Cu(II) species was additionally confirmed by *in situ* EPR spectroscopy, which revealed that up to 81% of the existing Cu(II) centers were EPR silent due to antiferromagnetic coupling (see Section 3.1). The presence of $[Cu_2(\mu\text{-}O)_2]^{2+}$ was further rationalized by its ability to release O_2, thus serving as a potential Cu(II) active site for N_2O decomposition. Reducing the temperature from 773 to 673 K caused a decrease in both the N_2O conversion and the absorbance of the spectral feature at 22 700 cm^{-1}. Simultaneously, an increase of two signals centered at 30 000 and 13 000 cm^{-1}, corresponding to an $O_{fw} \rightarrow$ Cu(II) LMCT and d–d transition of partially hydrated Cu(II), respectively, was observed. This behavior was attributed to the formation of a $[Cu_2(\mu\text{-}O)]^{2+}$ core, which was postulated to be an intermediate of $[Cu_2(\mu\text{-}O)_2]^{2+}$. The authors suggested that below 773 K, the N_2O decomposition reaction proceeds in two steps:

$$2Cu^+ + N_2O \rightarrow [Cu_2(\mu\text{-}O)]^{2+} + N_2 \quad (5.1)$$

$$[Cu_2(\mu\text{-}O)]^{2+} + N_2O \rightarrow [Cu_2(\mu\text{-}O)_2]^{2+} + N_2 \quad (5.2)$$

The first step would involve the generation of $[Cu_2(\mu\text{-}O)]^{2+}$ in a two-electron redox process *via* an O^{2-} transfer to a Cu(I) pair and the simultaneous release of N_2 (eqn (5.1)). The authors further suggested that the subsequent transformation of $[Cu_2(\mu\text{-}O)]^{2+}$ into $[Cu_2(\mu\text{-}O)_2]^{2+}$ (eqn (5.2)) is unfavorable at temperatures below 673 K, leading to an accumulation of the former Cu-oxo species at lower temperatures.

Following the initial identification of $[Cu_2(\mu\text{-}O)_2]^{2+}$ in Cu-MFI, *in situ* UV-Vis spectroscopy revealed that the intensity of the LMCT band at 22 700 cm^{-1} gradually decreased during interaction with CH_4, demonstrating the ability of this Cu(II) species to activate CH_4.[7] Woertink *et al.* employed Raman spectroscopy, using a laser with an appropriate wavelength to enhance the vibrations of this specific Cu(II) center, and identified both a pronounced ν_{sym}(Cu–O) at 456 cm^{-1} and a less intense ν_{asym}(Cu–O) at 870 cm^{-1}, revealing that the Cu(II) active site previously assumed to be a $[Cu_2(\mu\text{-}O)_2]^{2+}$ species (*vide supra*) actually corresponds to a $[Cu_2(\mu\text{-}O)]^{2+}$ center.[66] Normal coordinate analysis (NCA) of these vibrations highlighted that the Cu–O–Cu angle in $[Cu_2(\mu\text{-}O)]^{2+}$ is 140°. According to the authors, such a wide angle excludes the introduction of a second bridging O_{ef} atom, as would be necessary to form the $[Cu_2(\mu\text{-}O)_2]^{2+}$ site. DFT calculations suggested that the $[Cu_2(\mu\text{-}O)]^{2+}$ moiety is located within the 10-MR of MFI, with the two Al T-sites being separated by two intermediate Si T-sites. The assignment was based on a comparison of experimentally and theoretically determined geometric and electronic properties, revealing very similar features such as comparable Cu–O–Cu angles (138° theoretical *vs.* 140° experimental). Analyzing materials with various Cu/Al ratios revealed that the spectroscopic features of $[Cu_2(\mu\text{-}O)]^{2+}$ became more

prevalent in samples characterized by a higher Cu loading.[136] This is quite intuitive, as the formation of a $[Cu_2(\mu\text{-}O)]^{2+}$ active site requires two Cu(I) centers in close proximity to each other.

Further work has demonstrated that the $[Cu_2(\mu\text{-}O)]^{2+}$ motif may be present in multiple other zeolite topologies besides Cu-MFI, such as Cu–MOR[51,68] and Cu–CHA.[194] However, dependent on the topology of the zeolitic host, distinct differences in the geometric and electronic properties of the $[Cu_2(\mu\text{-}O)]^{2+}$ species have been shown to exist. Even within the same zeolite framework, slight variations in the geometric configuration of the $[Cu_2(\mu\text{-}O)]^{2+}$ center have been observed. Vanelderen *et al.* have shown that upon exposure of (auto)reduced $Cu_{0.43}MOR_{5.0}$ to N_2O, a LMCT band centered around 22 200 cm^{-1} emerged.[51] According to the authors, the band at 22 200 cm^{-1} can be deconvoluted into two separate LMCT bands at 21 900 and 23 100 cm^{-1}, suggesting that two $[Cu_2(\mu\text{-}O)]^{2+}$ species distinguishable from each other may simultaneously be present in Cu–MOR. Raman spectroscopy revealed that although both Cu(II) species formally correspond to $[Cu_2(\mu\text{-}O)]^{2+}$, they exhibit different ν_{asym}(Cu–O) and ν_{sym}(Cu–O) values. NCA highlighted that the two $[Cu_2(\mu\text{-}O)]^{2+}$ centers exhibit slightly different Cu–O–Cu angles (137° *vs.* 141°) and Cu–O bond strengths. Notably, these two Cu(II) sites are characterized by a substantially different reactivity toward CH_4; the Cu(II) species featuring a smaller Cu–O–Cu angle of 137° and a LMCT band at 21 900 cm^{-1} reduced less rapidly compared to the Cu(II) center characterized by the LMCT band at 23 100 cm^{-1} and the larger Cu–O–Cu angle of 141°. DFT models based on the experimental data suggested that two distinct $[Cu_2(\mu\text{-}O)]^{2+}$ sites are located at different positions within the framework: the less reactive Cu(II) species at the intersection of the side pockets and the 12-MR channels, and the more reactive Cu(II) center in the intersections of the side pockets and the 8-MR channels (Scheme 1).[51,69] The difference in reactivity of the two Cu(II) species toward HAA from CH_4 has been suggested to originate from the zeolite framework itself, with a confinement of CH_4 within the smaller side pockets of MOR suggested to lower the activation enthalpy required for HAA.[51,69] Recently, Plessers *et al.* identified a third $[Cu_2(\mu\text{-}O)]^{2+}$ site after interaction of (auto)reduced $Cu\text{–}MOR_{9.0}$ with N_2O.[68] Alternation of both the Cu loading (Cu/Al ratio between 0.09 and 0.45) as well as the nature of the alkali co-cation employed to further charge balance the zeolite framework resulted in a variation of the ratio of different Cu(II) species, *i.e.*, Cu^{2+} *vs.* $[CuOH]^+$ *vs.* $[Cu_2(\mu\text{-}O)]^{2+}$, in the studied Cu–MOR samples. The newly identified $[Cu_2(\mu\text{-}O)]^{2+}$ species exhibits a LMCT band at ~22 300 cm^{-1} after N_2O exposure. NCA of the ν_{sym}(Cu–O) and ν_{asym}(Cu–O) vibration of the new $[Cu_2(\mu\text{-}O)]^{2+}$ moiety revealed that its Cu–O–Cu angle is 127°, and therefore significantly smaller than the Cu–O–Cu angles determined for the other two identified $[Cu_2(\mu\text{-}O)]^{2+}$ centers in Cu–MOR (*vide supra*).[51,68] In Cu–CHA, Rhoda *et al.* revealed a further $[Cu_2(\mu\text{-}O)]^{2+}$ site by exposing (auto)reduced $Cu_{0.29}CHA_{15.7}$ to N_2O at 823 K, leading to the emergence of an intense LMCT band at 22 400 cm^{-1} as well as a weaker band at 6200 cm^{-1}, as illustrated in Fig. 8.[194] The reason for the high N_2O treatment temperature was not discussed in detail, which is surprising given that N_2O can already decompose

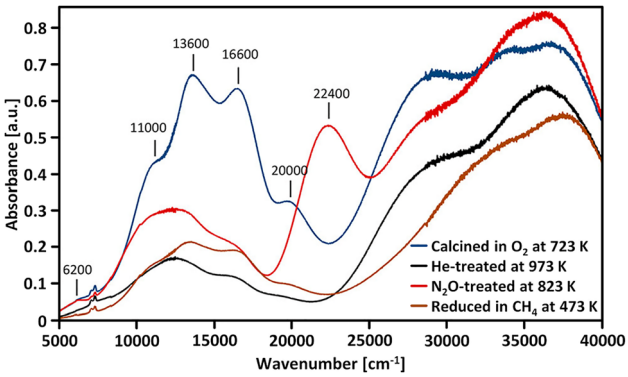

Fig. 8 UV-Vis spectra of $Cu_{0.29}CHA_{15.7}$ collected at ambient temperature after calcination in O_2 at 723 K (blue), (auto)reduction in He at 973 K (black), N_2O treatment at 823 K (red), and interaction with CH_4 at 473 K (brown). Adapted from ref. 194 with permission from the American Chemical Society (Copyright 2021).

into N_2 and O_2 at ~623 K in the case of $Cu_{0.4}CHA_{13.0}$.[13] As depicted in Fig. 8, exposure of activated $Cu_{0.29}CHA_{15.0}$ to CH_4 at 473 K induced a significant decrease in intensity of the LMCT band at 22 400 cm^{-1}, which is indicative of the reduction of $[Cu_2(\mu\text{-}O)]^{2+}$ to Cu(I). The combination of Raman spectroscopy of the N_2O-activated sample (ν_{sym}(Cu–O) = 581 cm^{-1}, ν_{asym}(Cu–O) = 837 cm^{-1}) with NCA revealed that the Cu–O–Cu angle corresponds to 120°. DFT calculations highlighted that a $[Cu_2(\mu\text{-}O)]^{2+}$ site with such a small angle can only be stabilized across the 8-MR of Cu–CHA, with three Si T-sites separating the Al T-sites. The bridging O_{ef} atom was determined to point out of the 8-MR and into the CHA cages themselves (Scheme 1).

A further factor affecting the performance of $[Cu_2(\mu\text{-}O)]^{2+}$ in C–H bond activation was suggested to stem from the Cu–O–Cu angle itself, as elucidated by Mahyuddin *et al.*[157] The authors suggested that a smaller Cu–O-Cu angle would result in greater overlap of the Cu d-orbitals, leading to a lowering of the energy of the acceptor orbital involved in C–H bond activation.

These discussed works show that a range of distinct $[Cu_2(\mu\text{-}O)]^{2+}$ centers in various Cu–zeolites with different topologies can be formed *via* the oxidation of Cu(I) pairs with N_2O.[66,68,124,194] Tsai *et al.* investigated this process primarily using DFT calculations.[124] Building on the previously determined geometric and spectroscopic features of $[Cu_2(\mu\text{-}O)]^{2+}$ in Cu-MFI,[66] the authors assessed which Cu(I) pair sites within the 10-MR of MFI would enable a low-barrier O^{2-} transfer from N_2O. A systematic variation of both the O_{fw}–Cu–O_{fw} bite angles, the CN (two and three) from the lattice to Cu(I), as well as the nature of the central atom (Si or Al) of the coordinating T-site, was performed. Two factors were determined to significantly increase the thermodynamic stability of a given Cu(I) pair: A linear O_{fw}–Cu–O_{fw} bite angle close to 180° and coordination to the O_{fw} atoms of Al T-sites instead of Si T-sites. The most stable Cu(I) pair configuration that is experimentally feasible exhibited two-coordinate Cu centers with an O_{Si}–Cu–O_{Al} bite angle of ~149° and a Cu(I)–Cu(I) distance of 4.17 Å, thereby minimizing electrostatic repulsion between the two Cu(I) ions. The $[Cu_2(\mu\text{-}O)]^{2+}$ species corresponding to a Cu(I) pair has a

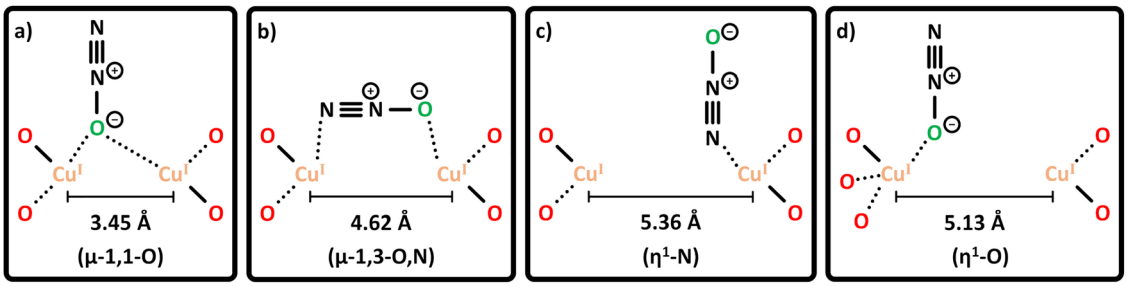

Fig. 9 Potential binding configurations of N_2O on Cu(I) pairs characterized by different Cu–Cu distances and coordination modes to the zeolite lattice. Structures (a)–(c) describe the interaction of N_2O with a Cu(I) pair, which features a Cu–Cu distance of 4.17 Å prior to N_2O adsorption. Each Cu(I) ion is coordinated by two O_{fw} atoms that are affiliated with an Al and Si T-site. In structure (d), the Cu–Cu distance before N_2O adsorption is 5.85 Å. One of the involved Cu(I) ions is coordinated by three O_{fw} atoms, two belonging to a single Al T-site, whereas the third O_{fw} atom originates from a Si T-site. Adapted from ref. 124 with permission from the American Chemical Society (Copyright 2014).

calculated Cu–O–Cu angle of 135°, and therefore is very similar to the value of 139° observed experimentally.[224] Both the calculated Raman vibrations (451 cm^{-1} and 842 cm^{-1}) and LMCT band (22 926 cm^{-1}) were very close to the experimentally obtained value by Woertink *et al.* (*vide supra*).[224]

Using the determined structure of the energetically favorable Cu(I) pair, three distinct N_2O binding modes were evaluated *via* DFT: η^1-N, μ-1,1-O, and μ-1,3-O,N, as depicted in Fig. 9a–c; all in the closed-shell singlet ground state. Notably, the η^1-N and μ-1,3-O,N binding modes exhibited an apparent activation energy of 250 and 21 kJ mol^{-1}, respectively, which is far from the experimentally determined value of 8 ± 2 kJ mol^{-1} for $[Cu_2(\mu\text{-}O)]^{2+}$ formation. Remarkably, the calculated value in the case of the μ-1,1-O binding mode (8 kJ mol^{-1}) matched the experiment well (Fig. 9a). The true activation energy for a μ-1,1-O binding mode was estimated at 46 kJ mol^{-1}. It should be noted that Mahyuddin *et al.* also investigated the μ-1,1-O binding mode on a Cu(I) pair in MFI, though determining an even lower true activation energy of ~26 kJ mol^{-1} for N–O bond cleavage.[154] These results indicate that the exact configuration of N_2O interaction with both Cu(I) centers is the determinative factor for the necessary activation energy, with non-bridging binding modes being characterized by a particularly high activation barrier. This, therefore, also directly influences the permittable Cu–Cu distance a Cu(I) pair may have for N_2O activation. Tsai *et al.* determined that a Cu(I)–Cu(I) distance above 4.17 Å restricts μ-1,1-O binding mode, hence prohibiting N_2O activation (Fig. 9d).[124]

The reaction was suggested to be initiated *via* a one-electron transfer from one of the Cu(I)'s to a π* orbital of N_2O, leading to a partial breaking of the N–O bond. This is followed by a further electron transfer from the second Cu(I), resulting in a cleavage of the N–O bond and formation of N_2 and $[Cu_2(\mu\text{-}O)]^{2+}$. The spin density distribution revealed that an electron is predominantly transferred from one of the two Cu(I)'s, thereby highlighting that it is a stepwise process, itself facilitated by the bent N–N–O geometry of 143° at the transition state (TS), stabilizing the π* and enhancing overlap with the d orbitals. Additionally, it is worth mentioning that during oxidation, a change in the coordination of Cu to the zeolite lattice occurs as well. Both Cu(I) centers are each coordinated to two O_{fw} separated by both an Al T-site and a Si T-site, while both of the resulting Cu(II)'s of $[Cu_2(\mu\text{-}O)]^{2+}$ are coordinated to two O_{fw} solely separated by one Al T-site.

Mahyuddin *et al.* investigated the same three proposed N_2O binding modes (Fig. 9a–c) *via* DFT calculations on a Cu(I) pair in Cu-AEI, with the site modelled to be located in the 8-MR of the zeolite.[157] N_2O would initially adsorb on one of the two Cu(I) centers with a binding energy of −25 to −47 kJ mol^{-1} (without and with dispersion correction). The μ-1,1-O binding mode (Fig. 9a) of N_2O was determined to be the only feasible pathway for an oxo-transfer from N_2O, which is highlighted in Scheme 11, with a determined true activation energy of ~5 to 8 kJ mol^{-1}, without and with dispersion correction, respectively, in the closed-shell singlet state.[157] This value of 8 kJ mol^{-1} for Cu-AEI[157] is significantly lower than that obtained for Cu-MFI by both Mahyuddin *et al.*[154] and Tsai *et al.*[124] (*vide supra*). Zhao *et al.* calculated an activation energy of 75 kJ mol^{-1} for the activation of a Cu(I) pair *via* the μ-1,1-O binding mode in Cu–MOR.[164] This value was determined for a $[Cu_2(\mu\text{-}O)]^{2+}$ species located in the 12-MR of MOR. The location of the Cu(I) pair within a given zeolite, as well as the topology, will significantly influence the characteristics of it, as well as the $[Cu_2(\mu\text{-}O)]^{2+}$ resulting from said Cu(I) pair. Such is the case when comparing AEI and MFI; in the 8-MR of AEI, the Cu–Cu distance of the Cu(I) pair was determined to be only 2.7 Å, with the resulting $[Cu_2(\mu\text{-}O)]^{2+}$ species exhibiting a Cu–O–Cu angle of ~84° in comparison to ~135° in the case of Cu-MFI.[124,157] These effects also extend to the TS of N_2O oxidation, with the N–O bond length at the TS evaluated to be slightly shorter at ~1.2 Å in Cu-AEI than for Cu-MFI at ~1.46 Å.[124,157] This suggests that the necessary energy investments for an oxo-transfer to a Cu(I) pair, and thereby an oxidation and formation of $[Cu_2(\mu\text{-}O)]^{2+}$, may significantly depend on framework topology, as well as location within a given topology. This is analogous to the influence that framework topology may have on a $[Cu_2(\mu\text{-}O)]^{2+}$ sites ability for HAA from CH_4.

In the case of Cu-MFI, Tsai *et al.* elucidated that the N_2O activation of paired Cu(I) proceeds along the singlet potential energy surface (PES).[124] Although two singlet–triplet crossing points at 1.35 and 1.55 Å were identified during N–O bond elongation, the TS was located at the intermediate N–O distance of 1.46 Å. This would therefore result in a spin-crossover to a triplet state after reconstitution of the active site.

Mahyuddin *et al.* suggested the same for Cu-AEI, with the re-oxidation occurring in the singlet state, followed by a spin crossover to a triplet state. This triplet state however, is almost isoenergetic to the singlet state (see Section 4.1).[157] Heyer *et al.* further investigated the ground state of both $[Cu_2(\mu\text{-}O)]^{2+}$ in Cu-MFI as well as Cu–CHA using VTVH MCD spectroscopy and DFT calculations.[67] Cu-MFI was found to adopt a singlet ground state due to the parallel arrangement of the bidentate coordinating Al T-sites of the framework, thereby maximizing the superexchange interaction between the two half-filled Cu(II) 3d orbitals. This, however, stands in contrast to the theoretical works by Tsai *et al.*, which determined $[Cu_2(\mu\text{-}O)]^{2+}$ in Cu-MFI to be present in a triplet ground state.[124] In Cu–CHA instead, Heyer *et al.*[67] elucidated that the $[Cu_2(\mu\text{-}O)]^{2+}$ site adopts a triplet ground state due to the perpendicular orientation of the coordinating Al T-sites of the framework, leading to a low orbital overlap of the O-bridged half-filled Cu(II) 3d orbitals. A triplet ground state for the $[Cu_2(\mu\text{-}O)]^{2+}$ site has also been suggested for Cu–MOR by Zhao *et al.*, due to the singlet state being 40 kJ mol^{-1} less stable.[164] The reaction, however, proceeds on a singlet PES *via* a Cu(I) pair and N_2O.[164] The authors did not calculate the activation barrier for a Cu(I) pair and N_2O *via* a triplet PES due to the instability of said state, resulting in a much higher activation barrier than in the case of a singlet PES. This implies that a spin inversion will occur after the TS if the $[Cu_2(\mu\text{-}O)]^{2+}$ site has a triplet spin state.

Göltl *et al.* computationally investigated Cu–CHA for Si/Al > 8, with theoretically predicted phase diagrams being employed to examine a range of Al configurations inside CHA, with two Al T-sites either being in a 3NN or 4NN configuration, or one of the two Al T-sites located in adjacent 6-MR and 8-MR.[72] The authors examined the effect of temperature and partial pressure of N_2O on the stability of the species with different configurations of two Al T-sites. In the case of one or zero Al T-sites being present in the 6-MR, and therefore respectively the necessary other two or one Al T-sites located in the 8-MR, the $[Cu_2(\mu\text{-}O)_2]^{2+}$ species were present under all examined conditions, including at ambient temperature. If, however, two Al T-sites are allowed to be located in the same 6-MR, Cu(II) will be present in a hydrated state at ambient temperature. Higher temperatures and low N_2O partial pressures could result in Cu migration and the formation of Cu^{2+}, assumedly in the 6-MR. However, an increase in the partial pressure of N_2O restricts such changes in Cu(II) speciation and will lead to the formation of $[Cu_2(\mu\text{-}O)_2]^{2+}$ instead. For example, at the typical activation temperature of 723 K, a partial pressure of ~10 mbar N_2O would suffice for the formation of $[Cu_2(\mu\text{-}O)_2]^{2+}$. When, however, the model was restricted to certain Al configurations, the phase diagrams showed that both $[Cu_2(cis\text{-}\mu\text{-}1,2\text{-}O_2)]^{2+}$ and $[Cu_2(\mu\text{-}OH)_2]^{2+}$, as well as bare and hydrated Cu(II), could all potentially be the thermodynamically preferred sites, dependent on both N_2O partial pressure and temperature. As experimental verification, a UV-Vis spectrum of a $Cu_{0.41}CHA_{14.7}$ sample at ambient temperature, previously activated at 723 K in N_2O, was collected, exhibiting both d–d transitions at 13 400 cm^{-1} and a broad LMCT band between 29 000–37 000 cm^{-1}. A comparison to theoretically predicted spectra suggested that these bands could be attributed to the suggested $[Cu_2(\mu\text{-}O)_2]^{2+}$ species. While the authors' theoretical findings showed that $[Cu_2(\mu\text{-}OH)_2]^{2+}$ can only form under an O_2 and not N_2O atmosphere, Raman spectroscopy revealed a band at 615 cm^{-1} attributed to said species. The authors, however, performed their activation procedure at 723 K, a temperature where Cu–CHA has been shown to be able to decompose N_2O to O_2 and N_2,[13] which could cause the resulting O_2 to be responsible for the formation of $[Cu_2(\mu\text{-}OH)_2]^{2+}$. An explanation of why both species are able to exist simultaneously within CHA is, however, not present. Moreover, the source of H^+ necessary to form $[Cu_2(\mu\text{-}OH)_2]^{2+}$ remains to be clarified. In addition, it needs to be noted that Zhao *et al.* calculated that for Cu–MOR that an O insertion into $[Cu_2(\mu\text{-}O)]^{2+}$ *via* a second N_2O to form $[Cu_2(\mu\text{-}1,2\text{-}O_2)]^{2+}$, while being exergonic at a temperature of 523 K, presented an insurmountable activation barrier of 244 kJ mol^{-1}.[164]

The vast majority of studies investigating the dimeric structures have been conducted on (auto)reduced materials that have been treated under He at elevated temperatures, followed by an exposure to N_2O. An overview of the different starting conditions is provided in Scheme 11.[51,66,68,194] Examining if the $[Cu_2(\mu\text{-}O)]^{2+}$ active site can be formed from an as-prepared/hydrated state by N_2O exposure has not received much attention, with solely one examination having been performed by Ipek *et al.*[13] As-prepared/hydrated $Cu_{0.4}CHA_{12.0}$ was exposed to 30% N_2O/He at 543 K, leading to absorption features at both 23 100 and 21 000 cm^{-1}, attributed to different $[Cu_2(\mu\text{-}O)]^{2+}$ species. The authors further examined the CH_3OH productivity at 473 K of the same material in the chemical looping process, studying different activation temperatures by keeping the duration and the N_2O concentration constant. An increase in activation temperature from 473 to 723 K led to an increase in CH_3OH productivity from ~13 to 35 $\mu mol_{CH_3OH}\ g_{ZEO}^{-1}$. The authors also highlighted that at temperatures above 623 K N_2O decomposition occurs, which would result in a lower amount of potential active sites for HAA. However, it should be noted that since the CH_4 exposure was always conducted at 473 K, well below the temperature regime where N_2O decomposition occurs, any resulting Cu(I) may be expected to undergo a re-oxidation by N_2O during the cool down. The changes in productivity might therefore be more related to the preceding dehydration of the material at higher temperatures.

5.1.2 Trimeric sites. Kim *et al.*[21] suggested that heating of a hydrated $Cu_{0.4}MOR_{20.0}$ sample in N_2O leads to the formation of $[Cu_3(\mu\text{-}O)_3]^{2+}$ species. *In situ* UV-vis spectra collected during an activation procedure in N_2O up to 873 K revealed LMCT bands at 30 000, 34 000, and 39 000 cm^{-1}, all attributed to $[Cu_3(\mu\text{-}O)_3]^{2+}$. The activation temperature during N_2O exposure was shown to have a significant effect on the CH_3OH productivity, with an increase from ~30 to 97 $\mu mol_{CH_3OH}\ g_{ZEO}^{-1}$ when increasing the activation temperature from 673 to 873 K. A consecutive cycle with a N_2O activation at 873 K exhibited a similar productivity to the first cycle, as well as the presence of LMCT bands at 34 000–39 000 cm^{-1}, thereby showing that the $[Cu_3(\mu\text{-}O)_3]^{2+}$ species can be reconstituted from a reduced state (Scheme 11). A slight bathochromic shift of the band at

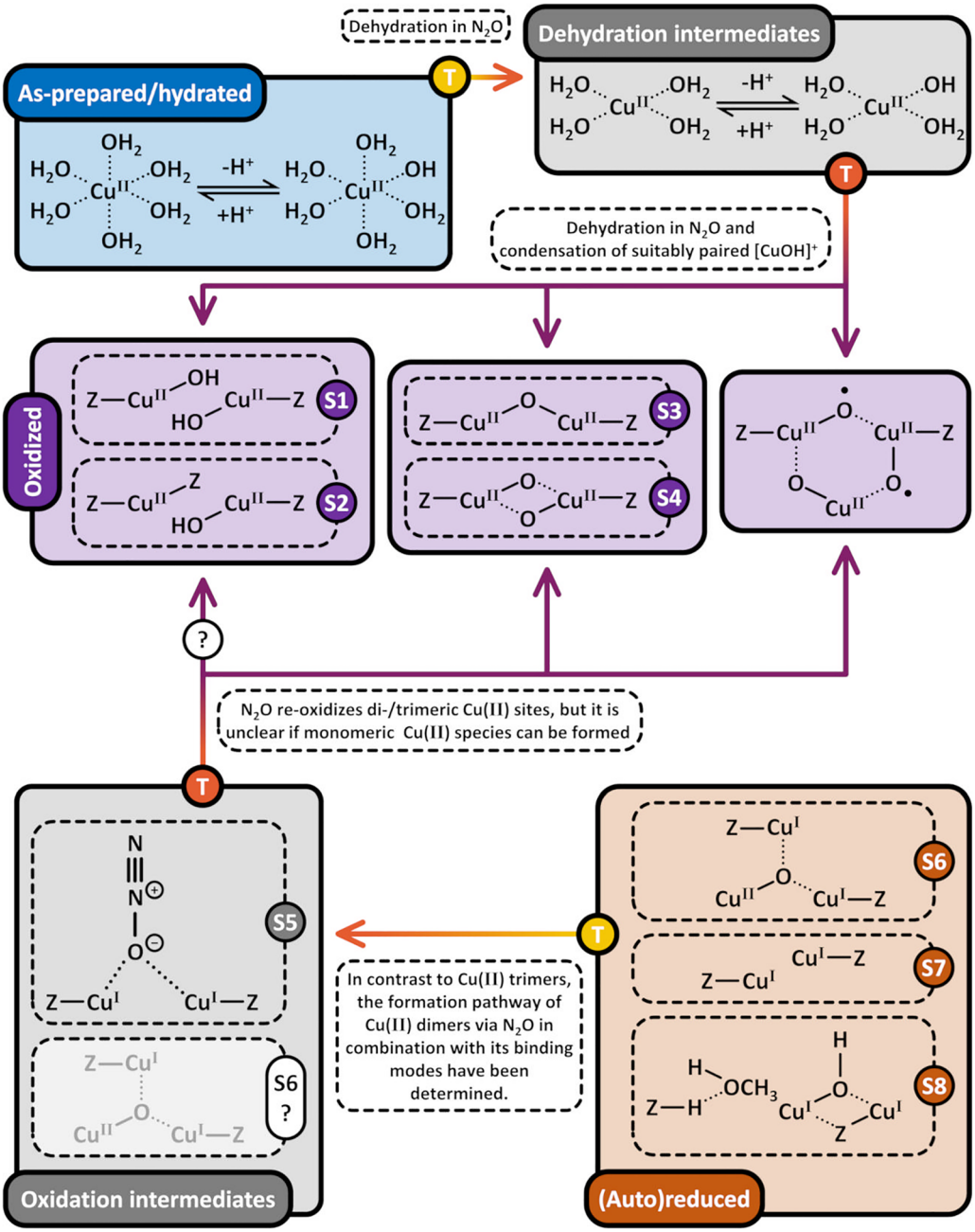

Scheme 11 Formation pathways of $[CuOH]^+$/$[CuOH]^+$ (S1), Cu^{2+}/$[CuOH]^+$ (S2), $[Cu_2(\mu\text{-}O)]^{2+}$ (S3), $[Cu_2(\mu\text{-}O)_2]^{2+}$ (S4), and $[Cu_3(\mu\text{-}O)_3]^{2+}$ (violet background) by treatment of as-prepared/hydrated (blue background) and (auto)reduced (brown background) Cu–zeolites with N_2O in the chemical looping process. The transformation of Cu(II)-aqua complexes into the Cu-oxo species proceeds *via* the dehydration intermediates $[Cu(H_2O)_4]^{2+}$ and $[Cu(OH)(H_2O)_3]^+$ (grey background). Interaction of N_2O with paired Cu(I) (S7) yields S3 and S4 *via* the adsorption intermediate (S5) (grey background). The reaction mechanism of $[Cu_3(\mu\text{-}O)_3]^{2+}$ generation starting from $[Cu_3(\mu\text{-}O)]^{2+}$ (S6) has not been investigated yet, and potentially involved intermediates are not known (structure with transparent overlay and marked with a question mark). Similarly, it is not clear whether monomeric Cu(II) species can be re-oxidized by treatment of (auto)reduced Cu–zeolites with N_2O, either from a state without a given H^+ source (S7) or with (S8) (pathway marked with a question mark). Dotted bonds correspond to dative interactions. The term "Z" describes the negatively charged zeolite lattice. The color gradient from yellow to violet of the different starting points and arrows indicates the progressively increasing temperature.

39 000 to 38 500 cm^{-1} was observed, suggesting that the LMCT band at 34 000 cm^{-1} was related to the $[Cu_3(\mu\text{-}O)_3]^{2+}$ site, with the other bands originating from inactive Cu-oxo clusters present in the material.

While the $[Cu_3(\mu\text{-}O)_3]^{2+}$ site may seemingly be generated from an as-prepared/hydrated state, Kim *et al.* suggested that during the activation procedure under N_2O, an initial dehydration would lead to a reduction of Cu(II) to Cu(I), as well as the

formation of square planar Cu(II). N_2O activation would then lead to the formation of $[Cu_3(\mu\text{-}O)_3]^{2+}$ from these intermediates. Experimental verification was delivered by first exposing $Cu_{0.4}MOR_{20.0}$ to N_2 at 723 K, leading to the appearance of a d–d transition at 16 700 cm^{-1}, attributed to square planar Cu(II). Exposure to N_2O at 523 K led to an increase in absorbance at 34 000 cm^{-1}, and disappearance of the feature at 16 700 cm^{-1}, attributed to square planar Cu(II) being incorporated into a $[Cu_3(\mu\text{-}O)_3]^{2+}$ species (Scheme 11). Therefore, while $[Cu_3(\mu\text{-}O)_3]^{2+}$ can be formed from an as-prepared/hydrated material, an initial (auto)reduction of a fraction of the Cu is necessary. Therefore $[Cu_3(\mu\text{-}O)_3]^{2+}$ will not be able to be formed directly from the hydrated as-prepared state. Similar suggestions were made by Ikuno *et al.* for $Cu_{0.31}MOR_{11.0}$.[19] While no spectroscopic characterization for the N_2O-activated material is shown, the obtained CH_3OH productivity of $Cu_{0.31}MOR_{11.0}$ is equivalent to the O_2-activated material over a range of activation temperatures (473–773 K), for which a detailed characterization of the active site has been performed. The formation of $[Cu_3(\mu\text{-}O)_3]^{2+}$ under O_2 exposure is discussed in greater detail in Section 4.2.2.

More definite characterizations of the $[Cu_3(\mu\text{-}O)_3]^{2+}$ active site formable by N_2O have, to our knowledge, only been performed in the case of Cu–MOR.[19,21] Whether this site is even able to be formed in other zeolitic frameworks is a matter of debate. Göltl *et al.*, for one, suggested that in the case of Cu–CHA of Si/Al > 8, trimeric species cannot be stabilized under any conditions in the course of N_2O treatment.[72]

5.1.3 Monomeric sites. While primarily examining the formation of $[Cu_2(\mu\text{-}O)_2]^{2+}$ sites (see Section 5.1.1), Göltl *et al.* provided direct spectroscopic evidence of $[CuOH]^+$ forming from an as-prepared/hydrated state by N_2O exposure.[72] Following an N_2O activation at 723 K of an as-prepared/hydrated $Cu_{0.41}CHA_{14.7}$, a UV-Vis spectrum collected at ambient temperature revealed a d–d transition at 11 500 cm^{-1}, attributed to a defect-bound $[CuOH]^+$. Plessers *et al.* delivered further evidence for both $[CuOH]^+$ and bare Cu^{2+} being able to form from an as-prepared/hydrated state by N_2O exposure. As-prepared/hydrated Cu–$MOR_{9.0}$ with Cu/Al ratios varying from 0.09–0.45, was exposed to N_2O at 523 K. EPR spectroscopy revealed spectroscopic fingerprints of both $[CuOH]^+$ and Cu^{2+}, with the fraction of $[CuOH]^+$ increasing with the Cu/Al ratio.

Examining if $[CuOH]^+$ can be re-constituted by oxidation with N_2O from a reduced Cu(I) state has not yet been clearly shown. $[CuOH]^+$ is typically suggested to be more resistant toward (auto)reduction in an inert atmosphere than $[Cu_2(\mu\text{-}O)]^{2+}$, necessitating the use of reducing agents such as CH_4.[62] By simply performing one reaction cycle using the looping procedure followed by an exposure of the material to N_2O, this question could easily be answered. However, such an examination is at this point lacking in the literature. Tsai *et al.*, however, suggested that any mononuclear Cu(I) site would be unable to be activated by N_2O, based on a very high activation energy due to the necessary η^1-O binding mode (Fig. 9d).[124] Such a binding mode would be necessary due to either a Cu(I) being completely isolated or sufficiently far (>5 Å) from another Cu(I), thereby excluding a bridged N_2O binding mode. In any case, a bridged binding mode would only allow for the re-oxidation of one Cu(I) to form $[CuOH]^+$, while HAA from CH_4 would necessitate two proximal $[CuOH]^+$. The determined activation energy for N_2O activation in the case of a Cu–Cu distance of ~5.13 Å, and therefore necessitating a terminal η^1-O binding mode over a single Cu(I), was determined to be ~67 kJ mol^{-1}. While being higher than the activation energy of N_2O activation *via* a Cu(I) pair (see Section 5.1.1), the value suggests that the reaction could be feasible at elevated temperatures.

Evidence for the involvement of monomeric Cu(I) species in N_2O decomposition suggests that these species can undergo reversible redox processes in the presence of N_2O. For example, Smeets *et al.* investigated N_2O decomposition over a range of Cu–zeolites (MOR, MFI, FER, BEA). At Cu/Al ≤ 0.23, almost all Cu was EPR visible, indicating an exclusively monomeric configuration. At elevated temperatures of 723–773 K, N_2O conversion was low (0–5%).[225] However, adding 0.1% NO to the feed increased N_2O conversion by ~12–20% for all Cu–zeolites examined, suggesting that monomeric Cu species can be activated under these conditions. Notably, above ~750 K, $Cu_{0.22}MFI_{12.0}$ began exhibiting intrinsic activity toward N_2O decomposition, achieving ~10% conversion at ~830 K.[207,225] It needs to be mentioned that the type of monomeric Cu(II) has not been revealed in this study (Scheme 11). Further, Fanning *et al.* performed extensive diffuse reflectance FTIR spectroscopy (DRIFTS) studies on $Cu_{0.55–0.6}$-$MFI_{10.7–13.5}$ to examine the Cu(II) species formed by N_2O oxidation of Cu(I).[226] At the initial stage, the materials were exposed to Ar at 773 K. In the case of $Cu_{0.6}MFI_{13.5}$, a hypsochromic shift of a band at ~930 to ~970 cm^{-1} was associated with the reduction of Cu(II) to Cu(I). Further evidence for the reduction of Cu(II) was provided by complementary EPR measurements, which showed that 96% of the signal intensity decreased during the pretreatment. The observation of CO in the DRFITS suggests that the primary origin of the reduction is the presence of carbonaceous species from the $Cu(CH_3COO)_2$ precursors. A bathochromic shift of the band at 970 to 930–910 cm^{-1} was observed after the exposure to N_2O at 583–643 K. This band was assigned to asymmetric framework vibrations perturbed by either $[CuOH]^+$ or $[CuO^\bullet]^+$, a species for which any definite characterization is lacking in the literature (see Section 3.2). However, it should be noted that the assignment of the 930–910 cm^{-1} bands to monomeric species is contested, as dimeric sites have been assigned to similar bands.[227] Further, this study suggests that the identified $[CuOH]^+$ species, or their precursors, are reducible during an inert gas treatment at 773 K, which stands in contrast to other literature.[42,62]

The potential source of the necessary H atom for the reconstitution of $[CuOH]^+$, as is the case for the formation of said species by O_2 oxidation in Section 4.2.2, remains unresolved. Fanning *et al.* therefore suggested that Cu(I) could be re-oxidized by N_2O, with a BAS or terminal Si–OH group donating a H atom for $[CuOH]^+$ formation (eqn (5.3)). Another feasible source could be the simultaneous conversion of a Cu(I) pair *via* both N_2O and H_2O, as depicted in eqn (5.4), which would therefore require a close proximity of the two Cu(I)'s. However, below a certain Cu–Cu distance, the more likely result would be

the formation of $[Cu_2(\mu\text{-}O)]^{2+}$ species, as discussed in Section 5.1.1 and depicted in eqn (5.1).

$$Cu^+ + N_2O + SiOH \rightarrow [CuOH]^+ + N_2 + SiO^\bullet \quad (5.3)$$

$$2Cu^+ + N_2O + H_2O \rightarrow 2[CuOH]^+ + N_2 \quad (5.4)$$

5.2 Formation of Cu(II) sites using N_2O during catalytic selective CH_4 oxidation

While the continuous CH_4-to-CH_3OH conversion using N_2O as an oxidant has received some attention and has been shown to be a plausible route, identification of the potential active sites responsible for HAA from CH_4 is often lacking. This is primarily due to many spectroscopic techniques not being able to derive the same amount of information in continuous *vs.* cyclic CH_4-to-CH_3OH conversion. A prime example of this is UV-Vis spectroscopy. As mentioned in section 4.3.1, and will be discussed in more detail in Section 10.3, the presence of H_2O traces may already significantly reduce the LMCT transitions of $[Cu_2(\mu\text{-}O)]^{2+}$. As the feed-gas composition in catalytic operational mode often contains >3 vol% H_2O, an identification of $[Cu_2(\mu\text{-}O)]^{2+}$ using UV-Vis spectroscopy becomes impossible for the continuous CH_4-to-CH_3OH conversion. Significant emphasis has therefore been placed on drawing comparisons to active sites characterized in stepwise operational mode, as well as a reliance on DFT calculations.

Ipek *et al.*, as well as Memioglu *et al.*, investigated various Cu–zeolites, including Cu-exchanged MOR, CHA, AEI, MFI, and MAZ, which all exhibited activity in the continuous CH_4-to-CH_3OH conversion using N_2O as the oxidant.[13,228] Most emphasis was placed on $Cu_{0.4}CHA_{12.0}$.[13,228] Increasing the reaction temperature from 523 to 573 K entailed an increase in productivity from 12 to 55 $\mu mol_{CH_3OH}\ g_{ZEO}^{-1}\ h^{-1}$. *In situ* UV-Vis spectroscopy under an N_2O atmosphere at 543 K revealed absorption features at 21 000 and 23 100 cm^{-1}, both attributed to $[Cu_2(\mu\text{-}O)]^{2+}$ species near to the 8-MR of the CHA topology. This could be considered valid evidence that $[Cu_2(\mu\text{-}O)]^{2+}$ species in $Cu_{0.4}CHA_{12.0}$ would be responsible for HAA from CH_4 in continuous operational mode. The authors, however, also suggested that a different active species could form due to the presence of H_2O in the feed, which is still able to perform an HAA from CH_4, as previously suggested by Alayon *et al.*[173] The authors also posited that, just as suggested by Yumura *et al.*, a $[Cu_2(\mu\text{-}O)(OH)_2]^{2+}$ or $[(HO)Cu(\mu\text{-}OH)Cu(O)]^{2+}$ species could be the true active species under continuous conditions, and even cleave the C–H bond of CH_4 more efficiently than the $[Cu_2(\mu\text{-}O)]^{2+}$ species, as evidenced from theoretical calculations.[208] However, experimental verification of such species remains elusive (see Section 12.3).

Xiao *et al.* investigated the potential of $Cu_{0.03-0.22}AEI_{7.7-11.6}$ for the catalytic CH_4 oxidation using N_2O as the oxidant.[229,230] By increasing the calcination temperature from 823 to 1223 K, the authors decreased the amount of Al T-site pairs, from 57% to 8%, together with the fraction of total Al T-sites, from 98% to 51%. All examined Cu-AEI samples exhibited activity, with the highest activity achieved by the sample with the highest fraction of Al T-site pairs, that being the sample calcined at the lowest temperature of 823 K. Alternating these parameters, as well as varying Cu/Al ratio, culminated in $Cu_{0.09}AEI_{11.4}$ achieving impressive CH_3OH productivities up to 2448 $\mu mol_{CH_3OH}\ g_{ZEO}^{-1}\ h^{-1}$ at a selectivity of 45% at 623 K. In samples with Al T-site pairs, the authors suggested the $[Cu_2(\mu\text{-}O_2)]^{2+}$ species to be responsible for CH_4 activation. Based on the results of FTIR spectroscopy conducted at 298 K following an evacuation procedure at 773 K, the authors concluded that N_2O would bind to a $[Cu_2(\mu\text{-}O)]^{2+}$ site in either a η^1-N or η^1-O binding mode (Fig. 9). It should, however, be noted that such high-temperature conditions have previously been shown to be able to cause (auto)reduction of $[Cu_2(\mu\text{-}O)]^{2+}$ species.[62,66] The authors may therefore have been probing N_2O binding modes to (auto)reduced Cu(I) sites rather than the intended $[Cu_2(\mu\text{-}O)]^{2+}$ species, which raises questions about their structural assignments. Nevertheless, characteristic bands at 2292 and 2248 cm^{-1}, attributed to η^1-N and η^1-O binding modes, respectively, were observed (Fig. 9). The authors also did not exclude the possibility of a μ-1,3-O,N binding mode. According to their proposed mechanism, the resulting $[Cu_2(\mu\text{-}O_2)]^{2+}$ species would serve as the active site for HAA from CH_4.[230] Critically, however, no spectral evidence for the formation of this proposed active $[Cu_2(\mu\text{-}O_2)]^{2+}$ species was reported.[229] The suggested reaction scheme is depicted in eqn (5.5).

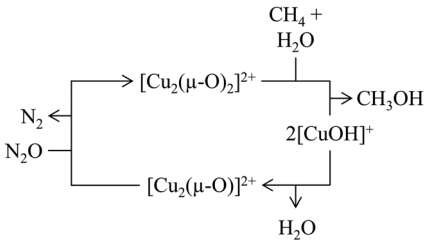

(5.5)

As highlighted by eqn (5.5), an O insertion into $[Cu_2(\mu\text{-}O)]^{2+}$ by N_2O leads to the formation of the proposed $[Cu_2(\mu\text{-}O_2)]^{2+}$ species, which then may be responsible for CH_4 hydroxylation. A Cu reduction leads to a $[CuOH]^+/[CuOH]^+$ pair, which, through H_2O desorption, may reconstitute the $[Cu_2(\mu\text{-}O)]^{2+}$ site. The authors also suggested that CH_3OH could desorb without the addition of H_2O, thereby omitting the formation of $[CuOH]^+/[CuOH]^+$. The mechanism of such a H_2O free desorption of CH_3OH was not described. The authors also examined Cu-AEI samples containing a very low fraction of Al pairs, as determined by Co^{2+} titration studies (Co/Al $\sim$ 0.02). NO-FTIR conducted at 153 K unraveled bands at 1887 and 1900 cm^{-1}, which the authors attributed to $[CuOH]^+$. Activity for this sample was reported for more than 24 h on stream, suggesting that the Cu(I) can be oxidized to $[CuOH]^+$ by N_2O. In addition, it has to be noted that the selectivity over all samples significantly decreased above 573 K, where the authors also showed that N_2O decomposition started to play a role.

Chen *et al.*, Xu *et al.*, and Dai *et al.* examined the mechanism of the active site formation in the catalytic CH_4-to-CH_3OH conversion using N_2O in multiple Cu-exchanged zeolite topologies, such as Cu-BEA, Cu–CHA, and Cu-MFI, in more detail.[231–233] In a combinatorial approach of experiments and DFT calculations, the authors suggested that for Cu-BEA and

Cu-MFI a re-oxidation of the $[Cu_2(\mu\text{-}O)]^{2+}$ core *via* a μ-1,3-O,N binding mode to a Cu(I) pair would occur (Fig. 9). Furthermore, a mechanism of N_2O activation over isolated Cu(I) sites was proposed as well.[231,232] A Cu–CHA sample was prepared *via* solid-state ion exchange under a wet NH_3 atmosphere with the aim of obtaining exclusively isolated Cu(II) in the 6-MR of the zeolite.[232] Due to the lack of proximal Cu(I) the authors claim that the mechanism would proceed *via* a η^1-O binding mode, as shown in Fig. 9d. The activation energy was calculated to be ~130 kJ mol^{-1} for both single Cu(I) in CHA and MFI, and the reaction would proceed *via* eqn (5.6).

$$Cu^+ + N_2O \rightarrow [CuO^\bullet]^+ + N_2 \quad (5.6)$$

The authors proposed that the active species is an oxo-monomeric $[CuO^\bullet]^+$ site rather than $[CuOH]^+$. However, their suggested mechanism for Cu–CHA contains a critical thermodynamic inconsistency. According to their data, after CH_3OH desorption occurs, there is an enormous energy barrier of approximately 800 kJ mol^{-1} between the resulting Cu(I) species and the subsequent N_2O adsorption step (*via* η^1-O binding mode in the pre-TS). This energy barrier is thermodynamically insurmountable under realistic reaction conditions. A second cycle would thus not be possible, thereby making the claims doubtful.

6. Cu(II) active site formation using either O_2 or N_2O and impact on CH_3OH productivity

In light of the discussion in Sections 4 and 5, it is clear that the activation of (auto)reduced Cu–zeolites using either O_2 or N_2O may proceed in fundamentally different manners. Apart from the distinct formation mechanism of isostructural Cu-oxo sites (*e.g.*, $[Cu_2(\mu\text{-}O)]^{2+}$, see Sections 4.2.2 and 5.1.1), activation with O_2 or N_2O has been reported to result in the development of entirely different oxygenated Cu(II) centers within the same material. Owing to the oxidant-dependent variation in the Cu speciation, the CH_3OH productivity of a given sample may significantly differ following treatment with O_2 or N_2O under otherwise identical conditions. In the following section, the impact of the oxidant type on the CH_3OH output will be assessed and correlated to the differences in the nature and abundance of the generated Cu-oxo sites. This analysis will primarily be framed in the context of CH_4 partial oxidation *via* non-isothermal looping, as the limited amount of available literature does not allow for a direct comparison of activation by O_2 and N_2O in other operation modes of CH_4 hydroxylation.

As outlined in Section 4.2.2, the CH_3OH productivity of most Cu–zeolites increases upon raising the calcination temperature.[13–16,18,19] A similar relationship between the material performance in CH_4 partial oxidation and the temperature during N_2O treatment has been established.[13,19,21] However, conflicting observations regarding the relative CH_3OH productivity after interaction with either O_2 or N_2O in specific temperature regimes have been reported. Ipek *et al.* investigated the behavior of $Cu_{0.4}CHA_{12.0}$ in CH_4 partial oxidation following activation in O_2 or N_2O at temperatures ranging from 473 to 723 K.[13] At 473 and 573 K, treatment with N_2O resulted in a higher CH_3OH output compared to calcination. The greater CH_3OH productivity after N_2O treatment in this temperature regime was attributed to a higher fraction of formed oxygenated Cu(II) active centers. This was supported by complementary UV-Vis experiments, which demonstrated that the absorbance of two spectral features at 23 100 and 21 000 cm^{-1}, attributed to two different $[Cu_2(\mu\text{-}O)]^{2+}$ motifs, was more intense after N_2O exposure at 543 K than after O_2 treatment. Notably, upon increasing the activation temperature to 723 K, the reverse trend was observed, with the CH_3OH output being higher after interaction with O_2 than after N_2O treatment. This phenomenon was related to the (auto)reduction of $[Cu_2(\mu\text{-}O)]^{2+}$, driven by the catalytic decomposition of N_2O into N_2 and O_2, which effectively decreases the number of dimeric Cu(II) active sites. Nevertheless, Ipek *et al.* conducted the CH_4 partial oxidation experiments at 473 K following a cool down from the activation temperature in the presence of the oxidant. Considering the discussion in Sections 4.2.5 and 5.1.1, the $[Cu_2(\mu\text{-}O)]^{2+}$ (auto)-reduction should have been reversed throughout the temperature decrease prior to the CH_4 hydroxylation, assuming that its re-oxidation *via* N_2O is not kinetically limited.

Rhoda *et al.* reported an increase in the CH_3OH productivity from 64 to 82 $\mu mol_{CH_3OH}\ g_{ZEO}^{-1}$ after activation of $Cu_{0.29}CHA_{15.7}$ at 823 K in N_2O *vs.* O_2.[194] Similar to the UV-Vis study by Ipek *et al.*, an amplification of the band of the LMCT transition of $[Cu_2(\mu\text{-}O)]^{2+}$ at 22 400 cm^{-1} upon exchanging O_2 for N_2O was observed. This coincides with observations from Brenig *et al.*, who detected a significant gain in the absorbance of the LMCT transition of a $[Cu_2(\mu\text{-}O)]^{2+}$ species at 22 100 cm^{-1} after interaction of $Cu_{0.35}CHA_{11.0}$ with N_2O instead of O_2 at 723 K.[50] Likewise, Plessers *et al.* identified that the intensity of the LMCT transition of three distinct types of $[Cu_2(\mu\text{-}O)]^{2+}$ sites centered at 22 300 cm^{-1} was more pronounced after activation of Cu–MOR in N_2O at 523 K than after exposure to O_2.[51,68] A noteworthy exception to this general trend is the work by Sheppard *et al.*, who determined that the band of $[Cu_2(\mu\text{-}O)]^{2+}$ in $Cu_{0.28}MFI_{12.0}$ at 22 200–22 000 cm^{-1} was more intense after exposure of the (auto)reduced sample to O_2 at 673 K than after interaction with N_2O.[85]

Based on the spectroscopic studies by Ipek *et al.*, Rhoda *et al.*, and Brenig *et al.*, the enhanced CH_3OH output of N_2O-activated Cu–zeolites originates from the more facile $[Cu_2(\mu\text{-}O)]^{2+}$ generation compared to O_2-treated samples. This is also evident from the variation in the threshold temperature required to observe the LMCT transition of the dimeric Cu-oxo centers during interaction of (auto)reduced Cu–zeolites with either N_2O or O_2. As mentioned in Section 4.2.2, Woertink *et al.* demonstrated that a minimal temperature of 448 K is necessary to trigger the appearance of the feature at 22 700 cm^{-1} throughout interaction of (auto)reduced $Cu_{0.54}MFI_{12.0}$ with O_2 (Fig. 10).[224] On the contrary, this signal could already be identified at ambient temperature upon exposing the material to N_2O.[147]

The difference in the efficiency of $[Cu_2(\mu\text{-}O)]^{2+}$ formation by N_2O and O_2 has also been highlighted by DFT calculations of Mahyuddin *et al.*, which indicate that the nature of the oxidant governs the magnitude of the activation energy of the rate-

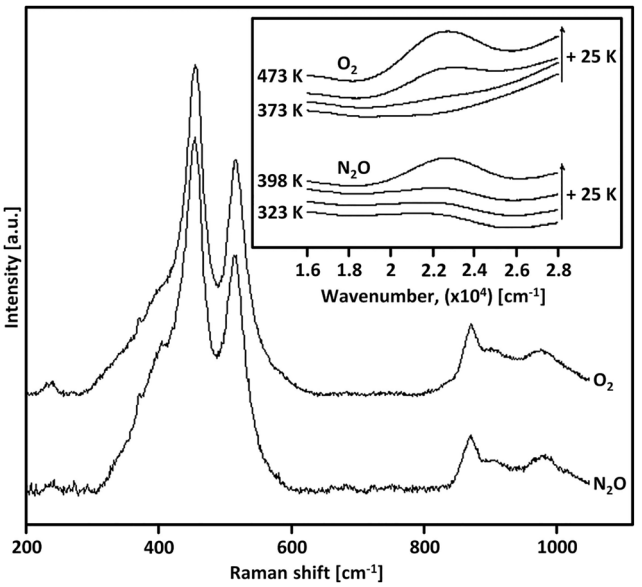

Fig. 10 Raman spectra (λ_{ex} = 457.9 nm) of $Cu_{0.54}MFI_{12.0}$ activated in either O_2 or N_2O. The inset displays UV-Vis spectra recorded at ambient temperature after interaction of $Cu_{0.54}MFI_{12.0}$ with either O_2 or N_2O at temperatures ranging from 373 to 473 K and 323 to 398 K, respectively. The arrows in the inset represent the increasing temperature of the O_2 and N_2O treatment. Adapted from ref. 224 with permission from the National Academy of Sciences (Copyright 2009).

determining step in the generation mechanism of the oxygenated Cu(II) species.[157,179] For example, the transformation of paired Cu(I) into $[Cu_2(\mu\text{-}O)]^{2+}$ in Cu-AEI and Cu-MFI by N_2O exhibits a true activation energy of approximately 8 and 26 kJ mol^{-1}, respectively.[157,163] On the contrary, the activation energy of the rate-determining step in the formation of two $[Cu_2(\mu\text{-}O)]^{2+}$ sites *via* oxidation of proximal Cu(I) pairs, situated in the opposing 8-MRs of the MOR side pocket (Scheme 1), with O_2 amounts to ~50 kJ mol^{-1}.[179] Although the energetic barrier of $[Cu_2(\mu\text{-}O)]^{2+}$ formation by O_2 is still low enough to proceed at moderate temperatures, the considerably smaller activation energy of $[Cu_2(\mu\text{-}O)]^{2+}$ generation by N_2O indicates that this reaction is more facile. The difference between the true activation energy of $[Cu_2(\mu\text{-}O)]^{2+}$ formation by O_2 and N_2O is highlighted in Scheme 12, which also illustrates the corresponding oxidation intermediates. Notably, a higher true activation energy of 46 kJ mol^{-1} for the formation of $[Cu_2(\mu\text{-}O)]^{2+}$ during activation of Cu-MFI with N_2O has been reported by Tsai *et al.*[124] At present, the origin of the considerable difference between the true activation energies for the development of $[Cu_2(\mu\text{-}O)]^{2+}$ in Cu-MFI *via* interaction with N_2O, as determined by Mahyuddin *et al.* and Tsai *et al.*, remains unclear.

The preferential formation of $[Cu_2(\mu\text{-}O)]^{2+}$ *via* treatment of Cu–zeolites in N_2O instead of O_2 also becomes apparent when comparing the generation mechanisms of the dimeric Cu-oxo site in the presence of the two oxidants (eqn (5.1) and (4.7)–(4.10)). In the case of N_2O, the reaction proceeds *via* a simple two-electron redox process and involves the direct transfer of a single O moiety to two Cu(I) ions as well as the simultaneous release of N_2.[9,19,51,52,95,124,149,158] On the contrary, the O–O bond cleavage occurring throughout $[Cu_2(\mu\text{-}O)]^{2+}$ evolution in O_2 requires that the second O moiety must be accommodated either within the zeolite lattice or at a nearby Cu(I) pair.[147,179] Keeping in mind that the former process is characterized by an excessively high true activation energy of 250 kJ mol^{-1} (see Section 4.2.2), it is reasonable to assume that the transformation of a proximal Cu(I) pair into another oxygenated Cu(II) center by the liberated O group is preferred. However, this implies that the development of $[Cu_2(\mu\text{-}O)]^{2+}$ in O_2 might be inhibited in the absence of neighboring Cu(I) ions, as there is no place to host the second O moiety. Activation in N_2O thus enables the generation of isolated $[Cu_2(\mu\text{-}O)]^{2+}$, which might not be possible in the case of O_2 treatment. Scheme 12 illustrates the distinct formation mechanism of $[Cu_2(\mu\text{-}O)]^{2+}$ in either O_2 or N_2O and emphasizes

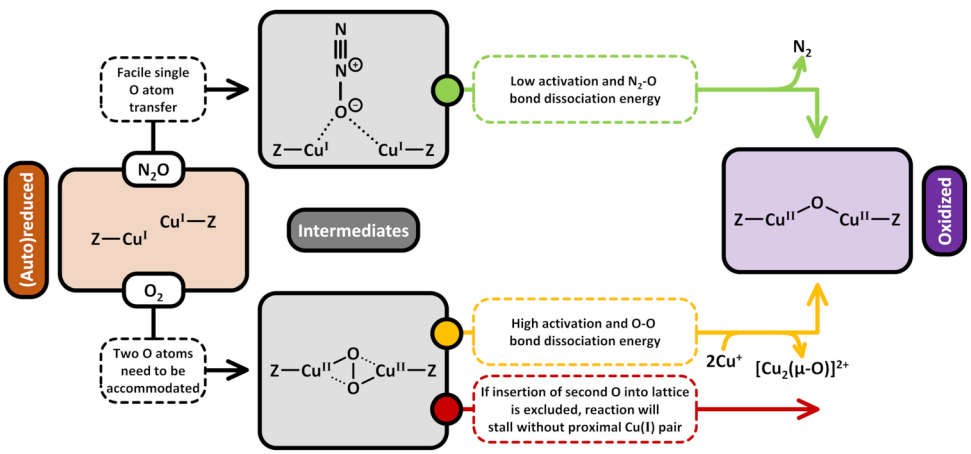

Scheme 12 Transformation of Cu(I) (brown background) into $[Cu_2(\mu\text{-}O)]^{2+}$ (violet background) using either O_2 or N_2O as the oxidant. The generation of $[Cu_2(\mu\text{-}O)]^{2+}$ *via* interaction of (auto)reduced Cu–zeolites with O_2 proceeds *via* a $[Cu_2(\mu\text{-}O)_2]^{2+}$ intermediate (grey background) and cannot resume without a location to accommodate the second O moiety. In contrast, material activation by N_2O, which proceeds *via* a particular adsorption complex (grey background), enables the formation of isolated $[Cu_2(\mu\text{-}O)]^{2+}$ as only a single O atom is transferred. Compared to treatment in O_2, $[Cu_2(\mu\text{-}O)]^{2+}$ generation by N_2O is thermodynamically more facile as the true activation energy and N_2–O bond dissociation energy are lower. Dotted bonds correspond to dative interactions. The term "Z" describes the negatively charged zeolite lattice.

the necessity of a location to accommodate the liberated O group in the case of Cu–zeolite activation by O_2.

The greater efficiency of $[Cu_2(\mu\text{-}O)]^{2+}$ generation using N_2O compared to O_2 can also be rationalized by taking into account that the energy required for N_2–O bond cleavage is significantly smaller than that of O–O bond rupture. Based on tabulated formation enthalpies at 0 K, the N_2–O bond dissociation energy amounts to just $\sim$161 kJ mol^{-1}, whereas that of O–O equals 494 kJ mol^{-1}, which is also described in Scheme 12.[234] Importantly, this consideration is not exclusive to the generation of $[Cu_2(\mu\text{-}O)]^{2+}$ since N_2–O and O–O bond cleavage is involved in the formation mechanism of other Cu-oxo species by N_2O or O_2, too. Similar to the results of Ipek *et al.*, Kim *et al.* found that the CH_3OH productivity of $Cu_{0.4}MOR_{20.0}$ was higher after interaction with N_2O than after calcination in O_2 at activation temperatures in the 573–623 K range. These authors also observed that this trend is reversed when further increasing the activation temperature to 673 K.[21] However, upon raising the activation temperature to 773 K, the CH_3OH output was again greater following exposure to N_2O than after O_2 treatment. Kim *et al.* ascribed the better performance in CH_4 partial oxidation after activation in N_2O at temperatures below 673 K and above 773 K to the thermodynamically favored transformation of a reduced Cu precursor into $[Cu_3(\mu\text{-}O)_3]^{2+}$. On the contrary, the formation of $[Cu_3(\mu\text{-}O)_3]^{2+}$ in the presence of O_2 was proposed to occur *via* an O_2-bridged intermediate (see Section 4.2.2), which was deemed to be responsible for the diminished CH_3OH productivity. At low activation temperatures, the necessary O–O bond scission was suggested to be kinetically limited, whereas high activation temperatures were hypothesized to induce the desorption of O_2 from the intermediate. The reason for the higher CH_3OH productivity after interaction with O_2 compared to N_2O at intermediate activation temperatures from 673 to 723 K has yet to be explained.

Then again, Ikuno *et al.* did not observe any strong variation in the CH_3OH output of $Cu_{0.31}MOR_{11.0}$ after activation of the material in either N_2O or O_2 at temperatures ranging from 473 to 773 K.[19] Hence, these authors argued that the generation of the Cu-oxo active site, which was proposed to correspond to a $[Cu_3(\mu\text{-}O)_3]^{2+}$ species, is equally efficient in O_2 and N_2O, suggesting that O–O bond cleavage is not a limiting factor.

Finally, Göltl *et al.* noted a rise in the CH_3OH productivity from 10 to 23 $\mu mol_{CH_3OH}\ g_{ZEO}^{-1}$ when activating $Cu_{0.41}CHA_{14.7}$ in N_2O at 723 K instead of O_2.[72] This was attributed to an oxidant-controlled variation in the nature of the Cu(II) active center. Theoretically predicated phase diagrams revealed that, depending on the specific Al T-site arrangement, $[Cu_2(\mu\text{-}O)_2]^{2+}$ and $[Cu_2(cis\text{-}\mu\text{-}1,2\text{-}O_2)]^{2+}$ are the thermodynamically preferred Cu-oxo species in Cu–CHA at 0.9 mbar N_2O and 473 K, *i.e.*, the conditions prior to CH_4 hydroxylation. On the contrary, $[Cu_2(\mu\text{-}OH)_2]^{2+}$ as well as $[Cu_2(\mu\text{-}OH)]^{2+}$ (Scheme S1x) were identified as the most favorable Cu(II) sites at 0.9 mbar O_2 and 473 K.[72,168] Complementary DFT calculations indicated that $[Cu_2(\mu\text{-}O)_2]^{2+}$ and $[Cu_2(cis\text{-}\mu\text{-}1,2\text{-}O_2)]^{2+}$ are capable of performing two consecutive CH_4 partial oxidations. In contrast, $[Cu_2(\mu\text{-}OH)_2]^{2+}$ can convert only a single CH_4 molecule into CH_3OH, whereas $[Cu_2(\mu\text{-}OH)]^{2+}$ was found to be inactive toward CH_4 hydroxylation.[72] Göltl *et al.* thus suggested that the higher CH_3OH productivity of N_2O-activated materials arises from the formation of oxygenated Cu(II) centers, which intrinsically yield more CH_3OH compared to the Cu-oxo species generated in the presence of O_2. Unfortunately, no mechanism for the formation of any of the proposed oxygenated Cu(II) active sites was provided. Consequently, the source of H^+ necessary for the (re-)generation of $[Cu_2(\mu\text{-}OH)_2]^{2+}$ is not clear. It could be envisioned that the latter is formed *via* interaction of $[Cu_2(\mu\text{-}O)]^{2+}$ with H_2O, though this remains purely speculative. Moreover, it remains elusive how the O–O bond in $[Cu_2(cis\text{-}\mu\text{-}1,2\text{-}O_2)]^{2+}$ during interaction of the sample with N_2O is formed. The latter question is particularly important since theoretical calculations by Zhao *et al.* have demonstrated that the formation of $[Cu_2(\mu\text{-}1,2\text{-}O_2)]^{2+}$ *via* oxidation of $[Cu_2(\mu\text{-}O)]^{2+}$ with N_2O is characterized by an insurmountable free energy barrier of 244 kJ mol^{-1} at 523 K.[164] The inability of N_2O to generate Cu-oxo centers featuring O–O bonds has also been emphasized by Rhoda *et al.*, who noted that, unlike activation in O_2, treatment with N_2O cannot result in the development of end-on/side-on $[Cu(\eta\text{-}O_2^{\bullet})]^+$.[194] Likewise, the formation of $[Cu_2(\mu\text{-}\eta^2\text{:}\eta^2\text{-}O)]^{2+}$ has only been observed through activation in the presence of O_2 but not N_2O.[147]

7. Formation of active Cu(II) species with H_2O in stepwise and catalytic CH_4-to-CH_3OH conversion

7.1. Formation of Cu(II) sites using H_2O during the stepwise CH_4-to-CH_3OH conversion *via* looping

A discussion on whether H_2O is able to oxidize Cu(I) centers in zeolites has been present long before Cu(II) zeolites were shown to be active for CH_4 activation. Anaerobic oxidation of Cu(I) to Cu(II) in zeolites has been suggested to be both impossible[99] and possible,[143] as well as both O_2 and H_2O being necessary simultaneously.[98,99,235] This discussion has continued into the field of CH_4-to-CH_3OH conversion *via* Cu–zeolites.

Alayon *et al.*, using $Cu_{0.38}MOR$, reported the first anaerobic oxidation of Cu(I) to Cu(II) by H_2O, following a Cu(II) reduction in CH_4.[116] During the following H_2O exposure, a marked decrease in the Cu(I) 1s $\rightarrow$ 4p transition at $\sim$8983 eV and an increase in the 1s $\rightarrow$ 3d transition of Cu(II) at $\sim$8978 eV *via in situ* high-energy resolution fluorescence detection (HERFD) XAS were observed. In addition, a hypsochromic shift of the edge was observed, a further indication of Cu oxidation occurring. Pappas *et al.*, also using *in situ* XAS, showed that an anaerobic Cu(I) to Cu(II) oxidation was also observable for both $Cu_{0.2}FER_{11.0}$[169] and $Cu_{0.5}CHA_{12.0}$.[16] It also was the case for $Cu_{0.38}MOR$ as reported by Alayon *et al.*,[116] H_2O was not able to fully re-oxidize all Cu(I) reduced during the preceding CH_4 exposure over the examined timeframes.

7.1.1 Dimeric sites. A more detailed examination regarding the applicability of H_2O as an oxidant for the CH_4-to-CH_3OH conversion in the chemical looping approach was provided by Sushkevich *et al.* using Cu–$MOR_{13.0}$.[88] The cycling sequence consisted of an initial exposure to He at 673 K, followed by the subsequent dosage of CH_4 and H_2O, both at 473 K, to desorb

any produced CH_3OH. Besides CH_3OH desorption during H_2O exposure, XAS revealed a decrease in the 1s → 4p transition at ~8984 eV and an increase in white-line intensity at ~8997 eV, as depicted in Fig. 11a, demonstrating the oxidation of Cu(I) to Cu(II). Further evidence of an anaerobic oxidation was delivered by CO- and NO-FTIR spectroscopy, showing a decrease in bands associated with Cu(I) species (both $[Cu(CO)]^+$ at 2159 cm^{-1} and $[Cu(CO)_2]^+$ at 2151 and 2179 cm^{-1}, Fig. 11b), and a simultaneous increase in bands associated with Cu(II) species ($[Cu_X(NO)]^{2+}$ at 1909, 1958, 1995 cm^{-1}, Fig. 11c) during H_2O exposure. Besides CH_3OH, molecular H_2 was observed using MS (Fig. 11e, Scheme 13). This suggested that the mechanism of Cu(I) re-oxidation to Cu(II) by H_2O involves a two-electron reduction process, resulting in the formation of H_2 and a reconstitution of the $[Cu_2(\mu\text{-}O)]^{2+}$ active site, as shown in eqn (7.1). The activation energy of said re-oxidation step was calculated to be 102 kJ mol^{-1}.

The proposed mechanism was verified by using $H_2{}^{18}O$ during steam exposure, with the O insertion by H_2O into the Cu(I) pair being confirmed by the subsequent catalytic cycle yielding $CH_3{}^{18}OH$, as shown in Fig. 11d.

$$2Cu^+ + H_2O \rightarrow [Cu_2(\mu\text{-}O)]^{2+} + H_2 \qquad (7.1)$$

The quick formation of molecular H_2 indicates that a re-oxidation proceeds relatively rapidly over ~10 min at 473 K (Fig. 11e). When including a high-temperature activation procedure (673 K in He), the productivity and selectivity increased when compared to the first cycle, as may be seen in Fig. 11f (87% and 0.142 mol_{CH_3OH} $mol_{Cu}{}^{-1}$ *vs.* 97% and 0.202 mol_{CH_3OH} $mol_{Cu}{}^{-1}$). This productivity and selectivity were reproducible for three further cycles using the outlined anaerobic looping procedure. It should be noted that if a high-temperature treatment was omitted, with the activation in He instead conducted at 473 K,

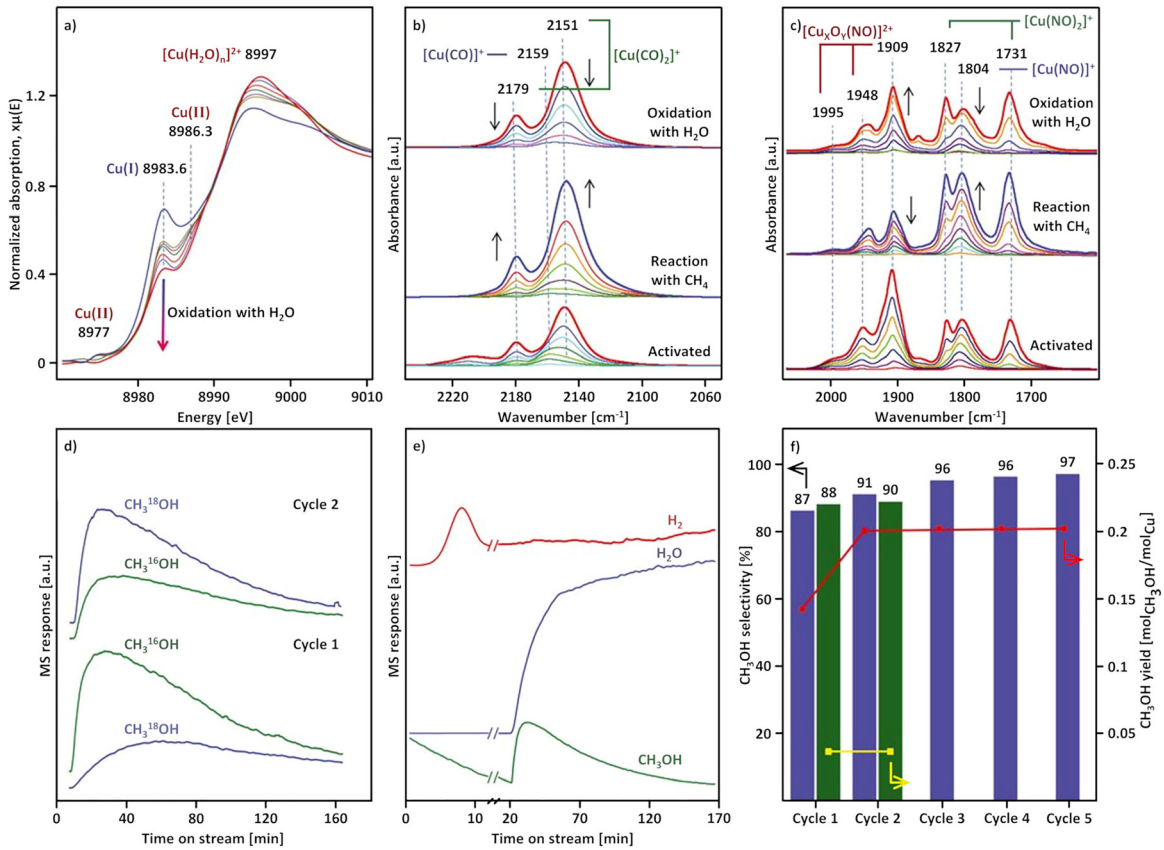

Fig. 11 *In situ* XANES spectra of Cu–$MOR_{13.0}$ recorded during interaction with H_2O at 473 K after reaction with CH_4 at the same temperature (a). The arrow describes the temporal development of the Cu(I) pre-edge feature. FTIR spectra recorded at 100 K of CO adsorbed on Cu–$MOR_{13.0}$ after treatment in vacuum at 673 K (bottom, b), reaction with CH_4 at 473 K (middle, b) and re-oxidation with H_2O at 473 K (top, b). The color gradient indicates the progressively increasing CO dosage. Arrows describe the evolution of the intensity of absorption bands, originating from the interaction of CO with Cu(I), after material exposure to CH_4 and H_2O. FTIR spectra recorded at 100 K of NO adsorbed on Cu–$MOR_{13.0}$ after treatment in vacuum at 673 K (bottom, c), reaction with CH_4 at 473 K (middle, c) and re-oxidation with H_2O at 473 K (top, c). The color gradient indicates the progressively increasing NO dosage. Arrows describe the evolution of the intensity of absorption bands, originating from the interaction of NO with Cu(I) and Cu(II), after material exposure to CH_4 and H_2O. MS responses of unlabeled (*m/z* = 31) and ^{18}O-labeled (*m/z* = 33) CH_3OH after two consecutive reaction cycles of Cu–$MOR_{13.0}$, using labeled $H_2{}^{18}O$ for CH_3OH desorption and reactivation (d). MS responses of H_2 (*m/z* = 2), H_2O (*m/z* = 18), and CH_3OH (*m/z* = 31) after interaction of Cu–$MOR_{13.0}$ with 7 bar CH_4 at 473 K, followed by a purge with H_2O in He (2.6 vol%, 1 bar, total flow of 40 ml min^{-1}, e). CH_3OH yield and selectivity across multiple cycles, each involving a He activation at either 673 K (red line and blue bars) or 473 K (yellow line and green bars), followed by CH_4 reaction and then catalyst reactivation by H_2O at 473 K (f). Adapted from ref. 88 with permission from Science (Copyright 2017).

a significantly lower CH_3OH productivity (0.04 mol_{CH_3OH} mol_{Cu}^{-1}) is achieved. Such observations are in line with previous studies, where an isothermal looping procedure at 473 K resulted in a poisoning of active Cu(II) by H_2O and precluded the interaction of CH_4 with the O_{ef} ligands of the active sites.[173,202] For a more detailed discussion on the ability of H_2O to act as a poison for active Cu(II), the reader is referred to Section 10.1.

The claim that H_2O may act as an oxidant for Cu(I) centers in zeolites has, however, proven to be very contentious. One source of scrutiny stems from the re-oxidation of Cu(I) being thermodynamically unfavorable at 473 K under standard conditions (ΔG_{473K} = 130 kJ mol^{-1}), as detailed by Periana.[236] While a valid criticism, these values are only applicable to bulk crystalline copper oxides and not the $[Cu_2(\mu\text{-}O)]^{2+}$ species itself, and do not include any stabilizing effects that additional H_2O molecules would exhibit. In response, a more thorough explanation of the anaerobic re-oxidation mechanism was presented by Sushkevich *et al.*[189] Following the formation of $[Cu_2(\mu\text{-}O)]^{2+}$ from one H_2O molecule and a binuclear Cu(I) center, as shown in eqn (7.1), a second H_2O molecule would lead to the formation of a $[Cu_2(\mu\text{-}OH)_2]^{2+}$ species, calculated to be significantly more stable than the $[Cu_2(\mu\text{-}O)]^{2+}$ species ($\Delta\Delta G_{473K}$ = −117 kJ mol^{-1}). A ΔG_{473K} = 58 kJ mol^{-1} was calculated as the upper limit for the re-oxidation to the $[Cu_2(\mu\text{-}OH)_2]^{2+}$ species. While endergonic, the reaction was suggested to still be able to proceed at 473 K primarily due to the further stabilization effects of additional H_2O molecules on Cu(II), as well as the low adsorption of H_2 relative to H_2O. Both these factors would lead to a significant decrease in ΔG, making the reaction thermodynamically feasible. A high-temperature activation (673 K in He) would result in the $[Cu_2(\mu\text{-}O)]^{2+}$ active site *via* a dehydration and unpoisoning of the $[Cu_2(\mu\text{-}OH)_2]^{2+}$ species, as depicted in eqn (7.2).[88,202]

$$[Cu_2(\mu\text{-}OCH_3)]^+ + H^+ + 2H_2O \rightarrow [Cu_2(\mu\text{-}OH)_2]^{2+} + CH_3OH + H_2 \rightarrow [Cu_2(\mu\text{-}O)]^{2+} + H_2O \quad (7.2)$$

A similar criticism as Periana[236] was brought forward by Mahyuddin *et al.*[151,158] The authors, employing DFT calculations, determined the activation energy of the overall reaction for an anaerobic re-oxidation of the binuclear Cu(I) center to $[Cu_2(\mu\text{-}O)]^{2+}$ to be ~290 kJ mol^{-1}. In comparison, the necessary energy investment for the desorption of H_2O from the Cu(I) pair is significantly lower at ~220 kJ mol^{-1}. Notably, the authors also suggested that a single H_2O molecule would reduce the CH_3OH desorption energy by ~50%, thereby highlighting that the effects of H_2O extend far beyond solely being an extraction medium, or as in the discussed case, an oxidizing agent. This motivated a careful re-examination of the anaerobic oxidation mechanism *via* DFT calculations and molecular dynamics simulations by Palagin *et al.* to carefully examine the role of H_2O for the suggested oxidation reaction.[237] Multiple H_2O molecules were not only suggested to be necessary for the mechanism, but also crucial for decreasing both the high activation barrier for H_2 release and Cu(I) oxidation. The suggested mechanism for re-oxidation is depicted in Fig. 12.

A first H_2O molecule is responsible for the conversion of a CH_3O group to molecular CH_3OH adsorbed on a $[Cu_2(\mu\text{-}OH)]^+$ species. The Cu oxidation would be initiated by the adsorption of a second H_2O molecule, as depicted in Fig. 12. The second H_2O molecule transfers a H^+ from a proximal BAS, whose own formation was shown to be coupled to CH_3O group formation (Fig. 13),[88] to the $[Cu_2(\mu\text{-}OH)]^+$ species. This transfer results in the oxidation of both Cu(I) centers of $[Cu_2(\mu\text{-}OH)]^+$, resulting in the formation of a $[Cu_2(\mu\text{-}OH)(\mu\text{-}H)]^{2+}$ intermediate. The activation energy for Cu(I) oxidation was calculated at ~80–105 kJ mol^{-1}, dependent on the number of H_2O molecules coordinated to the intermediate. These values are significantly lower than the activation energy of 290 kJ mol^{-1} as suggested by Mahyuddin *et al.* (*vide supra*).[158,237] A third H_2O molecule would be necessary in the release of H_2, leading to a reformation of the $[Cu_2(\mu\text{-}O)]^{2+}$ active site. However, the formed $[Cu_2(\mu\text{-}O)]^{2+}$ will be poisoned by transformation into the energetically more favorable $[Cu_2(\mu\text{-}OH)_2]^{2+}$ species *via* the addition of a fourth H_2O molecule. A regeneration of the active site able to activate CH_4 would then proceed *via* eqn (7.2) by employment of a high-temperature activation procedure. This transformation from Cu(I) pair to $[Cu_2(\mu\text{-}O)]^{2+}$ *via* the H_2O poisoned intermediate $[Cu_2(\mu\text{-}OH)_2]^{2+}$ is further illustrated in Scheme 13. However, it needs to be noted that a definite spectroscopic identification of the $[Cu_2(\mu\text{-}OH)_2]^{2+}$ intermediate is lacking, and therefore the suggested transformation into the $[Cu_2(\mu\text{-}O)]^{2+}$ active site upon dehydration remains to be proven under the examined conditions.

Heyer *et al.* experimentally investigated the anaerobic Cu(I) oxidation in $Cu_{0.45}MOR_{9.0}$.[238] On the basis of the amount of EPR silent Cu(II) sites, the amount of $[Cu_2(\mu\text{-}O)]^{2+}$ species in the system was estimated to be 36 ± 14% of the total Cu present in the material. Following an activation in He at 773 K, UV-Vis and Raman spectroscopies determined that solely mononuclear Cu(II) remains oxidized, with the $[Cu_2(\mu\text{-}O)]^{2+}$ sites in the system having been (auto)reduced.[62,238] No Cu(I) to Cu(II) oxidation was observed *via in situ* XAS when the (auto)reduced material was exposed to H_2O at 473 K, the same temperature at which Sushkevich *et al.* first characterized the anaerobic oxidation of a Cu(I) pair to $[Cu_2(\mu\text{-}O)]^{2+}$ (*vide supra*). At first glance, the results of Heyer *et al.* and Sushkevich *et al.* may therefore seem contradictory.[88,238] A marked difference, however, lies in the fact that Sushkevich *et al.* performed a full cycle, consisting of the subsequent dosage of O_2–CH_4–H_2O, before examining a re-oxidation of Cu–$MOR_{13.0}$. Heyer *et al.* instead investigated the oxidation of an (auto)reduced Cu(I) pair to $[Cu_2(\mu\text{-}O)]^{2+}$ by H_2O in $Cu_{0.45}MOR_{9.0}$. While this difference may sound inconsequential, the proposed mechanism suggested by Palagin *et al.*[237] requires the transfer of H^+ from a proximal BAS to form the necessary $[Cu_2(\mu\text{-}OH)(\mu\text{-}H)]^{2+}$ intermediate, with the proximal BAS only forming following a C–H bond cleavage of CH_4, as has been determined experimentally (Fig. 13).[88] An (auto)reduction procedure will instead lead to no change in the charge balancing ability of Cu toward the framework, and therefore no BAS formation. The high Cu/Al exchange degree of 0.45 also suggests that a low amount of BAS would be present before the (auto)-reduction procedure. However, attributing the conflicting observations reported by Sushkevich *et al.*[88] and Heyer *et al.*[238] to the lack of a proximal BAS to a Cu(I) pair entirely relies on the

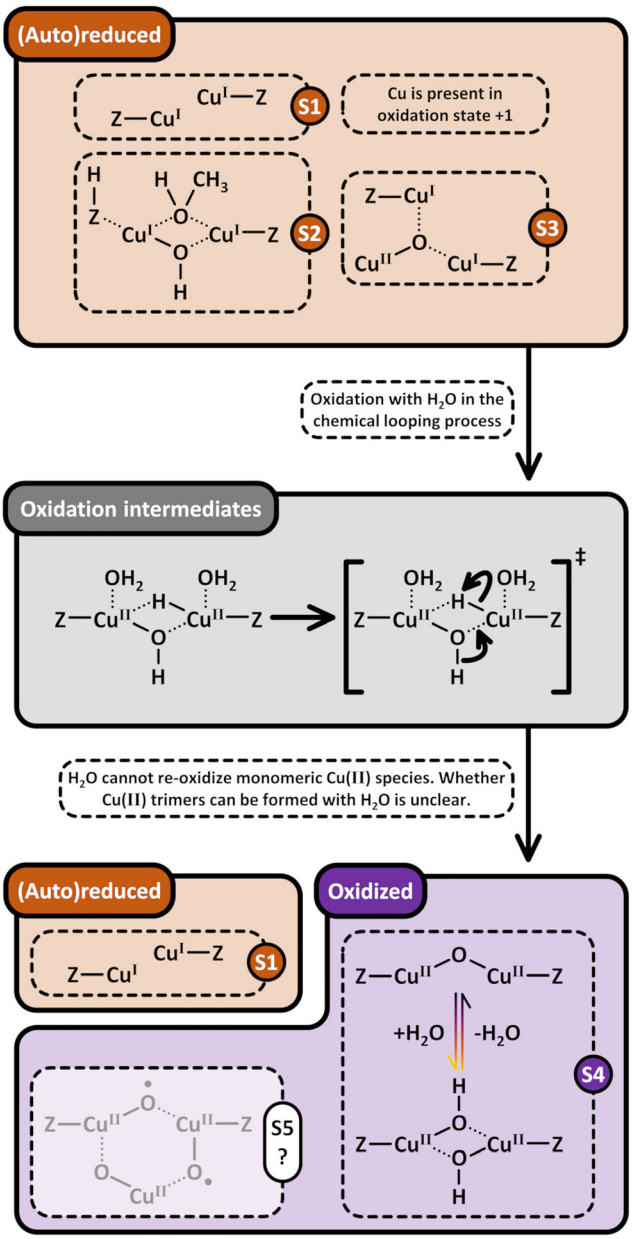

Scheme 13 Formation pathways of Cu-oxo centers (violet background) *via* activation of (auto)reduced Cu–zeolites (brown background) with H_2O in the chemical looping process. (Auto)reduced monomeric Cu(II) active sites (S1), such as $[CuOH]^+$/$[CuOH]^+$ or Cu^{2+}/$[CuOH]^+$, cannot be re-oxidized with H_2O. Dimeric Cu(II) active sites (S1), (auto)reduced to a Cu(I) pair under high temperature inert conditions or vacuum, can also not be re-oxidized with H_2O. The transformation of the Cu(I) pair (S2), which hosts CH_3OH, into $[Cu_2(\mu\text{-}O)]^{2+}$ and $[Cu_2(\mu\text{-}OH)_2]^{2+}$ (S4) proceeds *via* a hydride intermediate (grey background). Whether H_2O is capable of re-oxidizing $[Cu_3(\mu\text{-}O)]^{2+}$ into $[Cu_3(\mu\text{-}O)_3]^{2+}$ (S5) has not been investigated yet (structure is highlighted by a transparent overlay and marked with a question mark). Dotted bonds correspond to dative interactions. The term "Z" describes the negatively charged zeolite lattice. The color gradient from yellow to violet of the arrows in (S4) indicates the progressively increasing temperature.

premise that the mechanism proposed by Palagin *et al.*[237] is in fact valid. An alternative source of the discrepancy between these works may instead stem from Cu–MOR samples with different characteristics. Cu–MOR exhibits a variety of $[Cu_2(\mu\text{-}O)]^{2+}$ active sites, which exhibit different abilities toward being oxidized and (auto)reduced.[51,68] It may be entirely possible that one variation of the active site is able to be re-oxidized by H_2O under the examined conditions due to favorable geometric effects by, for example, a variation in Al T-site distribution throughout the zeolite lattice. The significant impact that the Al T-site distribution in MOR may have is illustrated by the fact that only certain Al T-site arrangements, as well as the need for non-conventional ion-exchange procedures, allow for the $[Cu_3(\mu\text{-}O)_3]^{2+}$ species to be formed.[96] In addition, the *in situ* XANES spectra of Cu–$MOR_{13.0}$ recorded during H_2O exposure has highlighted that not all Cu(II) reduced *via* CH_4 is able to be re-oxidized by H_2O (Fig. 13). While this may also stem from the inability of other active sites to be re-oxidized *via* H_2O exposure (see Section 7.1.2), this may also indicate the inability of certain dimeric Cu(I) motifs to be re-oxidized *via* H_2O exposure.

A further point of criticism regarding the feasibility of H_2O as an oxidant for Cu(I) in zeolites has been the source of the molecular H_2 formed during re-oxidation. An alternative source of H_2 was proposed to stem from a decomposition of HCOOH to CO_2 and H_2 ($\Delta G_{473K} = -63$ kJ mol^{-1}) over the material.[90,238] $HCOO^-$ bands were detected by FTIR in the original work by Sushkevich *et al.*,[88] which may lead to HCOOH formation during H_2O exposure, which could subsequently decompose into CO_2 and H_2 over Cu(I).[90,238] When Heyer included a CH_4 exposure following the activation in He at 773 K (*vide supra*), the authors observed that CO_2 and H_2 are produced in a ratio of 1 : 1 during H_2O exposure, a strong indication that the source is from an oxidation of HCOOH ($\Delta G_{473K} = -63$ kJ mol^{-1}) instead of a re-oxidation of Cu(I) pairs.[238] Any oxidation of Cu(I) witnessed in the work by Sushkevich *et al.* under H_2O was instead suggested to stem from O_2 impurities or potential leaks, or could also stem from a water-gas shift reaction occurring during H_2O exposure ($\Delta G_{473K} = -21$ kJ mol^{-1}).[90,238] Any presence of O_2 will definitely lead to re-oxidation. If these, however, were the sole sources of H_2, it would be reasonable for Cu–zeolites solely exhibiting $[CuOH]^+$ sites to also result in H_2 formation during H_2O exposure. This, however, is not the case, as shown by Sushkevich *et al.*[65] $[CuOH]^+$ sites are suggested not to be able to be re-oxidized *via* H_2O from their Cu(I) precursor (see Section 7.1.2). $Cu_{0.6}MOR_{46.0}$, assumed to solely exhibit $[CuOH]^+$ sites due to its high Si/Al ratio, was shown not to release H_2 during H_2O exposure, while FTIR was still able to identify both CO species (2157 cm^{-1}) and $HCOO^-$ species (1619 cm^{-1}) during CH_4 exposure. If both a decomposition of HCOOH or a water-gas shift reaction are the only potential sources of H_2, then it would be only logical that $Cu_{0.6}MOR_{46.0}$ would also lead to H_2 formation. The conflicting results and interpretations of said results emphasize that to make definite statements on the ability, or inability, of H_2O to be able to oxidize a Cu(I) motif to result in a $[Cu_2(\mu\text{-}O)]^{2+}$ species, further investigations will be needed to identify the origin of this divergence in findings reported in this section.

7.1.2 Monomeric sites. *In situ* XANES spectroscopy has highlighted that, unlike O_2, an H_2O exposure is not able to

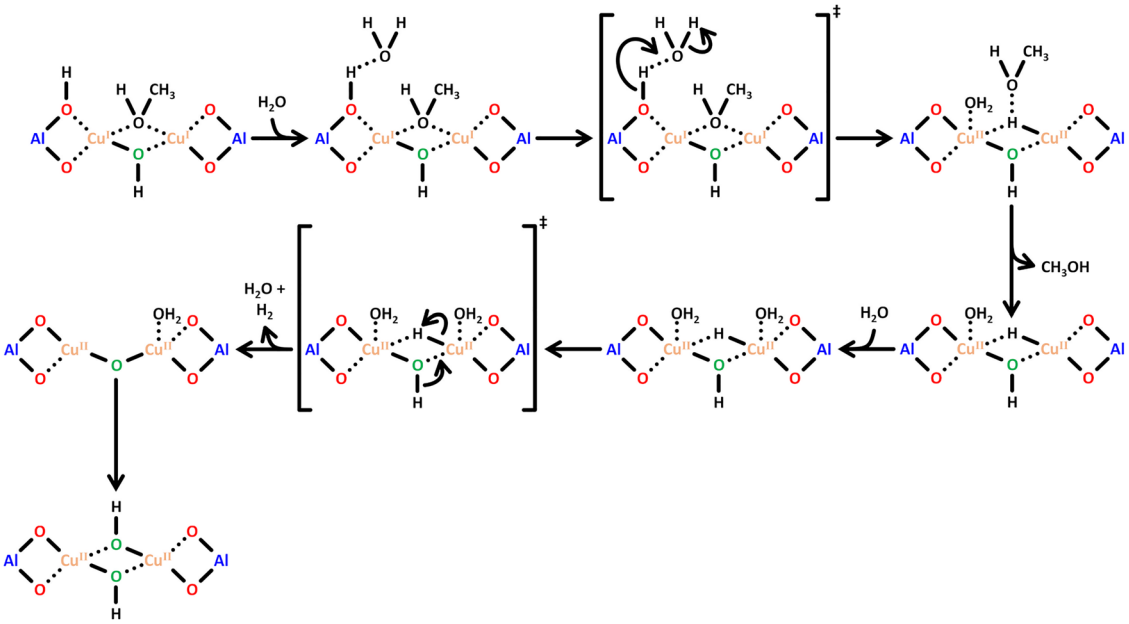

Fig. 12 Suggested mechanism of $[Cu_2(\mu\text{-}O)]^{2+}$ and $[Cu_2(\mu\text{-}OH)_2]^{2+}$ formation *via* oxidation of a Cu(I) pair, hosting CH_3OH, with H_2O. Adapted from ref. 237 with permission from the American Chemical Society (Copyright 2019).

fully re-oxidize all Cu(I) in zeolites previously reduced by CH_4.[16,88,116,169] In the case of Sushkevich *et al.*, an LCF of the collected XAS spectra revealed that only 30% of all Cu of Cu–$MOR_{13.0}$ experienced a change in oxidation state during H_2O exposure, while a total of 70% had been reduced under CH_4 exposure.[88] Cu–MOR has been shown to be able to host a variety of Cu-active sites for the CH_4-to-CH_3OH conversion.[46,51,62,68] The disparity in the amount of Cu experiencing a change in oxidation state during CH_4 and H_2O exposure by Sushkevich *et al.* highlights that not all Cu(II) active sites may be re-oxidized by H_2O, as illustrated in Scheme 13.[88]

Based on these observations, Sushkevich *et al.* investigated Cu–MOR at varying Si/Al and Cu/Al ratios, resulting in samples with differing ratios of monomeric *vs.* dimeric Cu(II) sites.[65] A high Si/Al ratio would entail a low fraction of proximal Al T-sites throughout the zeolite lattice, thereby reducing the amount of dimeric Cu species present in MOR. $Cu_{0.6}MOR_{46.0}$ would therefore result in primarily monomeric Cu(II), with active Cu being present as $[CuOH]^+$. $Cu_{0.38}MOR_{6.5}$ and $Cu_{0.4}MOR_{10.0}$ with lower Si/Al and higher Cu/Al would shift the equilibrium toward the formation of dimeric active sites. While the first cycle following a high-temperature activation procedure (673 K in He) resulted in CH_3OH production in the case of $Cu_{0.6}MOR_{46.0}$, no quantifiable CH_3OH productivity was observed in a second cycle activated under the same conditions (673 K in He) following H_2O exposure to desorb CH_3OH. Both $Cu_{0.38}MOR_{6.5}$ and $Cu_{0.4}MOR_{10.0}$, however, exhibited CH_3OH productivity under the same conditions as $Cu_{0.6}MOR_{46.0}$. This is a strong indication that in the case of monomeric Cu(I), H_2O is not able to re-oxidize Cu and reconstitute the $[CuOH]^+$ species, as depicted in Scheme 13.

Heyer *et al.* arrived at conclusions similar to those of Sushkevich *et al.*[88,238] As previously mentioned in Section 7.1.1, an initial activation procedure (773 K in He) resulted in solely mononuclear $[CuOH]^+$ remaining in a +2 oxidation state. H_2O exposure at 473 K following CH_4 exposure at the same temperature led to an increase in absorption in the XANES spectrum at ~8985 eV, associated with the 1s → 4p transition of Cu(I). An oxidation of Cu(I) to Cu(II) is typically associated with the opposite behavior, namely a decrease in the 1s → 4p transition at ~8985 eV. This increase was instead suggested to be a spectroscopic fingerprint of a linear two-coordinate Cu(I)-aqua complex. *In situ* EPR spectroscopy distinguished a Cu species with a g_{II} value of 2.4, attributed to hydrated Cu(II) in zeolites. More importantly, however, no increase in the amount of EPR active Cu was observed, thereby highlighting that no increase in EPR-visible Cu(II), such as $[CuOH]^+$, occurred (Scheme 13).

Contrasting claims regarding the ability of $[CuOH]^+$ to be reconstituted *via* an oxidation of a mononuclear Cu(I) by H_2O have been made by Pereira *et al.* for Cu-$MAZ_{2.7}$ samples with Cu/Al ratios ranging from 0.15 to 0.27.[239] UV-Vis spectra of $Cu_{0.23}MAZ_{2.7}$ following O_2 exposure at 723 K revealed broad LMCT bands at ~30 000–45 000 cm^{-1}, with an absorbance maximum at ~ 41 200 cm^{-1}. A comparison to DFT calculated UV-Vis spectra suggested that these bands could be associated with $[CuOH]^+$. Following a high-temperature activation under either O_2 or CO_2, the sample was exposed to CH_4 at 523 K. A following H_2O exposure at 523 K was suggested to re-oxidize Cu(I) to $[CuOH]^+$. To unpoison the active sites, the material was exposed to CO_2 at 723 K. The obtained yield of the following cycle was equivalent to the yield of the first cycle. No spectra are provided following H_2O exposure, as well as following the consecutive reactivation under CO_2 atmosphere at 723 K. As CO_2 is considered a potential oxidant for Cu(I) to Cu(II) in zeolites (see Section 8), it is impossible to evaluate which of the two suggested oxidants is responsible for a Cu(I) re-oxidation.

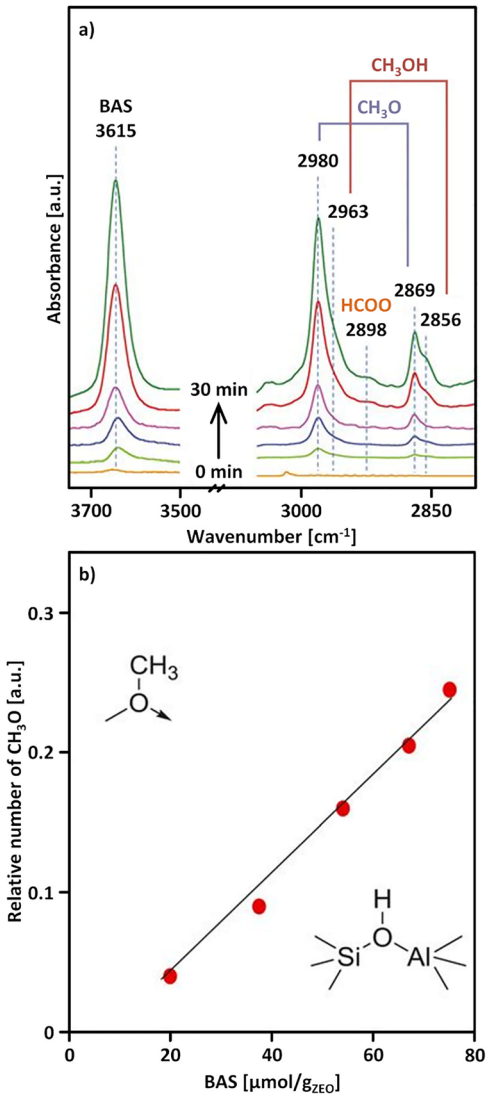

Fig. 13 Time-resolved *in situ* FTIR spectra of adsorbed surface species formed during the interaction of Cu–$MOR_{13.0}$ (pretreated in a flow of He) with 7 bar CH_4 at 473 K (a). Relative number of CH_3O species *vs.* number of BASs formed during the interaction of CH_4 with Cu–$MOR_{13.0}$ at 473 K within 5 to 120 min (b). Adapted from ref. 88 with permission from Science (Copyright 2017).

7.2 Formation of Cu(II) sites using H_2O during catalytic selective CH_4 oxidation

7.2.1 Commonly proposed species (monomeric, dimeric, and trimeric Sites). Jeong *et al.* investigated both Cu–MOR with either H^+ or Na^+ as counter ions in the continuous anaerobic CH_4-to-CH_3OH conversion.[240] The catalyst was examined at 623 and 673 K over a range of both Cu/Al (0.05–0.54) and Si/Al (7.5 and 15.0) ratios. All examined Cu–MOR catalysts, except for low Cu loaded $Cu_{0.05}MOR_{15.0}$, were able to catalytically convert CH_4 into CH_3OH using H_2O as the sole oxidant. At both examined Si/Al ratios, an intermediate Cu/Al ratio of ~0.15–0.19 exhibited the highest CH_3OH productivity when normalized to the Cu loading. While the total CH_4 conversion rates were very similar under the same conditions (same zeolite, same Cu/Al), the blockage of BAS by Na^+ cations increased the selectivity toward CO_2. This is in line with what has been observed for Cu–MOR in the cyclic CH_4-to-CH_3OH conversion.[241] DFT calculations suggested a plausible mechanism focused on the $[Cu_2(\mu\text{-}O)]^{2+}$ active site; however, other active sites for Cu–MOR were not ruled out. The authors, for example, suggested that at higher Cu/Al, Cu–MOR would exhibit $[Cu_3(\mu\text{-}O)_3]^{2+}$ species. Depending on the Cu/Al and Si/Al ratios of Cu–MOR examined by Jeong *et al.*, various active sites and their corresponding Cu(I) precursors may be present in each sample. The authors suggested that after CH_3OH desorption, a remaining $[Cu_2(\mu\text{-}OH_2)]^{2+}$ motif (Scheme S1y) can be re-oxidized by H_2O adsorption and H_2 evolution. This would be followed by H_2O desorption and thereby an unpoisoning of the active site, as shown in eqn (7.3).

$$[Cu_2(\mu\text{-}OH_2)]^{2+} + H_2O \rightarrow [Cu_2(\mu\text{-}OH)_2]^{2+} + H_2 \rightarrow [Cu_2(\mu\text{-}O)]^{2+} + H_2O \quad (7.3)$$

At first glance, the postulated re-oxidation mechanism seems in line with the mechanism suggested in the cyclic anaerobic CH_4-to-CH_3OH conversion, as shown in Section 7.1.1.[237] The DFT calculated mechanism however suggests that the re-oxidized $[Cu_2(\mu\text{-}O)]^{2+}$ active site has a free energy ~91 kJ mol^{-1} higher than the initial $[Cu_2(\mu\text{-}O)]^{2+}$ site, which seems implausible and therefore makes the postulated re-oxidation mechanism questionable.

Koishybay *et al.* compared both anaerobic and aerobic CH_4-to-CH_3OH conditions for $Cu_{0.33}CHA_{10.0}$, and observed exclusive formation of CO_2 under aerobic conditions.[242] The authors assumed that solely non-selective sites, suggested to be $[Cu_3(\mu\text{-}O)_3]^{2+}$ and $[Cu_2(\mu\text{-}O)_2]^{2+}$, would be oxidized by O_2 and not H_2O. Therefore, selective sites, claimed to be represented by $[CuOH]^+$ and $[Cu_2(\mu\text{-}O)]^{2+}$ can be reconstituted from their reduced state under anaerobic CH_4-to-CH_3OH conversion conditions, leading to a selectivity of 100%. Jeong *et al.*, using Cu–MOR without Na^+ co-cations (*vide supra*), also solely observed the formation of CO_2 when adding O_2 in the feed, however, in tandem with a significant increase in the CH_3OH formation rates.[240] A low O_2 amount (85 ppm) was shown to increase CH_3OH productivity by a factor of ~5.[240] However, instead of suggesting that O_2 is responsible for a more rapid Cu(I) re-oxidation in comparison to H_2O, the authors suggested another entirely different role (see Section 7.2.3).

7.2.2 Newly proposed active site configurations. Zhou *et al.* showed that Cu–$CHA_{10.0}$, Cu–$MOR_{11.0}$, and Cu–$MFI_{15.0}$, with 2.1, 2.2, and 1.9 wt% Cu, respectively, were active in the anaerobic continuous CH_4-to-CH_3OH conversion between 473–723 K.[243] The examined Cu–CHA significantly outperformed the other two topologies, with a CH_3OH productivity of ~190 $\mu mol_{CH_3OH}\ g_{ZEO}^{-1}\ h^{-1}$ being achievable at 623 K, in comparison to ~20 $\mu mol_{CH_3OH}\ g_{ZEO}^{-1}\ h^{-1}$ at 473 K. A further temperature increase to 723 K however resulted in a sharp decrease in activity (~30 $\mu mol_{CH_3OH}\ g_{ZEO}^{-1}\ h^{-1}$). The increase in activity observed upon increasing the temperature to 623 K was suggested to stem from more Cu(II) sites being catalytically active at higher temperatures. A temperature-programmed

reduction (TPR) in H_2 was used to assign different Cu sites present in the catalyst, with the highest temperature of a H_2 consumption peak, and therefore the least reducible species, attributed to isolated bare Cu^{2+} in the 6-MR of CHA, typically considered to be inactive toward CH_4 activation.[16] *In situ* UV-Vis spectra revealed d–d transitions at 13 600 and 16 500 cm^{-1}, both attributed to bare Cu^{2+} by the authors. A decrease in absorbance was observed when the sample was exposed to a mixture of CH_4 and H_2O above 573 K, which originated from the reduction of Cu^{2+} sites. FTIR spectroscopy in the region of structural vibrations revealed two bands associated with different Cu species, namely at 900 cm^{-1}, attributed to bare Cu^{2+}, and at ~950 cm^{-1}, attributed to $[CuOH]^+$. This, however, contrasts their findings using EPR spectroscopy, which, according to the authors, showed the presence of only bare Cu^{2+}, while $[CuOH]^+$ is an EPR visible species as well (see Section 2.1.2). When examining the system under an atmosphere of CH_4 and H_2O (573–673 K) using *in situ* FTIR spectroscopy, the band at ~950 cm^{-1}, previously assigned to a $[CuOH]^+$ species, was instead attributed to a Cu-CH_3 species in the 6-MR of CHA. On the basis of these findings, the authors postulated that bare Cu^{2+} in the 6-MR can be active for CH_4 activation. To further support this claim, *in situ* FTIR spectroscopy of Cu–$CHA_{10.0}$ in a quasi-looping manner was performed. Following an activation in He at 573–673 K, the sample was exposed to CH_4 at the same temperature. A decrease in 900 cm^{-1} (bare Cu^{2+}), and an increase in 950 cm^{-1} (Cu–CH_3, no oxidation state of Cu suggested) and 2153 cm^{-1} ($[Cu(CO)]^+$) bands were observed over the examined temperature range. Exposure of the sample to H_2O resulted in a decrease in the band at 950 cm^{-1} and an increase in 900 cm^{-1}. While no mechanistic scheme is presented, this would suggest that the reaction proceeds *via* eqn (7.4).

$$[CuCH_3]^+ + H^+ + H_2O \rightarrow Cu^{2+} + CH_3OH + H_2 \quad (7.4)$$

This, however, would suggest that no change in oxidation state of Cu has taken place, remaining in a +2 oxidation state throughout the reaction. A reduction is, however, suggested to occur by the authors upon CH_4 exposure, as highlighted by both *in situ* UV-Vis and FTIR measurements (*vide supra*). Additionally, both Cu–CH_3 and $[CuOH]^+$ being attributed to bands at ~950 cm^{-1} shows that the assignment of various Cu-species in the far FTIR region is not as straightforward as suggested. Both monomeric and dimeric sites have been assigned to the FTIR region of 930–910 cm^{-1}, complicating matters further.[226,227] In addition, the presence of dimeric sites was determined using UV-Vis spectroscopy, based on observed LMCT transitions at ~30 000 cm^{-1}. Based on these interpretations by the authors, the ability of bare Cu^{2+} to activate CH_4, and therefore any re-oxidation of Cu(I) to bare Cu^{2+} being possible, remains to be proven. In a subsequent publication, Zhang *et al.* examined $Cu_{0.05}CHA_{10.0}$, which the authors suggested to solely exhibit bare Cu^{2+} sites in the 6-MR due to the low Cu/Al ratio.[244] Reaction temperatures between 473–773 K were examined, with 673 K exhibiting the highest CH_3OH productivity and selectivity (2678 $mmol_{CH_3OH}$ mol_{Cu}^{-1} h^{-1}, 93% selectivity toward CH_3OH). A comparison to Cu–$CHA_{10.0}$ with higher Cu/Al showed that the site-specific yield at such a low Cu/Al greatly outperformed the other Cu–$CHA_{10.0}$ catalysts at 673 K. Two species were detected using EPR spectroscopy, both attributed to bare Cu^{2+} in the 6-MR. Cu K-edge FT-EXAFS of the material revealed a Cu first shell CN of 4 for $Cu_{0.05}CHA_{10.0}$, which decreased with increasing Cu/Al. The conditions under which the XAS and EPR spectra were recorded were, however, not mentioned. Similar to their previous work,[243] both the observed d–d transitions band at ~13 000 cm^{-1} in the UV-Vis spectra as well as a band at 900 cm^{-1} in the FTIR spectra were used to identify bare Cu^{2+} in the 6-MR of CHA as the potential active site. In contrast to previous work, which claimed bare Cu^{2+} to be the active site (*vide supra*),[243] the authors suggested that in an initial stage, bare Cu(II) would be converted into a $[CuOH]^+$ species through the combination of both H_2O and CH_4 exposure, as shown by eqn (7.5).

$$Cu^{2+} + CH_4 \rightarrow [CuCH_3]^+ + H^+ \xrightarrow{+H_2O} [(H_2O)CuCH_3]^+ + H^+ \rightarrow [CuOH]^+ + CH_4 + H^+ \quad (7.5)$$

The formed $[CuOH]^+$ species in the 6-MR of CHA was suggested to be responsible for any CH_4-to-CH_3OH conversion. The reaction of C–H bond scission over bare Cu^{2+} was calculated to have an activation energy of ~160 kJ mol^{-1}, while $[CuOH]^+$ in the 6-MR had a lower value of activation energy of ~60 kJ mol^{-1}. These 6-MR $[CuOH]^+$ species were additionally suggested to be more active than both single $[CuOH]^+$ sites in the 8-MR as well as any $[Cu_2(\mu\text{-}O)]^{2+}$ species due to stronger spatial confinement effects by the zeolite framework. Following CH_3OH desorption, a reconstitution of the proposed active site would proceed *via* eqn (7.6).

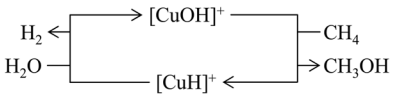

(7.6)

However, just as in previous work (*vide supra*), eqn (7.5) and (7.6) at no point entail a change in the oxidation state of Cu.

7.2.3 The role of O_2. O_2 is the most commonly examined oxidant for the re-oxidation of Cu(I) to Cu(II) in Cu–zeolites. Its role, however, in the scope of the catalytic CH_4-to-CH_3OH conversion, has also been suggested to be an entirely different one. Jeong *et al.* proposed that even with the addition of O_2 to the feed, the mechanism of active site reactivation and oxidation would still proceed anaerobically.[240] O_2 would instead be responsible for H_2 removal/oxidation, thereby shifting the reaction equilibrium in eqn (7.7) toward CH_3OH formation and making the anaerobic oxidation of Cu(I) motifs *via* H_2O thermodynamically favorable.

$$CH_4 + H_2O \leftrightarrow CH_3OH + H_2 \quad (7.7)$$

Koishybay *et al.*, using $Cu_{0.33}CHA_{10.0}$, suggested the same as Joeng *et al.*[242] By comparing feed gas compositions with and without O_2 at 498 K, the authors showed that in both cases, the anaerobic oxidation pathway of Cu(I) to Cu(II) *via* H_2 abstraction is the preferred Cu(I) oxidation pathway. This conclusion was

based on *in situ* far FTIR spectroscopy of the C–O stretching region, wherein the authors inferred the C–O stretch to stem solely from CH_3OH, in combination with the utilization of isotopically labelled $H_2{}^{18}O$. The catalyst was first exposed to air at 823 K, followed by an exposure to CH_4 at 498 K. After 40 min, the catalyst was exposed to either aerobic ($^{16}O_2$, $H_2{}^{18}O$, CH_4) or anaerobic ($H_2{}^{18}O$, CH_4) feed gas compositions at 498 K. In both cases, following a switch from CH_4 to catalytic conditions, a disappearance of the C–O stretching band at 1033 cm^{-1} ($C^{16}O$) is observed over time, which is associated with the desorption of $CH_3{}^{16}OH$. A $C^{18}O$ stretching band at 1007 cm^{-1}, however, remained, suggesting a continued formation of $CH_3{}^{18}OH$. The authors did, however, not track the isotopically labelled products such as $CH_3{}^{18}OH$ with MS, which could have been a strong validation of the reactivation of Cu species proceeding by H_2O and not O_2.

7.2.4 The need for elevated temperatures. After a pretreatment at 823 K in air, Koishybay *et al.* showed that a catalytically operational anaerobic CH_4 oxidation was possible at 498 K. The productivity was however very low at $\sim$5 $\mu mol_{CH_3OH}\ g_{ZEO}^{-1}\ h^{-1}$. A reason for this low activity could be associated with the reversible poisoning effects of H_2O at low temperatures, thereby inhibiting CH_4 activation.[88,202] This suggests that higher operational temperatures are indeed necessary in catalytic operational mode. Jeong *et al.* performed their anaerobic cycling studies using Cu–MOR at temperatures between 623–673 K, and suggested that even at these comparatively high temperatures, the unpoisoning of the active site would remain an integral part of the mechanism (see Section 7.2.1).[240] When using H_2O as an oxidant itself therefore, significant attention must also be given toward the potential inhibiting ability of the oxidant itself, with this effect clearly being temperature dependent. A more detailed discussion on both the inhibiting and promoting effects of H_2O for the CH_4-to-CH_3OH conversion may be found in Section 10.

7.2.5 Influence of H_2O partial pressure. Zhou *et al.*[243] investigated the effect of H_2O partial pressure (7.5–32.5 mbar) on the performance of Cu–$CHA_{10.0}$. The authors found that the reaction order of H_2O on the CH_3OH formation rate varies with temperature. While at relatively low temperatures at 473 K, they observed a reaction order of 0.11, at elevated temperatures at 623 K, they reported a reaction order of 0.89. This could potentially be related to the poisoning effect of H_2O experienced at lower temperatures (see Sections 7.2.4 and 10.1).

8. Less common oxidants (NO, CO_2, H_2O_2) for the formation of active Cu-oxo species

8.1. NO

The use of NO as an oxidizing agent has not been explored thoroughly so far. One study by Sheppard *et al.*[85] reported the isothermal looping at 423 K with NO as the oxidizing agent over a $Cu_{0.28}MFI_{12.0}$, followed by the reaction with CH_4 and the extraction with H_2O vapor. In a schematic description of the mechanism, the authors assume that NO binds to individual Cu(I) centers and forms N_2O as well as a $[Cu_2(\mu\text{-}O)]^{2+}$ species. Subsequently, the thus formed N_2O is further capable of oxidizing another Cu(I) pair. The mechanism is based on the earlier work from Modén *et al.* on the NO decomposition over Cu-ZSM-5 (Fig. 14).[245]

Interestingly, in the same studies, the authors found that the amount of CH_3OH extracted from Cu-MFI was 2–6 times greater when H_2O vapor was used to perform the extraction compared to when liquid H_2O was used. Using *in situ* UV-Vis spectroscopy, the authors monitored the re-oxidation by following the absorption band at 22 000 cm^{-1}. This band, attributed to the $[Cu_2(\mu\text{-}O)]^{2+}$ active site, disappeared in the following exposure to CH_4, demonstrating that the re-oxidized species is active in the CH_4-to-CH_3OH conversion. Further, the authors revealed that at these low temperatures, only a fraction of Cu species can be re-oxidized, since the intensity of the UV-Vis band was much more intense after high temperature activation in O_2 or N_2O. No details about the kinetics of monomeric species are provided, as UV-Vis is not able to give detailed insights into their behavior. However, given the fact that only a small fraction of the Cu can be oxidized, it can be speculated that the vast majority of them are dimeric species since their oxidation is generally believed to be faster. The generation of monomeric Cu(II) from Cu(I) with NO has been shown earlier by Lamberti *et al.*[246] In this study, a series of MFI zeolites with low Al content (Si/Al = 180–100) was reacted with gaseous CuCl at 573 K, and an exchange level of 200% was assumed. After exposure to 8 mbar of NO for 10 min and again after evacuation for 60 min at ambient temperature, the EPR signal intensity showed an increase by a factor of 17 and 30, respectively, demonstrating that the oxidation of monomeric centers is possible. Complementary FTIR results indicate that this corresponds to a total amount of 28% of the Cu present in the

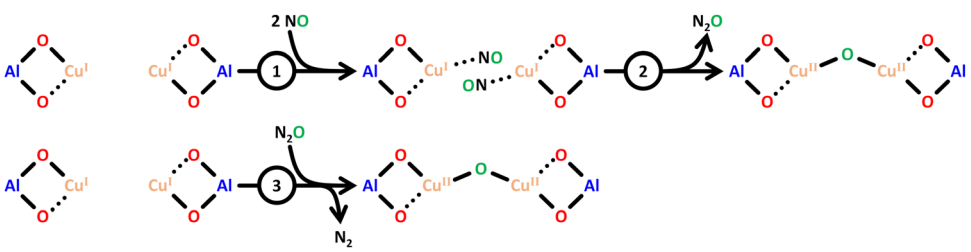

Fig. 14 Suggested mechanism of $[Cu_2(\mu\text{-}O)]^{2+}$ formation *via* oxidation of a Cu(I) pair using NO or *in situ* generated N_2O. Adapted from ref. 85 with permission from the Royal Society of Chemistry (Copyright 2014).

sample. While the material has not been tested for the conversion of CH_4 to CH_3OH, it shows that, in principle, monomeric species can be formed. The authors pointed out that the coordination and subsequent oxidation of the Cu(I) sites with NO is complicated by the decomposition reaction of NO into N_2O and NO_2, which can take place even at ambient temperature.

8.2. CO_2

The possibility of employing CO_2 as an activation agent has been explored by Pereira *et al.*[239] and Vieira *et al.*[247] Starting from the initial as-prepared/hydrated state, Pereira *et al.* exposed $Cu_{0.23}MAZ_{2.7}$ to CO_2 at 723 K, with UV-Vis spectra revealing a broad LMCT band around $\sim$41 200 cm^{-1}. A comparison to DFT calculated reference spectra suggested the species exhibiting the broad LMCT band to be $[CuOH]^+$ pairs. A low intensity band at 10 000–15 000 cm^{-1} was attributed to d–d transitions of Cu^{2+}. Using said activation procedure in CO_2 at 723 K, followed by CH_4 and H_2O exposure at 523 K, resulted in increasing productivity values as a function of the Cu/Al ratio, with the highest value of 163 $\mu mol_{CH_3OH}\ g_{ZEO}^{-1}$ achieved in the case of $Cu_{0.27}MAZ_{2.7}$. Notably, when an (auto)reduction procedure preceded CO_2 exposure at 723 K, the productivity significantly decreased. In the case of $Cu_{0.15}MAZ_{2.7}$ the observed CH_3OH productivity dropped from 94 to 43 $\mu mol_{CH_3OH}\ g_{ZEO}^{-1}$, which would suggest that the species able to be (auto)reduced are not able to be re-oxidized *via* CO_2 exposure. The authors further suggested that the species able to be re-oxidized *via* CO_2 exposure from an (auto)reduced state would be $Cu_{(x>3)}O_y$ species, with $[CuOH]^+$ suggested not to be able to be re-oxidized by CO_2 directly. Instead, any LMCT bands attributed to $[CuOH]^+$ observed after a high-temperature activation at 723 K in CO_2 in a following cycle were instead attributed to stem from a re-oxidation by H_2O during CH_3OH extraction (see Section 7.1.2).

Vieira *et al.*[247] also investigated the effect of CO_2 on $Cu_{0.1}CHA_{4.7}$. The authors employed an isothermal looping protocol, using CO_2 instead of O_2, over a range of temperatures. The highest CH_3OH productivity of 132 $\mu mol_{CH_3OH}\ g_{ZEO}^{-1}$ was observed at 673 K, with however a second consecutively performed cycle leading to a drastic decline in activity to $\sim$ 40 $\mu mol_{CH_3OH}\ g_{ZEO}^{-1}$. This stark decrease in productivity was attributed to both coke formation as well as incomplete Cu(I) oxidation. DFT calculations determined a true activation energy for the re-oxidation of a Cu(I) pair to $[Cu_2(\mu\text{-}O)]^{2+}$ and CO at 259 kJ mol^{-1}, therefore giving credence to the claim of incomplete Cu(I) oxidation. In addition, an (auto)reduction of $[CuOH]^+$ at elevated temperatures under a CO_2 atmosphere was suggested to occur. The authors, however, stated that the (auto)-reduction of $[CuOH]^+$ would not proceed in the first cycle due to an enhanced stability of $[CuOH]^+$. The source of the enhanced stability in the first cycle was, however, not further elucidated. In comparison, using O_2 as the oxidant led to an increase in CH_3OH productivity over consecutive cycles at 673 K. When comparing the spectra obtained at 673 K in a CO_2 atmosphere in Cu–CHA to the same conditions using O_2, a broader band at 40 000–45 000 cm^{-1}, attributed to both $[CuOH]^+$ and $[Cu_2(\mu\text{-}O)]^{2+}$ species, was observed. This broadening was assumed to mean a greater variety of the active Cu species following a CO_2 activation. A performed peak fitting of the spectra suggested a higher fraction of $[CuOH]^+$ pairs being present under a CO_2 atmosphere than under a O_2 atmosphere, which could indicate less condensation of $[CuOH]^+$ pairs to $[Cu_2(\mu\text{-}O)]^{2+}$ at 673 K. Since online MS or similar data are not provided, the role of CO_2 remains elusive, especially since the H_2O vapor from the product extraction might contribute to the oxidation, as suggested in the previous work of Pereira *et al.*[239]

8.3. H_2O_2

The use of H_2O_2 as an oxidizing agent for CH_4-to-CH_3OH conversion is more frequently reported over Fe-zeolites and over Cu-promoted Fe-zeolites.[248–252] Recently, Cu–zeolites have been investigated.[253–255] The use of H_2O_2 as an oxidizing agent has often been dismissed because of its higher economic value than CH_3OH. However, the reaction still attracts scientific interest, due to its high selectivity and mild conditions. In an early study, Armstrong *et al.*,[253] tested the low-temperature (323 K) conversion of CH_4, C_2H_6, and C_3H_8 in a batch reactor over Cu-MFI with varying Cu/Al and Si/Al ratios under elevated pressure (30–20 bar). A Cu-MFI yielded 49.86 $mmol_{CH_3OH}$, which equals 96.1% selectivity towards CH_3OH and a productivity of 3.7 $mol_{CH_3OH}\ kg_{ZEO}^{-1}\ h^{-1}$. They further found evidence by NO-FTIR measurements that isolated Cu(II) species characterized by a band at 1913 cm^{-1} are responsible for the selective conversion, however, the exact structure or sitting site has yet to be revealed. In over-exchanged zeolites, the authors reported an increase in overoxidation, while no further structural details have been provided on the active Cu site. Building on these results, Tang *et al.*[256] reported a Cu-MFI material featuring mostly monomeric Cu(II) species yielding 12 000 $\mu mol_{CH_3OH}\ g_{ZEO}^{-1}$ within 30 min at 343 K. The authors utilized a combination of *ex situ* XAS, high-angle annular dark-filed scanning transmission electron microscopy (HAADF-STEM), and EPR to characterize the isolated Cu(II) atoms and concluded that it is a bare Cu^{2+} site coordinated by four O_{fw} moieties in the 6-MR in the MFI framework. It should, however, be pointed out that the material was hydrated during these spectroscopic experiments, and the formation of species with higher nuclearity during the reaction cannot be ruled out based on these data. They further showed that the low loading, which presumably leads to only bare Cu^{2+} centers, significantly reduced the overoxidation of reaction intermediates to CO_2, which is observed with a reference material with higher Cu loading. This was further explained by DFT calculations that indicated that these proposed bare Cu^{2+} sites exhibit a uniquely reversed C–H bond activation trend, where the C–H bond of CH_4 is more readily activated than that of CH_3OH due to entropic and solvation contributions.[256] However, experimental evidence for the proposed conversion of CH_4-to-CH_3OH with H_2O_2 at an isolated Cu^{2+} site still needs to be shown. Further, it should be noted that the turnover frequency for these materials is rather low, with up to 340 h^{-1} and an overall CH_4 conversion of below 1%, accompanied by a H_2O_2 consumption of up to 80%. The reported CH_3OH selectivity is about 80%. The ratio between C1 oxygenates and the consumed H_2O_2 was found to be between 0.2–0.4. Further support for the proposed monomeric

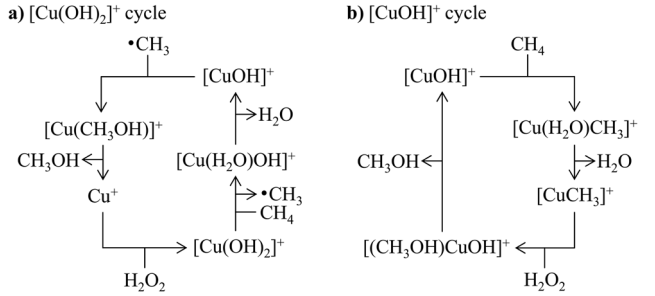

Scheme 14 The reaction network of catalytic CH_4-to-CH_3OH conversion in Cu-MFI based on H_2O_2 as an oxidant. The Cu(II) active site in cycles (a) and (b) corresponds to $[Cu(OH)_2]^+$ or $[CuOH]^+$, respectively. Adapted from ref. 254 with permission from Elsevier (Copyright 2023).

site as the active centers comes from a theoretical study by Cheng *et al.*[254] Their theoretical calculations revealed that the O–O bond of H_2O_2 can be broken to form surface-reactive hydroxyl groups through a H_2O-mediated mechanism at mononuclear Cu–zeolites, forming monomeric $[Cu(OH)_2]^+$ species (Scheme 14 and Scheme S1z). The authors further performed kinetic analysis and found that the resulting homolytic C–H bond activation mechanism leads to a trade-off between selectivity and activity of these sites, which are also responsible for H_2O_2 self-decomposition.

9. Influence of the material's state on the possibility of forming active species

The formation pathways of the most commonly observed Cu active site motifs in Cu-exchanged zeolites, beginning from either the as-prepared/hydrated state (left side of the scheme) or the (auto-)reduced state (right side of the scheme) under various activation conditions employed in the CH_4-to-CH_3OH conversion, are illustrated in Scheme 15. As emphasized throughout this review, the initial state of the zeolite sample has a profound effect on the type of species formed during the activation procedure.

9.1 As-prepared/hydrated state

The as-prepared/hydrated state on the left side of Scheme 15 represents a common starting point for materials evaluation and spectroscopic investigations. In this state, the Cu(II) species exist primarily as $[Cu(H_2O)_6]^{2+}$ and $[Cu(OH)(H_2O)_5]^+$. Subjecting hydrated samples to heat and gas flow or vacuum will first lead to a partial dehydration of the Cu(II) ions and subsequently to their attachment to the zeolite framework, where the respective active sites are formed, as demonstrated by spectroscopic interrogation and quantitative mechanical modelling.[45]

Samples used in their as-prepared/hydrated state without calcination exhibit markedly different activation behavior, particularly under inert conditions or vacuum, compared to properly calcined samples due to the presence of organic residues. The influence of sample pretreatment has been, for example, shown by Sushkevich *et al.*[101] The authors employed *in situ* XANES spectroscopy to compare the temperature-induced Cu(I) generation in as-prepared/hydrated *vs.* pre-calcined Cu–MOR during treatment in He from 300 to 1100 K. A pronounced increase in the Cu(I) fraction at approximately 495 K was observed in the as-prepared/hydrated material, whereas temperatures above 650 K were necessary to induce noticeable decreases in Cu(II) in the pre-calcined samples. Exposing uncalcined samples to a heat treatment under an inert atmosphere or vacuum may therefore entail a substantial reduction of Cu(II) to Cu(I). This phenomenon has at times been misinterpreted to be a result of (auto)reduction.[98,99] This reduction coincides with the formation of radical coke species, as evidenced in the EPR spectra, providing proof that carbonaceous residues are responsible for the reduction of Cu(II) during thermal treatment under inert conditions.

9.1.1 Monomeric sites. As indicated on the left side of the Scheme 15, the formation of monomeric species, from the hydrated/as prepared state, including bare Cu^{2+} and $[CuOH]^+$, has been observed under various conditions, including the application of vacuum and inert conditions as well as in the presence of O_2, N_2O, and CO_2. EPR spectroscopy has been proven to be a valuable tool to trace the formation of these species, since the H_2O coordinated Cu(II) ions exhibit a distinct spectroscopic fingerprint in comparison to Cu(II) centers attached to the framework.[42,43,45,46,111] The formation of bare Cu^{2+} sites proceeds *via* stepwise dehydration of $[Cu(H_2O)_6]^{2+}$, whereas the formation of a $[CuOH]^+$ species originates, for example, from $[Cu(OH)(H_2O)_5]^+$, but the deprotonation can also occur at a different stage during dehydration. The latter is formed due to the transformation of ligated H_2O into OH^-, which is facilitated by the electrostatic field imposed by the framework and yields H^+ as a charge balancing ion.[94] As already highlighted by Kucherov *et al.* for calcined Cu–zeolites with exclusively monomeric species, the EPR intensity will remain unaffected by heat treatment in an inert atmosphere up to 723 K, and reduction is more likely due to carbonaceous species rather than (auto)reduction.[42] This further suggests that monomeric species, including bare Cu^{2+} as well as $[CuOH]^+$, are comparatively stable towards (auto)reduction in vacuum or inert atmosphere, which has also been highlighted by Heyer *et al.* and Brenig *et al.*[62,127]

9.1.2 Dimeric species. Dimeric sites can be formed in analogy to the monomeric species in inert conditions or under vacuum, as well as in the presence of O_2, NO, N_2O, and CO_2 from the as-prepared/hydrated state, as indicated on the left-hand side of the Scheme 15. Typically, $[Cu_2(\mu\text{-}O)]^{2+}$ can form *via* the condensation of two $[CuOH]^+$ species upon the removal of a H_2O molecule. In comparison to monomeric species, however, dimeric species are more prone toward (auto)reduction at elevated temperatures in the absence of carbonaceous compounds.[62,101,127,131] It is important to point out that incomplete oxidation of Cu(I) species at high temperatures above 650 K has been observed even in the presence of oxidizing agents such as N_2O or O_2. This phenomenon has for example been extensively studied for the catalytic N_2O decomposition ability of Cu–zeolites, typically performed at ~723 K. This incomplete formation of active Cu(II) species for the subsequent application in the CH_4-to-CH_3OH

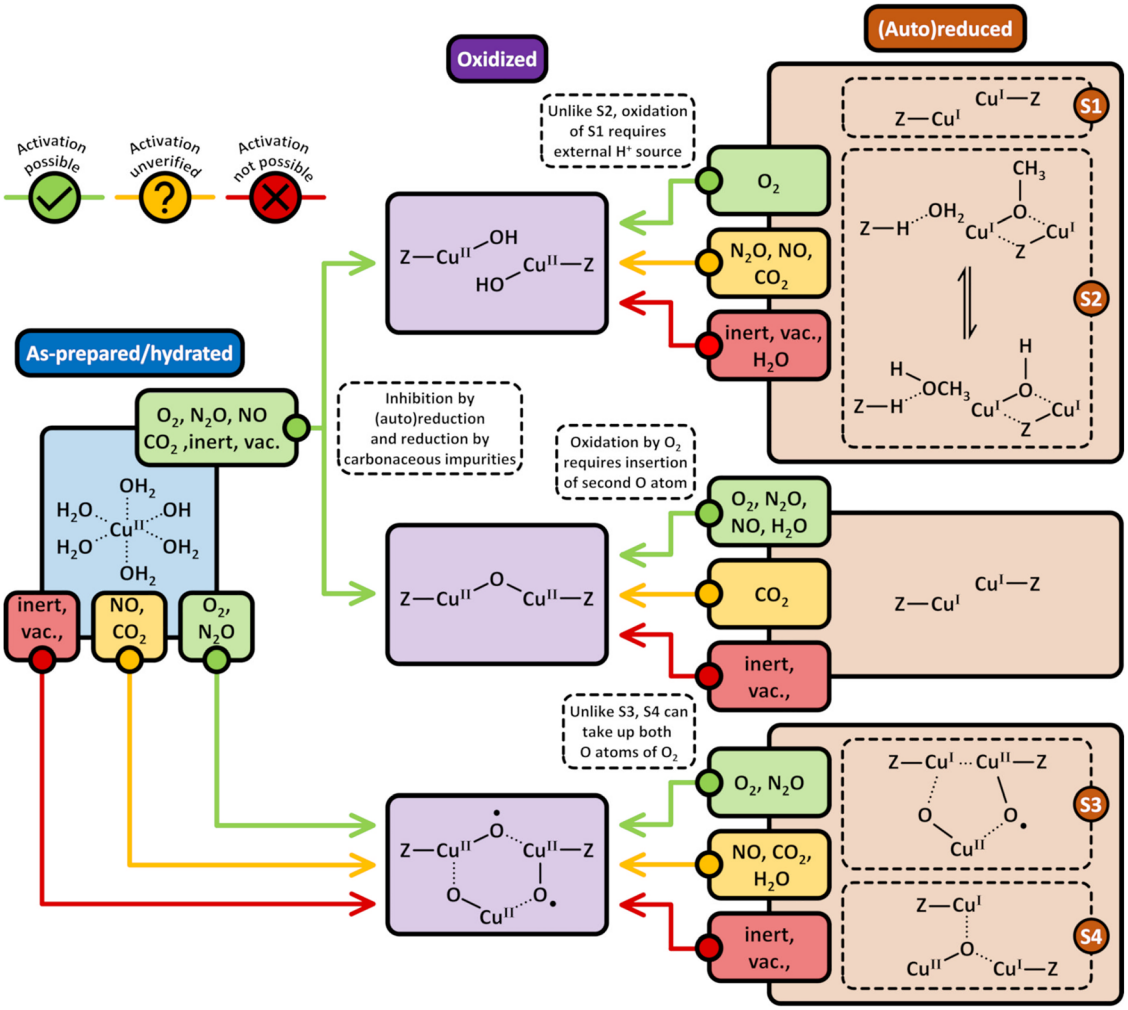

Scheme 15 The possibility to form Cu-oxo active sites (violet background) with a certain oxidant in Cu-exchanged zeolites, beginning from either the as-prepared/hydrated state (blue background) or the (auto)reduced state (brown background). Arrows and oxidants highlighted in green, red, and yellow indicate whether the generation of a certain oxygenated Cu(II) species by a specific oxidant is possible, not possible, or has not yet been verified. (Auto)reduced $[CuOH]^+$/$[CuOH]^+$ may exist either as two plain Cu(I) ions (S1), or as a BAS containing site (S2). This distinction is important as, unlike in the case of S2, the generation of $[CuOH]^+$/$[CuOH]^+$ from S1 necessitates an external H^+ source. Unlike the reaction of $[Cu_3(\mu\text{-}O)_2]^{2+}$ (S3) with O_2, the formation of $[Cu_3(\mu\text{-}O)_3]^{2+}$ *via* interaction of $[Cu_3(\mu\text{-}O)]^{2+}$ (S4) with O_2 does not require a location to accommodate the second O moiety. Dotted bonds correspond to dative interactions. The term "Z" describes the negatively charged zeolite lattice.

conversion can be avoided by cooling the sample to reaction conditions after high-temperature treatment under oxidizing conditions, which leads to the more favorable oxidation of Cu(I) to Cu(II) at lower temperatures.[127] This, in turn, questions the origin of the effects of difference in activity observed in high-temperature activation conducted at different temperatures and durations, which are typically attributed to changes in the active site speciation due to the high-temperature treatment. However, since the reaction is conducted at a lower temperature, it can be expected that even if changes occur at high temperature, they are reversible upon cooling the sample in oxidation conditions to the reaction temperature if these processes are not kinetically hindered.

9.1.3 Trimeric centers. Contrary to monomeric and dimeric species, the formation of trimeric species from the as-prepared/hydrated state requires the presence of oxidizing agents such as N_2O and O_2, as indicated by the red and green colors in Scheme 15. The use of NO in the formation of trimeric species has not yet been thoroughly tested; however, since the activation of NO is believed to result in the *in situ* generation of N_2O, one might argue that trimeric formation could be possible with NO as well. Similarly, the use of CO_2 has not yet been clarified, therefore the path is marked with yellow color in the Scheme 15.[245]

9.2 (Auto)reduced state

Starting from a fully (auto)reduced material (*e.g.*, after CH_4 treatment), oxidizing agents are necessary for the reformation of all Cu-oxo active sites, whereas treatment under inert conditions, *e.g.*, He or vacuum, will not lead to the generation of active sites as indicated on the right-hand side of the Scheme 15.

9.2.1 Monomeric centers. Monomeric species, including bare Cu^{2+} and $[CuOH]^+$, are reported to form upon exposure to

molecular O_2.[43,45,46,50,58,109,127,141] Similar to the as-prepared/hydrated state, it is necessary to carefully distinguish between a reduced material without and with CH_x residues, such as adsorbed CH_3O species, denoted in Scheme 15 as S1 and S2, respectively. In the presence of carbonaceous species, exposure to O_2 at high temperature will lead to the formation of CO_2 and H_2O, which may act as a H^+ source for the formation of $[CuOH]^+$ sites. In their absence, another H^+ source is necessary to generate the $[CuOH]^+$ species, such as neighboring BAS. In a first step, the interaction of O_2 with isolated Cu(I) sites is proposed to result in the generation of both $[Cu(\eta^1\text{-}O_2^{\bullet})]^+$ and $[Cu(\eta^2\text{-}O_2^{\bullet})]^+$ species, while it remains to be determined how these centers can convert into Cu^{2+} and $[CuOH]^+$. Besides O_2, only a few accounts of the application of different oxidants for the regeneration of monomeric species can be found. For example, Lamberti *et al.* reported an increase in the EPR spectrum of Cu-MFI after 8 mbar of NO is dosed. It should be noted that the oxidized material was not employed in the CH_4-to-CH_3OH conversion.[246] Further, the participation of EPR active monomeric species in N_2O decomposition has been reported in the presence of a reducing agent, which opens an O migration pathway, suggesting that they can be oxidized by N_2O.[207] It should also be emphasized that high-temperature N_2O activation might lead to catalytic N_2O decomposition over dimeric species, resulting in the *in situ* generation of O_2 capable of re-oxidizing monomeric species. Similar to inert conditions, the use of CO_2 and H_2O has been shown to be insufficient to form monomeric Cu^{2+} centers from the reduced state.

9.2.1 Dimeric species. The formation of the $[Cu_2(\mu\text{-}O)]^{2+}$ core from the fully reduced state has been much more carefully assessed compared to the monomeric species. Analogous to the regeneration of monomeric species, treatment in vacuum or inert gas does not induce the formation of dimeric species, while the usage of CO_2 is still debated. Exposure to O_2, NO, NO_2, and H_2O has been shown to lead to $[Cu_2(\mu\text{-}O)]^{2+}$ formation, as shown in the Scheme 15. While the regeneration with O_2 is suggested to proceed *via* $[Cu_2(\mu\text{-}\eta^2\text{:}\eta^2\text{-}O_2)]^{2+}$ as a precursor, the usage of N_2O most likely leads to the formation of a μ-1,1-O binding state prior to the regeneration of $[Cu_2(\mu\text{-}O)]^{2+}$.[66,145] Sheppard *et al.* reported the formation of the $[Cu_2(\mu\text{-}O)]^{2+}$ with NO at temperatures as low as 423 K. While no mechanistic study was conducted, the authors assumed NO condensation over nearby sites, which was previously reported for the NO decomposition reaction.[85] The formation of the $[Cu_2(\mu\text{-}O)]^{2+}$ core with H_2O has been reported to evolve *via* a $[Cu_2(\mu\text{-}OH)(\mu\text{-}H)]^{2+}$ intermediate and the subsequent generation of H_2 upon contacting the reduced materials with H_2O. As discussed above, the formation of active dimeric centers is usually not complete at high temperatures due to their pronounced (auto)reduction.[88]

9.2.3 Trimeric sites. For the regeneration of trimeric species from a fully reduced sample, two initial conditions need to be distinguished, denoted as S1 and S2 in Scheme 15. The former requires the insertion of a second O atom from an O_2 molecule into a different structural position, in analogy to the formation of the $[Cu_2(\mu\text{-}O)]^{2+}$ species. In contrast, this issue does not arise in the case of the transformation of $[Cu_3(\mu_3\text{-}O)]^{2+}$ (S2) into $[Cu_3(\mu\text{-}O)_3]^{2+}$, since the latter can accommodate two additional O^{2-} ions. The formation of trimers was also investigated *via* N_2O using $Cu_{0.4}MOR_{20.0}$, where a reactivation at 873 K of the material in N_2O, following a complete cycle, once again resulted in the observation of LMCT bands at 34 000–39 000 cm^{-1}, thereby showing that the trimeric species was able to be reconstituted from a reduced state.

10. The role of H_2O in Cu–zeolite for CH_4-to-CH_3OH conversion

As outlined in previous sections, especially in Section 7, the formation of active Cu(II) sites in zeolites for CH_4-to-CH_3OH conversion is highly influenced by the presence of H_2O, independent of the activation and starting conditions employed. However, the exact role, especially in continuous catalytic CH_4-to-CH_3OH conversion, remains a subject of debate. In the following, the different roles of H_2O are outlined besides its discussed role as an oxidizing agent.

10.1 H_2O as an inhibitor of active sites

Complete dehydration of Cu–zeolite materials is particularly important to achieve high activity, as the strongly hydrophilic Cu-oxo species readily adsorb H_2O. This adsorption saturates the coordination sphere of the Cu(II) active sites, rendering them inaccessible to CH_4 and effectively poisoning them. Sushkevich *et al.* emphasized this phenomenon by combining FTIR spectroscopy with NO probe molecule adsorption, demonstrating that the interaction of even a single H_2O molecule with $[Cu_2(\mu\text{-}O)]^{2+}$ and $[CuOH]^+$ species is sufficient to completely deactivate these active centers when a low CH_4 partial pressure is employed (see Section 4.3).[202] The impact of incomplete dehydration was further illustrated by Tomkins *et al.*, who compared the CH_3OH output of Cu–MOR during interaction with 1 bar CH_4 at 473 K after activation in 1 bar O_2 at either 723 K for 4 h or 473 K for 13 h.[17] The authors observed a significant decrease in CH_3OH productivity from approximately 45.3 to 2.1 $\mu mol_{CH_3OH}\ g_{ZEO}{}^{-1}$ with the isothermal looping process, likely due to incomplete dehydration. The same was observed by Wieser *et al.* in the case of Cu-MAZ using the isothermal looping procedure.[111,205] When increasing the cycling temperature from 473 to 548 K, a significant increase in yield from ~75 to 275 $\mu mol_{CH_3OH}\ g_{ZEO}{}^{-1}$ per cycle was observed. A LCF analysis of the spectra collected *via in situ* XANES spectroscopy further revealed a significant decrease in the fraction of hydrated Cu(II) during O_2 exposure when increasing the cycling temperature. Although elevated CH_4 pressures can partially mitigate the inhibitory effect of competitive H_2O adsorption, the disparity in CH_3OH output between the two procedures generally persists.[17,201,203,205]

10.2 H_2O-induced enhancement of CH_3OH productivity

A distinction must be made between the documented poisoning effect of H_2O on active sites and its role in enhancing CH_3OH productivity across sequential redox cycles (see Section 4.2.6). Bozbag *et al.* reported that the CH_3OH productivity of

Cu–MOR increased by approximately 30% between the first and second cycle and remained relatively constant thereafter.[199] This enhancement was attributed to facilitated Cu(II) active site formation during the second calcination period, resulting from material hydration throughout the aqueous CH_3OH extraction of the first cycle. Similar productivity enhancements over multiple redox cycles have been reported by Pappas *et al.* for Cu-FER and Cu–CHA.[89,169] These improvements were attributed to hydration-induced displacement of residual Cu(II) species from redox-inert positions during CH_3OH extraction and their subsequent transformation into oxygenated Cu(II) active centers during O_2 treatment in the following reaction cycle. Inactive Cu(II) species usually correspond to isolated bare Cu^{2+} ions, and the formation of these Cu(II) centers is characterized by a significantly lower Gibbs free energy compared to that of any active mono- or multimeric Cu-oxo species under the conditions of Cu–zeolite activation. Therefore, the driving force for this redistribution phenomenon is not clear and deserves further attention.[103] Interestingly, a drop in the CH_3OH output of Cu-MAZ by $\sim$40% during four consecutive cycles has been reported by Wieser *et al.* and Knorpp *et al.*, which was associated with a gradual migration of active Cu(II) species from the 8-MR channel to an inert position in the 6-MR.[111,200] The origin of this rearrangement phenomenon was related to the extensive dehydration of the material throughout activation at 723 K under an O_2 atmosphere, which was proposed to enable the transfer of Cu between the different ion exchange positions. Notably, the migration of Cu(I) ions should not be influenced by H_2O, since they exhibit diminishing affinity to H_2O ligands, which makes migration during activation in the presence of an oxidation agent more likely. Nevertheless, it remains uncertain why this migration occurs over multiple redox cycles and is not complete after the very first activation from the hydrated or reduced state. As discussed above, for an accurate description of the effects related to Cu migration, a detailed analysis of the Cu speciation after each cycle is required to quantify the effect and evaluate the significance of these rearrangements, and whether they can explain the changes in activity. This is further complicated by the influence of H_2O on the spectroscopic signatures of the active sites.

10.3 Spectroscopic identification

Contact with H_2O not only inhibits catalytic activity but also suppresses the characteristic spectroscopic UV-Vis fingerprints of active dimeric Cu(II) sites, complicating the identification of existing species. Smeets *et al.* observed the reversible disappearance of the UV-Vis band at 22 700 cm^{-1}, associated with the active $[Cu_2(\mu\text{-}O)]^{2+}$ center in Cu-MFI, upon switching between H_2O-saturated N_2O streams at 637 and 723 K and pure N_2O flow.[207] Similarly, Brenig *et al.* observed decreased absorbance of the LMCT bands of two different $[Cu_2(\mu\text{-}O)]^{2+}$ motifs at $\sim$26 700 and $\sim$22 400 cm^{-1} in the UV-Vis spectrum of calcined and O_2-treated Cu–CHA during interaction with H_2O at 473 K.[127] This suggests that intact $[Cu_2(\mu\text{-}O)]^{2+}$ centers could be present after calcination at 473 K but remain undetectable *via* UV-Vis spectroscopy due to high residual H_2O content. Similarly, UV-Vis spectra from Sheppard *et al.* demonstrated the disappearance of the band at 22 000 cm^{-1}, attributed to $[Cu_2(\mu\text{-}O)]^{2+}$ species, after switching from NO to H_2O containing gas feed in $Cu_{0.8}MFI_{12.0}$.[85] Remarkably, the introduction of NO after H_2O exposure and purging with He led to the appearance of a weak UV-Vis signal despite incomplete dehydration in the same study. Similarly, the exposure to H_2O is expected to alter the appearance of the EPR signal of the monomeric species. Even though no systematic study exists in which the EPR signal of activated zeolites was recorded upon dosing traces of H_2O, the fact that the EPR signal is very different prior to dehydration indicates that H_2O will have an effect on the EPR signal. These limitations pose significant challenges for identifying active species in the presence of H_2O, particularly in catalytic CH_4-to-CH_3OH conversion and even more severe in liquid-phase processes employing H_2O_2 as an oxidizing agent. Under these conditions, the absence of UV-Vis fingerprints for active dimeric cores is not sufficient evidence to rule out their presence. For example, Narsimhan *et al.* exposed (auto)reduced Cu-MFI to an $O_2/CH_4/H_2O$ feed and observed the onset of steady-state CH_3OH production. However, they ruled out the presence of $[Cu_2(\mu\text{-}O)]^{2+}$ since complementary UV-Vis spectra collected throughout the induction period did not display a pronounced LMCT band at $\sim$22 700 cm^{-1}.[209] Conversely, in a subsequent study by the same research group, $[Cu_2(\mu\text{-}O)]^{2+}$ was identified as the Cu(II) active site for catalytic CH_4 partial oxidation in Cu–CHA through analysis of EXAFS spectra collected at 543 K under steady-state CH_3OH production.[212] The extent to which species observed under dry conditions prevail under wet conditions remains debated, with theoretical investigations instead suggesting the emergence of distinct different species under wet conditions.

In that line, a $[(HO)Cu(\mu\text{-}OH)Cu(O)]^{2+}$ core has been proposed as the active species in partially hydrated Cu–zeolites by Yumura *et al.*, who studied the interaction of O_2 and H_2O with reduced Cu-MFI using DFT.[208] This species originates from a $[Cu_2(trans\text{-}\mu\text{-}1,2\text{-}O_2)(H_2O)]^{2+}$ intermediate, which is transformed into $[Cu_2(trans\text{-}\mu\text{-}1,2\text{-}OOH)(OH)]^{2+}$ *via* H atom transfer from the H_2O ligand onto the bridging O_2 moiety. Further, another H atom transfer and simultaneous O-OH bond cleavage result in a $[Cu_2(\mu\text{-}O)(OH)_2]^{2+}$ species, which is the direct precursor for the active site. Similarly, Ipek *et al.* suggested this same species during continuous CH_4-to-CH_3OH conversion with N_2O as an oxidizing agent, and theoretical calculations indicated that the site could cleave the C–H bond of CH_4 more efficiently than the $[Cu_2(\mu\text{-}O)]^{2+}$ species.[13,228] However, experimental evidence for such a dimeric structure remains elusive. The first experimental identification of an active site during the cyclic, isothermal CH_4-to-CH_3OH conversion is a paired $[CuOH]^+$ site in Cu-MAZ.[111] Currently, it remains unclear whether dimeric and trimeric Cu-oxo centers can develop under the activation conditions employed in isothermal CH_4 hydroxylation and whether their structures resemble those generated during high-temperature calcination in non-isothermal CH_4 hydroxylation. Experimental evidence from EPR measurements of fully hydrated samples indicates that all or at least an overwhelming majority of the Cu(II) within the framework are present as monomeric species,

raising questions about the formation of multimeric sites, at least in fully hydrated samples.[43,46]

10.4 H_2O in liquid-phase H_2O_2 oxidation

The role of H_2O becomes even less clear, and experimental evidence is scarcer, for active Cu(II) species existing in the liquid phase during H_2O_2 oxidation (see Section 8.3). Typically, materials are analyzed prior to catalytic testing in either the hydrated state or after dehydration, and spectroscopic signatures are assigned to distinct species by analogy to literature focusing on dehydrated species. However, these species might not be present in this composition under actual reaction conditions.

A notable exception is a study by Yashnik *et al.*, who employed mixed Fe-/Cu–zeolites and recorded *ex situ* UV-Vis spectra at specific points during the reaction, suggesting the presence of both monomeric and dimeric Cu(II) species.[257] Their UV-Vis measurements indicated the existence of terminal peroxo complexes (Cu–OOH, LMCT at 36 000 cm^{-1}) originating from isolated Cu(II) ions in the presence of H_2O_2, as well as binuclear Cu(II) peroxo complexes connected *via* terminal OOH groups (LMCT at 20 700 cm^{-1}) or bridging OO groups (LMCT at 26 700 cm^{-1}). It should be noted, however, that the samples were measured *ex situ*, and contributions of Fe(III) species were not accounted for in the UV-Vis spectra, raising questions about the transferability of these results to pure Cu–zeolite materials.

Theoretical investigations by Cheng *et al.* demonstrated that the H_2O_2 O–O bond could be readily cleaved through an H_2O-mediated mechanism at monomeric Cu(II) sites in zeolites to form reactive $[Cu(OH)_2]^+$.[254] These sites were proposed to be responsible for C–H bond activation at low temperatures, overoxidation of CH_3OH, and the self-decomposition of H_2O_2. Tang *et al.* also proposed monomeric Cu^{2+} sites attached solely to framework O atoms within the 6-MR as active sites even in the presence of H_2O.[256] This assignment, however, is in contrast to the EPR spectra of hydrated materials, which usually show no indication of a framework-bound species.[43,45,46]

11. The need for examination of Cu(I) speciation

As outlined in this review, substantial work has been conducted to elucidate the structural characteristics of the Cu(II) sites present in zeolitic hosts. The complexity of this task is highlighted by the ongoing debates regarding the exact location and configuration of various species. However, when compared to the knowledge gained on Cu(II) sites, the current insights into the nature of Cu(I) species are extremely limited. Very few studies have investigated Cu(I) speciation in Cu-exchanged zeolites. Notable exceptions include work by Dědeček *et al.* and Wichterlová *et al.*, who utilized NO-FTIR and PL spectroscopy to provide indirect information about Cu(I) speciation and demonstrate correlations between different Cu(I) and Cu(II) sites.[44,258] These investigations showed the existence of at least four distinct Cu(I) species, revealing that the speciation of Cu(I) sites exhibits a complexity and variety comparable to that of Cu(II) sites. Furthermore, complementary EPR measurements using NO as a probe molecule confirmed the presence of multiple Cu(I) sites in MFI and MCM-22 zeolites. This was evidenced by the formation of Cu(I)–NO adsorption complexes originating from two distinct Cu(I) sites within the zeolite framework, each coordinated by different numbers of framework oxygen ligands.[259–261] Further work on the photocatalytic decomposition of NO over Cu(I) sites has revealed three distinct Cu(I) species by synchronous PL spectroscopy in MFI, including two monomers, previously identified with NO-EPR, and one Cu(I)–Cu(I) dimer structure.[262] Further evidence for a distinct Cu(I) speciation and a resulting difference in reactivity comes from early work on photocatalytic decomposition of N_2O. For example Anpo *et al.* investigated the reaction of N_2O with Cu(I) species in Cu-FAU and found that dependent on the Si/Al ratio, two distinct isolated linear coordinated Cu(I) monomers as well as a dimer can exist and concluded that monomeric Cu(I) will be the more active of the two in the photocatalytic N_2O decomposition at ambient temperature.[263] Yamashita *et al.* investigated Cu–$MOR_{14.9}$ with a weight loading of 1.9 wt% Cu, and by the utilization of CO probe molecules and XAS experiments revealed that isolated Cu(I) monomers with planar three-fold or linear two-fold coordinate geometry exist within the framework.[264] Wieser *et al.* were able to pinpoint the exact locations of Cu during CH_4 exposure with *in situ* AXRPD.[111] While no verification of the oxidation state was delivered, Rietveld analysis was able to identify a CH_3O species bound to a Cu moiety, thereby implying that a reduction to Cu(I) during CH_4 exposure had occurred. In general, however, the exact location and structural arrangement of Cu(I) centers remain largely unresolved. Since Cu(I) species serve as precursors for both bare Cu(II) and active Cu(II)-oxo sites, their structural elucidation is a prerequisite to gaining mechanistic insights regarding Cu(II) formation. Therefore, methods suitable for direct structural characterization, such as advanced synchrotron techniques including EXAFS, AXRPD, or pair distribution function (PDF), should be applied. Additionally, complementary studies employing probe molecules and indirect spectroscopic methods, such as PL, NO-EPR, and NO-FTIR, reinforced by computational modeling, can contribute invaluable information and may allow for unambiguous identification of the respective location. Starting with materials with very low Cu loading and probing the reducibility of bare Cu^{2+} sites with CH_4, the Cu(I) speciation can be varied by increasing Cu/Al and changing the Si/Al ratio. This approach can establish a path toward a comprehensive understanding of these critical precursors to active sites in Cu-exchanged zeolites for CH_4-to-CH_3OH conversion.

12. Conclusion and outlook

Cu(II) species can form within zeolitic matrices, ranging from isolated bare Cu^{2+} and $[CuOH]^+$ ions over a variety of different dimeric species, including $[Cu_2(\mu\text{-}O)]^{2+}$ to trimeric $[Cu_3(\mu\text{-}O)_3]^{2+}$ species. The local environment of the zeolite topology, defined by the Al content and distribution throughout the framework,

governs the type and the proximity of Cu(II) centers and therefore the redox activity and stability of these species. Their (re)generation is determined by complex (inter-)dependencies, which include the initial state of the material, the zeolite framework properties, as well as exposure temperature and duration to a given activation process.

As demonstrated above, the starting condition of the material and the pretreatment play significant roles in the formation of the active Cu sites and, therefore, in the material's performance in CH_4-to-CH_3OH conversion. Unfortunately, in various studies, the starting conditions of the material are ill-defined, leading to ambiguities in interpretation and conflicting results. This also holds for the reproducibility test and the influence of the H_2O steaming or wet extraction, which has been claimed to have various influences on the materials' performance. Authors need to be clearer about the starting states of their materials and catalysts at the beginning of each cycle to be able to unravel the source of the large number of conflicting reports in the literature. Systematic studies from well-defined states, such as carefully calcined hydrated samples or after an *in situ* calcination, will help clarify the influence of the material's state on its performance in the CH_4-to-CH_3OH conversion and lead to more consistent results. Importantly, the Cu speciation as well as the presence of carbonaceous residues need to be assessed prior to every cycle. Since no single spectroscopic technique is capable of providing complete insights, a combination of various methods, including but not limited to UV-Vis, EPR, XANES, FTIR, and Raman, is necessary to identify the relative presence of monomeric, dimeric, and multimeric species in a given sample. While *in situ* and *operando* measurements provide important information about the state of the samples, *ex situ* measurements of carefully prepared sealed samples can also contribute greatly. Furthermore, the influence of CH_x and H_2O on the active site formation needs to be assessed. One potential approach could be by using different reducing agents than CH_4, such as CO and H_2. Employing CO would preclude the formation of H_2O, while H_2 would preclude the formation of CH_x species after careful pretreatment. A comparison of the different states could allow for further studies to unravel both the influence of CH_x and H_2O on active site formation.

Besides the importance of the material's state, as indicated in the Scheme 15, several open questions regarding the formation of specific sites under certain oxidation conditions persist. This includes a thorough investigation of the formation of $[CuOH]^+$ upon exposure of reduced material to NO and N_2O. This question is especially important to study in the present and absence of H_2O as a potential proton source. Additional questions remain about the relative fraction of various Cu species after exposure to N_2O and O_2. Despite the belief that both oxidants form isostructural Cu-oxo sites, the activation of Cu–zeolites using either O_2 or N_2O proceeds through fundamentally different pathways, resulting in distinct Cu-oxo species with varying methanol productivity in the CH_4-to-CH_3OH conversion. Importantly, O_2 activation requires accommodating the second oxygen atom from O–O bond cleavage at nearby Cu(I) sites, potentially limiting the formation of isolated $[Cu_2(\mu\text{-}O)]^{2+}$ centers. Future research should focus on *in situ* characterization techniques that can directly observe the formation and transformation of active sites under reaction conditions, such as XANES or FTIR. For example, treatment at different temperatures in N_2O and O_2 could resolve the structural rearrangements that occur during the transformation of Cu(I) into active Cu(II) centers. Facilitating the identification and structural characterization of potential active site precursors.

Similarly, the active site identification and structural characterization of species existing in the presence of H_2O in the isothermal (catalytic) schemes deserves some attention. While different sites such as the $[(HO)Cu(\mu\text{-}OH)Cu(O)]^{2+}$ core have been proposed, which could theoretically be active in the CH_4-to-CH_3OH, a detailed spectroscopic characterization is missing. A major factor for the lack of properly characterized active sites in the isothermal (catalytic) scheme is that a structural characterization remains challenging, especially because UV-Vis bands tend to diminish in the presence of H_2O. Therefore, a set of spectroscopic tools needs to be developed that can trace the fate of Cu motifs under catalytic conditions, with high accuracy, to reveal the active fraction. It can be expected that only a small fraction of the present Cu(II) will be active, since the majority will exhibit a H_2O coordination shell. This problem also extends to the liquid state and the use of H_2O_2, where the characterization of the potential Cu(II) active sites is even more difficult. The extraction of spectroscopic fingerprints of species that are obscured by spectator species can be done by applying spectroscopic methods under the paradigm of modulation-excitation with phase-resolved detection (MES-PSD).[265–268] MES-PSD is a transient response method that relies on periodic perturbation of the system under investigation. This perturbation can be achieved by modulation of the gas feed of the reaction. After data treatment, the resulting spectra in the phase domain exclusively show those species undergoing reversible changes with the same frequency as the applied perturbation. The background, as well as static signals arising from spectator sites, are sufficiently suppressed. Variation in the gas feed between O_2/N_2O, H_2O, and reducing agent, while monitoring the material with XANES, FTIR, or EPR, could lead to the identification of the spectroscopic fingerprints of the truly active species and subsequently to their full characterization. *In situ* AXRPD has also proven to be a very powerful technique, and is not restricted to any particular temperature range. A multimodal operational scheme of combining AXRPD with spectroscopic techniques, such as XANES and UV-Vis spectroscopy, may also prove to be a useful tool for unraveling the different Cu sites in a given zeolite framework.

In conclusion, this review summarizes the significant progress and also some persistent lack thereof made over the last decades in understanding the formation of the active Cu(II) site in CH_4-to-CH_3OH conversion and highlights common misconceptions and knowledge gaps. Common assumptions about Cu(II) site formation are challenged, and a more holistic view of the CH_4-to-CH_3OH, including the active site formation and Cu(I) speciation, is encouraged. Only by understanding and controlling all of these steps can a given material's performance

be understood, and an efficient, selective, and scalable CH_4 oxidation can be achieved.

Author contributions

J. W. A. F. conceptualization, writing the original draft, review, and editing. A. B. conceptualization, writing the original draft, review, and editing. J. W. conceptualization, writing the original draft, review, and editing. J. A. B. review and editing. V. L. S. conceptualization, supervision, review, and editing. All authors contributed to the editing of the final version of the manuscript.

Conflicts of interest

There are no conflicts to declare.

Data availability

No primary research results, software, or code have been included, and no new data were generated or analyzed as part of this review.

Acknowledgements

J. W. A. F. gratefully acknowledges support through a JSPS Postdoctoral Fellowship (PE24052). J. W. A. F., A. B., J. A. vB. and V. L. S. thank ETH Research Grant ETH-48 20–1.

References

1 S. Thomas and R. A. Dawe, Review of ways to transport natural gas energy from countries which do not need the gas for domestic use, *Energy*, 2003, **28**, 1461–1477.
2 Z. Zakaria and S. K. Kamarudin, Direct conversion technologies of methane to methanol: An overview, *Renewable Sustainable Energy Rev.*, 2016, **65**, 250–261.
3 U. Olsbye, S. Svelle, M. Bjørgen, P. Beato, T. V. W. Janssens, F. Joensen, S. Bordiga and K. P. Lillerud, Conversion of Methanol to Hydrocarbons: How Zeolite Cavity and Pore Size Controls Product Selectivity, *Angew. Chem., Int. Ed.*, 2012, **51**, 5810–5831.
4 D. J. Wilhelm, D. R. Simbeck, A. D. Karp and R. L. Dickenson, Syngas production for gas-to-liquids applications: technologies, issues and outlook, *Fuel Process. Technol.*, 2001, **71**, 139–148.
5 R. J. Bunting, P. S. Rice, J. Thompson and P. Hu, Investigating the innate selectivity issues of methane to methanol: consideration of an aqueous environment, *Chem. Sci.*, 2021, **12**, 4443–4449.
6 V. I. Sobolev, K. A. Dubkov, O. V. Panna and G. I. Panov, Selective oxidation of methane to methanol on a FeZSM-5 surface, *Catal. Today*, 1995, **24**, 251–252.
7 M. H. Groothaert, P. J. Smeets, B. F. Sels, P. A. Jacobs and R. A. Schoonheydt, Selective Oxidation of Methane by the Bis(μ-oxo)dicopper Core Stabilized on ZSM-5 and Mordenite Zeolites, *J. Am. Chem. Soc.*, 2005, **127**, 1394–1395.
8 K. T. Dinh, M. M. Sullivan, P. Serna, R. J. Meyer, M. Dincă and Y. Román-Leshkov, Viewpoint on the Partial Oxidation of Methane to Methanol Using Cu- and Fe-Exchanged Zeolites, *ACS Catal.*, 2018, **8**, 8306–8313.
9 B. E. R. Snyder, M. L. Bols, R. A. Schoonheydt, B. F. Sels and E. I. Solomon, Iron and Copper Active Sites in Zeolites and Their Correlation to Metalloenzymes, *Chem. Rev.*, 2018, **118**, 2718–2768.
10 J.-P. Lange and P. J. A. Tijm, Processes for converting methane to liquid fuels: Economic screening through energy management, *Chem. Eng. Sci.*, 1996, **51**, 2379–2387.
11 J.-P. Lange, Catalysis for biorefineries – performance criteria for industrial operation, *Catal. Sci. Technol.*, 2016, **6**, 4759–4767.
12 M. Ravi, M. Ranocchiari and J. A. van Bokhoven, The Direct Catalytic Oxidation of Methane to Methanol—A Critical Assessment, *Angew. Chem., Int. Ed.*, 2017, **56**, 16464–16483.
13 B. Ipek and R. F. Lobo, Catalytic conversion of methane to methanol on Cu-SSZ-13 using N_2O as oxidant, *Chem. Commun.*, 2016, **52**, 13401–13404.
14 M. B. Park, S. H. Ahn, A. Mansouri, M. Ranocchiari and J. A. van Bokhoven, Comparative Study of Diverse Copper Zeolites for the Conversion of Methane into Methanol, *ChemCatChem*, 2017, **9**, 3705–3713.
15 R. Oord, J. E. Schmidt and B. M. Weckhuysen, Methane-to-methanol conversion over zeolite Cu-SSZ-13, and its comparison with the selective catalytic reduction of NO_x with NH_3, *Catal. Sci. Technol.*, 2018, **8**, 1028–1038.
16 D. K. Pappas, E. Borfecchia, M. Dyballa, I. A. Pankin, K. A. Lomachenko, A. Martini, M. Signorile, S. Teketel, B. Arstad, G. Berlier, C. Lamberti, S. Bordiga, U. Olsbye, K. P. Lillerud, S. Svelle and P. Beato, Methane to Methanol: Structure–Activity Relationships for Cu-CHA, *J. Am. Chem. Soc.*, 2017, **139**, 14961–14975.
17 P. Tomkins, A. Mansouri, S. E. Bozbag, F. Krumeich, M. B. Park, E. M. C. Alayon, M. Ranocchiari and J. A. van Bokhoven, Isothermal Cyclic Conversion of Methane into Methanol over Copper-Exchanged Zeolite at Low Temperature, *Angew. Chem., Int. Ed.*, 2016, **55**, 5467–5471.
18 J. Zheng, I. Lee, E. Khramenkova, M. Wang, B. Peng, O. Y. Gutiérrez, J. L. Fulton, D. M. Camaioni, R. Khare, A. Jentys, G. L. Haller, E. A. Pidko, M. Sanchez-Sanchez and J. A. Lercher, Importance of Methane Chemical Potential for Its Conversion to Methanol on Cu-Exchanged Mordenite, *Chem. – Eur. J.*, 2020, **26**, 7563–7567.
19 T. Ikuno, S. Grundner, A. Jentys, G. Li, E. Pidko, J. Fulton, M. Sanchez-Sanchez and J. A. Lercher, Formation of Active Cu-oxo Clusters for Methane Oxidation in Cu-Exchanged Mordenite, *J. Phys. Chem. C*, 2019, **123**, 8759–8769.
20 B. Ipek, M. J. Wulfers, H. Kim, F. Göltl, I. Hermans, J. P. Smith, K. S. Booksh, C. M. Brown and R. F. Lobo, Formation of $[Cu_2O_2]^{2+}$ and $[Cu_2O]^{2+}$ toward C–H Bond Activation in Cu-SSZ-13 and Cu-SSZ-39, *ACS Catal.*, 2017, **7**, 4291–4303.

21 Y. Kim, T. Y. Kim, H. Lee and J. Yi, Distinct activation of Cu-MOR for direct oxidation of methane to methanol, *Chem. Commun.*, 2017, **53**, 4116–4119.
22 D. T. Bregante, L. N. Wilcox, C. Liu, C. Paolucci, R. Gounder and D. W. Flaherty, Dioxygen Activation Kinetics over Distinct Cu Site Types in Cu-Chabazite Zeolites, *ACS Catal.*, 2021, **11**, 11873–11884.
23 M. Álvarez, P. Marín and S. Ordóñez, Direct oxidation of methane to methanol over Cu-zeolites at mild conditions, *Mol. Catal*, 2020, **487**, 110886.
24 C. Colella and W. S. Wise, The IZA Handbook of Natural Zeolites: A tool of knowledge on the most important family of porous minerals, *Microporous Mesoporous Mater.*, 2014, **189**, 4–10.
25 Christian Baerlocher, Lynne McCusker, Database of Zeolite Structures, can be found under https://www.iza-structure.org/databases/, (accessed 23 May 2025), n.d.
26 W. Loewenstein, The distribution of aluminum in the tetrahedra of silicates and aluminates, *Am. Mineral.*, 1954, **39**, 92–96.
27 M. Sato, K. Maeda and K. Hirasawa, in *Studies in Surface Science and Catalysis*, ed. J. Weitkamp, H. G. Karge, H. Pfeifer and W. Hölderich, Elsevier, 1994, pp. 589–596.
28 V. Gábová, J. Dědeček and J. Čejka, Control of Al distribution in ZSM-5 by conditions of zeolite synthesis, *Chem. Commun.*, 2003, 1196–1197.
29 D. E. Perea, I. Arslan, J. Liu, Z. Ristanović, L. Kovarik, B. W. Arey, J. A. Lercher, S. R. Bare and B. M. Weckhuysen, Determining the location and nearest neighbours of aluminium in zeolites with atom probe tomography, *Nat. Commun.*, 2015, **6**, 7589.
30 O. H. Han, C.-S. Kim and S. B. Hong, Direct Evidence for the Nonrandom Nature of Al Substitution in Zeolite ZSM-5: An Investigation by 27Al MAS and MQ MAS NMR, *Angew. Chem., Int. Ed.*, 2002, **41**, 469–472.
31 R. Szostak, *Molecular Sieves: Principles of Synthesis and Identification*, Springer Netherlands, Dordrecht, 1989.
32 M. B. Z. Gili and M. T. Conato, Synthesis and characterization of mordenite-type zeolites with varying Si/Al ratio, *Mater. Res. Express*, 2018, **6**, 015515.
33 S. Ghojavand, E. B. Clatworthy, A. Vicente, E. Dib, V. Ruaux, M. Debost, J. El Fallah and S. Mintova, The role of mixed alkali metal cations on the formation of nano-sized CHA zeolite from colloidal precursor suspension, *J. Colloid Interface Sci.*, 2021, **604**, 350–357.
34 Q.-F. Lin, Z. R. Gao, C. Lin, S. Zhang, J. Chen, Z. Li, X. Liu, W. Fan, J. Li, X. Chen, M. A. Camblor and F.-J. Chen, A stable aluminosilicate zeolite with intersecting three-dimensional extra-large pores, *Science*, 2021, **374**, 1605–1608.
35 E. Jang, L. Choi, J. Kim, Y. Jeong, H. Baik, C. Y. Kang, C. H. Kim, K.-Y. Lee and J. Choi, A copper-impregnated BEA zeolite for adsorption and oxidation of aromatic species during vehicle cold starts, *Appl. Catal., B*, 2021, **287**, 119951.
36 Z. Li, K. Xie and R. C. T. Slade, Studies of the interaction between CuCl and HY zeolite for preparing heterogeneous CuI catalyst, *Appl. Catal., A*, 2001, **209**, 107–115.
37 R. G. Moore and J. M. Crawford, Isolated and Paired Metal Sites in Zeolites Using Solid-State Ion Exchange, *Angew. Chem., Int. Ed.*, 2025, **64**, e202505186.
38 Y. Xin, Q. Li and Z. Zhang, Zeolitic Materials for DeNO Selective Catalytic Reduction, *ChemCatChem*, 2018, **10**, 29–41.
39 F. Gao, E. D. Walter, N. M. Washton, J. Szanyi and C. H. F. Peden, Synthesis and evaluation of Cu/SAPO-34 catalysts for NH3-SCR 2: Solid-state ion exchange and one-pot synthesis, *Appl. Catal., B*, 2015, **162**, 501–514.
40 D. Wang, F. Gao, C. H. F. Peden, J. Li, K. Kamasamudram and W. S. Epling, Selective Catalytic Reduction of NO with NH_3 over a Cu-SSZ-13 Catalyst Prepared by a Solid-State Ion-Exchange Method, *ChemCatChem*, 2014, **6**, 1579–1583.
41 L. Ren, Y. Zhang, S. Zeng, L. Zhu, Q. Sun, H. Zhang, C. Yang, X. Meng, X. Yang and F.-S. Xiao, Design and Synthesis of a Catalytically Active Cu-SSZ-13 Zeolite from a Copper-Amine Complex Template, *Chin. J. Catal.*, 2012, **33**, 92–105.
42 A. V. Kucherov, A. A. Slinkin, D. A. Kondrat'ev, T. N. Bondarenko, A. M. Rubinstein and Kh. M. Minachev, Cu^{2+}-cation location and reactivity in mordenite and ZSM-5: e.s.r.-study, *Zeolites*, 1985, **5**, 320–324.
43 A. Godiksen, F. N. Stappen, P. N. R. Vennestrøm, F. Giordanino, S. B. Rasmussen, L. F. Lundegaard and S. Mossin, Coordination Environment of Copper Sites in Cu-CHA Zeolite Investigated by Electron Paramagnetic Resonance, *J. Phys. Chem. C*, 2014, **118**, 23126–23138.
44 J. Dedecek, Z. Sobalik, Z. Tvaruazkova, D. Kaucky and B. Wichterlova, Coordination of Cu Ions in High-Silica Zeolite Matrixes. Cu^{+} Photoluminescence, IR of NO Adsorbed on Cu^{2+}, and Cu^{2+} ESR Study, *J. Phys. Chem.*, 1995, **99**, 16327–16337.
45 P. C. Bruzzese, E. Salvadori, S. Jäger, M. Hartmann, B. Civalleri, A. Pöppl and M. Chiesa, 17O-EPR determination of the structure and dynamics of copper single-metal sites in zeolites, *Nat. Commun.*, 2021, **12**, 4638.
46 J. W. A. Fischer, A. Brenig, D. Klose, J. A. van Bokhoven, V. L. Sushkevich and G. Jeschke, Methane Oxidation over $Cu^{2+}/[CuOH]^{+}$ Pairs and Site-Specific Kinetics in Copper Mordenite Revealed by *Operando* Electron Paramagnetic Resonance and UV/Visible Spectroscopy, *Angew. Chem., Int. Ed.*, 2023, **135**, e202303574.
47 A. Godiksen, P. N. R. Vennestrøm, S. B. Rasmussen and S. Mossin, Identification and Quantification of Copper Sites in Zeolites by Electron Paramagnetic Resonance Spectroscopy, *Top. Catal.*, 2017, **60**, 13–29.
48 K. Pierloot, A. Delabie, M. H. Groothaert and R. A. Schoonheydt, A reinterpretation of the EPR spectra of Cu(II) in zeolites A, Y and ZK4, based on ab initio cluster model calculations, *Phys. Chem. Chem. Phys.*, 2001, **3**, 2174–2183.
49 F. Göltl, P. Sautet and I. Hermans, Can Dynamics Be Responsible for the Complex Multipeak Infrared Spectra of NO Adsorbed to Copper(II) Sites in Zeolites?, *Angew. Chem., Int. Ed.*, 2015, **54**, 7799–7804.
50 A. Brenig, J. W. A. Fischer, D. Klose, G. Jeschke, J. A. van Bokhoven and V. L. Sushkevich, Redox and Kinetic

Properties of Composition-Dependent Active Sites in Copper-Exchanged Chabazite for Direct Methane-to-Methanol Oxidation, *Angew. Chem., Int. Ed.*, 2024, **63**, e202411662.

51 P. Vanelderen, B. E. R. Snyder, M.-L. Tsai, R. G. Hadt, J. Vancauwenbergh, O. Coussens, R. A. Schoonheydt, B. F. Sels and E. I. Solomon, Spectroscopic Definition of the Copper Active Sites in Mordenite: Selective Methane Oxidation, *J. Am. Chem. Soc.*, 2015, **137**, 6383–6392.

52 P. Vanelderen, J. Vancauwenbergh, B. F. Sels and R. A. Schoonheydt, Coordination chemistry and reactivity of copper in zeolites, *Coord. Chem. Rev.*, 2013, **257**, 483–494.

53 C. Negri, M. Signorile, N. G. Porcaro, E. Borfecchia, G. Berlier, T. V. W. Janssens and S. Bordiga, Dynamic Cu^{II}/Cu^{I} speciation in Cu-CHA catalysts by *in situ* Diffuse Reflectance UV-vis-NIR spectroscopy, *Appl. Catal., A*, 2019, **578**, 1–9.

54 H. Li, C. Paolucci, I. Khurana, L. N. Wilcox, F. Göltl, J. D. Albarracin-Caballero, A. J. Shih, F. H. Ribeiro, R. Gounder and W. F. Schneider, Consequences of exchange-site heterogeneity and dynamics on the UV-visible spectrum of Cu-exchanged SSZ-13, *Chem. Sci.*, 2019, **10**, 2373–2384.

55 A. Godiksen, O. L. Isaksen, S. B. Rasmussen, P. N. R. Vennestrøm and S. Mossin, Site-Specific Reactivity of Copper Chabazite Zeolites with Nitric Oxide, Ammonia, and Oxygen, *ChemCatChem*, 2018, **10**, 366–370.

56 M. H. Mahyuddin, E. T. Lasiman, A. G. Saputro, S. V. Casuarina, N. Nugraha and H. K. Dipojono, Conditions to meet for the $[CuOH]^{+}$ site to be favorable and reactive toward the conversion of methane to methanol over Cu-MOR zeolite, *Catal. Sci. Technol.*, 2023, **13**, 5767–5775.

57 C. Paolucci, A. A. Parekh, I. Khurana, J. R. Di Iorio, H. Li, J. D. Albarracin Caballero, A. J. Shih, T. Anggara, W. N. Delgass, J. T. Miller, F. H. Ribeiro, R. Gounder and W. F. Schneider, Catalysis in a Cage: Condition-Dependent Speciation and Dynamics of Exchanged Cu Cations in SSZ-13 Zeolites, *J. Am. Chem. Soc.*, 2016, **138**, 6028–6048.

58 P. C. Bruzzese, E. Salvadori, B. Civalleri, S. Jäger, M. Hartmann, A. Pöppl and M. Chiesa, The Structure of Monomeric Hydroxo-Cu^{II} Species in Cu-CHA. A Quantitative Assessment, *J. Am. Chem. Soc.*, 2022, **144**, 13079–13083.

59 M. H. Groothaert, K. Pierloot, A. Delabie and R. A. Schoonheydt, Identification of Cu(II) coordination structures in Cu-ZSM-5, based on a DFT/ab initio assignment of the EPR spectra, *Phys. Chem. Chem. Phys.*, 2003, **5**, 2135–2144.

60 P. Vanelderen, J. Vancauwenbergh, M.-L. Tsai, R. G. Hadt, E. I. Solomon, R. A. Schoonheydt and B. F. Sels, Spectroscopy and Redox Chemistry of Copper in Mordenite, *Chem. Phys. Chem.*, 2014, **15**, 91–99.

61 A. Delabie, K. Pierloot, M. H. Groothaert, B. M. Weckhuysen and R. A. Schoonheydt, The siting of Cu(II) in mordenite: a theoretical spectroscopic study, *Phys. Chem. Chem. Phys.*, 2002, **4**, 134–145.

62 A. J. Heyer, D. Plessers, A. Braun, H. M. Rhoda, M. L. Bols, B. Hedman, K. O. Hodgson, R. A. Schoonheydt, B. F. Sels and E. I. Solomon, Methane Activation by a Mononuclear Copper Active Site in the Zeolite Mordenite: Effect of Metal Nuclearity on Reactivity, *J. Am. Chem. Soc.*, 2022, **144**, 19305–19316.

63 V. L. Sushkevich, M. Artsiusheuski, D. Klose, G. Jeschke and J. A. Bokhoven, Identification of Kinetic and Spectroscopic Signatures of Copper Sites for Direct Oxidation of Methane to Methanol, *Angew. Chem., Int. Ed.*, 2021, **60**, 15944–15953.

64 D. Palagin, V. L. Sushkevich, A. J. Knorpp, M. Ranocchiari and J. A. van Bokhoven, Mapping Vibrational Spectra to the Structures of Copper Species in Zeolites Based on Calculated Stretching Frequencies of Adsorbed Nitrogen and Carbon Monoxides, *J. Phys. Chem. C*, 2021, **125**, 12094–12106.

65 V. L. Sushkevich, D. Palagin and J. A. van Bokhoven, The Effect of the Active-Site Structure on the Activity of Copper Mordenite in the Aerobic and Anaerobic Conversion of Methane into Methanol, *Angew. Chem., Int. Ed.*, 2018, **57**, 8906–8910.

66 J. S. Woertink, P. J. Smeets, M. H. Groothaert, M. A. Vance, B. F. Sels, R. A. Schoonheydt and E. I. Solomon, A $[Cu_2O]^{2+}$ core in Cu-ZSM-5, the active site in the oxidation of methane to methanol, *Proc. Natl. Acad. Sci. U. S. A.*, 2009, **106**, 18908–18913.

67 A. J. Heyer, D. Plessers, J. Ma, B. E. R. Snyder, R. A. Schoonheydt, B. F. Sels and E. I. Solomon, Magnetic Exchange Coupling in Zeolite Copper Dimers and Its Contribution to Methane Activation, *J. Am. Chem. Soc.*, 2024, **146**, 6061–6071.

68 D. Plessers, A. J. Heyer, H. M. Rhoda, M. L. Bols, E. I. Solomon, R. A. Schoonheydt and B. F. Sels, Tuning Copper Active Site Composition in Cu-MOR through Co-Cation Modification for Methane Activation, *ACS Catal.*, 2023, **13**, 1906–1915.

69 B. E. R. Snyder, P. Vanelderen, R. A. Schoonheydt, B. F. Sels and E. I. Solomon, Second-Sphere Effects on Methane Hydroxylation in Cu-Zeolites, *J. Am. Chem. Soc.*, 2018, **140**, 9236–9243.

70 G. Brezicki, J. Zheng, C. Paolucci, R. Schlögl and R. J. Davis, Effect of the Co-cation on Cu Speciation in Cu-Exchanged Mordenite and ZSM-5 Catalysts for the Oxidation of Methane to Methanol, *ACS Catal.*, 2021, **11**, 4973–4987.

71 M. A. Artsiusheuski, J. A. van Bokhoven and V. L. Sushkevich, Structure of Selective and Nonselective Dicopper(II) Sites in CuMFI for Methane Oxidation to Methanol, *ACS Catal.*, 2022, **12**, 15626–15637.

72 F. Göltl, S. Bhandari, E. A. Lebrón-Rodríguez, J. I. Gold, D. J. Hutton, S. I. Zones, I. Hermans, J. A. Dumesic and M. Mavrikakis, Exploring the Impact of Active Site Structure on the Conversion of Methane to Methanol in Cu-Exchanged Zeolites, *Angew. Chem., Int. Ed.*, 2024, **63**, e202403179.

73 S. Grundner, M. A. C. Markovits, G. Li, M. Tromp, E. A. Pidko, E. J. M. Hensen, A. Jentys, M. Sanchez-Sanchez and J. A. Lercher, Single-site trinuclear copper oxygen clusters in mordenite for selective conversion of methane to methanol, *Nat. Commun.*, 2015, **6**, 7546–7555.

74 G. Li, P. Vassilev, M. Sanchez-Sanchez, J. A. Lercher, E. J. M. Hensen and E. A. Pidko, Stability and reactivity of copper oxo-clusters in ZSM-5 zeolite for selective methane oxidation to methanol, *J. Catal.*, 2016, **338**, 305–312.

75 D. Palagin, A. J. Knorpp, A. B. Pinar, M. Ranocchiari and J. A. van Bokhoven, Assessing the relative stability of copper oxide clusters as active sites of a CuMOR zeolite for methane to methanol conversion: size matters?, *Nanoscale*, 2017, **9**, 1144–1153.
76 M. A. Artsiusheuski, O. Safonova, D. Palagin, J. A. van Bokhoven and V. L. Sushkevich, Structural Evolution of Copper-Oxo Sites in Zeolites upon the Reaction with Methane Investigated by Means of Cu K-edge X-ray Absorption Spectroscopy, *J. Phys. Chem. C*, 2023, **127**, 9603–9615.
77 V. L. Sushkevich, O. V. Safonova, D. Palagin, M. A. Newton and J. A. van Bokhoven, Structure of copper sites in zeolites examined by Fourier and wavelet transform analysis of EXAFS, *Chem. Sci.*, 2020, **11**, 5299–5312.
78 M. H. Mahyuddin, Y. Shiota, A. Staykov and K. Yoshizawa, Theoretical Overview of Methane Hydroxylation by Copper–Oxygen Species in Enzymatic and Zeolitic Catalysts, *Acc. Chem. Res.*, 2018, **51**, 2382–2390.
79 Q. M. Phung, T. Yanai, D. Plessers, B. F. Sels, R. A. Schoonheydt and K. Pierloot, Homolytic versus Heterolytic Methane Hydroxylation in Copper Zeolites, *ACS Catal.*, 2025, **15**, 1249–1264.
80 M. J. Wulfers, S. Teketel, B. Ipek and R. F. Lobo, Conversion of methane to methanol on copper-containing small-pore zeolites and zeotypes, *Chem. Commun.*, 2015, **51**, 4447–4450.
81 M. Ravi, V. L. Sushkevich, A. J. Knorpp, M. A. Newton, D. Palagin, A. B. Pinar, M. Ranocchiari and J. A. van Bokhoven, Misconceptions and challenges in methane-to-methanol over transition-metal-exchanged zeolites, *Nat. Catal*, 2019, **2**, 485–494.
82 A. A. Latimer, A. Kakekhani, A. R. Kulkarni and J. K. Nørskov, Direct Methane to Methanol: The Selectivity–Conversion Limit and Design Strategies, *ACS Catal.*, 2018, **8**, 6894–6907.
83 A. Blankenship, M. Artsiusheuski, V. Sushkevich and J. A. van Bokhoven, Recent trends, current challenges and future prospects for syngas-free methane partial oxidation, *Nat. Catal.*, 2023, **6**, 748–762.
84 M. Ahlquist, R. J. Nielsen, R. A. Periana and W. A. Goddard III, Product Protection, the Key to Developing High Performance Methane Selective Oxidation Catalysts, *J. Am. Chem. Soc.*, 2009, **131**, 17110–17115.
85 T. Sheppard, C. D. Hamill, A. Goguet, D. W. Rooney and J. M. Thompson, A low temperature, isothermal gas-phase system for conversion of methane to methanol over Cu–ZSM-5, *Chem. Commun.*, 2014, **50**, 11053–11055.
86 P. Tomkins, A. Mansouri, V. L. Sushkevich, L. I. van der Wal, S. E. Bozbag, F. Krumeich, M. Ranocchiari and J. A. van Bokhoven, Increasing the activity of copper exchanged mordenite in the direct isothermal conversion of methane to methanol by Pt and Pd doping, *Chem. Sci.*, 2018, **10**, 167–171.
87 R. J. Passini, M. Picinini, J. M. C. Bueno and E. A. Urquieta-Gonzalez, Direct methane to methanol stepwise conversion over Cu-oxo species in zeolites – Insights on the Cu-zeolite activation in air or helium from *in situ* UV-Vis analyses, *Mol. Catal.*, 2022, **530**, 112605.
88 V. L. Sushkevich, D. Palagin, M. Ranocchiari and J. A. van Bokhoven, Selective Anaerobic Oxidation of Methane Enables Direct Synthesis of Methanol, *Science*, 2017, **356**, 523–527.
89 D. K. Pappas, E. Borfecchia, M. Dyballa, K. A. Lomachenko, A. Martini, G. Berlier, B. Arstad, C. Lamberti, S. Bordiga, U. Olsbye, S. Svelle and P. Beato, Understanding and Optimizing the Performance of Cu-FER for The Direct CH_4 to CH_3OH Conversion, *ChemCatChem*, 2019, **11**, 621–627.
90 G. Brezicki, J. D. Kammert, T. B. Gunnoe, C. Paolucci and R. J. Davis, Insights into the Speciation of Cu in the Cu-H-Mordenite Catalyst for the Oxidation of Methane to Methanol, *ACS Catal.*, 2019, **9**, 5308–5319.
91 M. C. Alvarez-Galvan, N. Mota, M. Ojeda, S. Rojas, R. M. Navarro and J. L. G. Fierro, Direct methane conversion routes to chemicals and fuels, *Catal. Today*, 2011, **171**, 15–23.
92 D. K. Pappas, A. Martini, M. Dyballa, K. Kvande, S. Teketel, K. A. Lomachenko, R. Baran, P. Glatzel, B. Arstad, G. Berlier, C. Lamberti, S. Bordiga, U. Olsbye, S. Svelle, P. Beato and E. Borfecchia, The Nuclearity of the Active Site for Methane to Methanol Conversion in Cu-Mordenite: A Quantitative Assessment, *J. Am. Chem. Soc.*, 2018, **140**, 15270–15278.
93 J. O. Petunchi, G. Marcelin and W. K. Hall, Studies of the changes occurring on reduction and reoxidation of CuY zeolites, *J. Phys. Chem.*, 1992, **96**, 9967–9975.
94 C. M. Naccache and Y. B. Taarit, Oxidizing and acidic properties of copper-exchange Y zeolite, *J. Catal.*, 1971, **22**, 171–181.
95 L. Tao, I. Lee and M. Sanchez-Sanchez, Cu oxo nanoclusters for direct oxidation of methane to methanol: formation, structure and catalytic performance, *Catal. Sci. Technol.*, 2020, **10**, 7124–7141.
96 S. Grundner, W. Luo, M. Sanchez-Sanchez and J. A. Lercher, Synthesis of single-site copper catalysts for methane partial oxidation, *Chem. Commun.*, 2016, **52**, 2553–2556.
97 M. Lo Jacono, G. Fierro, R. Dragone, X. Feng, J. d'Itr and W. K. Hall, Zeolite Chemistry of CuZSM-5 Revisited, *J. Phys. Chem. B*, 1997, **101**, 1979–1984.
98 G. Turnes Palomino, P. Fisicaro, S. Bordiga, A. Zecchina, E. Giamello and C. Lamberti, Oxidation States of Copper Ions in ZSM-5 Zeolites. A Multitechnique Investigation, *J. Phys. Chem. B*, 2000, **104**, 4064–4073.
99 F. X. Llabrés i Xamena, P. Fisicaro, G. Berlier, A. Zecchina, G. T. Palomino, C. Prestipino, S. Bordiga, E. Giamello and C. Lamberti, Thermal Reduction of Cu^{2+}–Mordenite and Re-oxidation upon Interaction with H_2O, O_2, and NO, *J. Phys. Chem. B*, 2003, **107**, 7036–7044.
100 E. M. C. Alayon, M. Nachtegaal, A. Bodi, M. Ranocchiari and J. A. van Bokhoven, Bis(μ-oxo) versus mono(μ-oxo)dicopper cores in a zeolite for converting methane to methanol: an *in situ* XAS and DFT investigation, *Phys. Chem. Chem. Phys.*, 2015, **17**, 7681–7693.
101 V. L. Sushkevich and J. A. van Bokhoven, Revisiting copper reduction in zeolites: the impact of autoreduction and

sample synthesis procedure, *Chem. Commun.*, 2018, **54**, 7447–7450.

102 A. Martini, E. Borfecchia, K. A. Lomachenko, I. A. Pankin, C. Negri, G. Berlier, P. Beato, H. Falsig, S. Bordiga and C. Lamberti, Composition-driven Cu-speciation and reducibility in Cu-CHA zeolite catalysts: a multivariate XAS/FTIR approach to complexity, *Chem. Sci.*, 2017, **8**, 6836–6851.

103 C. W. Andersen, E. Borfecchia, M. Bremholm, M. R. V. Jørgensen, P. N. R. Vennestrøm, C. Lamberti, L. F. Lundegaard and B. B. Iversen, Redox-Driven Migration of Copper Ions in the Cu-CHA Zeolite as Shown by the *In Situ* PXRD/XANES Technique, *Angew. Chem., Int. Ed.*, 2017, **56**, 10367–10372.

104 E. Borfecchia, K. A. Lomachenko, F. Giordanino, H. Falsig, P. Beato, A. V. Soldatov, S. Bordiga and C. Lamberti, Revisiting the nature of Cu sites in the activated Cu-SSZ-13 catalyst for SCR reaction, *Chem. Sci.*, 2014, **6**, 548–563.

105 A. Wijerathne, A. Sawyer, R. Daya and C. Paolucci, Competition between Mononuclear and Binuclear Copper Sites across Different Zeolite Topologies, *JACS Au*, 2024, **4**, 197–215.

106 L. N. Wilcox, J. Rebolledo-Oyarce, A. D. Mikes, Y. Wang, W. F. Schneider and R. Gounder, Structure and Reactivity of Binuclear Cu Active Sites in Cu-CHA Zeolites for Stoichiometric Partial Methane Oxidation to Methanol, *ACS Catal.*, 2024, **14**, 3647–3663.

107 A. R. Kulkarni, Z.-J. Zhao, S. Siahrostami, J. K. Nørskov and F. Studt, Monocopper Active Site for Partial Methane Oxidation in Cu-Exchanged 8MR Zeolites, *ACS Catal.*, 2016, **6**, 6531–6536.

108 V. L. Sushkevich, R. Verel and J. A. Bokhoven, Pathways of Methane Transformation over Copper-Exchanged Mordenite as Revealed by *In Situ* NMR and IR Spectroscopy, *Angew. Chem.*, 2019, **132**, 920–928.

109 V. L. Sushkevich, M. Artsiusheuski, D. Klose, G. Jeschke and J. A. van Bokhoven, Identification of Kinetic and Spectroscopic Signatures of Copper Sites for Direct Oxidation of Methane to Methanol, *Angew. Chem., Int. Ed.*, 2021, **60**, 15944–15953.

110 A. J. Knorpp, A. B. Pinar, C. Baerlocher, L. B. McCusker, N. Casati, M. A. Newton, S. Checchia, J. Meyet, D. Palagin and J. A. van Bokhoven, Paired Copper Monomers in Zeolite Omega: The Active Site for Methane-to-Methanol Conversion, *Angew. Chem., Int. Ed.*, 2021, **60**, 5854–5858.

111 J. Wieser, D. Wardecki, J. W. A. Fischer, M. A. Newton, C. Dejoie, A. J. Knorpp, G. Jeschke, P. Rzepka and J. A. van Bokhoven, Quantifying the Hydration-Dependent Dynamics of Copper Migration and Activity in Zeolite Omega for the Partial Oxidation of Methane, *Angew. Chem., Int. Ed.*, 2024, e202407395.

112 F. Giordanino, P. N. R. Vennestrøm, L. F. Lundegaard, F. N. Stappen, S. Mossin, P. Beato, S. Bordiga and C. Lamberti, Characterization of Cu-exchanged SSZ-13: a comparative FTIR, UV-Vis, and EPR study with Cu-ZSM-5 and Cu-β with similar Si/Al and Cu/Al ratios, *Dalton Trans.*, 2013, **42**, 12741–12761.

113 J. A. Duffy, *Novel Chemical Effects of Electronics Behaviour.*, Springer, Berlin, Heidelberg, 1977, pp. 147–166.

114 C. E. Housecroft and A. G. Sharpe, *Inorganic Chemistry*, Pearson Education Limited, Essex, 2008.

115 R. Boča, *Electronic Energy Levels of Transition Metal Complexes*, Elsevier, Amsterdam, 2025.

116 E. M. C. Alayon, M. Nachtegaal, E. Kleymenov and J. A. van Bokhoven, Determination of the electronic and geometric structure of Cu sites during methane conversion over Cu-MOR with X-ray absorption spectroscopy, *Microporous Mesoporous Mater.*, 2013, **166**, 131–136.

117 M. A. Newton, A. J. Knorpp, V. L. Sushkevich, D. Palagin and J. A. van Bokhoven, Active sites and mechanisms in the direct conversion of methane to methanol using Cu in zeolitic hosts: a critical examination, *Chem. Soc. Rev.*, 2020, **49**, 1449–1486.

118 A. Martini, E. Alladio and E. Borfecchia, Determining Cu–Speciation in the Cu–CHA Zeolite Catalyst: The Potential of Multivariate Curve Resolution Analysis of *In Situ* XAS Data, *Top. Catal.*, 2018, **61**, 1396–1407.

119 J. L. DuBois, P. Mukherjee, T. D. P. Stack, B. Hedman, E. I. Solomon and K. O. Hodgson, A Systematic K-edge X-ray Absorption Spectroscopic Study of Cu(III) Sites, *J. Am. Chem. Soc.*, 2000, **122**, 5775–5787.

120 M. L. Baker, M. W. Mara, J. J. Yan, K. O. Hodgson, B. Hedman and E. I. Solomon, K- and L-edge X-ray absorption spectroscopy (XAS) and resonant inelastic X-ray scattering (RIXS) determination of differential orbital covalency (DOC) of transition metal sites, *Coord. Chem. Rev.*, 2017, **345**, 182–208.

121 H. Yamashita, M. Matsuoka, K. Tsuji, Y. Shioya, M. Anpo and M. Che, *In Situ* XAFS, Photoluminescence, and IR Investigations of Copper Ions Included within Various Kinds of Zeolites. Structure of Cu(I) Ions and Their Interaction with CO Molecules, *J. Phys. Chem.*, 1996, **100**, 397–402.

122 L. S. Kau, D. J. Spira-Solomon, J. E. Penner-Hahn, K. O. Hodgson and E. I. Solomon, X-ray absorption edge determination of the oxidation state and coordination number of copper. Application to the type 3 site in Rhus vernicifera laccase and its reaction with oxygen, *J. Am. Chem. Soc.*, 1987, **109**, 6433–6442.

123 E. I. Solomon, D. E. Heppner, E. M. Johnston, J. W. Ginsbach, J. Cirera, M. Qayyum, M. T. Kieber-Emmons, C. H. Kjaergaard, R. G. Hadt and L. Tian, Copper Active Sites in Biology, *Chem. Rev.*, 2014, **114**, 3659–3853.

124 M.-L. Tsai, R. G. Hadt, P. Vanelderen, B. F. Sels, R. A. Schoonheydt and E. I. Solomon, $[Cu_2O]^{2+}$ Active Site Formation in Cu–ZSM-5: Geometric and Electronic Structure Requirements for N_2O Activation, *J. Am. Chem. Soc.*, 2014, **136**, 3522–3529.

125 C. Buono, A. Martini, I. A. Pankin, D. K. Pappas, C. Negri, K. Kvande, K. A. Lomachenko and E. Borfecchia, Local structure of Cu(I) ions in the MOR zeolite: A DFT-assisted XAS study, *Radiat. Phys. Chem.*, 2020, **175**, 108111.

126 F. Gao, E. D. Walter, M. Kollar, Y. Wang, J. Szanyi and C. H. F. Peden, Understanding ammonia selective catalytic reduction kinetics over Cu/SSZ-13 from motion of the Cu ions, *J. Catal.*, 2014, **319**, 1–14.

127 A. Brenig, J. W. A. Fischer, D. Klose, G. Jeschke, J. A. van Bokhoven and V. L. Sushkevich, Tracking Active Site Formation during Oxidative Activation of Copper-Exchanged Zeolites for Methane-to-Methanol Conversion, *Adv. Sci.*, 2025, **12**, 2413870–2413883.

128 M. Occhiuzzi, G. Fierro, G. Ferraris and G. Moretti, Unusual Complete Reduction of Cu^{2+} Species in Cu-ZSM-5 Zeolites under Vacuum Treatment at High Temperature, *Chem. Mater.*, 2012, **24**, 2022–2031.

129 C. Chao and J. H. Lunsford, EPR Study of Copper(II) Ion Pairs in Y-Type Zeolites, *J. Chem. Phys.*, 1972, **57**, 2890–2898.

130 J. Valyon and W. K. Hall, Effects of reduction and reoxidation on the infrared spectra from Cu-Y and Cu-ZSM-5 zeolites, *J. Phys. Chem.*, 1993, **97**, 7054–7060.

131 V. L. Sushkevich, A. V. Smirnov and J. A. van Bokhoven, Autoreduction of Copper in Zeolites: Role of Topology, Si/Al Ratio, and Copper Loading, *J. Phys. Chem. C*, 2019, **123**, 9926–9934.

132 F. Gao, N. M. Washton, Y. Wang, M. Kollár, J. Szanyi and C. H. F. Peden, Effects of Si/Al ratio on Cu/SSZ-13 NH3-SCR catalysts: Implications for the active Cu species and the roles of Brønsted acidity, *J. Catal.*, 2015, **331**, 25–38.

133 M. H. Groothaert, K. Lievens, H. Leeman, B. M. Weckhuysen and R. A. Schoonheydt, An *operando* optical fiber UV-vis spectroscopic study of the catalytic decomposition of NO and N_2O over Cu-ZSM-5, *J. Catal.*, 2003, **220**, 500–512.

134 M. Iwamoto, H. Yahiro, K. Tanda, N. Mizuno, Y. Mine and S. Kagawa, Removal of nitrogen monoxide through a novel catalytic process. 1. Decomposition on excessively copper-ion-exchanged ZSM-5 zeolites, *J. Phys. Chem.*, 1991, **95**, 3727–3730.

135 D. J. Hutton, D. H. Lopez and F. Göltl, Thermodynamic driving forces for autoreduction of Cu sites in the zeolite SSZ-13 *React*, *Chem. Eng.*, 2024, **9**, 1685–1695.

136 P. J. Smeets, M. H. Groothaert and R. A. Schoonheydt, Cu based zeolites: A UV-vis study of the active site in the selective methane oxidation at low temperatures, *Catal. Today*, 2005, **110**, 303–309.

137 G. Deplano, A. Martini, M. Signorile, E. Borfecchia, V. Crocellà, S. Svelle and S. Bordiga, Copper Pairing in the Mordenite Framework as a Function of the Cu^{I}/Cu^{II} Speciation, *Angew. Chem., Int. Ed.*, 2021, **60**, 25891–25896.

138 A. Martini, M. Signorile, C. Negri, K. Kvande, K. A. Lomachenko, S. Svelle, P. Beato, G. Berlier, E. Borfecchia and S. Bordiga, EXAFS wavelet transform analysis of Cu-MOR zeolites for the direct methane to methanol conversion, *Phys. Chem. Chem. Phys.*, 2020, **22**, 18950–18963.

139 K. Kvande, B. Garetto, G. Deplano, M. Signorile, B. G. Solemsli, S. Prodinger, U. Olsbye, P. Beato, S. Bordiga, S. Svelle and E. Borfecchia, Understanding C–H activation in light alkanes over Cu-MOR zeolites by coupling advanced spectroscopy and temperature-programmed reduction experiments, *Chem. Sci.*, 2023, **14**, 9704–9723.

140 C. Dossi, A. Fusi, G. Moretti, S. Recchia and R. Psaro, On the role of carbonaceous material in the reduction of Cu^{2+} to Cu^{+} in Cu-ZSM-5 catalysts, *Appl. Catal., A*, 1999, **188**, 107–119.

141 A. V. Kucherov, H. G. Karge and R. Schlögl, Quantitative ESR study of the CuH-ZSM-5 system: influence of preparation and pretreatment techniques on the valence state of copper, *Microporous Mesoporous Mater.*, 1998, **25**, 7–14.

142 P. D. Costa, B. Modén, G. D. Meitzner, D. K. Lee and E. Iglesia, Spectroscopic and chemical characterization of active and inactive Cu species in NO decomposition catalysts based on Cu-ZSM5, *Phys. Chem. Chem. Phys.*, 2002, **4**, 4590–4601.

143 S. C. Larsen, A. Aylor, A. T. Bell and J. A. Reimer, Electron Paramagnetic Resonance Studies of Copper Ion-Exchanged ZSM-5, *J. Phys. Chem.*, 1994, **98**, 11533–11540.

144 M. H. Groothaert, J. A. van Bokhoven, A. A. Battiston, B. M. Weckhuysen and R. A. Schoonheydt, Bis(μ-oxo)dicopper in Cu-ZSM-5 and Its Role in the Decomposition of NO: A Combined in Situ XAFS, UV-Vis-Near-IR, and Kinetic Study, *J. Am. Chem. Soc.*, 2003, **125**, 7629–7640.

145 M. H. Groothaert, K. Lievens, J. A. van Bokhoven, A. A. Battiston, B. M. Weckhuysen, K. Pierloot and R. A. Schoonheydt, Bis(μ-oxo)dicopper as Key Intermediate in the Catalytic Decomposition of Nitric Oxide, *Chem. Phys. Chem.*, 2003, **4**, 626–630.

146 E. A. Pidko, E. J. M. Hensen and R. A. van Santen, Self-organization of extraframework cations in zeolites, *Proc. R. Soc. Math. Phys. Eng. Sci.*, 2012, **468**, 2070–2086.

147 P. J. Smeets, R. G. Hadt, J. S. Woertink, P. Vanelderen, R. A. Schoonheydt, B. F. Sels and E. I. Solomon, Oxygen Precursor to the Reactive Intermediate in Methanol Synthesis by Cu-ZSM-5, *J. Am. Chem. Soc.*, 2010, **132**, 14736–14738.

148 A. Delabie, K. Pierloot, M. H. Groothaert, R. A. Schoonheydt and L. G. Vanquickenborne, The Coordination of Cu(II) in Zeolites – Structure and Spectroscopic Properties, *Eur. J. Inorg. Chem.*, 2002, 515–530.

149 P. J. Smeets, J. S. Woertink, B. F. Sels, E. I. Solomon and R. A. Schoonheydt, Transition-Metal Ions in Zeolites: Coordination and Activation of Oxygen, *Inorg. Chem.*, 2010, **49**, 3573–3583.

150 U. Engedahl, A. Boje, H. Ström, H. Grönbeck and A. Hellman, Complete Reaction Cycle for Methane-to-Methanol Conversion over Cu-SSZ-13: First-Principles Calculations and Microkinetic Modeling, *J. Phys. Chem. C*, 2021, **125**, 14681–14688.

151 M. Haris Mahyuddin, Y. Shiota and K. Yoshizawa, Methane selective oxidation to methanol by metal-exchanged zeolites: a review of active sites and their reactivity, *Catal. Sci. Technol.*, 2019, **9**, 1744–1768.

152 H. Liu, J. Wang, T. Yu, S. Fan and M. Shen, The role of various iron species in Fe-β catalysts with low iron loadings for NH3-SCR, *Catal. Sci. Technol.*, 2014, **4**, 1350–1356.

153 A. I. Olivos-Suarez, À. Szécsényi, E. J. M. Hensen, J. Ruiz-Martinez, E. A. Pidko and J. Gascon, Strategies for the Direct Catalytic Valorization of Methane Using Heterogeneous Catalysis: Challenges and Opportunities, *ACS Catal.*, 2016, **6**, 2965–2981.

154 M. H. Mahyuddin, H. K. Dipojono and K. Yoshizawa, in *Direct Hydroxylation Methane Interplay Theory Experiment*, ed. K. Yoshizawa, Springer, Singapore, 2020, pp. 75–86.

155 S. Santra, T. Archipov, A. B. Ene, H. Komnik, H. Stoll, E. Roduner and G. Rauhut, Adsorption of dioxygen to copper in CuHY zeolite, *Phys. Chem. Chem. Phys.*, 2009, **11**, 8855–8866.

156 L. Vilella and F. Studt, The Stability of Copper Oxo Species in Zeolite Frameworks, *Eur. J. Inorg. Chem.*, 2016, 1514–1520.

157 M. H. Mahyuddin, A. Staykov, Y. Shiota, M. Miyanishi and K. Yoshizawa, Roles of Zeolite Confinement and Cu–O–Cu Angle on the Direct Conversion of Methane to Methanol by $[Cu_2(\mu\text{-}O)]^{2+}$-Exchanged AEI, CHA, AFX, and MFI Zeolites, *ACS Catal.*, 2017, **7**, 3741–3751.

158 M. H. Mahyuddin, T. Tanaka, Y. Shiota, A. Staykov and K. Yoshizawa, Methane Partial Oxidation over $[Cu_2(\mu\text{-}O)]^{2+}$ and $[Cu_3(\mu\text{-}O)_3]^{2+}$ Active Species in Large-Pore Zeolites, *ACS Catal.*, 2018, **8**, 1500–1509.

159 M. H. Mahyuddin, A. Staykov, A. G. Saputro, M. K. Agusta, H. K. Dipojono and K. Yoshizawa, Novel Mechanistic Insights into Methane Activation over Fe and Cu Active Sites in Zeolites: A Comparative DFT Study Using Meta-GGA Functionals, *J. Phys. Chem. C*, 2020, **124**, 18112–18125.

160 D. Panthi, O. Adeyiga and S. O. Odoh, DFT Analysis of Methane C−H Activation and Over-Oxidation by $[Cu_2O]^{2+}$ and $[Cu_2O_2]^{2+}$ Sites in Zeolite Mordenite: Intra- versus Inter-site Over-Oxidation, *ChemPhysChem*, 2021, **22**, 2517–2525.

161 K. D. Vogiatzis, G. Li, E. J. M. Hensen, L. Gagliardi and E. A. Pidko, Electronic Structure of the $[Cu_3(\mu\text{-}O)_3]^{2+}$ Cluster in Mordenite Zeolite and Its Effects on the Methane to Methanol Oxidation, *J. Phys. Chem. C*, 2017, **121**, 22295–22302.

162 V. L. Sushkevich, R. Verel and J. A. van Bokhoven, Pathways of Methane Transformation over Copper-Exchanged Mordenite as Revealed by In Situ NMR and IR Spectroscopy, *Angew. Chem.*, 2020, **132**, 920–928.

163 M. H. Mahyuddin, in *Direct Hydroxylation Methane*, ed. K. Yoshizawa, Springer Singapore, Singapore, 2020, pp. 87–100.

164 Z.-J. Zhao, A. Kulkarni, L. Vilella, J. K. Nørskov and F. Studt, Theoretical Insights into the Selective Oxidation of Methane to Methanol in Copper-Exchanged Mordenite, *ACS Catal.*, 2016, **6**, 3760–3766.

165 X. Liu, Y. Ryabenkova and M. Conte, Catalytic oxygen activation versus autoxidation for industrial applications: a physicochemical approach, *Phys. Chem. Chem. Phys.*, 2014, **17**, 715–731.

166 N. Dietl, C. van der Linde, M. Schlangen, M. K. Beyer and H. Schwarz, Diatomic $[CuO]^+$ and Its Role in the Spin-Selective Hydrogen- and Oxygen-Atom Transfers in the Thermal Activation of Methane, *Angew. Chem., Int. Ed.*, 2011, **50**, 4966–4969.

167 O. Suleiman, O. Adeyiga, D. Panthi and S. O. Odoh, Copper-Oxo Active Sites in the 8MR of Zeolite Mordenite: DFT Investigation of the Impact of Acid Sites on Methanol Yield and Selectivity, *J. Phys. Chem. C*, 2021, **125**, 6684–6693.

168 F. Göltl, S. Bhandari and M. Mavrikakis, Thermodynamics Perspective on the Stepwise Conversion of Methane to Methanol over Cu-Exchanged SSZ-13, *ACS Catal.*, 2021, **11**, 7719–7734.

169 D. K. Pappas, E. Borfecchia, K. A. Lomachenko, A. Lazzarini, E. S. Gutterød, M. Dyballa, A. Martini, G. Berlier, S. Bordiga, C. Lamberti, B. Arstad, U. Olsbye, P. Beato and S. Svelle, Cu-Exchanged Ferrierite Zeolite for the Direct CH_4 to CH_3OH Conversion: Insights on Cu Speciation from X-Ray Absorption Spectroscopy, *Top. Catal.*, 2019, **62**, 712–723.

170 A. J. Knorpp, A. B. Pinar, M. A. Newton, V. L. Sushkevich and J. A. van Bokhoven, Copper-Exchanged Omega (MAZ) Zeolite: Copper-concentration Dependent Active Sites and its Unprecedented Methane to Methanol Conversion, *ChemCatChem*, 2018, **10**, 5593–5596.

171 A. J. Knorpp, M. A. Newton, A. B. Pinar and J. A. van Bokhoven, Conversion of Methane to Methanol on Copper Mordenite: Redox Mechanism of Isothermal and High-Temperature-Activation Procedures, *Ind. Eng. Chem. Res.*, 2018, **57**, 12036–12039.

172 E. Borfecchia, P. Beato, S. Svelle, U. Olsbye, C. Lamberti and S. Bordiga, Cu-CHA – a model system for applied selective redox catalysis, *Chem. Soc. Rev.*, 2018, **47**, 8097–8133.

173 E. M. C. Alayon, M. Nachtegaal, A. Bodi and J. A. van Bokhoven, Reaction Conditions of Methane-to-Methanol Conversion Affect the Structure of Active Copper Sites, *ACS Catal.*, 2014, **4**, 16–22.

174 J. H. Kwak, T. Varga, C. H. F. Peden, F. Gao, J. C. Hanson and J. Szanyi, Following the movement of Cu ions in a SSZ-13 zeolite during dehydration, reduction and adsorption: A combined *in situ* TP-XRD, XANES/DRIFTS study, *J. Catal.*, 2014, **314**, 83–93.

175 E. Borfecchia, D. K. Pappas, M. Dyballa, K. A. Lomachenko, C. Negri, M. Signorile and G. Berlier, Evolution of active sites during selective oxidation of methane to methanol over Cu-CHA and Cu-MOR zeolites as monitored by *operando* XAS, *Catal. Today*, 2019, **333**, 17–27.

176 R. Bulanek, K. Frolich, P. Cicmanec, D. Nachtigallova, A. Pulido and P. Nachtigall, Combined Experimental and Theoretical Investigations of Heterogeneous Dual Cation Sites in Cu,M-FER Zeolites, *J. Phys. Chem. C*, 2011, **115**, 13312–13321.

177 U. Engedahl, H. Grönbeck and A. Hellman, First-Principles Study of Oxidation State and Coordination of Cu-Dimers in Cu-SSZ-13 during Methane-to-Methanol Reaction Conditions, *J. Phys. Chem. C*, 2019, **123**, 26145–26150.

178 Y. Pérez-Badell, X. Solans-Monfort, M. Sodupe and L. A. Montero, A DFT periodic study on the interaction between O2 and cation exchanged chabazite MCHA (M = H^+, Na^+ or Cu^+): effects in the triplet–singlet energy gap, *Phys. Chem. Chem. Phys.*, 2009, **12**, 442–452.

179 M. H. Mahyuddin, T. Tanaka, A. Staykov, Y. Shiota and K. Yoshizawa, Dioxygen Activation on Cu-MOR Zeolite: Theoretical Insights into the Formation of Cu_2O and Cu_3O_3 Active Species, *Inorg. Chem.*, 2018, **57**, 10146–10152.

180 T. Yumura, M. Takeuchi, H. Kobayashi and Y. Kuroda, Effects of ZSM-5 Zeolite Confinement on Reaction Intermediates during Dioxygen Activation by Enclosed Dicopper Cations, *Inorg. Chem.*, 2009, **48**, 508–517.

181 Y. Zhu, K. Mimura and M. Isshiki, Oxidation Mechanism of Cu_2O to CuO at 600–1050 °C, *Oxid. Met.*, 2004, **62**, 207–222.
182 Z. Grzesik and M. Migdalska, Oxidation Mechanism of Cu_2O and Defect Structure of CuO at High Temperatures, *High Temp. Mater. Process*, 2011, **30**, 277–287.
183 C. K. Clayton and K. J. Whitty, Measurement and modeling of decomposition kinetics for copper oxide-based chemical looping with oxygen uncoupling, *Appl. Energy*, 2014, **116**, 416–423.
184 C. K. Clayton, H. Y. Sohn and K. J. Whitty, Oxidation Kinetics of Cu_2O in Oxygen Carriers for Chemical Looping with Oxygen Uncoupling, *Ind. Eng. Chem. Res.*, 2014, **53**, 2976–2986.
185 janaf.nist.gov/tables/O-029.html, can be found under https://janaf.nist.gov/tables/O-029.html, (accessed 14 January 2026), n.d.
186 janaf.nist.gov/tables/Cu-019.html, can be found under https://janaf.nist.gov/tables/Cu-019.html, (accessed 14 January 2026), n.d.
187 janaf.nist.gov/tables/Cu-015.html, can be found under https://janaf.nist.gov/tables/Cu-015.html, (accessed 14 January 2026), n.d.
188 Y. Wang, H. Liu, Q. Duan, Z. Li, Y. Wang, H. Liu, Q. Duan and Z. Li, Understanding the Negative Apparent Activation Energy for Cu_2O and CoO Oxidation Kinetics at High Temperature near Equilibrium, *Catalysts*, 2024, **14**, 832.
189 V. L. Sushkevich, D. Palagin, M. Ranocchiari and J. A. van Bokhoven, Response to Comment on 'Selective anaerobic oxidation of methane enables direct synthesis of methanol', *Science*, 2017, **358**, eaan6083.
190 M. Dyballa, K. Thorshaug, D. K. Pappas, E. Borfecchia, K. Kvande, S. Bordiga, G. Berlier, A. Lazzarini, U. Olsbye, P. Beato, S. Svelle and B. Arstad, Zeolite Surface Methoxy Groups as Key Intermediates in the Stepwise Conversion of Methane to Methanol, *ChemCatChem*, 2019, **11**, 5022–5026.
191 K. Kvande, D. K. Pappas, E. Borfecchia and K. A. Lomachenko, Advanced X-ray Absorption Spectroscopy Analysis to Determine Structure-Activity Relationships for Cu-Zeolites in the Direct Conversion of Methane to Methanol, *ChemCatChem*, 2020, **12**, 2385–2405.
192 I. A. Pankin, E. Borfecchia, A. Martini, K. A. Lomachenko, C. Lamberti and A. V. Soldatov, DFT-assisted XANES simulations to discriminate different monomeric Cu^{II} species in CHA catalysts, *Radiat. Phys. Chem.*, 2020, **175**, 108510.
193 K. Kvande, D. K. Pappas, M. Dyballa, C. Buono, M. Signorile, E. Borfecchia, K. A. Lomachenko, B. Arstad, S. Bordiga, G. Berlier, U. Olsbye, P. Beato and S. Svelle, Comparing the Nature of Active Sites in Cu-loaded SAPO-34 and SSZ-13 for the Direct Conversion of Methane to Methanol, *Catalysts*, 2020, **10**, 191.
194 H. M. Rhoda, D. Plessers, A. J. Heyer, M. L. Bols, R. A. Schoonheydt, B. F. Sels and E. I. Solomon, Spectroscopic Definition of a Highly Reactive Site in Cu-CHA for Selective Methane Oxidation: Tuning a Mono-μ-Oxo Dicopper(II) Active Site for Reactivity, *J. Am. Chem. Soc.*, 2021, **143**, 7531–7540.
195 M. A. Artsiusheuski, J. A. van Bokhoven and V. L. Sushkevich, Modeling and Experiment for Oxygen Isotope Exchange over Copper-Containing Mordenite, *J. Phys. Chem. C*, 2021, **125**, 12366–12373.
196 M. A. Artsiusheuski, J. A. van Bokhoven and V. L. Sushkevich, Oxygen Isotope Exchange over Copper-Containing Mordenite: The Effect of Copper Loading and Si/Al Ratio, *J. Phys. Chem. C*, 2021, **125**, 26512–26521.
197 K. A. Lomachenko, A. Martini, D. K. Pappas, C. Negri, M. Dyballa, G. Berlier, S. Bordiga, C. Lamberti, U. Olsbye, S. Svelle, P. Beato and E. Borfecchia, The impact of reaction conditions and material composition on the stepwise methane to methanol conversion over Cu-MOR: An *operando* XAS study, *Catal. Today*, 2019, **336**, 99–108.
198 M. Dyballa, D. K. Pappas, K. Kvande, E. Borfecchia, B. Arstad, P. Beato, U. Olsbye and S. Svelle, On How Copper Mordenite Properties Govern the Framework Stability and Activity in the Methane-to-Methanol Conversion, *ACS Catal.*, 2019, **9**, 365–375.
199 S. E. Bozbag, E. M. C. Alayon, J. Pecháček, M. Nachtegaal, M. Ranocchiari and J. A. van Bokhoven, Methane to methanol over copper mordenite: yield improvement through multiple cycles and different synthesis techniques, *Catal. Sci. Technol.*, 2016, **6**, 5011–5022.
200 A. J. Knorpp, *Direct Conversion of Methane to Methanol over Copper-Exchanged Zeolite Omega (MAZ)*, ETH Zürich, 2019.
201 A. J. Knorpp, M. A. Newton, S. C. M. Mizuno, J. Zhu, H. Mebrate, A. B. Pinar and J. A. van Bokhoven, Comparative performance of Cu-zeolites in the isothermal conversion of methane to methanol, *Chem. Commun.*, 2019, **55**, 11794–11797.
202 V. L. Sushkevich and J. A. van Bokhoven, Kinetic study and effect of water on methane oxidation to methanol over copper-exchanged mordenite, *Catal. Sci. Technol.*, 2020, **10**, 382–390.
203 P. Tomkins, M. Ranocchiari and J. A. van Bokhoven, Direct Conversion of Methane to Methanol under Mild Conditions over Cu-Zeolites and beyond, *Acc. Chem. Res.*, 2017, **50**, 418–425.
204 V. L. Sushkevich and J. A. van Bokhoven, Methane-to-Methanol: Activity Descriptors in Copper-Exchanged Zeolites for the Rational Design of Materials, *ACS Catal.*, 2019, **9**, 6293–6304.
205 J. Wieser, A. J. Knorpp, D. C. Stoian, P. Rzepka, M. A. Newton and J. A. van Bokhoven, Assessing the Productivity of the Direct Conversion of Methane-to-Methanol over Copper-Exchanged Zeolite Omega (MAZ) via Oxygen Looping, *Angew. Chem., Int. Ed.*, 2023, **62**, e202305140.
206 J. Zhu, V. L. Sushkevich, A. J. Knorpp, M. A. Newton, S. C. M. Mizuno, T. Wakihara, T. Okubo, Z. Liu and J. A. van Bokhoven, Cu-Erionite Zeolite Achieves High Yield in Direct Oxidation of Methane to Methanol by Isothermal Chemical Looping, *Chem. Mater.*, 2020, **32**, 1448–1453.
207 P. J. Smeets, B. F. Sels, R. M. van Teeffelen, H. Leeman, E. J. M. Hensen and R. A. Schoonheydt, The catalytic performance of Cu-containing zeolites in N2O decomposition and

the influence of O_2, NO and H_2O on recombination of oxygen, *J. Catal.*, 2008, **256**, 183–191.

208 T. Yumura, Y. Hirose, T. Wakasugi, Y. Kuroda and H. Kobayashi, Roles of Water Molecules in Modulating the Reactivity of Dioxygen-Bound Cu-ZSM-5 toward Methane: A Theoretical Prediction, *ACS Catal.*, 2016, **6**, 2487–2495.

209 K. Narsimhan, K. Iyoki, K. Dinh and Y. Román-Leshkov, Catalytic Oxidation of Methane into Methanol over Copper-Exchanged Zeolites with Oxygen at Low Temperature, *ACS Cent. Sci.*, 2016, **2**, 424–429.

210 J. Ohyama, A. Hirayama, Y. Tsuchimura, N. Kondou, H. Yoshida, M. Machida, S. Nishimura, K. Kato, I. Miyazato and K. Takahashi, Catalytic direct oxidation of methane to methanol by redox of copper mordenite, *Catal. Sci. Technol.*, 2021, **11**, 3437–3446.

211 A. Hirayama, Y. Tsuchimura, H. Yoshida, M. Machida, S. Nishimura, K. Kato, K. Takahashi and J. Ohyama, Catalytic oxidation of methane to methanol over Cu-CHA with molecular oxygen, *Catal. Sci. Technol.*, 2021, **11**, 6217–6224.

212 K. T. Dinh, M. M. Sullivan, K. Narsimhan, P. Serna, R. J. Meyer, M. Dincă and Y. Román-Leshkov, Continuous Partial Oxidation of Methane to Methanol Catalyzed by Diffusion-Paired Copper Dimers in Copper-Exchanged Zeolites, *J. Am. Chem. Soc.*, 2019, **141**, 11641–11650.

213 J. Pokhrel and D. F. Shantz, Continuous partial oxidation of methane to methanol over Cu-SSZ-39 catalysts, *J. Catal.*, 2023, **421**, 300–308.

214 Y. Fan, W. Zhou, X. Qiu, H. Li, Y. Jiang, Z. Sun, D. Han, L. Niu and Z. Tang, Selective photocatalytic oxidation of methane by quantum-sized bismuth vanadate, *Nat. Sustainable*, 2021, **4**, 509–515.

215 Z. R. Jovanovic, J.-P. Lange, M. Ravi, A. J. Knorpp, V. L. Sushkevich, M. A. Newton, D. Palagin and J. A. van Bokhoven, Oxidation of methane to methanol over Cu-exchanged zeolites: Scientia gratia scientiae or paradigm shift in natural gas valorization?, *J. Catal.*, 2020, **385**, 238–245.

216 C. Paolucci, I. Khurana, A. A. Parekh, S. Li, A. J. Shih, H. Li, J. R. Di Iorio, J. D. Albarracin-Caballero, A. Yezerets, J. T. Miller, W. N. Delgass, F. H. Ribeiro, W. F. Schneider and R. Gounder, Dynamic multinuclear sites formed by mobilized copper ions in NOx selective catalytic reduction, *Science*, 2017, **357**, 898–903.

217 F. Gao, D. Mei, Y. Wang, J. Szanyi and C. H. F. Peden, Selective Catalytic Reduction over Cu/SSZ-13: Linking Homo- and Heterogeneous Catalysis, *J. Am. Chem. Soc.*, 2017, **139**, 4935–4942.

218 K. M. MacKay, R. A. MacKay and W. Henderson, *Introduction to Modern Inorganic Chemistry*, CRC Press, Cheltenham, 2017.

219 J. Blumberger, L. Bernasconi, I. Tavernelli, R. Vuilleumier and M. Sprik, Electronic Structure and Solvation of Copper and Silver Ions: A Theoretical Picture of a Model Aqueous Redox Reaction, *J. Am. Chem. Soc.*, 2004, **126**, 3928–3938.

220 Y. Kuroda, R. Kumashiro and M. Nagao, Prominent redox feature of copper ion exchanged in ZSM-5-type zeolite, *Appl. Surf. Sci.*, 2002, **196**, 408–422.

221 Y. Kuroda, S. Konno, Y. Yoshikawa, H. Maeda, Y. Kubozono, H. Hamano, R. Kumashiro and M. Nagao, Stabilization of copper metal clusters in mordenite micropores, *J. Chem. Soc., Faraday Trans.*, 1997, **93**, 2125–2130.

222 M. Signorile, E. Borfecchia, S. Bordiga and G. Berlier, Influence of ion mobility on the redox and catalytic properties of Cu ions in zeolites, *Chem. Sci.*, 2022, **13**, 10238–10250.

223 P. J. Smeets, M. H. Groothaert, R. M. van Teeffelen, H. Leeman, E. J. M. Hensen and R. A. Schoonheydt, in *Studies in Surface Science and Catalysis*, ed. R. Xu, Z. Gao, J. Chen and W. Yan, Elsevier, 2007, pp. 1080–1087.

224 J. S. Woertink, P. J. Smeets, M. H. Groothaert, M. A. Vance, B. F. Sels, R. A. Schoonheydt and E. I. Solomon, A $[Cu_2O]^{2+}$ core in Cu-ZSM-5, the active site in the oxidation of methane to methanol, *Proc. Natl. Acad. Sci. U. S. A.*, 2009, **106**, 18908–18913.

225 P. J. Smeets, M. H. Groothaert, R. M. van Teeffelen, H. Leeman, E. J. M. Hensen and R. A. Schoonheydt, Direct NO and N_2O decomposition and NO-assisted N_2O decomposition over Cu-zeolites: Elucidating the influence of the CuCu distance on oxygen migration, *J. Catal.*, 2007, **245**, 358–368.

226 P. E. Fanning and M. A. Vannice, A DRIFTS Study of Cu–ZSM-5 Prior to and during Its Use for N2O Decomposition, *J. Catal.*, 2002, **207**, 166–182.

227 G. D. Lei, B. J. Adelman, J. Sarkany and W. M. H. Sachtler, Identification of copper(II) and copper(I) and their interconversion in Cu/ZSM-5 De-NOx catalysts, *Appl. Catal., B*, 1995, **5**, 245–256.

228 O. Memioglu and B. Ipek, A potential catalyst for continuous methane partial oxidation to methanol using N2O: Cu-SSZ-39, *Chem. Commun.*, 2021, **57**, 1364–1367.

229 P. Xiao, Y. Wang, Y. Lu, T. De Baerdemaeker, A.-N. Parvulescu, U. Müller, D. De Vos, X. Meng, F.-S. Xiao, W. Zhang, B. Marler, U. Kolb, H. Gies and T. Yokoi, Effects of Al distribution in the Cu-exchanged AEI zeolites on the reaction performance of continuous direct conversion of methane to methanol, *Appl. Catal., B*, 2023, **325**, 122395.

230 P. Xiao, Y. Wang, K. Nakamura, Y. Lu, T. De Baerdemaeker, A.-N. Parvulescu, U. Müller, D. De Vos, X. Meng, F.-S. Xiao, W. Zhang, B. Marler, U. Kolb, R. Osuga, M. Nishibori, H. Gies and T. Yokoi, Highly Effective Cu/AEI Zeolite Catalysts Contribute to Continuous Conversion of Methane to Methanol, *ACS Catal.*, 2023, **13**, 11057–11068.

231 C. Dai, Y. Zhang, N. Liu, G. Yu, N. Wang, R. Xu and B. Chen, Mechanistic insight into the effect of active site motif structures on direct oxidation of methane to methanol over Cu-ZSM-5, *Phys. Chem. Chem. Phys.*, 2023, **25**, 24894–24903.

232 Y. Chen, N. Liu, C. Dai, R. Xu, G. Yu, N. Wang and B. Chen, Continuous oxidation of methane into methanol by N_2O over Cu-Zeolite: A combined experimental and theoretical study, *Catal. Today*, 2024, **442**, 114934.

233 R. Xu, N. Liu, C. Dai, Y. Li, J. Zhang, B. Wu, G. Yu and B. Chen, H_2O-Built Proton Transfer Bridge Enhances Continuous Methane Oxidation to Methanol over Cu-BEA Zeolite, *Angew. Chem.*, 2021, **133**, 16770–16776.

234 D. D. Wagman, *Selected Values of Chemical Thermodynamic Properties*, Institute For Materials Research, National Bureau of Standards, 1965.
235 P. H. Kasai and R. J. Bishop Jr., Thermochemical decomposition of water catalyzed by zeolites, *J. Phys. Chem.*, 1977, **81**, 1527–1529.
236 R. A. Periana, Comment on 'Selective anaerobic oxidation of methane enables direct synthesis of methanol', *Science*, 2017, **358**, eaan5970.
237 D. Palagin, V. L. Sushkevich and J. A. van Bokhoven, Water Molecules Facilitate Hydrogen Release in Anaerobic Oxidation of Methane to Methanol over Cu/Mordenite, *ACS Catal.*, 2019, **9**, 10365–10374.
238 A. J. Heyer, J. Ma, D. Plessers, A. Braun, M. L. Bols, H. M. Rhoda, R. A. Schoonheydt, B. F. Sels and E. I. Solomon, Spectroscopic Investigation of the Role of Water in Copper Zeolite Methane Oxidation, *J. Am. Chem. Soc.*, 2024, **146**, 21208–21213.
239 T. Caroline., P. Pereira, J. V. R. Vieira, C. H. F. Da Cunha, S. C. M. Mizuno, Y. O. Carvalho, T. Faheina, M. Picinini, A. L. Blanco, A. C. M. Tello, E. A. Urquieta-Gonzalez, A. Lopez-Castillo, A. M. De Lima, J. B. O. D. Santos and J. M. C. Bueno, Conversion of methane to methanol over Cu-MAZ (zeolite omega): An oxygen-free process using H_2O and CO_2 as oxidants, *Appl. Catal., B*, 2024, **342**, 123370.
240 Y. R. Jeong, H. Jung, J. Kang, J. W. Han and E. D. Park, Continuous Synthesis of Methanol from Methane and Steam over Copper-Mordenite, *ACS Catal.*, 2021, **11**, 1065–1070.
241 V. L. Sushkevich and J. A. van Bokhoven, Effect of Brønsted acid sites on the direct conversion of methane into methanol over copper-exchanged mordenite, *Catal. Sci. Technol.*, 2018, **8**, 4141–4150.
242 A. Koishybay and D. F. Shantz, Water Is the Oxygen Source for Methanol Produced in Partial Oxidation of Methane in a Flow Reactor over Cu-SSZ-13, *J. Am. Chem. Soc.*, 2020, **142**, 11962–11966.
243 C. Zhou, S. Li, S. He, Z. Zhao, Y. Jiao and H. Zhang, Temperature-dependant active sites for methane continuous conversion to methanol over Cu-zeolite catalysts using water as the oxidant, *Fuel*, 2022, **329**, 125483.
244 H. Zhang, P. Han, D. Wu, C. Du, J. Zhao, K. H. L. Zhang, J. Lin, S. Wan, J. Huang, S. Wang, H. Xiong and Y. Wang, Confined Cu–OH single sites in SSZ-13 zeolite for the direct oxidation of methane to methanol, *Nat. Commun.*, 2023, **14**, 7705.
245 B. Modén, P. Da Costa, B. Fonfé, D. K. Lee and E. Iglesia, Kinetics and Mechanism of Steady-State Catalytic NO Decomposition Reactions on Cu–ZSM5, *J. Catal.*, 2002, **209**, 75–86.
246 C. Lamberti, S. Bordiga, M. Salvalaggio, G. Spoto, A. Zecchina, F. Geobaldo, G. Vlaic and M. Bellatreccia, XAFS, IR, and UV−Vis Study of the CuI Environment in CuI-ZSM-5, *J. Phys. Chem. B*, 1997, **101**, 344–360.
247 J. V. R. Vieira, T. C. P. Pereira, C. H. F. da Cunha, D. D. Petrolini, A. C. M. Tello, A. M. Lima, Y. O. Carvalho, A. L. R. Garcia, E. A. Urquieta-Gonzalez, J. B. O. dos Santos, P. M. Lima and J. M. C. Bueno, Isothermal conversion of methane to methanol over Cu-CHA using different oxidants, *Catal. Today*, 2025, **446**, 115121.
248 S. J. Freakley, N. Dimitratos, D. J. Willock, S. H. Taylor, C. J. Kiely and G. J. Hutchings, Methane Oxidation to Methanol in Water, *Acc. Chem. Res.*, 2021, **54**, 2614–2623.
249 C. Hammond, M. M. Forde, M. H. Ab Rahim, A. Thetford, Q. He, R. L. Jenkins, N. Dimitratos, J. A. Lopez-Sanchez, N. F. Dummer, D. M. Murphy, A. F. Carley, S. H. Taylor, D. J. Willock, E. E. Stangland, J. Kang, H. Hagen, C. J. Kiely and G. J. Hutchings, Direct Catalytic Conversion of Methane to Methanol in an Aqueous Medium by using Copper-Promoted Fe-ZSM-5, *Angew. Chem., Int. Ed.*, 2012, **51**, 5129–5133.
250 C. Hammond, N. Dimitratos, J. A. Lopez-Sanchez, R. L. Jenkins, G. Whiting, S. A. Kondrat, M. H. Ab Rahim, M. M. Forde, A. Thetford, H. Hagen, E. E. Stangland, J. M. Moulijn, S. H. Taylor, D. J. Willock and G. J. Hutchings, Aqueous-Phase Methane Oxidation over Fe-MFI Zeolites; Promotion through Isomorphous Framework Substitution, *ACS Catal.*, 2013, **3**, 1835–1844.
251 C. Hammond, N. Dimitratos, R. L. Jenkins, J. A. Lopez-Sanchez, S. A. Kondrat, M. Hasbi ab Rahim, M. M. Forde, A. Thetford, S. H. Taylor, H. Hagen, E. E. Stangland, J. H. Kang, J. M. Moulijn, D. J. Willock and G. J. Hutchings, Elucidation and Evolution of the Active Component within Cu/Fe/ZSM-5 for Catalytic Methane Oxidation: From Synthesis to Catalysis, *ACS Catal.*, 2013, **3**, 689–699.
252 T. Yu, Z. Li, L. Lin, S. Chu, Y. Su, W. Song, A. Wang, B. M. Weckhuysen and W. Luo, Highly Selective Oxidation of Methane into Methanol over Cu-Promoted Monomeric Fe/ZSM-5, *ACS Catal.*, 2021, **11**, 6684–6691.
253 R. D. Armstrong, V. Peneau, N. Ritterskamp, C. J. Kiely, S. H. Taylor and G. J. Hutchings, The Role of Copper Speciation in the Low Temperature Oxidative Upgrading of Short Chain Alkanes over Cu/ZSM-5 Catalysts, *Chem. Phys. Chem.*, 2018, **19**, 469–478.
254 L. Cheng, X. Chen, P. Hu and X.-M. Cao, Advantages and limitations of hydrogen peroxide for direct oxidation of methane to methanol at mono-copper active sites in Cu-exchanged zeolites, *Chin. J. Catal.*, 2023, **51**, 135–144.
255 J. Ohyama, A. Hirayama, N. Kondou, H. Yoshida, M. Machida, S. Nishimura, K. Hirai, I. Miyazato and K. Takahashi, Data science assisted investigation of catalytically active copper hydrate in zeolites for direct oxidation of methane to methanol using H_2O_2, *Sci. Rep.*, 2021, **11**, 2067.
256 X. Tang, L. Wang, B. Yang, C. Fei, T. Yao, W. Liu, Y. Lou, Q. Dai, Y. Cai, X.-M. Cao, W. Zhan, Y. Guo, X.-Q. Gong and Y. Guo, Direct oxidation of methane to oxygenates on supported single Cu atom catalyst, *Appl. Catal., B*, 2021, **285**, 119827.
257 S. A. Yashnik, V. V. Boltenkov, D. E. Babushkin, O. P. Taran and V. N. Parmon, Methane Oxidation by H2O2 over Different Cu-Species of Cu-ZSM-5 Catalysts, *Top. Catal.*, 2020, **63**, 203–221.

258 B. Wichterlová, J. Dědeček, Z. Sobalík, A. Vondrová and K. Klier, On the Cu Site in ZSM-5 Active in Decomposition of NO: Luminescence, FTIR Study, and Redox Properties, *J. Catal.*, 1997, **169**, 194–202.

259 V. Umamaheswari, M. Hartmann and A. Pöppl, EPR Spectroscopy of Cu(I)−NO Adsorption Complexes Formed over Cu−ZSM-5 and Cu−MCM-22 Zeolites, *J. Phys. Chem. B*, 2005, **109**, 1537–1546.

260 E. Giamello, D. Murphy, G. Magnacca, C. Morterra, Y. Shioya, T. Nomura and M. Anpo, The interaction of NO with copper ions in ZSM5: An EPR and IR investigation, *J. Catal.*, 1992, **136**, 510–520.

261 Z. Sojka, M. Che and E. Giamello, EPR Investigation of the Electronic Structure of Mononuclear Copper(I) Nitric Oxide Adduct Formed upon Low-Pressure Adsorption of NO onto Cu/ZSM-5 Zeolite, *J. Phys. Chem. B*, 1997, **101**, 4831–4838.

262 M. Anpo, Y. Shioya, H. Yamashita, E. Giamello, C. Morterra, M. Che, H. H. Patterson, S. Webber and S. Ouellette, Preparation and Characterization of the Cu+/ZSM-5 Catalyst and Its Reaction with NO under UV Irradiation at 275 K. In situ Photoluminescence, EPR, and FT-IR Investigations, *J. Phys. Chem.*, 1994, **98**, 5744–5750.

263 M. Anpo, M. Matsuoka, K. Hano, H. Mishima, T. Ono and H. Yamashita, Photocatalytic decomposition of N2O on Cu+/Y-zeolite catalysts prepared by ion-exchange, *Korean J. Chem. Eng.*, 1997, **14**, 498–501.

264 H. Yamashita, M. Matsuoka, K. Tsuji, Y. Shioya, M. Anpo and M. Che, *In Situ* XAFS, Photoluminescence, and IR Investigations of Copper Ions Included within Various Kinds of Zeolites. Structure of Cu(I) Ions and Their Interaction with CO Molecules, *J. Phys. Chem.*, 1996, **100**, 397–402.

265 D. Ferri, M. S. Kumar, R. Wirz, A. Eyssler, O. Korsak, P. Hug, A. Weidenkaff and M. A. Newton, First steps in combining modulation excitation spectroscopy with synchronous dispersive EXAFS/DRIFTS/mass spectrometry for *in situ* time resolved study of heterogeneous catalysts, *Phys. Chem. Chem. Phys.*, 2010, **12**, 5634–5646.

266 J. W. A. Fischer, F. Buttignol, A. Garbujo, D. Ferri and G. Jeschke, Elucidation of site-specific red-ox kinetics in the CO-assisted N_2O decomposition over Fe–ferrierite by combining modulation excitation with *operando* EPR spectroscopy, *Chem. Sci.*, 2025, **16**, 4884–4891.

267 A. Urakawa, T. Bürgi and A. Baiker, Sensitivity enhancement and dynamic behavior analysis by modulation excitation spectroscopy: Principle and application in heterogeneous catalysis, *Chem. Eng. Sci.*, 2008, **63**, 4902–4909.

268 F. Buttignol, J. W. A. Fischer, A. H. Clark, M. Elsener, A. Garbujo, P. Biasi, I. Czekaj, M. Nachtegaal, G. Jeschke, O. Kröcher and D. Ferri, Iron-catalysed cooperative redox mechanism for the simultaneous conversion of nitrous oxide and nitric oxide, *Nat. Catal.*, 2024, 1–11.

